

Bacterial metabolomics approach towards antimicrobials and resistance

Edited by

Vijay Soni, Vinayak Singh and Zhe Wang

Published in

Frontiers in Microbiology



FRONTIERS EBOOK COPYRIGHT STATEMENT

The copyright in the text of individual articles in this ebook is the property of their respective authors or their respective institutions or funders. The copyright in graphics and images within each article may be subject to copyright of other parties. In both cases this is subject to a license granted to Frontiers.

The compilation of articles constituting this ebook is the property of Frontiers.

Each article within this ebook, and the ebook itself, are published under the most recent version of the Creative Commons CC-BY licence. The version current at the date of publication of this ebook is CC-BY 4.0. If the CC-BY licence is updated, the licence granted by Frontiers is automatically updated to the new version.

When exercising any right under the CC-BY licence, Frontiers must be attributed as the original publisher of the article or ebook, as applicable.

Authors have the responsibility of ensuring that any graphics or other materials which are the property of others may be included in the CC-BY licence, but this should be checked before relying on the CC-BY licence to reproduce those materials. Any copyright notices relating to those materials must be complied with.

Copyright and source acknowledgement notices may not be removed and must be displayed in any copy, derivative work or partial copy which includes the elements in question.

All copyright, and all rights therein, are protected by national and international copyright laws. The above represents a summary only. For further information please read Frontiers' Conditions for Website Use and Copyright Statement, and the applicable CC-BY licence.

ISSN 1664-8714
ISBN 978-2-8325-2705-4
DOI 10.3389/978-2-8325-2705-4

About Frontiers

Frontiers is more than just an open access publisher of scholarly articles: it is a pioneering approach to the world of academia, radically improving the way scholarly research is managed. The grand vision of Frontiers is a world where all people have an equal opportunity to seek, share and generate knowledge. Frontiers provides immediate and permanent online open access to all its publications, but this alone is not enough to realize our grand goals.

Frontiers journal series

The Frontiers journal series is a multi-tier and interdisciplinary set of open-access, online journals, promising a paradigm shift from the current review, selection and dissemination processes in academic publishing. All Frontiers journals are driven by researchers for researchers; therefore, they constitute a service to the scholarly community. At the same time, the *Frontiers journal series* operates on a revolutionary invention, the tiered publishing system, initially addressing specific communities of scholars, and gradually climbing up to broader public understanding, thus serving the interests of the lay society, too.

Dedication to quality

Each Frontiers article is a landmark of the highest quality, thanks to genuinely collaborative interactions between authors and review editors, who include some of the world's best academicians. Research must be certified by peers before entering a stream of knowledge that may eventually reach the public - and shape society; therefore, Frontiers only applies the most rigorous and unbiased reviews. Frontiers revolutionizes research publishing by freely delivering the most outstanding research, evaluated with no bias from both the academic and social point of view. By applying the most advanced information technologies, Frontiers is catapulting scholarly publishing into a new generation.

What are Frontiers Research Topics?

Frontiers Research Topics are very popular trademarks of the *Frontiers journals series*: they are collections of at least ten articles, all centered on a particular subject. With their unique mix of varied contributions from Original Research to Review Articles, Frontiers Research Topics unify the most influential researchers, the latest key findings and historical advances in a hot research area.

Find out more on how to host your own Frontiers Research Topic or contribute to one as an author by contacting the Frontiers editorial office: frontiersin.org/about/contact

Bacterial metabolomics approach towards antimicrobials and resistance

Topic editors

Vijay Soni — Weill Cornell Medical Center, New York-Presbyterian, United States

Vinayak Singh — University of Cape Town, South Africa

Zhe Wang — Shanghai Jiao Tong University, China

Citation

Soni, V., Singh, V., Wang, Z., eds. (2023). *Bacterial metabolomics approach towards antimicrobials and resistance*. Lausanne: Frontiers Media SA.
doi: 10.3389/978-2-8325-2705-4

Table of contents

- 05 Editorial: Bacterial metabolomics approach towards antimicrobials and resistance
Vijay Soni, Zhe Wang and Vinayak Singh
- 08 Antibacterial Activity of the Essential Oil From *Litsea cubeba* Against *Cutibacterium acnes* and the Investigations of Its Potential Mechanism by Gas Chromatography-Mass Spectrometry Metabolomics
Jing Chen, Jianing Zhang, Longping Zhu, Chunguo Qian, Hongru Tian, Zhimin Zhao, Lu Jin and Depo Yang
- 22 A Selective Medium for Screening Ceftazidime/Avibactam Resistance in Carbapenem-Resistant *Enterobacterales*
Weiliang Zeng, Wenli Liao, Yajie Zhao, Lingbo Wang, Hongyun Shu, Huaiyu Jia, Tao Chen, Ying Zhang, Tieli Zhou and Qing Wu
- 32 A New Perspective on the Antimicrobial Mechanism of Berberine Hydrochloride Against *Staphylococcus aureus* Revealed by Untargeted Metabolomic Studies
Shu Wu, Kun Yang, Yuhang Hong, Yanju Gong, Jiajia Ni, Ni Yang and Weijun Ding
- 45 Biomarker enrichment medium: A defined medium for metabolomic analysis of microbial pathogens
Maryam Mapar, Thomas Rydzak, Ryan A. Groves and Ian A. Lewis
- 61 Microbial containment device: A platform for comprehensive analysis of microbial metabolism without sample preparation
Mehdi Mohammadi, Stephanie L. Bishop, Raied Aburashed, Saad Luqman, Ryan A. Groves, Dominique G. Bihan, Thomas Rydzak and Ian A. Lewis
- 74 Intramammary infusion of matrine-chitosan hydrogels for treating subclinical bovine mastitis —effects on milk microbiome and metabolites
Hua Zhang, Ziyue Wang, Hua Yao, Linshu Jiang and Jinjin Tong
- 88 Metabolomic profiling of polymyxin-B in combination with meropenem and sulbactam against multi-drug resistant *Acinetobacter baumannii*
Shixing Zhu, Jiayuan Zhang, Chu Song, Yuwei Liu, Charles Oo, M. Tobias Heinrichs, Zhihua Lv, Yuanqi Zhu, Sherwin K. B. Sy, Pan Deng and Mingming Yu
- 101 Exogenous D-ribose promotes gentamicin treatment of several drug-resistant *Salmonella*
Yanhong Zhou, Yan Yong, Chunyang Zhu, Heng Yang and Binghu Fang

- 117 **Comparison of freeze-thaw and sonication cycle-based methods for extracting AMR-associated metabolites from *Staphylococcus aureus***
Rita Singh, Lovnish Thakur, Ashok Kumar, Sevaram Singh, Shailesh Kumar, Manoj Kumar, Yashwant Kumar and Niraj Kumar
- 133 **Nitrogen metabolism in mycobacteria: the key genes and targeted antimicrobials**
Yufan Xu, Shiwei Ma, Zixin Huang, Longlong Wang, Sayed Haidar Abbas Raza and Zhe Wang



OPEN ACCESS

EDITED AND REVIEWED BY
Rustam Aminov,
University of Aberdeen, United Kingdom

*CORRESPONDENCE

Vijay Soni
✉ vis2032@med.cornell.edu;
✉ sonivijay07@gmail.com

RECEIVED 14 May 2023

ACCEPTED 17 May 2023

PUBLISHED 30 May 2023

CITATION

Soni V, Wang Z and Singh V (2023) Editorial:
Bacterial metabolomics approach towards
antimicrobials and resistance.
Front. Microbiol. 14:1222594.
doi: 10.3389/fmicb.2023.1222594

COPYRIGHT

© 2023 Soni, Wang and Singh. This is an
open-access article distributed under the terms
of the [Creative Commons Attribution License](https://creativecommons.org/licenses/by/4.0/)
(CC BY). The use, distribution or reproduction
in other forums is permitted, provided the
original author(s) and the copyright owner(s)
are credited and that the original publication in
this journal is cited, in accordance with
accepted academic practice. No use,
distribution or reproduction is permitted which
does not comply with these terms.

Editorial: Bacterial metabolomics approach towards antimicrobials and resistance

Vijay Soni^{1*}, Zhe Wang^{2,3} and Vinayak Singh^{4,5}

¹Division of Infectious Diseases, Weill Department of Medicine, Weill Cornell Medicine, New York, NY, United States, ²Shanghai Key Laboratory of Veterinary Biotechnology, School of Agriculture and Biology, Shanghai Jiao Tong University, Shanghai, China, ³Shanghai Collaborative Innovation Center of Agri-Seeds, School of Agriculture and Biology, Shanghai Jiao Tong University, Shanghai, China, ⁴Holistic Drug Discovery and Development Centre (H3D), University of Cape Town, Rondebosch, South Africa, ⁵South African Medical Research Council Drug Discovery and Development Research Unit, Institute of Infectious Disease and Molecular Medicine, University of Cape Town, Rondebosch, South Africa

KEYWORDS

antimicrobial resistance (AMR), drug mechanism of action, LC-MS, metabolomic biomarker, microbial metabolomics, novel drug candidates, pathogenic bacteria antimicrobial assay

Editorial on the Research Topic

Bacterial metabolomics approach towards antimicrobials and resistance

The rising prevalence of bacterial infections and antimicrobial resistance (AMR) are becoming a growing global concern. According to the United Nations Environment Programme, by 2050 AMR will be responsible for almost 10 million deaths every year and if not controlled it will cost around USD 3.4 trillion annually. Therefore, there is an urgent need to develop novel approaches and treatments. Metabolomics presents a promising solution by accelerating the discovery of microbial metabolic changes during infection and upon antibiotic treatment (Figure 1). Thus, enabling researchers to identify potential novel drug targets and strategies to develop better therapeutic interventions to combat AMR. In this Research Topic, we have compiled several interesting articles covering novel discoveries around this theme.

Wu et al. evaluated bacterial metabolomics of *Staphylococcus aureus* upon Berberine hydrochloride (BBR) treatment and found significant inhibition of cell wall biosynthesis, perturbation in shikimate metabolism and elevated amino sugar production, nucleic acid biosynthesis and nucleotide sugar metabolism. Two stress resistance-related biomarkers, pyridine dicarboxylic acids, were downregulated while oxidized phospholipid levels were increased.

In the same direction, Chen et al. reported the antimicrobial activity of essential oil (EO), isolated from fresh mature *Litsea cubeba*, against *Cutibacterium acnes*. Metabolomics upon EO treatment showed alteration of 86 metabolites and 34 of them belonged to cell wall pathways, amino acid biosynthesis, energy production, and carbohydrate metabolism. ATP levels were extremely low and the activities of glycolytic enzymes and the Wood-Werkman cycle (malate dehydrogenase, pyruvate kinase, and pyruvate carboxylase activities were decreased, and hexokinase activity was increased) were perturbed significantly upon EO treatment.

Further, Zhu et al. investigated the synergistic behavior of polymyxin-B, meropenem, and sulbactam against multi-drug resistant *Acinetobacter baumannii*. A short (15 min) treatment combination of all three antibiotics substantially affected the levels of metabolites

involved in the cell wall, cell outer membrane, peptidoglycan, fatty acid, lipopolysaccharide, glycerophospholipid, and nucleotide metabolism. Interestingly, a longer (1 h) treatment of the double and triple combinations significantly interrupted the amino acids and nucleotide biosynthesis and central carbon metabolism.

Zhou et al. reported an interesting example of discovering a metabolite-based antibiotic adjuvant by comparing the metabolic profiles of drug-sensitive (SCH-S) and gentamicin-resistant *Salmonella Choleraesuis* (SCH-R). Non-targeted metabolomics revealed extensive disruption in energy and central carbon metabolism along with the dysregulations of amino acid biosynthesis, nucleotide production, vitamin and cofactor metabolism, and fatty acid biogenesis. Remarkably, D-ribose was the most suppressed metabolite in SCH-R and enhanced the efficacy of gentamicin against SCH-R and clinical multidrug-resistant strains. They suggested that D-ribose activates pentose phosphate pathway, glycolysis, and tricarboxylic acid cycle which induced the NADH levels, polarizes the electron transport chain, and raises the proton motive force to increase drug uptake, and kills the bacteria.

Study by Zhang et al. revealed the application of matrine-chitosan hydrogels (MCH) to cure subclinical mastitis, a bacterial infection-mediated inflammation in bovine mammary glands. Using metabolomics and 16S sequencing they investigated the biological response to MCH in mastitis-affected cows. They discovered that relative abundances of bacterial communities such as *Staphylococcus*, *Aerococcus*, and *Corynebacterium_1* were reduced after 7 days of MCH treatment. MCH infusion was also found to be associated with differentially expressed metabolites in milk, such as fatty acyls, flavonoids, sphingolipids, and glycerophospholipids. This study provides new understandings about the immunoregulatory mechanisms to matrine and its role in controlling mastitis in dairy cows.

Moreover, Singh et al. compared different methods of metabolite extraction that included freeze-thaw cycle (FTC) and sonication cycle (SC) individually and in combination (FTC+SC). Using ESI-LC-MS/MS, they found that both FTC and SC methods were efficient in isolating AMR-associated metabolites from *S. aureus*, while combining these methods does not improve the efficiency. Basically, each method showed some level of selectivity toward metabolites and the selection of the right method should be based on the possible class and type of metabolites.

Mohammadi et al. developed Microbial Containment Device (MCD), a novel high-throughput 96-well sampling system, to simplify boundary flux analysis and captured complex microbial metabolic phenotypes. Using a semi-permeable membrane, MCD allowed diffusion of water-soluble metabolites from bacterial culture reservoir into a bacteria-free analytical well. MCD required minimal sample handling and enabled single-step metabolomics to identify different bacterial strains and their responses to antibiotics. This can be very useful for large-scale metabolomics studies as it is compatible with traditional commercial autosamplers of LC-MS systems.

Nutrients and growth conditions play a crucial role in metabolism, especially in detecting AMR. Zeng et al. developed *Salmonella-Shigella* (SS) ceftazidime/avibactam (CZA)-selective medium for clinical screening of CZA-resistant carbapenem-resistant Enterobacterales (CRE) isolates from pure culture and simulated clinical polymicrobial specimens such as stool samples. With 100% specificity and sensitivity, the screening efficiency of SS-CZA media remained natural for different resistance determinants that were found in tested isolates.

Consecutively, Mapar et al. reported how commercial media such as Mueller Hinton medium can affect the *in vitro* metabolic phenotypes and formulated Biomarker Enrichment Medium (BEM)—a complex defined media derived from Roswell Park

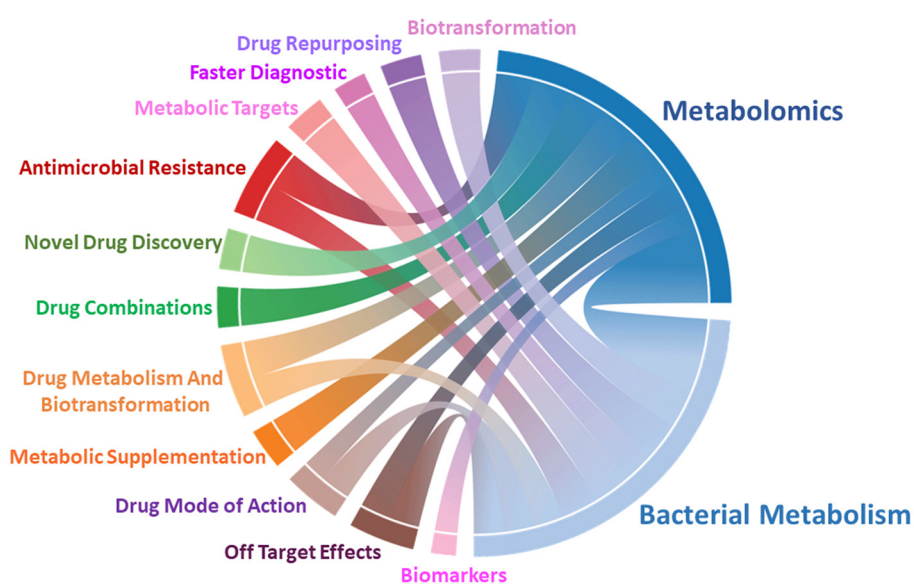


FIGURE 1

Metabolomics plays a central role in studying bacterial metabolism. Chord diagram representing correlations of metabolomics, microbial metabolism, and their application in drug development, diagnostic, and to understand mechanism of drug resistance and action.

Memorial Institute (RPMI) medium) as an alternative for metabolomic assays. Combining substrate exclusion, isotope-labeling, and nutritional supplementation methods they have identified specific nutrients required for unique biomarkers production by pathogenic bacteria. Using this information, they have proposed BEM as an alternative to complex undefined media for metabolomics experiments, clinical diagnostics, and drug discovery, where stable metabolic profiles play a crucial role.

A review from [Xu et al.](#) summarized the importance of nitrogen metabolism for Mycobacteria and showed the role of related genes and pathways in bacterial survival, virulence, and suggested a direction to develop novel targeted small molecular antimicrobials. Authors audited extensive literature to elaborate on the role of nitrogen metabolizing genes such as *glnA1*, *pknG*, *groES*, *groEL2*, *ansP2*, *ansA*, *Rv322c*, *argB*, and *argF*. Further, they have described the way forward, gaps, and recommendations to target nitrogen metabolism using specific inhibitors to control the emergence of AMR mycobacteria.

Finally, we want to express our gratitude to all contributing authors and reviewers who made it possible. We believe that this collection would assist readers to comprehend novel aspects of metabolomics and its applications in understanding the bacterial metabolism and controlling AMR.

Author contributions

VSo conceptualized, collected all information, and wrote the first draft. ZW participated in the writing of remaining sections. VSi and VSo edited the final draft. All authors contributed to the article and approved the submitted version.

Conflict of interest

The authors declare that the research was conducted in the absence of any commercial or financial relationships that could be construed as a potential conflict of interest.

Publisher's note

All claims expressed in this article are solely those of the authors and do not necessarily represent those of their affiliated organizations, or those of the publisher, the editors and the reviewers. Any product that may be evaluated in this article, or claim that may be made by its manufacturer, is not guaranteed or endorsed by the publisher.



Antibacterial Activity of the Essential Oil From *Litsea cubeba* Against *Cutibacterium acnes* and the Investigations of Its Potential Mechanism by Gas Chromatography-Mass Spectrometry Metabolomics

OPEN ACCESS

Edited by:

Zhe Wang,
Shanghai Jiao Tong University, China

Reviewed by:

Hyungjin Eoh,
University of Southern California,
United States
Xi Liu,
Shanghai Jiao Tong University, China

*Correspondence:

Lu Jin
jinlu5@mail.sysu.edu.cn
Depo Yang
lssydp@mail.sysu.edu.cn

Specialty section:

This article was submitted to
Antimicrobials, Resistance
and Chemotherapy,
a section of the journal
Frontiers in Microbiology

Received: 28 November 2021

Accepted: 28 January 2022

Published: 02 March 2022

Citation:

Chen J, Zhang J, Zhu L, Qian C,
Tian H, Zhao Z, Jin L and Yang D
(2022) Antibacterial Activity of the
Essential Oil From *Litsea cubeba*
Against *Cutibacterium acnes*
and the Investigations of Its Potential
Mechanism by Gas
Chromatography-Mass Spectrometry
Metabolomics.
Front. Microbiol. 13:823845.
doi: 10.3389/fmicb.2022.823845

Jing Chen¹, Jianing Zhang¹, Longping Zhu^{1,2}, Chunguo Qian^{1,2}, Hongru Tian^{1,2},
Zhimin Zhao^{1,2}, Lu Jin^{1,2*} and Depo Yang^{1,2*}

¹ School of Pharmaceutical Sciences, Sun Yat-sen University, Guangzhou, China, ² Guangdong Technology Research Center for Advanced Chinese Medicine, Guangzhou, China

Cutibacterium acnes (*C. acnes*) is an anaerobic Gram-positive bacterium generally considered as a human skin commensal, but is also involved in different infections, such as *acne* and surgical infections. Although there are a variety of treatments, the side effects and the problem of bacterial drug resistance still limit their clinical usage. In this study, we found that essential oil (EO) distilled from fresh mature *Litsea cubeba* possessed promising antibacterial activity against *C. acnes*. In order to elucidate its potential mechanism, bacteriostatic activity test, Live/Dead kit assay, scanning electron microscope (SEM), transmission electron microscope (TEM), and metabolomics were employed. In addition, the content of adenosine triphosphate (ATP) in bacterium and the activities of key enzymes involved in critical metabolic pathways were detected using a variety of biochemical assays. The results showed that EO exhibited significant antibacterial activity against *C. acnes* at a minimum inhibitory concentration (MIC) of 400 $\mu\text{g/mL}$ and a minimum bactericidal concentration (MBC) of 800 $\mu\text{g/mL}$, and EO could destroy *C. acnes* morphology and inhibit its growth. Moreover, results from our study showed that EO had a significant effect on the *C. acnes* normal metabolism. In total, 86 metabolites were altered, and 34 metabolic pathways related to the carbohydrate metabolism, energy metabolism, amino acid metabolism, as well as cell wall and cell membrane synthesis were perturbed after EO administration. The synthesis of ATP in bacterial cells was also severely inhibited, and the activities of key enzymes of the glycolysis and Wood-Werkman cycle were significantly affected (Pyruvate Carboxylase, Malate Dehydrogenase and Pyruvate kinase activities were decreased, and Hexokinase was increased). Taken together, these results illustrated that the bacteriostatic effect

of EO against *C. acnes* by breaking the bacterial cell morphology and perturbing cell metabolism, including inhibition of key enzyme activity and ATP synthesis. The results from our study may shed new light on the discovery of novel drugs with more robust efficacy.

Keywords: *Cutibacterium acnes*, *Litsea cubeba*, essential oil, GC-MS untargeted metabolomics, antibacterial

INTRODUCTION

Cutibacterium acnes (*C. acnes*) is considered to reside in the sebaceous glands of the skin, and plays an important role in maintaining skin pH by decomposing skin triglycerides and producing fatty acids (Gribbon et al., 1993; Webster, 1995). However, it is also a conditional pathogenic bacterium that is able to cause invasive infection of organs and tissues under specific cases, such as surgery or trauma (Achermann et al., 2014; Choi et al., 2021). In addition, studies have shown that *C. acnes* is one of the main culprits of *acne* (Dreno et al., 2018). As one of the most common skin diseases with high incidence in young adulthood, *acne* can cause physical discomfort, face skin defects, or disfigurement as the long-term chronic inflammations persist. It will even cause a tremendous psychological burden to the patients, causing anxiety and even severe mental illness (Gupta and Gupta, 1998; Thomas, 2004; Park et al., 2021).

In the past, the antibiotics, such as macrolides, clindamycin, and tetracyclines, were the most common medications prescribed for *acne* (Walsh et al., 2016). Although they are still largely active against the majority of *C. acnes*, the emerging of drug resistance becomes an urgent problem (Leyden, 1976); therefore, it is not appropriate to treat *acne* with a single antibiotic. Instead, a variety of antibiotics or the combination of antibiotics and other drugs are used, but there are still many problems with these drugs in clinical use, like irritation of the skin and mucous membranes (Nyirady et al., 2001; Archer and Chang, 2004; Strauss et al., 2007; Tanghetti and Popp, 2009). In recent years, more and more attention has been paid to natural products derived from plants due to their higher efficacy and lower toxicity, which can replace or assist antimicrobial agents in inhibiting the proliferation of *C. acnes* (De Canha et al., 2019; Di Lodovico et al., 2020; Wei et al., 2021). Accumulating evidence showed that many essential oils from plants such as cloves, cactus, tea tree, and so on possessed an inhibitory effect on *C. acnes* (Fu et al., 2009; Murbach Teles Andrade et al., 2018; Ossa-Tabares et al., 2020). However, there is a lack of research on the mechanism underlying the antibacterial activity.

Litsea cubeba (Lour) Pers. is a deciduous shrub or small tree belonging to the genus of *Litsea* of the Lauraceae family, and it is an economic crop for the production of essential oil (Chen Y.C. et al., 2020). Previous studies have demonstrated that the EO has promising anti-cancer (Dalimunthe et al., 2019; Pante et al., 2021), bacteriostatic (Liu and Yang, 2012; Li et al., 2014; Nguyen et al., 2018; Dai et al., 2021) and antifungal activities (Nardoni et al., 2019), insecticidal and mosquito repellent activities (Noosidum et al., 2008; Vongsombath et al., 2012), which has been widely used in daily chemical products and food as a flavoring and preservative (Agrawal et al., 2011).

Although EO has bacteriostatic activity against many kinds of bacteria, most of them are foodborne bacteria. The inhibitory activity against *C. acnes* has not been reported. Accordingly, we investigated the activity of *Litsea cubeba* essential oil against *C. acnes* and further explored its potential mechanism by GC-MS-based non-target metabolomics for the first time. This study may provide a new perspective to understand the mechanism of inhibiting *C. acnes* in more detail.

MATERIALS AND METHODS

Materials

Cutibacterium acnes (ATCC 6919, antibiotic-susceptible) strain was obtained from Guangdong Microbial Strain Preservation Center; The mediums of Brain Heart Infusion Broth and Reinforced Clostridium Aga were from HuanKai Microbial (Guangdong, China) and Shanghai Acme Biochemical Co., Ltd, respectively; Tween 80, Anhydrous sodium sulfate, 25% Glutaraldehyde, and TERT-butyl alcohol were obtained from DAMAO; Ampicillin was from Biofrox; Glucose, Absolute ethanol, and Sodium bisulfate dihydrate were provided from Sinopharm Chemical Reagent Co., Ltd.; Sodium hydroxide was from Guangzhou Chemical Reagent Factory, Methoxyamine hydrochloride, N-methyl-N-trimethylsilyltrifluoroacetanamide (MSTFA), and Adonitol were purchased from Sigma-Aldrich; Methanol HPLC/ACS was from Energy-chemical; Hypoxic conditions were generated using an AnaeroPack (Japan Mitsubishi MGC); C7-C40 n-alkanes was purchased from Shanghai Huicheng Biotechnology Co., Ltd.

Live/Dead BacLight Bacterial Viability Kits was obtained from Thermo (Invitrogen by Thermo Fisher Scientific, L7012), Enhanced BCA Protein Assay Kit was purchased from Beyotime, Micro Malate Dehydrogenase (MDH) Assay Kit, Micro Pyruvate Carboxylase (PC) Assay Kit, and Pyruvate kinase (PK) Assay Kit were provided from Solarbio; BacTiter-Glo™ Microbial Cell Viability Assay was from Promega.

Preparation of Essential Oil From *Litsea cubeba*

The mature fruits of *Litsea cubeba* (Lour.) were collected in mid-July from Conghua District, Guangzhou City, Guangdong Province, which were identified as *Litsea cubeba* (Lour.) according to their morphological characteristics by Professor Depo Yang of the botany of the School of Pharmaceutical Sciences, Sun Yat-sen University, and the certificate specimens were kept in the herbarium of Sun Yat-sen University. The fruits that were not eaten by insects or decayed were selected and

extracted by hydrodistillation for 5 h. After standing, anhydrous sodium sulfate was added to remove water, and *Litsea cubeba* essential oil (EO) was obtained. The EO was placed in a brown glass bottle, sealed, and stored at 4°C.

Gas Chromatography-Mass Spectrometry Analysis of the Essential Oil

EO was weighed accurately and then dissolved in chromatographic grade ethyl acetate to a final concentration of 1 mg/mL, and detected by gas chromatography-mass spectrometry (GC-MS, Thermo Scientific Trace DSQ II). The GC-MS conditions were performed as previously described (Hu et al., 2019), with slight modifications (**Supplementary File 1**). The retention indices (RI) were calculated for all EO components by the C7-C40 n-alkanes. Based on NIST 2017 mass spectrometry library, EO constituents were identified by comparing obtained RI and data already available in the literature (Jin et al., 2015).

Bacterial Activation and Culture

Cutibacterium acnes (*C. acnes*) were taken out from the ultra-low temperature refrigerator, melted and absorbed 200 μ L, evenly coated on the Reinforced Clostridium Agar (RCA) plate, and cultured inverted at 37°C for 72 h under anaerobic conditions by the AnaeroPack. Then, wet sterile cotton swabs were used to scrape the *C. acnes* from the plate, and the *C. acnes* was mixed in PBS to prepare the bacterial liquid. 200 μ L bacteria suspension was coated on the RCA plate and continued to culture for 72 h under anaerobic conditions at 37°C to obtain the activated bacterial cells.

Antibacterial Activity of Essential Oil Against *Cutibacterium acnes*

The Minimum Inhibitory Concentration

In order to study the antibacterial activity of the EO against *C. acnes*, the minimum inhibitory concentration of bacteria was detected using the micro-broth dilution method recommended by the Clinical and Laboratory Standard Institute (CLSI, 2017). Firstly, the bacterial strain was grown to the logarithmic growth phase and diluted by the BHI medium (10^4 – 10^5 CFU/mL). Then different concentrations of EO were added to the 96-well plate, and the final drug concentration was from 0.009375 to 19.2 mg/mL. According to the Clinical and Laboratory Standards Association 2017 (CLSI, 2017), when bacteria are not visible, the administration concentration is the minimum inhibitory concentration (MIC). At the same time, the absorbance data was obtained using 96-well microplate reader at 600 nm.

The Minimum Bactericidal Concentration

To determine the minimum bactericidal concentration (MBC), 10 μ L medium of each well with no visible bacteria growth was removed and inoculated in RCA plates. After 72 h of incubation under anaerobic conditions at 37°C, the number of surviving organisms was determined. According to the provisions of

CLSI (2017) drug sensitivity test, the lowest dose concentration that can kill 99.9% of bacteria is the MBC.

Bacteriostatic Curve

The medium was inoculated with *C. acnes* in the logarithmic phase and the final concentration was 10^8 CFU/mL. Then, bacteria were treated with different concentrations of EO that were dissolved with 0.1% Tween 80, respectively. And 0.1% Tween 80 was used as vehicle control. The final concentrations of EO were 4 MIC (1,600 μ g/mL), 2 MIC (800 μ g/mL), MIC (400 μ g/mL), and 1/2 MIC (200 μ g/mL). The growth of *C. acnes* in the Control and EO-treated groups was measured by monitoring the absorbance value of bacteria at 600 nm within 5 days according to literature (Kim et al., 2021).

Live/Dead Bacterial Viability Assay

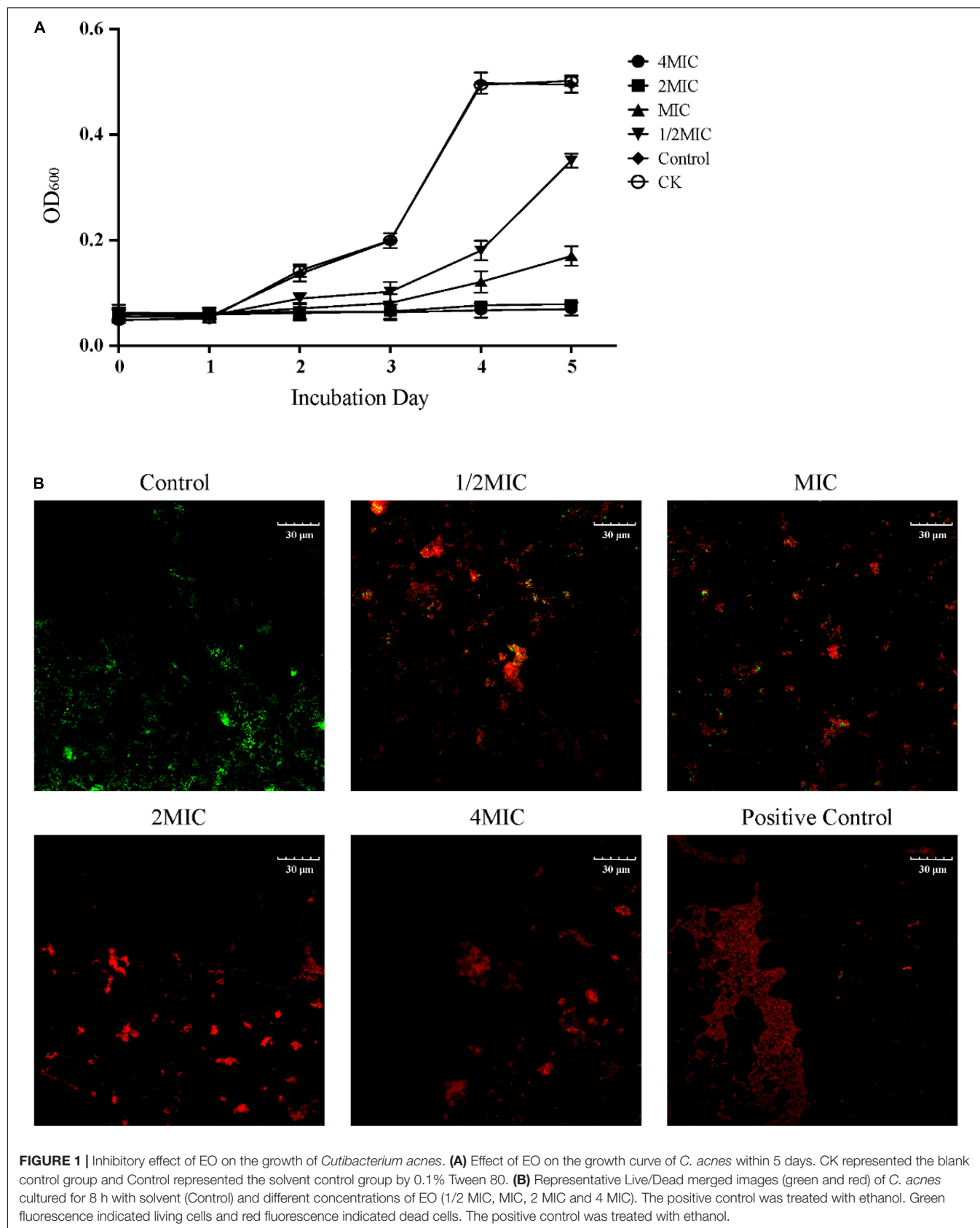
Live/Dead bacterial viability assay is a general method to determine bacterial activity according to membrane integrity (Emerson et al., 2017). Adjust the concentration of bacteria solution to 10^8 CFU/mL. As described in section “Bacteriostatic Curve” in method, prepare different concentrations of EO (4 MIC, 2 MIC, MIC, 1/2 MIC) and solvent (Control), and then adjust the concentration of bacteria again to 10^8 CFU/mL after anaerobic culture at 37°C and 180 rpm for 8 h. 70% ice ethanol was used as the positive control group. The staining was performed using the Live/Dead BacLight Bacterial Viability Kits (Invitrogen by Thermo Fisher Scientific, L7012), and the images were collected using the confocal microscope (Olympus FV3000).

Scanning Electron Microscope and Transmission Electron Microscope

The effect of the EO on *C. acnes* morphology can be observed using SEM and TEM following the previously described method with modifications (Zhou et al., 2020). *C. acnes* with EO or solvent were anaerobically cultured with shaking at 180 rpm at 37°C for 8 h. The bacteria were collected by centrifugation at 4,500 rpm for 10 min at 4°C and washed three times in PBS. 2.5% glutaraldehyde solution was added and stored in a refrigerator at 4°C overnight. The bacteria were washed with 0.1 M phosphate buffer, centrifuged at 4°C 4,500 rpm for 10 min, and the bacteria were collected for standby.

(1) SEM: Bacteria were soaked in ethanol solutions of different concentrations (30, 50, 70, 90, and 100%) to remove water, then replaced with tert-butyl alcohol, freeze-dried and gilded, then observed and photographed by Thermal Field Emission Environmental SEM-Eds-EBSD (Quanta 400FEG).

(2) TEM: Fixed the sample with 1% Osmic acid solution for 1–2 h, rinsed the sample with 0.1 M phosphate buffer three times, then used the gradient dehydration of ethanol solution (30, 50, 70, 80, 90, 95, and 100%), and then treated 20 min with pure acetone. The sample was embedded with a mixture of the embedding agent and acetone overnight at 70°C, and then sliced with LEICA EM UC7 ultra-thin slicer. The slices were stained with lead citrate solution and uranyl acetate 50% ethanol saturated solution for 5–10 min, respectively. After drying, the slices could be observed under transmission electron microscopy (HITACHI H-7650).



Metabonomics Studies

Sample Preparation

The GC-MS-based strategy was employed to analyze the metabolism profile of bacteria according to previous reports (Booth et al., 2015). 0.1% Tween 80 was also used as the solvent to enhance the EO solubility. Briefly, bacteria in the logarithmic phase were treated with EO (MIC) or solvent (Control) at 37°C for 8 h at 180 rpm, respectively. The bacteria were collected by centrifugation and washed three times in PBS. Then, 1 mL pre-cooled methanol was added to the quench, and the bacteria were lysed by a repeated freeze-thaw cycle followed by ultrasonication three times. The equal amount of the metabolites in the Control and MIC groups were mixed, respectively, with 8 μ L ribitol (0.5 mg/mL) that was the internal standard and concentrated again. Then the derivatization reaction by using MSTFA was performed according to the previously reported method (Chen J. et al., 2020; Tang et al., 2021), followed detection within 48 h by GC-MS (Agilent 7890A GC equipped with Agilent 5975 CVL MSD Detector).

Gas Chromatography-Mass Spectrometry Detection Conditions

GC-MS detection was conducted according to the previously reported conditions with slight modifications (Chen J. et al., 2020; Tang et al., 2021). In brief, the injection volume was 1 μ L in the split-less injection mode; Heating procedure: the initial temperature was 70°C, kept at the initial temperature for 3 min, then the temperature was heated to 285°C at 5°C/min, then to 310°C at 20°C/min, and kept at 310°C for 7 min; The ion source temperature was 230°C, and the four-stage rod temperature was 150°C. The carrier gas was He, and the flow rate was 1.0 mL/min.

Pre-processing of Metabolome Data

GC-MS data pre-processing was performed by Agilent Unknowns Analysis software version B.09.00. After peak identification and deconvolution, the metabolites were identified with NIST and Fiehn database. In addition, GC-MS data were subjected to the retention time correction and peak alignment. In addition, Metabolites signals were normalized using internal standards and quantile by R Statistical Computing Environment. These normalized data were used for subsequent analyses (The data of metabonomics included six biological replicates and two technical replicates for a total of 24 data).

Analysis of Metabolomics Data

Multivariate statistical analyses were carried out in R Statistical Computing Environment, including principal component analysis (PCA) and orthogonal partial least squares discriminant analysis (OPLS-DA). The metabolites of different groups can be screened by a combination of the variable importance projection (VIP) derived from the OPLS-DA model and the adjusted *p*-values (FDR, false discovery rate) of the Student's *t*-test analysis. Finally, metabolites (VIP ≥ 1 and *p*.adj < 0.05) were selected as differential metabolites. In the differential metabolites, biomarkers were further selected according to the correlation and covariance information provided by S-plot. MBRole 2.0 pathway analysis of the differential metabolites was conducted using the

KEGG database to determine that the metabolic pathways were considered significant with *p* < 0.05 (Lopez-Ibanez et al., 2016).

OmicStudio tools,¹ Origin software (Origin Lab), and Adobe Illustrator were used to perform partial bioinformatics analysis and visualization.

Detection of Enzyme Activity and Intracellular Adenosine Triphosphate Content

Enzyme Activity Assay

The bacteria concentration was adjusted to 10⁹ CFU/mL as described before, and cultured with shaking in BHI medium with EO or solvent for 8 h as described in section "Bacteriostatic Curve." After being washed twice in PBS, the bacteria were collected by centrifugation at 4,000 rpm at 4°C. According to the requirements of the kit, the extractant was added and extracted by the ultrasonic crusher for 10 min. The supernatant obtained by centrifugation was the extract, and BCA Protein Assay Kit detected the protein concentration. According to the instructions of the kits, detected the activities of the Pyruvate Decarboxylase (PC), Malate Dehydrogenase (MDH), Pyruvate kinase (PK), and Hexokinase (HK). Enzyme activity was expressed as units per milligram of protein. The detailed information of the enzymes activity determination process is depicted in **Supplementary File 1**.

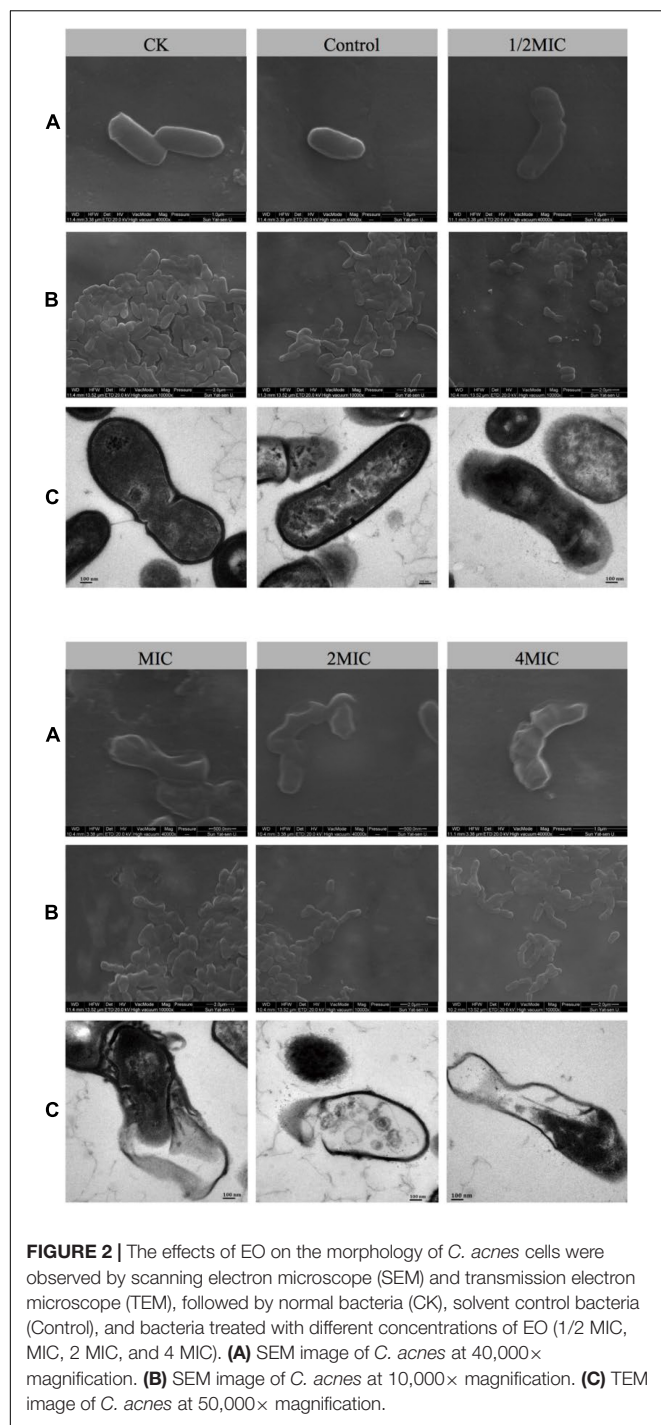
Adenosine Triphosphate Content Assay

The bacterial liquid was collected and adjusted to 1.0 $\times 10^8$ CFU/mL. The bacteria were treated, respectively, with EO at 1/2 MIC and MIC, or solvent (Control) as described in section "Bacteriostatic Curve," and were cultivated at 37°C with shaking at 180 rpm for 8 h. Next, the bacteria were collected by centrifugation and washed twice in PBS. Liquid nitrogen was used to quench metabolism. The bacterial pellet was resuspended in PBS, and the bacterial liquid was 1.0 $\times 10^8$ CFU/mL. Then, the volume of BacTiter-GloTM Reagent equal to the volume of the bacterial liquid in each well was added; after mixing and incubating for 5 min, the luminescence was recorded by an Infinite M1000 Proplate Reader (Tecan). In parallel, six adenosine triphosphate (ATP) concentration standards ranging from 2,500 pmol to 2,560 nmol were used to generate the ATP concentration standard curve by the BacTiter-Glo assay kit. Ultimately, the ATP concentration for each sample was calculated based on the standard curve.

Statistical Analysis

Except for the analysis of metabolomics data, all statistical analyses were conducted in GraphPad Prism version 8.0.2. All the experiments were carried out in triplicate, with at least three biological replicates. The data were analyzed by one-way analysis of variance (ANOVA), represented as mean \pm standard error of the mean (mean \pm SEM). *p* ≤ 0.05 were regarded to be significant (**p* ≤ 0.05 ; ***p* ≤ 0.01 ; ****p* ≤ 0.001 ; *****p* ≤ 0.0001 vs. control group).

¹<https://www.omicstudio.cn/tool>



RESULTS

Chemical Compositions of the Essential Oil

The major components of EO identified were listed in **Supplementary Table 1**. The top of 9 compounds accounted for 90.55%, which mainly included α -Citral (38.12%), β -Citral

(32.97%), Limonene (9.72%), Linalool (2.45%), (R)-(+)-Citronellal (1.82%), Terpinen-4-ol (1.62%), α -Thujene (1.51%), Eucalyptol (1.21%), Caryophyllene (1.13%), in which the relative contents of α -citral and β -citral were higher, which was same as previously reported in the literature (Hu et al., 2019). The contents of Geraniol, β -Pinene, α -Terpineol, Sabinene, β -Myrcene, Camphene ranged from 0.53 to 0.94%. The others were less than 0.50%.

Antibacterial Activity of Essential Oil Against *Cutibacterium acnes*

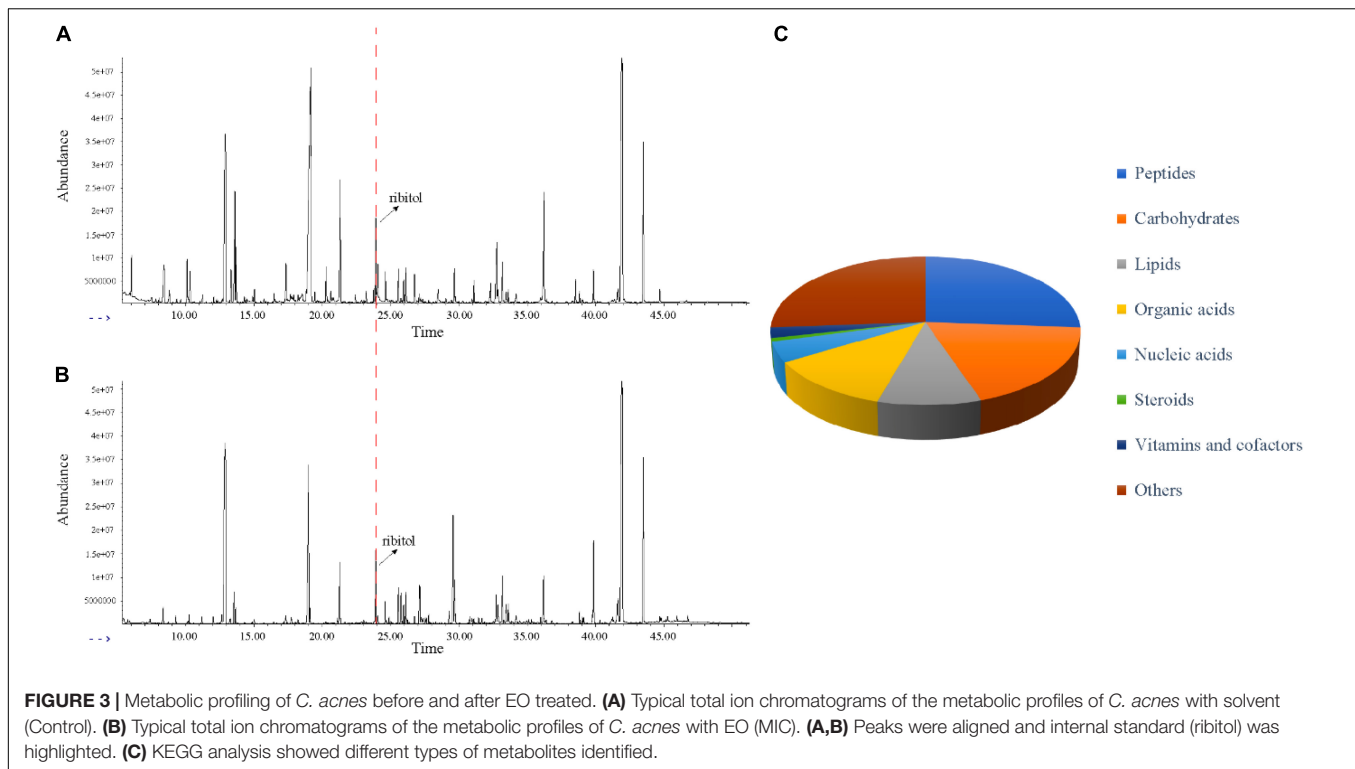
The inhibitory effect of EO on the growth of *C. acnes* was evaluated by measuring the minimum inhibitory concentration (MIC) and the minimum bactericidal concentration (MBC). This result showed that EO could inhibit the growth rate of *C. acnes* in a dose dependent manner, which the MIC and the MBC values were 400 and 800 μ g/mL, respectively (**Supplementary Figure 1**). As the results were shown in **Figure 1A**, there was no significant difference in bacterial growth between the solvent control group (Control) and the blank control group (CK), indicating that Tween 80 would not inhibit the growth of *C. acnes*. The growth of bacteria generally followed the model s-shaped growth curve, reached the logarithmic growth phase in 2 days and entered the platform phase 4 days later. The OD₆₀₀ of *C. acnes* that co-cultured with EO at 1/2 MIC and MIC in each growth stage was significantly lower than that of the control group, and its growth was significantly inhibited. In the treatment with EO at MIC, *C. acnes* entered the logarithmic growth period at 4, 2 days later than the Control and CK. When treated with EO at 2 MIC and 4 MIC, *C. acnes* stopped growing.

Bacterial Viability Test by Live/Dead Assay

The effect of EO on the activity of *C. acnes* was further observed by the Live/Dead BacLight Bacterial Viability assay, and each image represented the separate fluorescence channel (green and red) was shown in **Supplementary Figure 2**, the merge images was shown in **Figure 1B**. The cells produced green fluorescence but nearly undetectable red fluorescence in the control group, indicating the majority of cells were intact. After being cultured at 1/2 MIC and MIC in the medium with EO for 8 h, more spots with red fluorescence were observed. As the concentration of EO increased, the green fluorescence spots were gradually replaced by the red fluorescence spots, indicating that the number of bacterial death increased significantly and concentration-dependently. In the 2 MIC, and 4 MIC groups, the bacterial mortality rate was close to 100% (red fluorescence), which was similar to the positive control group.

Scanning Electron Microscope and Transmission Electron Microscope

In order to understand the intuitive effect of EO on the morphology of *C. acnes*, SEM and TEM techniques were used in this study (Wang et al., 2021). As shown in **Figure 2**, after 8 h of culture, the morphologies of the bacterium in the solvent control (Control) and the blank control group (CK) were complete, the



surface of cells was intact, smooth, and bright, as well as the cells were full of cytoplasmic material. Treatment with 1/2 MIC for 8 h, most of the cell membranes were intact, but slightly concave and wrinkled. As for MIC, the bacterial cell membrane became blurred, the concave and fold of the cell membrane became more obvious, and the number of bacterial cell membrane damage increased. Besides, while treated with 2MIC or 4MIC, almost all of the cell membranes and cell walls were ruptured (**Figure 2B**). TEM can explore not only the morphology of bacterial cells more clearly, but also intracellular alteration of the bacteria. As shown in **Figure 2C**, the cells in the high concentration EO treatment group (4MIC and 2MIC) lysed, and the cytoplasmic material flowed out. The result showed that compared with the control group, the cell membrane and cell wall of the groups with EO were damaged, and the degree of damage increased with the increase of EO concentration.

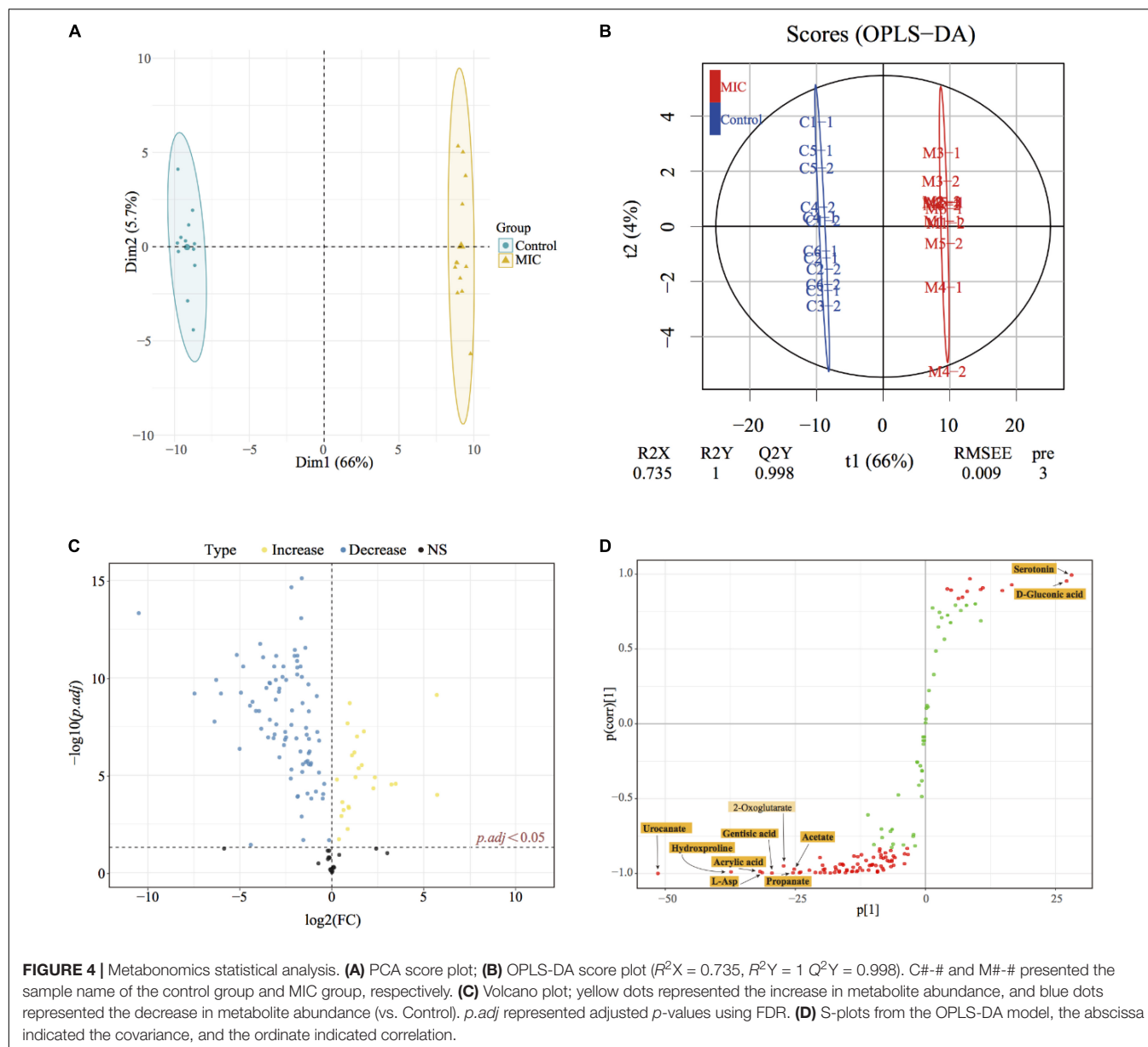
Metabonomics

Effect of Essential Oil on Metabolism of *Cutibacterium acnes*

In this study, GC-MS was used to analyze the effect of EO on bacterial metabolism. According to the result in **Figures 3A,B**, there were significant differences in the abundance of substances with the same retention time between the MIC and Control groups. As shown in **Figure 3C**, after GC-MS detection and data preprocessing of 24 groups of samples, a total of 133 metabolites were obtained, including peptides (26.3%), carbohydrates (18.8%), lipids (9.8%), organic acids (12.0%), nucleic acids (4.5%), vitamins and cofactors (2.3%), steroids (0.8%), and others (25.6%).

Analysis of Differential Metabolites

Multivariate statistical analysis and univariate statistical analysis were combined to study the metabolic differences between the EO-treated group (MIC) and the control group. The metabolites were analyzed by PCA, on the score plot (**Figure 4A**), the natural clustering trend among metabolites was observed, and it was found that MIC group and Control group could be obviously separated. The supervised OPLS-DA model was established to compare the metabolic changes between MIC and Control groups. The Q^2 value of the model was 0.998, indicating that it had high validated predictability and could be used for further screening of differential metabolites (**Figure 4B**). In the S-plot of OPLS-DA (**Figure 4D**), each spot was representative of a compound, and the further away from the origin, the more significant its contribution to clustering of the two groups. The contribution was represented by Variable Importance in Project (VIP) value, and the red spots in the figure indicated the compound with $VIP \geq 1$. 110 metabolites were selected by Student's *t*-test calculated significant differences between the two groups ($p_{adj} < 0.05$), and the Fold Change was calculated to quantify the degree of up/downregulation of metabolites, as shown in **Figure 4C**. Only if the VIP was above 1 and p_{adj} was below 0.05, the metabolites could be considered as differential metabolites. A total of 86 endogenous metabolites were selected as differential metabolites before and after the administration of EO and classified (**Supplementary Figure 3**). The heat map of differential metabolites showed that the abundance of *C. acnes* metabolites changed significantly after EO administration, with 74 metabolites decreased and 12 increased (**Figure 5A**). (Other detailed metabolic information,



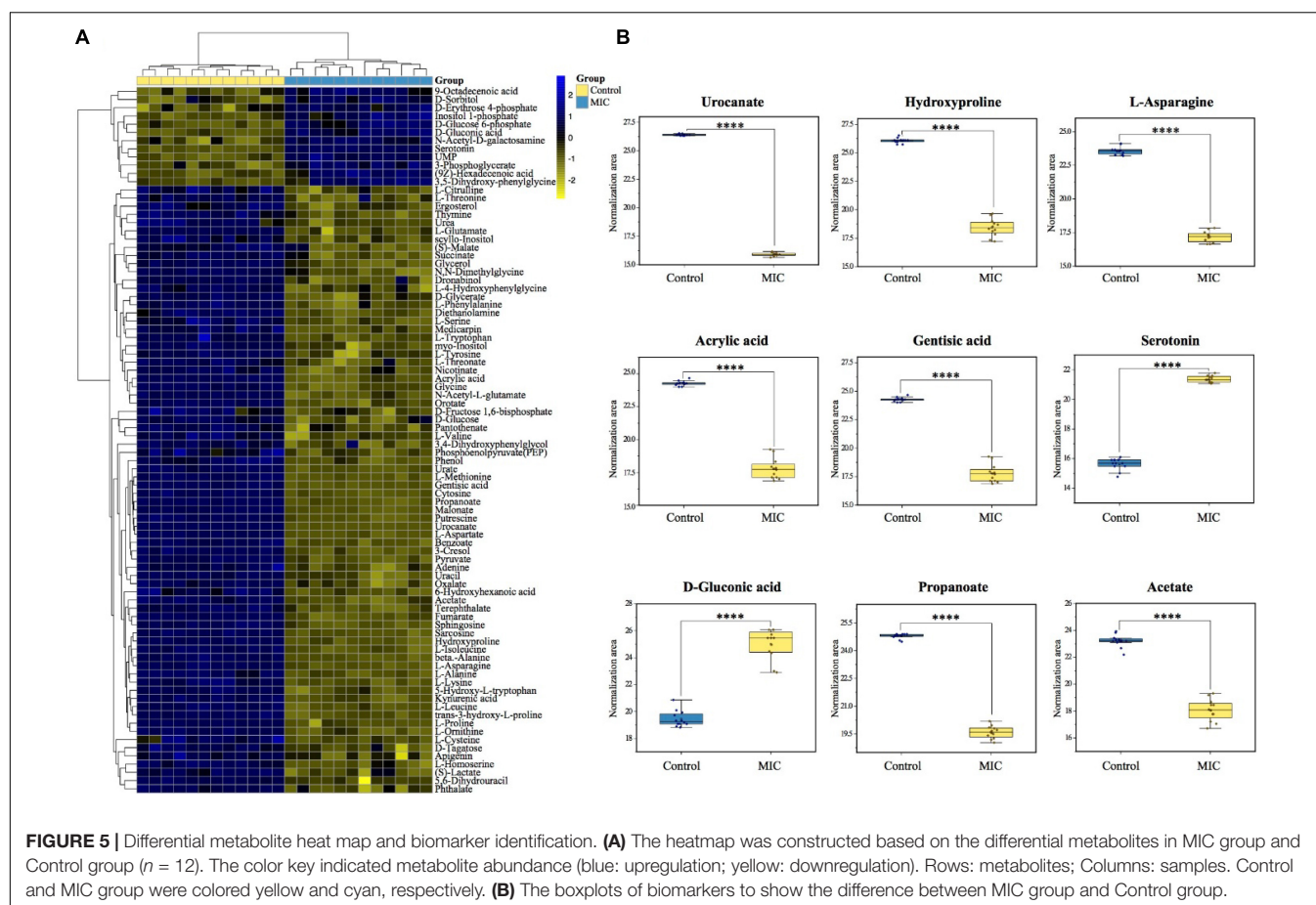
including VIP values in multivariate statistical analysis, p_{adj} and Fold Change in univariate statistical analysis, were listed in **Supplementary File 3**.)

Discovery of Biomarkers

Biomarker discovery is the critical step for metabolomics studies. According to the 86 differential metabolites that had been selected (**Figure 5A**), combined with 10 candidate biomarkers obtained by S-plot (highlighted in **Figure 4D**), it was found that 9 metabolites (**Figure 5B**) can be used as biomarkers, namely urocanate, hydroxyproline, L-asparagine, acrylic acid, gentisic acid, serotonin, D-gluconic acid, propanoate, and acetate, which belonged to peptides, organic acids, carbohydrates and other kinds, respectively. However, the 2-oxoglutarate was excluded because the p_{adj} was larger than 0.05.

Enrichment of Metabolic Pathway

A total of 34 metabolic pathways ($p_{adj} < 0.05$) were obtained by metabolic pathway enrichment analysis of 86 differential metabolites (**Supplementary File 4**). According to the order of p_{adj} from small to large (the smaller the p_{adj} , the more significant the impact on the metabolic pathway), the top 15 of them were shown in **Figure 6A**. 34 metabolic pathways were subdivided into the three kinds of KEGG main class, of which metabolism-related pathways accounted for 88.2%, including carbohydrate metabolism, amino acid metabolism and metabolism of cofactors and vitamins; In addition, 8.8% of environmental information processing-related pathways included membrane transport and signal transduction; and 3.0% of genetic information processing-related pathways included translation (**Supplementary File 4**). KEGG classification of the



top 15 metabolic pathways was shown in **Figure 6B**. Among the differential metabolites involved in the enrichment pathway, we found that pyruvate, L-aspartate, fumarate, and succinate were the critical intermediates of the metabolic pathway. Their abundance changes before and after EO administration were shown in **Figure 6C**.

Enzyme and Adenosine Triphosphate Content Test

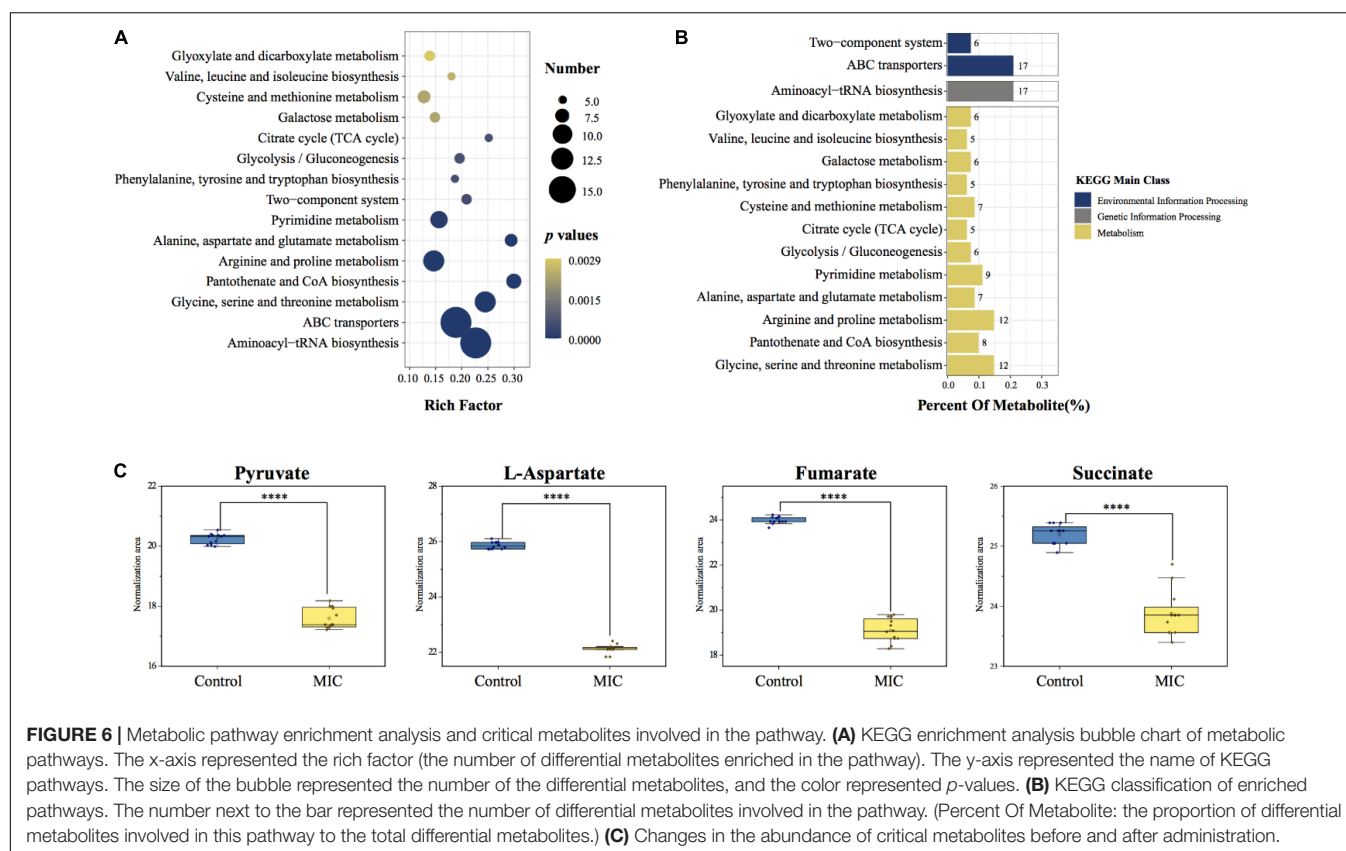
Based on the result from enrichment analysis, the metabolic pathways of *C. acnes* under the influence of EO were plotted (**Figure 7A**). In order to further verify the effect of EO on *C. acnes* metabolism, the activities of PC and MDH, enzymes related to the Wood-Werkman cycle, as well as the activity of HK and PK, the key enzyme in glycolysis were measured, and the change of intracellular ATP content was determined. The results were shown in **Figures 7B,C**. Compared with the control group, the activity of HK increased significantly, and the activities of PC, MDH, and PK decreased significantly after MIC treatment for 8 h, as well as the intracellular ATP content. After treating with EO, the activities of PC, MDH, and PK in the MIC group were lowered by approximately 57.85, 71.78, and 30.91%, respectively. However, the activity of HK was increased by 70.13% (**Figure 7B**). Additionally, the ATP content in the 1/2 MIC and MIC groups was downregulated 94.21 and 97.27% compared to the control group (**Figure 7C**).

DISCUSSION

In this study, we found that *Litsea cubeba* essential oil (EO) had sound antibacterial and bactericidal effects on *C. acnes* (ATCC6919), and the inhibitory effect on bacteria increased with the increase of the concentration of EO. This discovery not only expanded the use of EO, but also took the first step for us to find new drugs for the treatment of *C. acnes*-related diseases.

It is well known that the integrity of bacterial cell walls and cell membranes was the key factor for bacterial survival (Call and Klaenhammer, 2013). The bacterial cells stained by Live/Dead staining assay showed the cell viability of five groups of EO with different concentrations after co-culture with *C. acnes* for 8 h (**Figure 1B** and **Supplementary Figure 2**). The number of dead cells (red) in the administration groups increased significantly and showed concentration dependence, which was consistent with the antibacterial activity test results (**Figure 1A**). It also showed that the integrity of *C. acnes* cell membrane is damaged, which was more obvious in the images taken by SEM and TEM (**Figure 2**). The disrupted bacterial cellular integrity, as well as the emerging of cell debris, confirmed that the EO could alter the bacterial morphology.

Metabonomics is a qualitative and quantitative method of small molecular metabolites in the biological system utilizing LC-MS or GC-MS or NMR (Hu and Xu, 2014; Pang et al., 2019), which can understand the life activities of



organisms comprehensively and systematically. This method has been used to evaluate the mechanism of bacterial metabolism and bacteriostatic mechanism (Wong et al., 2018). In this study, non-target metabolomics based on GC-MS was used to explore the metabolic changes of *C. acnes* before and after the administration of EO, which has hardly ever been done in prior studies. Furthermore, the results from the perspective of metabolomics demonstrated that metabolic pathways of *C. acnes*, such as glycolysis, Wood-Werkman cycle and pentose phosphate pathway (Figures 6A,B), were similar to the *Propionibacterium* spp. though *C. acnes* has now been reclassified as *Cutibacterium* spp. (Scholz and Kilian, 2016), which was consistent with findings in most previous studies by other omics methods (McLaughlin et al., 2019). Therefore, the metabolomics study of other *Propionibacterium* spp. can provide references for us.

In this study, we identified a number of significantly altered metabolites (86 differential metabolites) after the administration of EO to *C. acnes*, in which the 9 metabolites was selected as biomarkers (the biomarker pattern is not unique to the antibacterial mechanism of EO) (Figure 5). Based on the above metabolomic analysis and previous studies on *Propionibacterium* spp., *C. acnes* showed a complex biological network to cope with EO-treated, which may be related to the carbohydrate metabolism, energy metabolism, amino acid metabolism, as well as cell wall and cell membrane synthesis (Figure 7A and Supplementary File 4).

Carbohydrate Metabolism

The glycolysis and propanoate production pathways are the central pathways of carbohydrate metabolism in *C. acnes*. Hexokinase (HK) and pyruvate kinase (PK) are rate-limiting enzymes in the glycolysis pathway. HK is the first enzyme of the glycolysis to catalyze the phosphorylation of glucose to glucose-6-phosphate, and pyruvate, the end product of the glycolysis pathway, is produced by PEP under PK. In our study, we observed a significant increase in the catalytic activity of HK, and the phenomenon may be caused by the defense response of *C. acnes* under environmental stress, which can avoid the damage of EO on bacterial metabolism by increasing glucose uptake, according to the literature investigation (Figures 6C, 7A,B; Wang et al., 2018). Pyruvate is the critical hub of the pathways in carbohydrate and amino acid metabolism, in the *Propionibacterium* genus, the synthesis of propanoate through the Wood-Werkman cycle is one of the essential pathways of pyruvate metabolism (McCubbin et al., 2020). Pyruvate forms oxaloacetate under pyruvate carboxylase (PC), which starts the first step of the propanoate synthesis. Malate dehydrogenase (MDH) converts oxaloacetate to malate, which is then converted to fumarate by succinate reductase, and fumarate yields succinyl-CoA and finally to propanoate. Our results demonstrated that, during this process, the abundance of 3 critical intermediates (pyruvate, fumarate, and succinate) of the metabolic pathway, and propanoate, the end product of the Wood-Werkman cycle after EO-treated decreased significantly (Figures 5B, 6C),

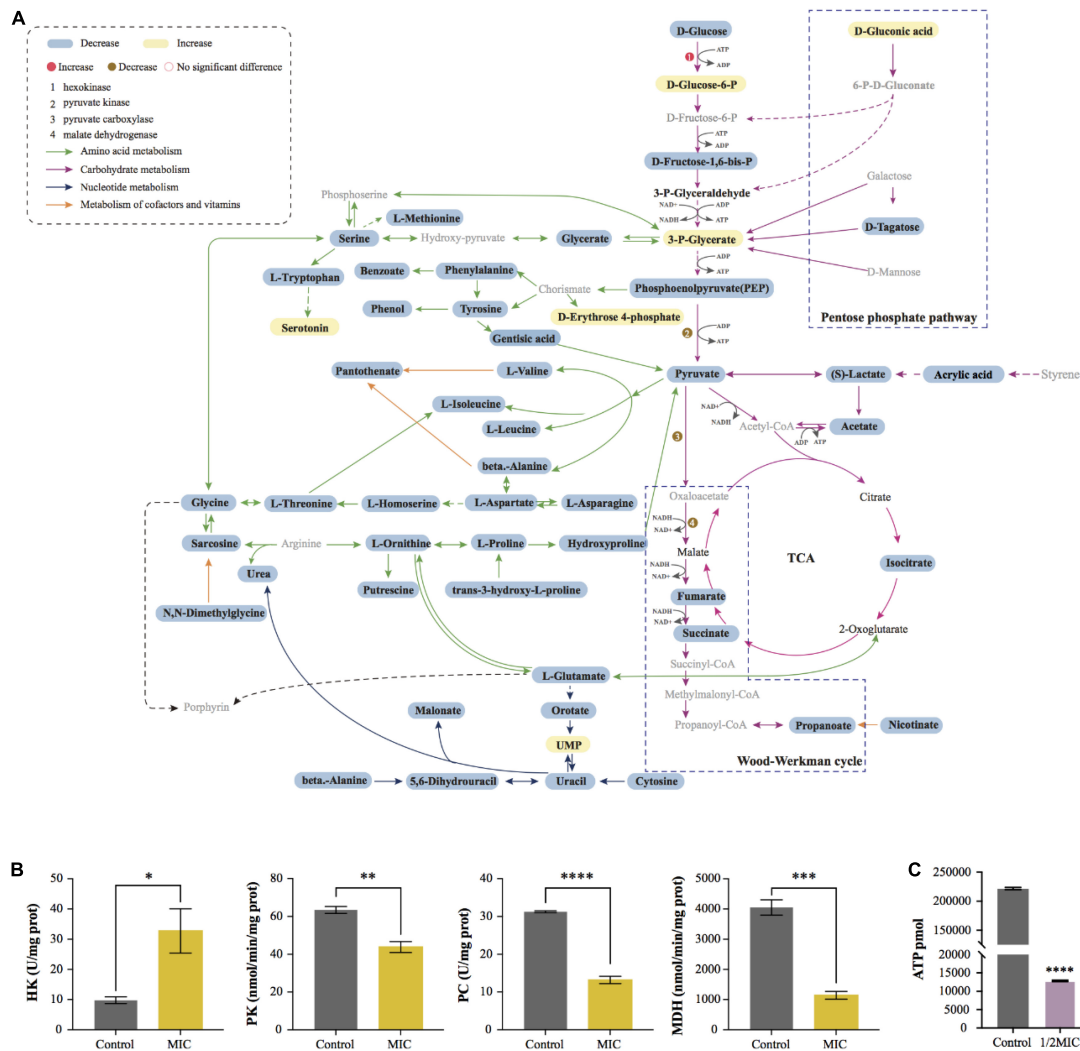


FIGURE 7 | Visualization of metabolic pathway and changes of key enzyme activity and ATP content before and after EO treatment. **(A)** Summary graph of metabolic pathways in MIC group (vs. Control). The black fonts indicated the detected metabolites (blue boxes were significantly down-regulated differential metabolites, yellow boxes were significantly up-regulated metabolites, and the rest are not differential metabolites), while the gray fonts indicated undetected metabolites. The activities of Hexokinase (HK), Pyruvate kinase (PK), Pyruvate Decarboxylase (PC) and Malate Dehydrogenase (MDH) are shown in **(B)**. **(C)** Effect of EO on ATP synthesis in *C. acnes* cells.

indicating that the Wood-Werkman cycle was inhibited. The activities of MDH and PC downregulated, which also confirmed this result (Figure 7B).

Energy Metabolism

ATP is the direct energy source for bacteria to maintain their life and normal physiological activities (Venkateswaran et al., 2003). Unlike other common aerobic bacteria, in *C. acnes*, the Wood-Werkman cycle, which can be coupled with an anaerobic electron transport chain (anaerobic respiration), is the primary energy supply pathway. NADH can provide H^+ , transfer H^+ to fumarate through a series of enzymes to drive the proton pump to synthesize ATP (de Vries et al., 1973). Moreover, *C. acnes* also utilize substrate-level phosphorylation to produce ATP, such as

glycolysis and pyruvate to acetate. Although acetate is a by-product of the metabolism, it is vital to *C. acnes* (McCubbin et al., 2020). Our result suggested that, as a biomarker, the abundance of acetate decreased significantly after EO treatment, indicating that the pathway of pyruvate to acetate was inhibited. Similarly, we found that other metabolisms related to ATP synthesis, including the Wood-Werkman cycle and glycolysis, were also disturbed, suggesting that EO inhibited the ATP synthesis of bacteria, leading to the inhibition of their growth. It was consistent with the result of ATP content in bacterial cells detected (Figure 7C).

Amino Acid Metabolism

The result indicated that EO also had a significant effect on the metabolism of amino acids in *C. acnes* because the abundance of

almost all amino acids in bacterial cells was significantly reduced after EO-treated (**Figure 7A**). Previous research has shown that L-Aspartate, the main precursor of amino acid synthesis in microorganisms, is key to amino acid metabolism and bacterial growth (Qiao et al., 2018). The results (**Figures 6C, 7A**) demonstrated that, as one of the four critical intermediates of the metabolic pathway, the inhibition of L-aspartate synthesis may cause the inhibition of the whole amino acid metabolism. Amino acid metabolism is a crucial metabolic pathway for bacterial cells to grow and maintain normal life activities (Afzal et al., 2016). It involves many aspects, such as protein synthesis, biological enzyme synthesis and regulation, gene expression, osmotic regulation, and so on (Wu, 2009). Therefore, disruption of amino acid metabolism will lead to abnormal physiological activities of bacteria. Apart from the above, amino acid metabolism also involves the synthesis of virulence factors in bacteria. *C. acnes* can secrete porphyrin, hyaluronidase, lipase, and others to cause cell inflammation, which is closely related to the pathogenesis of *acne* (De Canha et al., 2019; Spittaels et al., 2021). The disorder of amino acid metabolism may inhibit the ability of bacteria to secrete virulence factors and reduce their pathogenicity. However, this hypothesis needs to be tested further.

Cell Wall and Cell Membrane Synthesis

The cell wall of *C. acnes* is mainly composed of peptidoglycan, fatty acid and polysaccharide. Peptidoglycan is a disaccharide peptide consisting of sugar and amino acid, crossing links with each other to form a polymer network outside the cell membrane, which exists in almost all bacteria (Prasad et al., 2019). The results showed that the abundance of glucose decreased significantly, and the amino acid metabolism was disturbed (the abundance of alanine, glutamate, glycine and other amino acids decreased significantly). As the important precursors of synthetic peptidoglycan according to relevant literature (Johnson and Cummins, 1972), the decrease of their abundance indicated that the bacterial cell wall might be destroyed (**Figure 7A** and **Supplementary File 3**). It is worth noting that in *C. acnes* treated with EO, the abundance of these two unsaturated fatty acids 9-Octadecenoic acid and (9Z)-Hexadecenoic acid, main components of the cell wall and cell membrane, increased significantly, indicating that the synthesis and repair of the cell wall and cell membrane were strongly up-regulated (**Supplementary File 3**). It has been shown in the literature that microorganisms would protect themselves by the increase of unsaturated fatty acids to avoid damage caused by the administration, which was a stress response (Knoll et al., 2021). Therefore, it could be suggested that the damage of the EO to the cell wall and the cell membrane of the *C. acnes* may be indirectly caused by the influence of metabolism.

CONCLUSION

To sum up, we studied the antibacterial activity of *Litsea Cubeba* essential oil (EO) against *Cutibacterium acnes* (*C. acnes*) and established a metabonomics method based on GC-MS to investigate the related metabolic changes and the bacteriostatic

mechanism of *C. acnes* after administration. Our results demonstrated that EO could inhibit the growth of *C. acnes* and destroy bacterial cell structure. Metabolomics analysis showed that EO treatment could significantly affect 34 metabolic pathways of *C. acnes*, including carbohydrate metabolism, energy metabolism, amino acid metabolism, as well as cell wall and cell membrane synthesis, which finally disturbs normal bacterial metabolism. Overall, this discovery is expected to deepen the understanding of the activity of EO, widen its application range and improve its commercial value.

DATA AVAILABILITY STATEMENT

The original contributions presented in the study are included in the article/**Supplementary Material**, further inquiries can be directed to the corresponding author/s.

AUTHOR CONTRIBUTIONS

JC conducted the experiments. JC and JZ performed data analysis and wrote the manuscript. JC, JZ, LZ, CQ, and HT contributed to discussing the results and critical review of the manuscript. ZZ reviewed, edited the manuscript, and acquired funding. LJ performed data interpretation, reviewed, and edited the manuscript. DY performed data interpretation, reviewed and edited the manuscript, provided supervision and project administration, and acquired funding. All authors made significant contributions to this article and participated actively in the conception and design of the experiments, reading, and approving the final manuscript.

FUNDING

This work was supported by the Project for Provincial Agricultural Science and Technology Innovation and Promotion in Guangdong (Nos. 2019KJ142, 2020KJ142, 2021KJ142, 2021KJ268), the Provincial Key R&D Program of Guangdong (No. 2020B020221002), the Science and Technology Program of Guangdong Province (No. KTP20200014), and the National Natural Science Foundation of China (No. 82073735).

ACKNOWLEDGMENTS

We would like to thank the Instrumental Analysis and Research Center of Sun Yat-sen University for the sample detecting services. We also thank Jiali Chen, Xue Sheng, and Cailin Tang for technical support.

SUPPLEMENTARY MATERIAL

The Supplementary Material for this article can be found online at: <https://www.frontiersin.org/articles/10.3389/fmicb.2022.823845/full#supplementary-material>

REFERENCES

- Achermann, Y., Goldstein, E. J., Coenye, T., and Shirliff, M. E. (2014). *Propionibacterium acnes*: from commensal to opportunistic biofilm-associated implant pathogen. *Clin. Microbiol. Rev.* 27, 419–440. doi: 10.1128/CMR.00092-13
- Afzal, M., Shafeeq, S., and Kuipers, O. P. (2016). Methionine-mediated gene expression and characterization of the CmhR regulon in *Streptococcus pneumoniae*. *Microb. Genom.* 2:e000091. doi: 10.1099/mgen.0.000091
- Agrawal, N., Choudhary, A. S., Sharma, M. C., and Dobhal, M. P. (2011). Chemical constituents of plants from the genus *Litsea*. *Chem. Biodivers.* 8, 223–243. doi: 10.1002/cbdv.200900408
- Archer, J. S., and Chang, R. J. (2004). Hirsutism and acne in polycystic ovary syndrome. *Best Pract. Res. Clin. Obstet. Gynaecol.* 18, 737–754. doi: 10.1016/j.bpobgyn.2004.05.007
- Booth, S. C., Weljie, A. M., and Turner, R. J. (2015). Metabolomics reveals differences of metal toxicity in cultures of *Pseudomonas pseudoalcaligenes* KF707 grown on different carbon sources. *Front. Microbiol.* 6:827. doi: 10.3389/fmicb.2015.00827
- Call, E. K., and Klaenhammer, T. R. (2013). Relevance and application of sortase and sortase-dependent proteins in lactic acid bacteria. *Front. Microbiol.* 4:73. doi: 10.3389/fmicb.2013.00073
- Chen, J., Tang, C., Zhang, R., Ye, S., Zhao, Z., Huang, Y., et al. (2020). Metabolomics analysis to evaluate the antibacterial activity of the essential oil from the leaves of *Cinnamomum camphora* (Linn.) Presl. *J. Ethnopharmacol.* 253:112652. doi: 10.1016/j.jep.2020.112652
- Chen, Y. C., Li, Z., Zhao, Y. X., Gao, M., Wang, J. Y., Liu, K. W., et al. (2020). The *Litsea* genome and the evolution of the laurel family. *Nat. Commun.* 11:1675. doi: 10.1038/s41467-020-15493-5
- Choi, H. A., Ahn, S. O., Lim, H. D., and Kim, G. J. (2021). Growth suppression of a gingivitis and skin pathogen cutibacterium (*Propionibacterium*) *acnes* by medicinal plant extracts. *Antibiotics* 10:1092. doi: 10.3390/antibiotics10091092
- CLSI (2017). *Performance Standard for Antimicrobial Susceptibility Testing: Twenty-seventh Informational Supplement CLSI document M100-S27*. Atlanta: CSLI.
- Dai, J., Li, C., Cui, H., and Lin, L. (2021). Unraveling the anti-bacterial mechanism of *Litsea cubeba* essential oil against *E. coli* O157:H7 and its application in vegetable juices. *Int. J. Food Microbiol.* 338:108989. doi: 10.1016/j.jfoodmicro.2020.108989
- Dalimunthe, A., Hasibuan, P. A. Z., and Satria, D. (2019). The PI3KCA and AKT inhibitory activities of *litsea cubeba* lour. Fruits and heartwoods towards hela cells. *Open Access Maced. J. Med. Sci.* 7, 1422–1424. doi: 10.3889/oamjms.2019.317
- De Canha, M. N., Komarnytsky, S., Langhansova, L., and Lall, N. (2019). Exploring the anti-acne potential of impepho [*Helichrysum odoratissimum* (L.) sweet] to combat cutibacterium *acnes* virulence. *Front. Pharmacol.* 10:1559. doi: 10.3389/fphar.2019.01559
- de Vries, W., van Wyck-Kapteyn, W. M., and Stouthamer, A. H. (1973). Generation of ATP during cytochrome-linked anaerobic electron transport in propionic acid bacteria. *J. Gen. Microbiol.* 76, 31–41. doi: 10.1099/00221287-76-1-31
- Di Lodovico, S., Menghini, L., Ferrante, C., Recchia, E., Castro-Amorim, J., Gameiro, P., et al. (2020). Hop extract: an efficacious antimicrobial and anti-biofilm agent against multidrug-resistant *Staphylococci* strains and *Cutibacterium acnes*. *Front. Microbiol.* 11:1852. doi: 10.3389/fmicb.2020.01852
- Dreno, B., Pecastaings, S., Corvec, S., Veraldi, S., Khammari, A., and Roques, C. (2018). *Cutibacterium acnes* (*Propionibacterium acnes*) and acne vulgaris: a brief look at the latest updates. *J. Eur. Acad. Dermatol. Venereol.* 32(Suppl. 2), 5–14. doi: 10.1111/jdv.15043
- Emerson, J. B., Adams, R. I., Roman, C. M. B., Brooks, B., Coil, D. A., Dahlhausen, K., et al. (2017). Schrodinger's microbes: tools for distinguishing the living from the dead in microbial ecosystems. *Microbiome* 5:86. doi: 10.1186/s40168-017-0285-3
- Fu, Y., Chen, L., Zu, Y., Liu, Z., Liu, X., Liu, Y., et al. (2009). The antibacterial activity of clove essential oil against *Propionibacterium acnes* and its mechanism of action. *Arch. Dermatol.* 145, 86–88. doi: 10.1001/archdermatol.2008.549
- Gribbon, E. M., Cunliffe, W. J., and Holland, K. T. (1993). Interaction of *Propionibacterium acnes* with skin lipids in vitro. *J. Gen. Microbiol.* 139, 1745–1751. doi: 10.1099/00221287-139-8-1745
- Gupta, M. A., and Gupta, A. K. (1998). Depression and suicidal ideation in dermatology patients with acne, alopecia areata, atopic dermatitis and psoriasis. *Br. J. Dermatol.* 139, 846–850. doi: 10.1046/j.1365-2133.1998.02511.x
- Hu, C. X., and Xu, G. W. (2014). Metabolomics and traditional Chinese medicine. *Trends Anal. Chem.* 61, 207–214. doi: 10.1016/j.trac.2014.06.007
- Hu, W., Li, C. Z., Dai, J. M., Cui, H. Y., and Lin, L. (2019). Antibacterial activity and mechanism of *Litsea cubeba* essential oil against methicillin-resistant *Staphylococcus aureus* (MRSA). *Ind. Crops Prod.* 130, 34–41. doi: 10.1016/j.indcrop.2018.12.078
- Jin, J., Kim, M. J., Dhandapani, S., Tjhang, J. G., Yin, J. L., Wong, L., et al. (2015). The floral transcriptome of ylang ylang (*Cananga odorata* var. *fruticosa*) uncovers biosynthetic pathways for volatile organic compounds and a multifunctional and novel sesquiterpene synthase. *J. Exp. Bot.* 66, 3959–3975. doi: 10.1093/jxb/erv196
- Johnson, J. L., and Cummins, C. S. (1972). Cell wall composition and deoxyribonucleic acid similarities among the anaerobic coryneforms, classical propionibacteria, and strains of *Arachnia propionica*. *J. Bacteriol.* 109, 1047–1066. doi: 10.1128/jb.109.3.1047-1066.1972
- Kim, Y. G., Lee, J. H., and Lee, J. (2021). Antibiofilm activities of fatty acids including myristoleic acid against *Cutibacterium acnes* via reduced cell hydrophobicity. *Phytomedicine* 91:153710. doi: 10.1016/j.phymed.2021.153710
- Knoll, K. E., Lindeque, Z., Adeniji, A. A., Oosthuizen, C. B., Lall, N., and Loots, D. T. (2021). Elucidating the antimycobacterial mechanism of action of ciprofloxacin using metabolomics. *Microorganisms* 9:1158. doi: 10.3390/microorganisms9061158
- Leyden, J. J. (1976). Antibiotic resistant acne. *Cutis* 17, 593–596.
- Li, W. R., Shi, Q. S., Liang, Q., Xie, X. B., Huang, X. M., and Chen, Y. B. (2014). Antibacterial activity and kinetics of *Litsea cubeba* oil on *Escherichia coli*. *PLoS One* 9:e110983. doi: 10.1371/journal.pone.0110983
- Liu, T. T., and Yang, T. S. (2012). Antimicrobial impact of the components of essential oil of *Litsea cubeba* from Taiwan and antimicrobial activity of the oil in food systems. *Int. J. Food Microbiol.* 156, 68–75. doi: 10.1016/j.jfoodmicro.2012.03.005
- Lopez-Ibanez, J., Pazos, F., and Chagoyen, M. (2016). MBROLE 2.0-functional enrichment of chemical compounds. *Nucleic Acids Res.* 44, W201–W204. doi: 10.1093/nar/gkw253
- McCubbin, T., Gonzalez-Garcia, R. A., Palfreyman, R. W., Stowers, C., Nielsen, L. K., and Marcellin, E. (2020). A pan-genome guided metabolic network reconstruction of five propionibacterium species reveals extensive metabolic diversity. *Genes* 11:1115. doi: 10.3390/genes11101115
- McLaughlin, J., Watterson, S., Layton, A. M., Bjourson, A. J., Barnard, E., and McDowell, A. (2019). *Propionibacterium acnes* and acne vulgaris: new insights from the integration of population genetic, multi-omic, biochemical and host-microbe studies. *Microorganisms* 7:128. doi: 10.3390/microorganisms7050128
- Murbach Teles Andrade, B. F., Nunes Barbosa, L., Bergamo Alves, F. C., Pereira Marques, A. F., Albano, M., Mores Rall, V. L., et al. (2018). The impact of *Cymbopogon martinii* essential oil on *Cutibacterium* (formerly *Propionibacterium*) *acnes* strains and its interaction with keratinocytes. *J. Pharm. Pharmacol.* 70, 1688–1699. doi: 10.1111/jph.13011
- Nardoni, S., Najar, B., Fronte, B., Pistelli, L., and Mancianti, F. (2019). In vitro activity of essential oils against *Saprolegnia parasitica*. *Molecules* 24:1270. doi: 10.3390/molecules24071270
- Nguyen, H. V., Meile, J. C., Lebrun, M., Caruso, D., Chu-Ky, S., and Sarter, S. (2018). *Litsea cubeba* leaf essential oil from Vietnam: chemical diversity and its impacts on antibacterial activity. *Lett. Appl. Microbiol.* 66, 207–214. doi: 10.1111/lam.12837
- Noosidum, A., Prabaripai, A., Chareonviriyaphap, T., and Chandrapatya, A. (2008). Excito-repellency properties of essential oils from *Melaleuca leucadendron* L., *Litsea cubeba* (Lour.) Persoon, and *Litsea salicifolia* (Nees) on *Aedes aegypti* (L.) mosquitoes. *J. Vect. Ecol.* 33, 305–312. doi: 10.3376/1081-1710-33.2.305
- Nyirady, J., Grossman, R. M., Nighland, M., Berger, R. S., Jorizzo, J. L., Kim, Y. H., et al. (2001). A comparative trial of two retinoids commonly used in the treatment of acne vulgaris. *J. Dermatol. Treat.* 12, 149–157.
- Ossa-Tabares, J. C., Llanos, C. J., and Garcia, A. M. (2020). Evaluation of tea tree oil physicochemical features and its antimicrobial activity against *Cutibacterium acnes* (*Propionibacterium acnes*) ATCC 6919. *Biomedica* 40, 693–701. doi: 10.7705/biomedica.5122

- Pang, H., Jia, W., and Hu, Z. (2019). Emerging applications of metabolomics in clinical pharmacology. *Clin. Pharmacol. Ther.* 106, 544–556. doi: 10.1002/cpt.1538
- Pante, G. C., Castro, J. C., Lini, R. S., Romoli, J. C. Z., Almeida, R. T. R., Garcia, F. P., et al. (2021). *Litsea cubeba* essential oil: chemical profile, antioxidant activity, cytotoxicity, effect against *Fusarium verticillioides* and fumonisins production. *J. Environ. Sci. Health B* 56, 387–395. doi: 10.1080/03601234.2021.1890519
- Park, J., Schwardt, N. H., Jo, J. H., Zhang, Z., Pillai, V., Phang, S., et al. (2021). Shifts in the skin bacterial and fungal communities of healthy children transitioning through puberty. *J. Invest. Dermatol.* 142, 212–219. doi: 10.1016/j.jid.2021.04.034
- Prasad, M. A., Zolnik, C. P., and Molina, J. (2019). Leveraging phytochemicals: the plant phylogeny predicts sources of novel antibacterial compounds. *Future Sci OA* 5:FSO407. doi: 10.2144/fsoa-2018-0124
- Qiao, Y., Liu, G., Leng, C., Zhang, Y., Lv, X., Chen, H., et al. (2018). Metabolic profiles of cysteine, methionine, glutamate, glutamine, arginine, aspartate, asparagine, alanine and glutathione in *Streptococcus thermophilus* during pH-controlled batch fermentations. *Sci. Rep.* 8:12441. doi: 10.1038/s41598-018-30272-5
- Scholz, C. F. P., and Kilian, M. (2016). The natural history of cutaneous propionibacteria, and reclassification of selected species within the genus *Propionibacterium* to the proposed novel genera *Acidipropionibacterium* gen. nov., *Cutibacterium* gen. nov. and *Pseudopropionibacterium* gen. nov. *Int. J. Syst. Evol. Microbiol.* 66, 4422–4432. doi: 10.1099/ijsem.0.001367
- Spittaels, K. J., van Uytanghe, K., Zouboulis, C. C., Stove, C., Crabbe, A., and Coenye, T. (2021). Porphyrins produced by acneic *Cutibacterium acnes* strains activate the inflammasome by inducing K(+) leakage. *iScience* 24:102575. doi: 10.1016/j.isci.2021.102575
- Strauss, J. S., Krowchuk, D. P., Leyden, J. J., Lucky, A. W., Shalita, A. R., Siegfried, E. C., et al. (2007). Guidelines of care for acne vulgaris management. *J. Am. Acad. Dermatol.* 56, 651–663. doi: 10.1016/j.jaad.2006.08.048
- Tang, C., Chen, J., Zhou, Y., Ding, P., He, G., Zhang, L., et al. (2021). Exploring antimicrobial mechanism of essential oil of *Amomum villosum* Lour through metabolomics based on gas chromatography-mass spectrometry in methicillin-resistant *Staphylococcus aureus*. *Microbiol. Res.* 242:126608. doi: 10.1016/j.micres.2020.126608
- Tanghetti, E. A., and Popp, K. F. (2009). A current review of topical benzoyl peroxide: new perspectives on formulation and utilization. *Dermatol. Clin.* 27, 17–24. doi: 10.1016/j.det.2008.07.001
- Thomas, D. R. (2004). Psychosocial effects of acne. *J. Cutan. Med. Surg.* 8(Suppl. 4), 3–5. doi: 10.1007/s10227-004-0752-x
- Venkateswaran, K., Hattori, N., La Duc, M. T., and Kern, R. (2003). ATP as a biomarker of viable microorganisms in clean-room facilities. *J. Microbiol. Method* 52, 367–377. doi: 10.1016/S0167-7012(02)00192-6
- Vongsombath, C., Palsson, K., Bjork, L., Borg-Karlson, A. K., and Jaenson, T. G. (2012). Mosquito (Diptera: Culicidae) repellency field tests of essential oils from plants traditionally used in Laos. *J. Med. Entomol.* 49, 1398–1404. doi: 10.1603/me12025
- Walsh, T. R., Efthimiou, J., and Dreno, B. (2016). Systematic review of antibiotic resistance in acne: an increasing topical and oral threat. *Lancet Infect. Dis.* 16, e23–e33. doi: 10.1016/S1473-3099(15)00527-7
- Wang, X., Sakata, K., and Komatsu, S. (2018). An integrated approach of proteomics and computational genetic modification effectiveness analysis to uncover the mechanisms of flood tolerance in soybeans. *Int. J. Mol. Sci.* 19:1301. doi: 10.3390/ijms19051301
- Wang, Y., Li, J., Zhou, Z., Zhou, R., Sun, Q., and Wu, P. (2021). Halo-fluorescein for photodynamic bacteria inactivation in extremely acidic conditions. *Nat. Commun.* 12:526. doi: 10.1038/s41467-020-20869-8
- Webster, G. F. (1995). Inflammation in acne vulgaris. *J. Am. Acad. Dermatol.* 33(2 Pt 1), 247–253. doi: 10.1016/0190-9622(95)90243-0
- Wei, M. P., Qiu, J. D., Li, L., Xie, Y. F., Guo, Y. H., Yu, H., et al. (2021). The chemical profile and biological activity of different extracts of *Sapindus mukorossi* Gaertn. against *Cutibacterium acnes*. *Nat. Prod. Res.* 35, 4740–4745. doi: 10.1080/14786419.2020.1715399
- Wong, E. H. J., Ng, C. G., Goh, K. L., Vadivelu, J., Ho, B., and Loke, M. F. (2018). Metabolomic analysis of low and high biofilm-forming *Helicobacter pylori* strains. *Sci. Rep.* 8:1409. doi: 10.1038/s41598-018-19697-0
- Wu, G. (2009). Amino acids: metabolism, functions, and nutrition. *Amino Acids* 37, 1–17. doi: 10.1007/s00726-009-0269-0
- Zhou, X., Liu, Y., Gao, Y., Wang, Y., Xia, Q., Zhong, R., et al. (2020). Enhanced antimicrobial activity of N-terminal derivatives of a novel brevinin-1 peptide from the skin secretion of *Odorrana schmackeri*. *Toxins* 12:484. doi: 10.3390/toxins12080484

Conflict of Interest: The authors declare that the research was conducted in the absence of any commercial or financial relationships that could be construed as a potential conflict of interest.

Publisher's Note: All claims expressed in this article are solely those of the authors and do not necessarily represent those of their affiliated organizations, or those of the publisher, the editors and the reviewers. Any product that may be evaluated in this article, or claim that may be made by its manufacturer, is not guaranteed or endorsed by the publisher.

Copyright © 2022 Chen, Zhang, Zhu, Qian, Tian, Zhao, Jin and Yang. This is an open-access article distributed under the terms of the Creative Commons Attribution License (CC BY). The use, distribution or reproduction in other forums is permitted, provided the original author(s) and the copyright owner(s) are credited and that the original publication in this journal is cited, in accordance with accepted academic practice. No use, distribution or reproduction is permitted which does not comply with these terms.



A Selective Medium for Screening Ceftazidime/Avibactam Resistance in Carbapenem-Resistant *Enterobacterales*

Weiliang Zeng¹, Wenli Liao^{1,2}, Yajie Zhao³, Lingbo Wang¹, Hongyun Shu¹, Huaiyu Jia³, Tao Chen¹, Ying Zhang³, Tieli Zhou^{1*} and Qing Wu^{1*}

¹ Department of Clinical Laboratory, Key Laboratory of Clinical Laboratory Diagnosis and Translational Research of Zhejiang Province, The First Affiliated Hospital of Wenzhou Medical University, Wenzhou, China, ² Department of Laboratory, Yongzhou Central Hospital, Yongzhou, China, ³ Department of Medical Lab Science, School of Laboratory Medicine and Life Science, Wenzhou Medical University, Wenzhou, China

OPEN ACCESS

Edited by:

Vijay Soni,
NewYork-Presbyterian, United States

Reviewed by:

Saurabh Mishra,
Cornell University, United States
Arka Banerjee,
NewYork-Presbyterian, United States

*Correspondence:

Qing Wu
wuqing830@163.com
Tieli Zhou
wytli@163.com

Specialty section:

This article was submitted to
Antimicrobials, Resistance and
Chemotherapy,
a section of the journal
Frontiers in Microbiology

Received: 29 May 2022

Accepted: 17 June 2022

Published: 12 July 2022

Citation:

Zeng W, Liao W, Zhao Y, Wang L,
Shu H, Jia H, Chen T, Zhang Y, Zhou T
and Wu Q (2022) A Selective Medium
for Screening Ceftazidime/Avibactam
Resistance in Carbapenem-Resistant
Enterobacterales.
Front. Microbiol. 13:956044.
doi: 10.3389/fmicb.2022.956044

Ceftazidime/avibactam (CZA) is an alternative antibiotic used for the treatment of infections caused by carbapenem-resistant *Enterobacterales* (CRE). However, the CZA-resistant CRE strains have been detected worldwide. Therefore, it is critical to screen CZA-resistant CRE strains in colonized patients or a specific population so as to rapidly implement infection control measures to limit their transmission. In this study, we developed a *Salmonella-Shigella* (SS) CZA-selective medium and assessed its performance to screen for clinical CZA-resistant CRE isolates in both pure-strain specimens and stool samples. A total of 150 non-duplicated isolates, including 75 CZA-susceptible and 75 CZA-resistant CRE pathogens, were tested by using the broth microdilution method and the SS CZA medium, respectively. The bacterial suspensions were serially diluted in the SS CZA medium, which showed excellent screening performance in both pure CZA-resistant CRE strain and the stool samples with the lowest detection limit of 10^1 - 10^2 and 10^1 - 10^3 CFU/ml, respectively. Notably, none of the susceptible isolates showed growth even at the highest dilution concentration of 10^8 CFU/ml. Most importantly, the SS CZA medium demonstrated excellent performance in screening simulated clinical polymicrobial specimens. Moreover, its screening performance was unaffected by the different resistance determinants for tested isolates. Cumulatively, our data suggest that the SS CZA medium can be used as a promising selective medium to screen CZA-resistant CRE, irrespective of their resistance mechanisms.

Keywords: ceftazidime, avibactam, medium, CRE, resistance, screening

INTRODUCTION

Antibiotic resistance has become a major public health concern. Multidrug-resistant (MDR) pathogens are increasingly restricting the success of antibiotic treatments. In the past decades, carbapenems (such as imipenem, meropenem, and ertapenem) were demonstrated to possess a broad-spectrum antibacterial activity. In fact, they were considered the last resort for the treatment of infections caused by MDR *Enterobacterales* (including *Enterobacter cloacae*, *Escherichia coli*, and

Klebsiella pneumoniae). However, presently, carbapenem-resistant *Enterobacterales* (CRE) have been detected globally. CRE is resistant to several antibiotics and is associated with a mortality rate of up to 50% (Ackley et al., 2020). In addition, a prospective cohort study revealed that 57% of patients were colonized with CRE (van Duin et al., 2020). Therefore, there is an urgent need to develop novel antibiotics to combat CRE infections.

Ceftazidime/avibactam (CZA) is a novel synthetic β -lactamase inhibitor combination that consists of the third-generation cephalosporin ceftazidime (CAZ) and a newly developed β -lactamase inhibitor, avibactam (AVI). CZA is an effective antimicrobial agent against several enzyme-producing microorganisms, including extended-spectrum β -lactamases (ESBLs)-producing *Enterobacterales* (Zhang et al., 2018). Increasing evidence supports that CZA can be used to treat bacterial infections caused by MDR Gram-negative bacteria, including CRE infections (Shields et al., 2016; Caston et al., 2017; Krapp et al., 2017; Tumbarello et al., 2019). Unfortunately, resistance to CZA among CRE has gradually increased across the world with the extensive use of CZA in clinics (Koren et al., 2017; Shields et al., 2017). It has been widely reported that mutations in class A β -lactamase contribute to the development of increased CZA resistance. In *E. coli* and *K. pneumoniae*, the mutations at different sites of KPC increased the minimum inhibitory concentration (MIC) of CZA to various degrees (Haidar et al., 2017; Hemarajata and Humphries, 2019). Some mutations in *bla*_{CTX-M} (Livermore et al., 2018) and *bla*_{SHV} (Winkler et al., 2015) genes have also been reported to contribute to increased resistance to CZA. In addition, mutations in class C β -lactamase AmpC have been reported in several studies. Strains with AmpC mutations have been reported in *Enterobacterales* (Livermore et al., 2018). The base-pair substitutions of class D β -lactamase *bla*_{OXA-48} may induce resistance to CZA (Frohlich et al., 2019). The early detection of potentially CZA-resistant strains is extremely important to prevent further bacterial infections and transmission.

According to the guidelines of the Clinical and Laboratory Standards Institute (CLSI) (Prater et al., 2019), the broth microdilution (BMD) method was used as the reference method to detect the susceptibility of *Enterobacterales* to CZA. However, it is difficult to conduct this method in general clinical laboratories considering the associated complication and time investment. Therefore, effective screening mediums are essential for early, quick, and accurate detection of CZA-resistant CRE isolates. Recently, a CZA-resistance screening medium, called SuperCAZ/AVI, was developed by Sadek et al. to detect CZA resistance among *Enterobacterales* and *Pseudomonas aeruginosa* based on the CHROMagar™ Orientation medium (Sadek et al., 2020). According to their findings, the SuperCAZ/AVI medium contains CAZ, AVI, daptomycin, and amphotericin B, and is a selective medium with both 100% sensitivity and specificity when the lower limit of detection was greater than the cutoff value of 10^3 CFU/ml.

To design a screening medium appropriate for rectal swab specimens, it is important to select a selective medium that inherently inhibits contamination by Gram-positive bacteria

and fungi, such as *Enterococcus* and *Candida*. The *Salmonella-Shigella* (SS) agar medium is a commonly used strong selective medium for the isolation and detection of intestinal pathogens in most clinical microbiology laboratories, especially for the isolation and culture of *Salmonella* and *Shigella* strains. However, it is concerning that certain component of the SS agar medium, such as sodium citrate and bile salts, can prevent the growth of *Candida* and Gram-positive bacteria such as *Staphylococcus* and *Enterococcus* strains. In fact, with the popularity of CRE, carbapenem-drug discs are adhered to the SS agar medium to screen for CRE strains in some hospital laboratories (Aleem et al., 2021). In this study, we developed an SS CZA medium based on the SS agar medium and the SuperCAZ/AVI medium, followed by the assessment of its performance to screen for clinical CZA-resistant CRE strains.

MATERIALS AND METHODS

Bacterial Isolates

The tested strains were collected from the First Affiliated Hospital of the Wenzhou Medical University. The First Affiliated Hospital of Wenzhou Medical University of institutional ethics committee did not require the study to be reviewed or approved by an ethics committee considering its observational nature with the primary focus on bacteria and the no interventions made to patients.

A total of 150 non-duplicate CRE clinical isolates (56 *E. coli*, 60 *E. cloacae*, and 34 *K. pneumoniae*) were collected from the First Affiliated Hospital of Wenzhou Medical University, Wenzhou, Zhejiang, China. Species identification was performed by the matrix-assisted laser desorption ionization time-of-flight mass spectrometry (Bruker Daltonics, US). A total of 75 CZA-susceptible (28 *E. coli*, 30 *E. cloacae*, and 17 *K. pneumoniae*) and 75 CZA-resistant (28 *E. coli*, 30 *E. cloacae*, and 17 *K. pneumoniae*) CRE strains were selected and detected by BMD. *E. coli* ATCC 25922 and *K. pneumoniae* ATCC 700603 were used as the reference control strains. We had investigated the resistant mechanisms of *E. cloacae* previously (Liu et al., 2021).

Antimicrobial Susceptibility Testing

The assessment of the MICs of CZA was performed in triplicate on Cation-adjusted Mueller-Hinton broth by using the BMD. In accordance with the CLSI guidelines (Prater et al., 2019), the MIC breakpoint for CZA provided for *Enterobacterales* was $\leq 8/4 \mu\text{g/ml}$ (susceptible breakpoint) and $\geq 16/4 \mu\text{g/ml}$ (resistant breakpoint).

Polymerase Chain Reaction and DNA Sequencing

Genomic DNA of all tested clinical isolates was extracted using the Biospin Bacterial Genomic DNA Extraction Kit (Bioflux, Tokyo, Japan) in accordance with the instructions of the manufacturer. The resistant determinants, including carbapenem genes (*bla*_{KPC-2}, *bla*_{NDM}, *bla*_{IMP}, *bla*_{VIM}, and *bla*_{OXA-23}, *bla*_{OXA-48}), ESBL genes (*bla*_{SHV}, *bla*_{TEM}, *bla*_{CTX-M-1}, *bla*_{CTX-M-9}, and *bla*_{CTX-M-14}), the outer membrane porin genes (*ompC* and *ompF*), and cephalosporinase gene (*AmpC*),

TABLE 1 | PCR primers used in this study.

Genes	Sequence (5' → 3')	Annealing temperature (°C)	Amplicon size (bp)
<i>bla_{KPC}</i>	F: GCTACACCTAGCTCCACCTTC R: TCAGTGCTCTACAGAAAACC	52	1,050
<i>bla_{NDM}</i>	F: GGTTTGGCGATCTGGTTTTTC R: CGGAATGGCTCACGATC	52	621
<i>bla_{IMP}</i>	F: CATGGTTTGGTGGTTCTTGT R: ATAATTTGGCGGACTTTGGC	50	488
<i>bla_{VIM}</i>	F: GATGGTGTGGTGGTCGCATA R: CGAATGCGCAGCACCAG	58	390
<i>bla_{OXA-23}</i>	F: ACTTGCTATGTGGTTGCTTCTCTT R: TTCAGCTGTTTTAATGATTCATCA	55	797
<i>bla_{OXA-48}</i>	F: TTGGTGGCATCGATTATCGG R: GAGCACTTCTTTGTGATGGC	58	744
<i>bla_{SHV}</i>	F: AGCCGCTTGAGCAAATTAAC R: ATCCCGCAGATAAATCACCAC	60	713
<i>bla_{TEM}</i>	F: CATTTCCGTGTCGCCCTTATTC R: CGTTCATCCATAGTTGCCTGAC	60	800
<i>bla_{CTX-M-1}</i>	F: AAAAATCACTGCGTCAGTTCAC R: ACAAACCGTTGGTGACGATT	55	867
<i>bla_{CTX-M-9}</i>	F: TATTGGGAGTTTGAGATGGT R: TCCTTCAACTCAGCAAAGT	50	933
<i>bla_{CTX-M-14}</i>	F: CTGCTTAATCAGCCTGTGCA R: TCAGTGCGATCCAGACGAAA	50	230
<i>ompC</i>	F: GAGAATGGACTTGCCGACTG R: CGAACGGTCGCAAGAGTA	55	1,289
<i>ompF</i>	F: CAGAACTTATTGACGGCAG R: CGGGACGTTTCATCGGCAC	55	1,410
<i>bla_{AmpC}</i>	F: ACTTACTTCAACTCGCGACG R: TAAACACCACATATGTTCCG	55	663

were examined by PCR using specific primers (Table 1). The positive PCR products were subsequently sequenced.

Screening CZA Resistance in CRE Clinical Isolates Using the SS CZA Medium

Sadek et al.'s (2020) method was adopted, albeit with slight modifications, with at least two independent repeated experiments. The specific experimental procedure is illustrated in Figure 1 and described in the following steps.

Step 1: Preparation of the Culture Medium

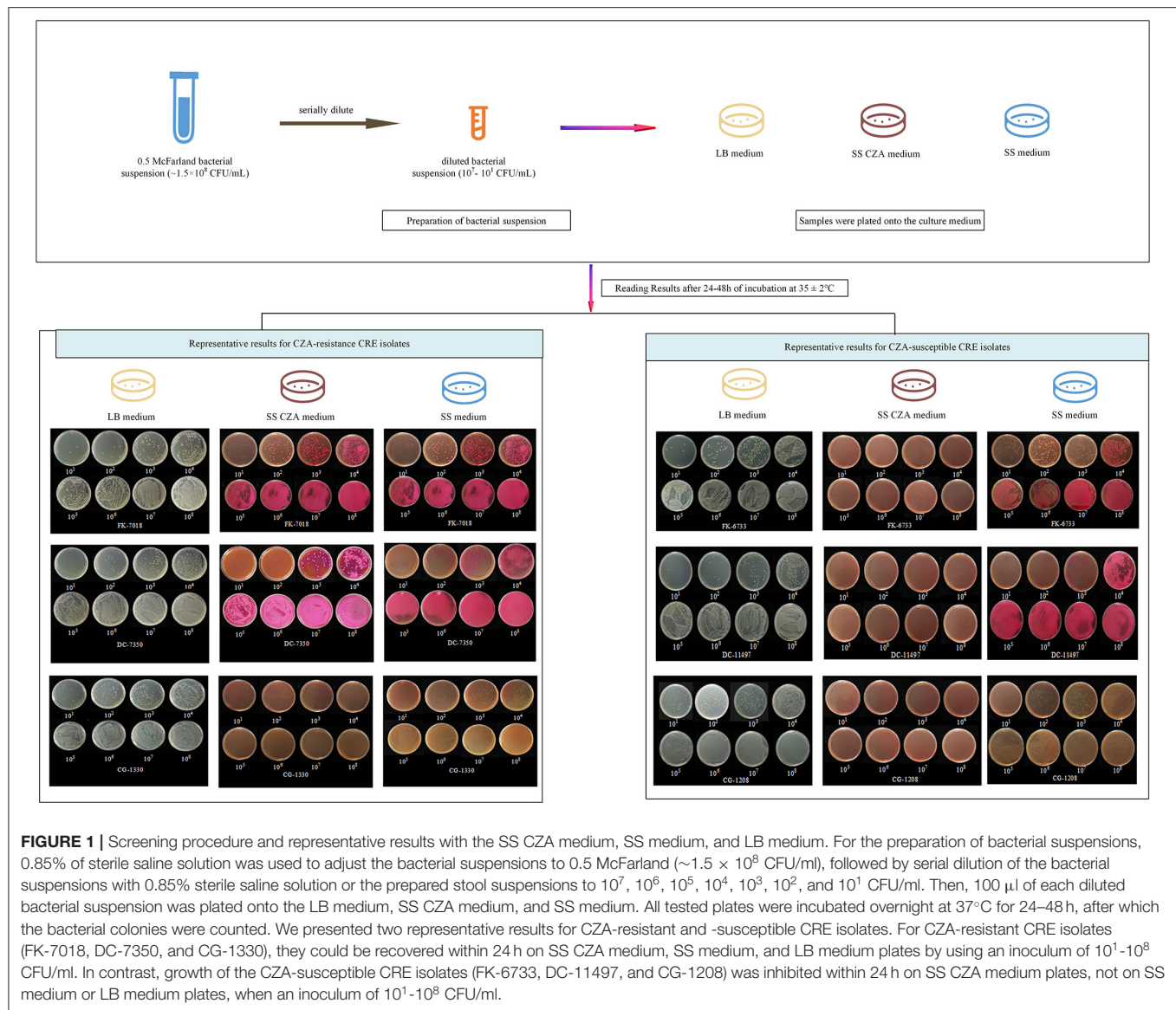
Three different culture media were prepared, including Luria–Bertani (LB) agar medium, SS agar medium, and SS agar medium with CZA (SS CZA medium). These media were prepared according to the instructions using the following formulas: (i) LB agar medium: tryptone 10 g/L, yeast extract 5 g/L, NaCl 10 g/L, agar 15 g/L, distilled water; (ii) SS agar medium: SS agar 62 g/L, distilled water; (iii) SS CZA medium: SS agar 62 g/L, distilled water, CAZ 6 mg/L, AVI 4 mg/L. Specifically, the LB and SS agar media were autoclaved at 121 and 105°C for 20 min, respectively, to dissolve them. After the SS CZA medium was cooled at 50°C for 1 h, the antibiotic stock solutions of CAZ (final concentration of 6 µg/ml) and AVI (final concentration of 4 µg/ml) were added

to it. These configured media were then poured into empty plates and stored at 4°C until further use.

Step 2: Preparation of Bacterial Suspensions and Clinical Simulated Stool Samples

For the preparation of bacterial suspensions, 0.85% sterile saline solution was used to adjust the bacterial suspensions to 0.5 McFarland ($\sim 1.5 \times 10^8$ CFU/ml), followed by serial dilution of the bacterial suspensions with 0.85% sterile saline solution to 10^7 , 10^6 , 10^5 , 10^4 , 10^3 , 10^2 , and 10^1 CFU/ml. The bacterial suspensions were used within 1.5 h of preparation. Then, 0.85% sterile saline solution with or without reference control strains (ATCC 25922 or ATCC 700603) was used as negative controls.

For the preparation of clinical simulated stool samples, fresh pooled feces from healthy volunteers were collected and prepared into suspensions (concentration of 10 g/100 ml) with 0.85% sterile saline solution. Meanwhile, 0.85% sterile saline solution was used to adjust the bacterial suspensions to 0.5 McFarland ($\sim 1.5 \times 10^8$ CFU/ml). Then, the clinically simulated stool samples were prepared and the bacterial suspensions were serially diluted with the prepared stool suspensions to 10^7 , 10^6 , 10^5 , 10^4 , 10^3 , 10^2 , and 10^1 CFU/ml. The clinical simulated stool samples



were to be used within 1.5 h of preparation. The stool suspensions with or without reference control strains (*E. coli* ATCC 25922 and *K. pneumoniae* ATCC 700603) were used as negative controls.

Step 3: Samples Were Plated Onto the Culture Medium

In this step, 100 μ l of each diluted bacterial suspension was plated onto the SS agar plates and SS CZA plates. Meanwhile, to quantify the viable bacterial count in each dilution step, LB agar plates were inoculated with the same amount of the abovementioned bacterial suspension. The screening procedure for clinically simulated fecal samples was the same as that for pure strains. To eliminate false-positive results contributed by fecal samples, 100 μ l of 0.85% sterile saline solution or fecal suspensions without the tested strains were plated onto these three media. All tested plates were incubated overnight at 37°C for 24 h, and the bacterial colonies were enumerated. If no bacterial growth was detected within 24 h, the plates were continuously cultured for 48 h to

assess the negativity of the culture. The lowest limit of detection for the studied strains was determined by the SS CAZ medium.

Step 4: Result Interpretations and Analysis

In this study, the sensitivity and specificity cutoff values for the detection of CZA-resistant CRE isolates were set to 1×10^3 CFU/ml (Nordmann et al., 2012). In other words, the results were considered positive when CZA-resistant CRE strains could grow on the SS CZA medium at $\leq 1 \times 10^3$ CFU/ml, while the CZA-susceptible CRE strains that showed a visible growth with an inoculum of $> 1 \times 10^3$ CFU/ml were considered as negative. In order to exclude the false-positive/-negative culture results, the results were considered interpretable under the following conditions: (i) the LB, SS, and SS CZA agar plates with 100 μ l of 0.85% sterile saline solution without tested strains showed no bacterial growth; (ii) bacterial growth was visible on the LB agar plate inoculated with 100 μ l of the fecal suspensions without tested strains, and no growth was detected on the SS and SS CZA

TABLE 2 | Summary of MIC values of the CZA for the tested isolates and the lowest detection limits of the SS CZA medium, SS medium, and LB medium.

Isolates	Species	MIC of CZA ($\mu\text{g/ml}$)	CZA Resistant Phenotype	Resistance determinant(s)	Lowest detection limit (CFU/ml) of					
					SS CZA medium ^a		SS medium		LB medium	
					Culture	Stools	Culture	Stools	Culture	Stools
DC-2003	<i>E. coli</i>	64	R	CTX-M-1, CTX-M-9, OmpF	10^1	10^3	10^1	10^1	10^1	10^1
DC-5128	<i>E. coli</i>	>256	R	NDM, CTX-M-1, CTX-M-9, OmpC, OmpF	10^1	10^1	10^1	10^1	10^1	10^1
DC-7114	<i>E. coli</i>	>256	R	NDM, TEM, CTX-M-1, OmpC	10^1	10^1	10^1	10^1	10^1	10^1
DC-7143	<i>E. coli</i>	>256	R	NDM, TEM, OmpC	10^1	10^1	10^1	10^1	10^1	10^1
DC-7333	<i>E. coli</i>	>256	R	NDM, TEM, CTX-M-1, CTX-M-9, OmpC	10^1	10^1	10^1	10^1	10^1	10^1
DC-7350	<i>E. coli</i>	>256	R	NDM, TEM, CTX-M-1	10^1	10^1	10^1	10^1	10^1	10^1
DC-7368	<i>E. coli</i>	>256	R	NDM, TEM, CTX-M-1	10^2	10^1	10^1	10^1	10^1	10^1
DC-7523	<i>E. coli</i>	>256	R	NDM, CTX-M-1, CTX-M-9, OmpC	10^1	10^1	10^1	10^1	10^1	10^1
DC-7658	<i>E. coli</i>	>256	R	NDM, TEM, CTX-M-1, CTX-M-9	10^1	10^1	10^1	10^1	10^1	10^1
DC-7706	<i>E. coli</i>	>256	R	NDM, TEM, CTX-M-1, CTX-M-9, OmpF	10^1	10^1	10^1	10^1	10^1	10^1
DC-7741	<i>E. coli</i>	>256	R	NDM, TEM, CTX-M-1, OmpC	10^1	10^1	10^1	10^1	10^1	10^1
DC-7781	<i>E. coli</i>	>256	R	NDM, TEM, CTX-M-1, OmpC	10^2	10^1	10^1	10^1	10^1	10^1
DC-7782	<i>E. coli</i>	>256	R	NDM, TEM, CTX-M-1, OmpC	10^1	10^1	10^1	10^1	10^1	10^1
DC-7911	<i>E. coli</i>	>256	R	NDM, CTX-M-9, OmpF	10^1	10^1	10^1	10^1	10^1	10^1
DC-7914	<i>E. coli</i>	>256	R	NDM, TEM, CTX-M-9, OmpF	10^1	10^2	10^1	10^1	10^1	10^1
DC-7956	<i>E. coli</i>	>256	R	NDM, TEM, CTX-M-9, OmpF	10^1	10^2	10^1	10^1	10^1	10^1
DC-8111	<i>E. coli</i>	>256	R	NDM, TEM, CTX-M-1, CTX-M-9, OmpC	10^1	10^2	10^1	10^1	10^1	10^1
DC-8439	<i>E. coli</i>	>256	R	NDM	10^2	10^1	10^1	10^1	10^1	10^1
DC-8466	<i>E. coli</i>	>256	R	NDM	10^1	10^1	10^1	10^1	10^1	10^1
DC-8647	<i>E. coli</i>	>256	R	NDM	10^1	10^1	10^1	10^1	10^1	10^1
DC-8823	<i>E. coli</i>	>256	R	NDM	10^1	10^1	10^1	10^1	10^1	10^1
DC-8855	<i>E. coli</i>	>256	R	NDM	10^1	10^1	10^1	10^1	10^1	10^1
DC-8896	<i>E. coli</i>	>256	R	NDM	10^1	10^1	10^1	10^1	10^1	10^1
DC-10494	<i>E. coli</i>	>256	R	NDM	10^2	10^3	10^1	10^1	10^1	10^1
DC-10527	<i>E. coli</i>	>256	R	NDM	10^1	10^1	10^1	10^1	10^1	10^1
DC-10921	<i>E. coli</i>	>256	R	NDM	10^2	10^3	10^1	10^1	10^1	10^1
DC-11403	<i>E. coli</i>	>256	R	NDM	10^1	10^1	10^1	10^1	10^1	10^1
DC-11552	<i>E. coli</i>	>256	R	NDM	10^1	10^1	10^1	10^1	10^1	10^1
ATCC 25922	<i>E. coli</i>	0.125	S	Reference	$>10^8$	$>10^8$	10^1	10^1	10^1	10^1
DC-1918	<i>E. coli</i>	4	S	CTX-M-9, OmpF	$>10^8$	$>10^8$	10^1	10^1	10^1	10^1
DC-3285	<i>E. coli</i>	0.5	S	KPC-2, CTX-M-1	$>10^8$	$>10^8$	10^1	10^1	10^1	10^1
DC-5113	<i>E. coli</i>	1	S	KPC-2, TEM, CTX-M-1, CTX-M-9	$>10^8$	$>10^8$	10^1	10^1	10^1	10^1
DC-5293	<i>E. coli</i>	0.125	S	TEM, SHV	$>10^8$	$>10^8$	10^1	10^1	10^1	10^1
DC-6669	<i>E. coli</i>	1	S	TEM, CTX-M-9, OmpF	$>10^8$	$>10^8$	10^1	10^1	10^1	10^1
DC-6834	<i>E. coli</i>	1	S	CTX-M-1, OmpF	$>10^8$	$>10^8$	10^1	10^1	10^1	10^1
DC-6856	<i>E. coli</i>	0.25	S	KPC-2, CTX-M-1, CTX-M-9, OmpF	$>10^8$	$>10^8$	10^1	10^1	10^1	10^1
DC-6896	<i>E. coli</i>	≤ 0.125	S	KPC-2, CTX-M-1, CTX-M-9, OmpF	$>10^8$	$>10^8$	10^1	10^1	10^1	10^1
DC-8535	<i>E. coli</i>	4	S	CTX-M-9, SHV	$>10^8$	$>10^8$	10^1	10^1	10^1	10^1
DC-8873	<i>E. coli</i>	1	S	TEM, SHV	$>10^8$	$>10^8$	10^1	10^1	10^1	10^1
DC-10694	<i>E. coli</i>	0.5	S	CTX-M-1, CTX-M-9, TEM, SHV	$>10^8$	$>10^8$	10^1	10^1	10^1	10^1
DC-10709	<i>E. coli</i>	0.25	S	CTX-M-1, TEM, SHV	$>10^8$	$>10^8$	10^1	10^1	10^1	10^1
DC-10740	<i>E. coli</i>	0.5	S	CTX-M-9, SHV	$>10^8$	$>10^8$	10^1	10^1	10^1	10^1
DC-11104	<i>E. coli</i>	0.25	S	CTX-M-1, TEM, SHV	$>10^8$	$>10^8$	10^1	10^1	10^1	10^1
DC-11305	<i>E. coli</i>	0.5	S	CTX-M-1, TEM, SHV	$>10^8$	$>10^8$	10^1	10^1	10^1	10^1
DC-11308	<i>E. coli</i>	0.5	S	CTX-M-1, TEM, SHV	$>10^8$	$>10^8$	10^1	10^1	10^1	10^1
DC-11497	<i>E. coli</i>	4	S	CTX-M-1	$>10^8$	$>10^8$	10^1	10^1	10^1	10^1

(Continued)

TABLE 2 | Continued

Isolates	Species	MIC of CZA ($\mu\text{g/ml}$)	CZA Resistant Phenotype	Resistance determinant(s)	Lowest detection limit (CFU/ml) of					
					SS CZA medium ^a		SS medium		LB medium	
					Culture	Stools	Culture	Stools	Culture	Stools
DC-11537	<i>E. coli</i>	0.5	S	CTX-M-1, TEM, SHV	$>10^8$	$>10^8$	10^1	10^1	10^1	10^1
DC-11581	<i>E. coli</i>	0.5	S	KPC-2	$>10^8$	$>10^8$	10^1	10^1	10^1	10^1
DC-11720	<i>E. coli</i>	2	S	KPC-2	$>10^8$	$>10^8$	10^1	10^1	10^1	10^1
DC-12735	<i>E. coli</i>	2	S	KPC-2	$>10^8$	$>10^8$	10^1	10^1	10^1	10^1
DC-13016	<i>E. coli</i>	1	S	CTX-M-9, SHV	$>10^8$	$>10^8$	10^1	10^1	10^1	10^1
DC-13149	<i>E. coli</i>	2	S	CTX-M-1, CTX-M-9	$>10^8$	$>10^8$	10^1	10^1	10^1	10^1
DC-13346	<i>E. coli</i>	4	S	CTX-M-1, TEM, SHV	$>10^8$	$>10^8$	10^1	10^1	10^1	10^1
DC-14122	<i>E. coli</i>	0.125	S	CTX-M-1	$>10^8$	$>10^8$	10^1	10^1	10^1	10^1
DC-14323	<i>E. coli</i>	0.5	S	CTX-M-1, CTX-M-9, TEM, SHV	$>10^8$	$>10^8$	10^1	10^1	10^1	10^1
DC-14324	<i>E. coli</i>	2	S	KPC-2	$>10^8$	$>10^8$	10^1	10^1	10^1	10^1
DC-14351	<i>E. coli</i>	1	S	CTX-M-9, SHV	$>10^8$	$>10^8$	10^1	10^1	10^1	10^1
CG-175 ^b (Liu et al., 2021)	<i>E. cloacae</i>	256	R	NDM, CTX-M-9, CTX-M-14	10^1	10^1	10^1	10^1	10^1	10^1
CG-586	<i>E. cloacae</i>	>256	R	NDM, CTX-M-1	10^1	10^1	10^1	10^1	10^1	10^1
CG-662	<i>E. cloacae</i>	>256	R	NDM	10^1	10^1	10^1	10^1	10^1	10^1
CG-698	<i>E. cloacae</i>	256	R	NDM	10^1	10^1	10^1	10^1	10^1	10^1
CG-749	<i>E. cloacae</i>	>256	R	NDM, efflux pump	10^1	10^1	10^1	10^1	10^1	10^1
CG-838	<i>E. cloacae</i>	64	R	NDM	10^1	10^2	10^1	10^1	10^1	10^1
CG-901	<i>E. cloacae</i>	>256	R	NDM	10^1	10^1	10^1	10^1	10^1	10^1
CG-983	<i>E. cloacae</i>	>256	R	NDM, efflux pump	10^1	10^1	10^1	10^1	10^1	10^1
CG-996	<i>E. cloacae</i>	128	R	OXA-23, TEM	10^1	10^1	10^1	10^1	10^1	10^1
CG-1045	<i>E. cloacae</i>	>256	R	IMP	10^1	10^1	10^1	10^1	10^1	10^1
CG-1075	<i>E. cloacae</i>	>256	R	NDM, efflux pump	10^1	10^1	10^1	10^1	10^1	10^1
CG-1090	<i>E. cloacae</i>	>256	R	NDM	10^1	10^1	10^1	10^1	10^1	10^1
CG-1608	<i>E. cloacae</i>	>256	R	NDM, SHV, efflux pump	10^1	10^1	10^1	10^1	10^1	10^1
CG-1819	<i>E. cloacae</i>	128	R	NDM, CTX-M-9	10^1	10^1	10^1	10^1	10^1	10^1
CG-1141	<i>E. cloacae</i>	>256	R	TEM, SHV	10^1	10^1	10^1	10^1	10^1	10^1
CG-1212	<i>E. cloacae</i>	>256	R	TEM, CTXM-14, impermeability, efflux pump	10^1	10^2	10^1	10^1	10^1	10^1
CG-1249	<i>E. cloacae</i>	64	R	AmpC, impermeability	10^1	10^2	10^1	10^1	10^1	10^1
CG-1257	<i>E. cloacae</i>	>256	R	IMP	10^1	10^1	10^1	10^1	10^1	10^1
CG-1280	<i>E. cloacae</i>	>256	R	impermeability	10^1	10^2	10^1	10^1	10^1	10^1
CG-1330	<i>E. cloacae</i>	>256	R	NDM	10^1	10^1	10^1	10^1	10^1	10^1
CG-1381	<i>E. cloacae</i>	>256	R	OXA-23	10^1	10^1	10^1	10^1	10^1	10^1
CG-1498	<i>E. cloacae</i>	>256	R	IMP	10^1	10^1	10^1	10^1	10^1	10^1
CG-1574	<i>E. cloacae</i>	>256	R	NDM, CTXM-14	10^1	10^1	10^1	10^1	10^1	10^1
CG-1591	<i>E. cloacae</i>	>256	R	IMP	10^1	10^1	10^1	10^1	10^1	10^1
CG-1593	<i>E. cloacae</i>	>256	R	IMP	10^1	10^1	10^1	10^1	10^1	10^1
CG-1737	<i>E. cloacae</i>	>256	R	NDM	10^2	10^3	10^1	10^1	10^1	10^1
CG-1778	<i>E. cloacae</i>	>256	R	NDM, efflux pump	10^1	10^1	10^1	10^1	10^1	10^1
CG-1779	<i>E. cloacae</i>	>256	R	NDM	10^1	10^1	10^1	10^1	10^1	10^1
CG-1781	<i>E. cloacae</i>	>256	R	NDM	10^1	10^1	10^1	10^1	10^1	10^1
CG-1813	<i>E. cloacae</i>	>256	R	IMP, efflux pump	10^1	10^1	10^1	10^1	10^1	10^1
CG-648	<i>E. cloacae</i>	≤ 0.125	S	KPC-2, AmpC	$>10^8$	$>10^8$	10^1	10^1	10^1	10^1
CG-701	<i>E. cloacae</i>	0.5	S	SHV, TEM, CTX-M-1, AmpC	$>10^8$	$>10^8$	10^1	10^1	10^1	10^1
CG-737	<i>E. cloacae</i>	0.5	S	AmpC	$>10^8$	$>10^8$	10^1	10^1	10^1	10^1
CG-741	<i>E. cloacae</i>	0.5	S	AmpC	$>10^8$	$>10^8$	10^1	10^1	10^1	10^1

(Continued)

TABLE 2 | Continued

Isolates	Species	MIC of CZA ($\mu\text{g/ml}$)	CZA Resistant Phenotype	Resistance determinant(s)	Lowest detection limit (CFU/ml) of					
					SS CZA medium ^a		SS medium		LB medium	
					Culture	Stools	Culture	Stools	Culture	Stools
CG-864	<i>E. cloacae</i>	1	S	AmpC	> 10 ⁸	> 10 ⁸	10 ¹	10 ¹	10 ¹	10 ¹
CG-934	<i>E. cloacae</i>	1	S	AmpC	> 10 ⁸	> 10 ⁸	10 ¹	10 ¹	10 ¹	10 ¹
CG-1038	<i>E. cloacae</i>	0.5	S	KPC-2, AmpC	> 10 ⁸	> 10 ⁸	10 ¹	10 ¹	10 ¹	10 ¹
CG-1048	<i>E. cloacae</i>	1	S	CTX-M-14, AmpC	> 10 ⁸	> 10 ⁸	10 ¹	10 ¹	10 ¹	10 ¹
CG-1050	<i>E. cloacae</i>	2	S	SHV, AmpC	> 10 ⁸	> 10 ⁸	10 ¹	10 ¹	10 ¹	10 ¹
CG-1051	<i>E. cloacae</i>	2	S	SHV, TEM, CTX-M-1, AmpC	> 10 ⁸	> 10 ⁸	10 ¹	10 ¹	10 ¹	10 ¹
CG-1479	<i>E. cloacae</i>	1	S	NDM, SHV, CTX-M-9, CTX-M-14, AmpC	> 10 ⁸	> 10 ⁸	10 ¹	10 ¹	10 ¹	10 ¹
CG-1506	<i>E. cloacae</i>	0.5	S	SHV, CTX-M-14	> 10 ⁸	> 10 ⁸	10 ¹	10 ¹	10 ¹	10 ¹
CG-1081	<i>E. cloacae</i>	4	S	TEM, AmpC, efflux pump	> 10 ⁸	> 10 ⁸	10 ¹	10 ¹	10 ¹	10 ¹
CG-1144	<i>E. cloacae</i>	0.25	S	impermeability	> 10 ⁸	> 10 ⁸	10 ¹	10 ¹	10 ¹	10 ¹
CG-1159	<i>E. cloacae</i>	2	S	AmpC, impermeability	> 10 ⁸	> 10 ⁸	10 ¹	10 ¹	10 ¹	10 ¹
CG-1181	<i>E. cloacae</i>	4	S	SHV, TEM, CTX-M-1, CTX-M-9, CTX-M-14, impermeability	> 10 ⁸	> 10 ⁸	10 ¹	10 ¹	10 ¹	10 ¹
CG-1208	<i>E. cloacae</i>	8	S	TEM, CTXM-9, CTXM-14, AmpC, impermeability	> 10 ⁸	> 10 ⁸	10 ¹	10 ¹	10 ¹	10 ¹
CG-1231	<i>E. cloacae</i>	1	S	AmpC, impermeability	> 10 ⁸	> 10 ⁸	10 ¹	10 ¹	10 ¹	10 ¹
CG-1236	<i>E. cloacae</i>	2	S	TEM, AmpC, impermeability	> 10 ⁸	> 10 ⁸	10 ¹	10 ¹	10 ¹	10 ¹
CG-1250	<i>E. cloacae</i>	2	S	AmpC, impermeability	> 10 ⁸	> 10 ⁸	10 ¹	10 ¹	10 ¹	10 ¹
CG-1252	<i>E. cloacae</i>	1	S	impermeability	> 10 ⁸	> 10 ⁸	10 ¹	10 ¹	10 ¹	10 ¹
CG-1281	<i>E. cloacae</i>	1	S	impermeability	> 10 ⁸	> 10 ⁸	10 ¹	10 ¹	10 ¹	10 ¹
CG-1457	<i>E. cloacae</i>	8	S	AmpC	> 10 ⁸	> 10 ⁸	10 ¹	10 ¹	10 ¹	10 ¹
CG-1461	<i>E. cloacae</i>	4	S	AmpC, impermeability	> 10 ⁸	> 10 ⁸	10 ¹	10 ¹	10 ¹	10 ¹
CG-1522	<i>E. cloacae</i>	4	S	TEM, CTX-M-1, AmpC, impermeability, efflux pump	> 10 ⁸	> 10 ⁸	10 ¹	10 ¹	10 ¹	10 ¹
CG-1532	<i>E. cloacae</i>	1	S	Impermeability, efflux pump	> 10 ⁸	> 10 ⁸	10 ¹	10 ¹	10 ¹	10 ¹
CG-1547	<i>E. cloacae</i>	2	S	KPC-2, SHV, TEX-M-9, CTXM-14, efflux pump	> 10 ⁸	> 10 ⁸	10 ¹	10 ¹	10 ¹	10 ¹
CG-1563	<i>E. cloacae</i>	4	S	SHV, TEM, CTX-M-14, impermeability	> 10 ⁸	> 10 ⁸	10 ¹	10 ¹	10 ¹	10 ¹
CG-1565	<i>E. cloacae</i>	4	S	SHV, AmpC, impermeability, efflux pump	> 10 ⁸	> 10 ⁸	10 ¹	10 ¹	10 ¹	10 ¹
CG-1581	<i>E. cloacae</i>	2	S	TEM, AmpC, impermeability, efflux pump	> 10 ⁸	> 10 ⁸	10 ¹	10 ¹	10 ¹	10 ¹
FK-2784	<i>K. pneumoniae</i>	64	R	KPC-2	10 ¹	10 ¹	10 ¹	10 ¹	10 ¹	10 ¹
FK-3246	<i>K. pneumoniae</i>	>256	R	KPC-2	10 ¹	10 ¹	10 ¹	10 ¹	10 ¹	10 ¹
FK-4722	<i>K. pneumoniae</i>	>256	R	KPC-2	10 ¹	10 ¹	10 ¹	10 ¹	10 ¹	10 ¹
FK-7018	<i>K. pneumoniae</i>	>256	R	NDM	10 ¹	10 ¹	10 ¹	10 ¹	10 ¹	10 ¹
FK-7079	<i>K. pneumoniae</i>	>256	R	CTX-M-9, SHV, TEM	10 ¹	10 ¹	10 ¹	10 ¹	10 ¹	10 ¹
FK-7173	<i>K. pneumoniae</i>	>256	R	NDM	10 ¹	10 ¹	10 ¹	10 ¹	10 ¹	10 ¹
FK-7513	<i>K. pneumoniae</i>	>256	R	NDM	10 ¹	10 ¹	10 ¹	10 ¹	10 ¹	10 ¹
FK-7710	<i>K. pneumoniae</i>	>256	R	NDM	10 ¹	10 ¹	10 ¹	10 ¹	10 ¹	10 ¹
FK-7786	<i>K. pneumoniae</i>	64	R	NDM	10 ¹	10 ¹	10 ¹	10 ¹	10 ¹	10 ¹
FK-7921	<i>K. pneumoniae</i>	>256	R	NDM	10 ¹	10 ¹	10 ¹	10 ¹	10 ¹	10 ¹
FK-7978	<i>K. pneumoniae</i>	>256	R	NDM	10 ¹	10 ¹	10 ¹	10 ¹	10 ¹	10 ¹
FK-8401	<i>K. pneumoniae</i>	>256	R	NDM	10 ¹	10 ¹	10 ¹	10 ¹	10 ¹	10 ¹
FK-8696	<i>K. pneumoniae</i>	>256	R	KPC-33, CTX-M-9, SHV, TEM	10 ¹	10 ¹	10 ¹	10 ¹	10 ¹	10 ¹
FK-8966	<i>K. pneumoniae</i>	>256	R	NDM	10 ¹	10 ¹	10 ¹	10 ¹	10 ¹	10 ¹
FK-9102	<i>K. pneumoniae</i>	>256	R	NDM	10 ¹	10 ¹	10 ¹	10 ¹	10 ¹	10 ¹
FK-9250	<i>K. pneumoniae</i>	>256	R	NDM	10 ¹	10 ¹	10 ¹	10 ¹	10 ¹	10 ¹
FK-9283	<i>K. pneumoniae</i>	>256	R	NDM	10 ¹	10 ¹	10 ¹	10 ¹	10 ¹	10 ¹

(Continued)

TABLE 2 | Continued

Isolates	Species	MIC of CZA ($\mu\text{g/ml}$)	CZA Resistant Phenotype	Resistance determinant(s)	Lowest detection limit (CFU/ml) of					
					SS CZA medium ^a		SS medium		LB medium	
					Culture	Stools	Culture	Stools	Culture	Stools
ATCC 700603	<i>K. pneumoniae</i>	≤ 0.125	S	Reference	$> 10^8$	$> 10^8$	10^1	10^1	10^1	10^1
FK-2731	<i>K. pneumoniae</i>	0.5	S	KPC-2	$> 10^8$	$> 10^8$	10^1	10^1	10^1	10^1
FK-2742	<i>K. pneumoniae</i>	0.5	S	KPC-2	$> 10^8$	$> 10^8$	10^1	10^1	10^1	10^1
FK-2836	<i>K. pneumoniae</i>	4	S	KPC-2, IMP	$> 10^8$	$> 10^8$	10^1	10^1	10^1	10^1
FK-2877	<i>K. pneumoniae</i>	2	S	KPC-2	$> 10^8$	$> 10^8$	10^1	10^1	10^1	10^1
FK-2970	<i>K. pneumoniae</i>	1	S	KPC-2	$> 10^8$	$> 10^8$	10^1	10^1	10^1	10^1
FK-3006	<i>K. pneumoniae</i>	1	S	KPC-2, IMP	$> 10^8$	$> 10^8$	10^1	10^1	10^1	10^1
FK-3020	<i>K. pneumoniae</i>	1	S	IMP	$> 10^8$	$> 10^8$	10^1	10^1	10^1	10^1
FK-3093	<i>K. pneumoniae</i>	4	S	KPC-2	$> 10^8$	$> 10^8$	10^1	10^1	10^1	10^1
FK-3142	<i>K. pneumoniae</i>	2	S	KPC-2	$> 10^8$	$> 10^8$	10^1	10^1	10^1	10^1
FK-6699	<i>K. pneumoniae</i>	0.5	S	KPC-2	$> 10^8$	$> 10^8$	10^1	10^1	10^1	10^1
FK-6701	<i>K. pneumoniae</i>	1	S	KPC-2	$> 10^8$	$> 10^8$	10^1	10^1	10^1	10^1
FK-6703	<i>K. pneumoniae</i>	1	S	KPC-2	$> 10^8$	$> 10^8$	10^1	10^1	10^1	10^1
FK-6719	<i>K. pneumoniae</i>	2	S	KPC-2	$> 10^8$	$> 10^8$	10^1	10^1	10^1	10^1
FK-6723	<i>K. pneumoniae</i>	2	S	KPC-2	$> 10^8$	$> 10^8$	10^1	10^1	10^1	10^1
FK-6728	<i>K. pneumoniae</i>	2	S	KPC-2	$> 10^8$	$> 10^8$	10^1	10^1	10^1	10^1
FK-6733	<i>K. pneumoniae</i>	8	S	KPC-2	$> 10^8$	$> 10^8$	10^1	10^1	10^1	10^1
FK-6735	<i>K. pneumoniae</i>	4	S	KPC-2	$> 10^8$	$> 10^8$	10^1	10^1	10^1	10^1

E. coli, *Escherichia coli*; *E. cloacae*, *Enterobacter cloacae*; *K. pneumoniae*, *Klebsiella pneumoniae*; MIC, minimal inhibitory concentration; CZA, ceftazidime-avibactam; R, resistant; S, susceptible; NDM, New Delhi Metallo-beta-lactamase; KPC, *K. pneumoniae* carbapenemase; TEM, Temoneira β -lactamase; CTX-M, cefotaxime-Munich-type β -lactamase; SHV, sulfhydryl reagent variable β -lactamase; OXA, oxacillinase; AmpC, AmpC-type β -lactamase; IMP, IMP-type metallo- β -lactamase; OmpC/OmpF, outer membrane porins genes.

^ameans that cutoff values were set at 1×10^3 CFU/mL, i.e., the results were considered as positive when CZA-resistant CRE strains can grow on SS CZA medium at $\leq 1 \times 10^3$ CFU/mL, while the CZA-susceptible CRE strains have a visible growth using an inoculum of $> 1 \times 10^3$ CFU/mL were considered as negative.

^bmeans that the resistant mechanisms of *E. cloacae* were investigated in our published study.

agar plates; and (iii) bacterial growth was observed on both the SS and LB agar plates inoculated with either the pure bacterial suspension or simulated specimen suspension, and the bacterial colonies on these media were enumerated to ensure the accuracy of the McFarland standard or the bacterial load and reliability of our findings.

RESULTS

The Tested CRE Clinical Strains Demonstrated Different Resistance Determinants

A total of 150 non-duplicate CRE clinical isolates were obtained, which included 75 CZA-resistant and 75 CZA-susceptible isolates, to evaluate the performances of the SS CZA medium. Their MIC of CZA ranged from ≤ 0.125 to $\geq 256 \mu\text{g/ml}$ (Table 2). The PCR results demonstrated that NDM was the main resistance determinant in CZA-resistant *E. coli* and *E. cloacae*. We also detected NDM in a CZA-susceptible *E. cloacae* strain (CG-1479). In addition, the resistance determinants of CZA-resistant *E. cloacae* CG-996 and CG-1045 were *bla*_{OXA-23} and IMP, respectively. KPC-2 was detected in *K. pneumoniae*. KPC-33, a KPC-2 variant with the D179Y mutation in the omega loop, was detected in FK-8696. A high expression of

AmpC, impermeability, or efflux pump was detected in CG1212, CG1249, and other strains (Liu et al., 2021). In addition, carbapenemase was found to coexist with other ESBP genes, such as *bla*_{TEM-1}, *bla*_{CTX-M-1}, *bla*_{CTX-M-9}, *bla*_{CTX-M-14}, *bla*_{SHV}, and *bla*_{TEM-1}, as well as the outer membrane porin-encoding genes *ompC* and *ompF* in several strains (Table 2).

SS CZA Medium Demonstrated a Great Ability for Screening CZA Resistance Among the CRE Isolates

The results of the SS CZA medium toward the detection of CZA-resistant and CZA-susceptible CRE isolates are shown in Table 2 and Figure 1. All CZA-resistant and -susceptible CRE isolates could be recovered within 24 h on SS medium and LB medium plates by using an inoculum of 10^1 – 10^8 CFU/ml. For CZA-resistant CRE isolates, they could be recovered within 24 h on SS CZA medium even at the low dilution gradient of 10^1 to 10^2 CFU/ml (below the cutoff value). In contrast, growth of the CZA-susceptible CRE isolates was inhibited within 24–48 h on SS CZA medium even at the highest dilution gradient of 10^8 CFU/ml (above the cutoff value). Furthermore, we assessed the ability of the SS CZA medium to screen the CZA-resistant CRE isolates from clinically simulated specimens. As expected, the clinically simulated stool samples with CZA-resistant CRE

isolates could grow on the SS CZA medium within 24 h using an inoculum of 10^1 to 10^3 CFU/ml (not greater than the cutoff value). In contrast, the clinically simulated stool samples with CZA-susceptible CRE isolates did not grow within 24–48 h even with an inoculum size of 10^8 CFU/ml (above the cutoff value). With the same cutoff value (setting at 1×10^3 CFU/ml), the lower detection limit for pure CZA-resistant CRE strains and clinically simulated stool samples with CZA-resistant CRE isolates ranged from 10^1 to 10^2 and 10^1 to 10^3 CFU/ml, respectively. In contrast, the lower detection limit for the pure CZA-susceptible isolates and clinically simulated stool samples with the CZA-susceptible isolates was $>10^8$ CFU/ml. These data indicate that the sensitivity and specificity of the SS CZA-selective medium for detecting CZA-resistant CRE isolates was 100% (using the same cutoff value, setting at 1×10^3 CFU/ml), both in pure clinical strain specimens and clinically simulated stool samples with CZA-resistant CRE isolates.

SS CZA Medium Had Great Storage Stability

In addition, the storage stability of the SS CZA medium was evaluated as per the method of Sadek et al. The reference strains (*Staphylococcus aureus* ATCC 25923, *Enterococcus faecalis* ATCC 29212, *E. coli* ATCC 25922, and *K. pneumoniae* ATCC 700603) were selected and subcultured every day onto the SS CZA medium from a single batch of medium stored at 4°C. No visible bacterial growth was observed for at least a 7-day period.

DISCUSSION

We designed an SS CZA medium based on the work of Sadek et al., albeit with some modifications (Sadek et al., 2020). Specifically, the SS agar medium is a strong selective medium containing sodium citrate and bile salts to inhibit the growth of *Candida* and Gram-positive bacteria, such as *Staphylococcus* and *Enterococcus* strains. Unlike the SuperCAZ/AVI medium, certain antibiotics that inhibit the growth of fungi and Gram-positive bacteria, such as amphotericin B and daptomycin, are not required to be added specifically to the SS CZA medium. Therefore, when compared with the SuperCAZ/AVI medium, our SS CZA medium eliminates several operational steps and saves on the incurred costs (only CZA needs to be added into the SS agar medium).

Next, we tested the performance of the SS CZA medium for screening CZA resistance among CRE. Consistent with the results of Sadek et al. (2020), we found that the lower detection limits for CZA-resistant CRE isolates were 10^1 to 10^3 CFU/ml. Moreover, all CZA-susceptible strains could grow on the LB and SS agar medium at the inoculum size of 10^1 to 10^8 CFU/ml, but not on the SS CZA medium plates, including strains showing an MIC close to that of the resistant breakpoint (such as FK-6733, DC-11497, and CG-1208 with an MIC at 8, 4, and 8 µg/ml, respectively), despite extending the incubation period to 48 h. However, different from the report of Sadek et al., which showed that the lower detection limits for CZA-susceptible *E. coli* and *K. pneumoniae* were 10^7 to $>10^8$ CFU/ml and 10^5 to $>10^8$ CFU/ml,

respectively, our study showed the lower detection limits for all CZA-susceptible isolates (including *E. coli* and *K. pneumoniae*) as both $>10^8$ CFU/ml. Given that the bacterial load in different clinical specimens is not consistent, a low detection limit of the SS CZA screening medium is more conducive to successful clinical application. Cumulatively, these data indicate that the SS CZA medium developed in this study contributes to an effective screening of CZA-resistant strains directly from clinical specimens and has significant clinical application value with the potential for development from the commercial perspective.

Most screening methods for CRE are performed with rectal swab specimens, which is a polymicrobial specimen. We, therefore, tested spiked stools with the same representative collection of CZA-resistant and CZA-susceptible CRE isolates using our SS CZA medium. As expected, the screening effect for simulated clinical specimens was similar to that of pure clinical isolates; the lower detection limits for stools containing the CZA-susceptible isolates and CZA-resistant isolates were $>10^8$ CFU/ml and 10^1 to 10^3 CFU/ml. These results implicate that the SS CZA medium is a promising selective medium for rapid and direct screening of clinical specimens suspected to contain CZA-resistant strains.

However, there are some limitations to our study. For instance, the SS CZA medium cannot give the exact MIC value, although it can help assign the susceptibility and resistance category quite rapidly, which is closely related to clinical medicine. In addition, we did not assess the screening effect of the SS CZA medium on *P. aeruginosa* or other Gram-negative bacteria, which should be explored in future studies.

CONCLUSION

The proposed SS CZA medium exhibited a significant performance for screening CZA-resistant CRE isolates with 100% sensitivity and specificity. Its screening performance was unaffected by the difference in the resistance determinants. In fact, the bacterial load of different clinical specimens was not consistent, and the low detection limit of the SS screening medium was found to be more conducive to its successful clinical application.

DATA AVAILABILITY STATEMENT

The original contributions presented in the study are included in the article/supplementary material, further inquiries can be directed to the corresponding author/s.

AUTHOR CONTRIBUTIONS

WZ conducted the experiments, analyzed the data, and wrote the manuscript. WL, YZ, and LW participated in experiments. HS and HJ took part in the analysis of results. TC and YZ participated in the analysis of results. TZ and QW helped design the study. All authors contributed to the article and approved the submitted version.

REFERENCES

- Ackley, R., Roshdy, D., Meredith, J., Minor, S., Anderson, W. E., Capraro, G. A., et al. (2020). Meropenem-Vaborbactam versus Ceftazidime-Avibactam for Treatment of Carbapenem-Resistant Enterobacteriaceae Infections. *Antimicrob. Agents Chemother.* 64:e02313-19. doi: 10.1128/aac.02313-19
- Aleem, M., Azeem, A. R., Rahmatullah, S., Vohra, S., Nasir, S., and Andleeb, S. (2021). Prevalence of bacteria and antimicrobial resistance genes in hospital water and surfaces. *Cureus* 13, e18738. doi: 10.7759/cureus.18738
- Caston, J. J., Lacort-Peralta, I., Martin-Davila, P., Loeches, B., Tabares, S., Temkin, L., et al. (2017). Clinical efficacy of ceftazidime/avibactam versus other active agents for the treatment of bacteremia due to carbapenemase-producing Enterobacteriaceae in hematologic patients. *Int. J. Infect. Dis.* 59, 118–123. doi: 10.1016/j.ijid.2017.03.021
- Frolich, C., Sorum, V., Thomassen, A. M., Johnsen, P. J., Leiros, H. S., and Samuelsen, O. (2019). OXA-48-mediated ceftazidime-avibactam resistance is associated with evolutionary trade-offs. *mSphere* 4:e00024-19. doi: 10.1128/mSphere.00024-19
- Haidar, G., Clancy, C. J., Shields, R. K., Hao, B., Cheng, S., and Nguyen, M. H. (2017). Mutations in blaKPC-3 that confer ceftazidime-avibactam resistance encode novel KPC-3 variants that function as extended-spectrum beta-lactamases. *Antimicrob. Agents Chemother.* 61:e02534-16. doi: 10.1128/AAC.02534-16
- Hemrajata, P., and Humphries, R. M. (2019). Ceftazidime/avibactam resistance associated with L169P mutation in the omega loop of KPC-2. *J. Antimicrob. Chemother.* 74, 1241–1243. doi: 10.1093/jac/dkz026
- Koren, S., Walenz, B. P., Berlin, K., Miller, J. R., Bergman, N. H., and Phillippy, A. M. (2017). Canu: scalable and accurate long-read assembly via adaptive -mer weighting and repeat separation. *Genome Res.* 27, 722–736. doi: 10.1101/gr.215087.116
- Krapp, F., Grant, J. L., Sutton, S. H., Ozer, E. A., and Barr, V. O. (2017). Treating complicated carbapenem-resistant enterobacteriaceae infections with ceftazidime/avibactam: a retrospective study with molecular strain characterisation. *Int. J. Antimicrob. Agents* 49, 770–773. doi: 10.1016/j.ijantimicag.2017.01.018
- Liu, S., Huang, N., Zhou, C., Lin, Y., Zhang, Y., Wang, L., et al. (2021). Molecular mechanisms and epidemiology of carbapenem-resistant enterobacter cloacae complex isolated from Chinese patients during 2004–2018. *Infect. Drug Resist.* 14, 3647–3658. doi: 10.2147/idr.S327595
- Livermore, D. M., Mushtaq, S., Doumith, M., Jamroz, D., Nichols, W. W., and Woodford, N. (2018). Selection of mutants with resistance or diminished susceptibility to ceftazidime/avibactam from ESBL- and AmpC-producing Enterobacteriaceae. *J. Antimicrob. Chemother.* 73, 3336–3345. doi: 10.1093/jac/dky363
- Nordmann, P., Girlich, D., and Poirel, L. (2012). Detection of carbapenemase producers in Enterobacteriaceae by use of a novel screening medium. *J. Clin. Microbiol.* 50, 2761–2766. doi: 10.1128/jcm.06477-11
- Prater, A. G., Mehta, H. H., Kosgei, A. J., Miller, W. R., Tran, T. T., Arias, C. A., et al. (2019). Environment shapes the accessible daptomycin resistance mechanisms in *Enterococcus faecium*. *Antimicrob. Agents Chemother.* 63:e00790-19. doi: 10.1128/AAC.00790-19
- Sadek, M., Poirel, L., Tinguely, C., and Nordmann, P. (2020). A selective culture medium for screening ceftazidime-avibactam resistance in Enterobacterales and *Pseudomonas aeruginosa*. *J. Clin. Microbiol.* 58:e00965-20. doi: 10.1128/jcm.00965-20
- Shields, R. K., Chen, L., Cheng, S., Chavda, K. D., Press, E. G., Snyder, A., et al. (2017). Emergence of ceftazidime-avibactam resistance due to plasmid-borne blaKPC-3 mutations during treatment of carbapenem-resistant *Klebsiella pneumoniae* infections. *Antimicrob. Agents Chemother.* 61:e02097-16. doi: 10.1128/AAC.02097-16
- Shields, R. K., Potoski, B. A., Haidar, G., Hao, B., Doi, Y., Chen, L., et al. (2016). Clinical outcomes, drug toxicity, and emergence of ceftazidime-avibactam resistance among patients treated for carbapenem-resistant Enterobacteriaceae infections. *Clin. Infect. Dis.* 63, 1615–1618. doi: 10.1093/cid/ciw636
- Tumbarello, M., Trecarichi, E. M., Corona, A., De Rosa, F. G., Bassetti, M., Mussini, C., et al. (2019). Efficacy of ceftazidime-avibactam salvage therapy in patients with infections caused by *Klebsiella pneumoniae* carbapenemase-producing *K. pneumoniae*. *Clin. Infect. Dis.* 68, 355–364. doi: 10.1093/cid/ciy492
- van Duin, D., Arias, C. A., Komarow, L., Chen, L., Hanson, B. M., Weston, G., et al. (2020). Molecular and clinical epidemiology of carbapenem-resistant Enterobacterales in the USA (CRACKLE-2): a prospective cohort study. *Lancet Infect. Dis.* 20, 731–741. doi: 10.1016/s1473-3099(19)30755-8
- Winkler, M. L., Papp-Wallace, K. M., Taracila, M. A., and Bonomo, R. A. (2015). Avibactam and inhibitor-resistant SHV beta-lactamases. *Antimicrob. Agents Chemother.* 59, 3700–3709. doi: 10.1128/AAC.04405-14
- Zhang, W., Guo, Y., Li, J., Zhang, Y., Yang, Y., Dong, D., et al. (2018). In vitro and in vivo bactericidal activity of ceftazidime-avibactam against Carbapenemase-producing *Klebsiella pneumoniae*. *Antimicrob. Resist. Infect. Control* 7, 142. doi: 10.1186/s13756-018-0435-9

Conflict of Interest: The authors declare that the research was conducted in the absence of any commercial or financial relationships that could be construed as a potential conflict of interest.

Publisher's Note: All claims expressed in this article are solely those of the authors and do not necessarily represent those of their affiliated organizations, or those of the publisher, the editors and the reviewers. Any product that may be evaluated in this article, or claim that may be made by its manufacturer, is not guaranteed or endorsed by the publisher.

Copyright © 2022 Zeng, Liao, Zhao, Wang, Shu, Jia, Chen, Zhang, Zhou and Wu. This is an open-access article distributed under the terms of the Creative Commons Attribution License (CC BY). The use, distribution or reproduction in other forums is permitted, provided the original author(s) and the copyright owner(s) are credited and that the original publication in this journal is cited, in accordance with accepted academic practice. No use, distribution or reproduction is permitted which does not comply with these terms.



A New Perspective on the Antimicrobial Mechanism of Berberine Hydrochloride Against *Staphylococcus aureus* Revealed by Untargeted Metabolomic Studies

Shu Wu^{1†}, Kun Yang^{1†}, Yuhang Hong², Yanju Gong¹, Jiajia Ni^{3,4}, Ni Yang¹ and Weijun Ding^{1*}

¹ School of Basic Medical Sciences, Chengdu University of Traditional Chinese Medicine, Chengdu, China, ² Key Laboratory of Application of Ecology and Environmental Protection in Plateau Wetland of Sichuan, Xichang University, Xichang, China, ³ Research and Development Center, Guangdong Meilong Bio-Sciences Ltd., Dongguan, China, ⁴ Dongguan Key Laboratory of Medical Bioactive Molecular Development and Translational Research, Guangdong Medical University, Dongguan, China

OPEN ACCESS

Edited by:

Vinayak Singh,
University of Cape Town, South Africa

Reviewed by:

Anand Anbarasu,
VIT University, India
Karishma R. Pardesi,
Savitribai Phule Pune University, India

*Correspondence:

Weijun Ding
Dingweijun@cdutcm.edu.cn

[†]These authors have contributed
equally to this work and share first
authorship

Specialty section:

This article was submitted to
Antimicrobials, Resistance and
Chemotherapy,
a section of the journal
Frontiers in Microbiology

Received: 11 April 2022

Accepted: 09 June 2022

Published: 13 July 2022

Citation:

Wu S, Yang K, Hong Y, Gong Y, Ni J,
Yang N and Ding W (2022) A New
Perspective on the Antimicrobial
Mechanism of Berberine
Hydrochloride Against
Staphylococcus aureus Revealed by
Untargeted Metabolomic Studies.
Front. Microbiol. 13:917414.
doi: 10.3389/fmicb.2022.917414

Berberine hydrochloride (BBR) is a natural product widely used in clinical medicine and animal production. It has a variety of antimicrobial effects, but its complex antimicrobial mechanism has not been clarified. This study aimed to discover the metabolic markers and gain a new perspective on the antibacterial mechanism of BBR. The effects of different inhibitory concentrations of BBR on the survival and growth of standard strain *Staphylococcus aureus* ATCC 25923 were analyzed by the bacteriostatic activity test. Differences in intracellular metabolites of *S. aureus* following 19 $\mu\text{g/ml}$ BBR exposure for 1 h were investigated by combining non-targeted metabolomics techniques of gas chromatography-mass spectrometry (GC-MS) and liquid chromatography-mass spectrometry (LC-MS). The results showed that the minimum inhibitory concentration of BBR against *S. aureus* was 51 $\mu\text{g/ml}$. A total of 368 and 3,454 putative metabolites were identified by GC-MS and LC-MS analyses, respectively. Principal component analysis showed the separation of intracellular metabolite profiles between BBR-exposed samples and non-exposed controls. Pathway activity profiling analysis indicated a global inhibition of metabolisms by BBR exposure, while enhancement was also found in nucleic acid metabolism, amino sugar, and nucleotide sugar metabolism. Several metabolic markers were screened out mainly based on their variable importance of projection values. Two pyridine dicarboxylic acids were significantly downregulated, suggesting the reduction of stress resistance. The oxidized phospholipid (PHOOA-PE) was accumulated, while lipid antioxidant gamma-tocopherol was decreased, and farnesyl PP, the synthetic precursor of another antioxidant (staphyloxanthin), was decreased below the detection threshold. This evidence indicates that BBR reduced the antioxidant capacity of *S. aureus*. Accumulation of the precursors (UDP-GlcNAc, CDP-ribitol, and CDP-glycerol) and downregulation of the key metabolite D-Ala-D-Ala suggest the inhibition of cell wall synthesis, especially the peptidoglycan synthesis. Metabolites involved in the shikimate pathway (such as 3-dehydroshikimate) and downstream

aromatic amino acid synthesis were disturbed. This study provides the first metabolomics information on the antibacterial mechanism of BBR against *S. aureus*. The key metabolic markers screened in this study suggest that the shikimate pathway, staphyloxanthin synthesis, and peptidoglycan biosynthesis are new directions for further study of BBR antibacterial mechanism in the future.

Keywords: GC-MS untargeted metabolomics, LC-MS untargeted metabolomics, natural antimicrobial, metabolic markers, mechanism

INTRODUCTION

Staphylococcus aureus is a common bacterial colonizer of human and a variety of animal species which can cause many infectious diseases, such as mastitis, endocarditis, septic arthritis, and sepsis. In the treatment of infectious diseases, antibiotics were initially highly effective, but they currently show several limitations, including widespread resistance, toxicity, and residues. *S. aureus* has developed resistance to various antibiotics including vancomycin (Ragunathan et al., 2018). We need to understand the resistance mechanism of microorganisms to existing antibiotics and develop antibiotics with new antimicrobial mechanisms (Anitha et al., 2016). As complementary or alternative drugs for the treatment or prevention of infection, natural products such as medicinal plants and their extracted components are a good choice (Herrmann et al., 2016; Newman and Cragg, 2016; Kokoska et al., 2019). Some natural compounds are considered to have multiple potential antimicrobial targets (Miryala et al., 2021, 2022). One of the natural anti-infective products is berberine, which is commonly used in clinical medicine, as well as in livestock production and aquaculture.

Berberine is an isoquinoline alkaloid found mainly in the form of hydrochloride (berberine hydrochloride) in many medicinal plants, such as *Coptis chinensis*, *Phellodendron amurense*, and *Berberis vulgaris* (Imenshahidi and Hosseinzadeh, 2016). It exhibits various pharmacological activities, including prominent anti-inflammatory and anti-infective effects, antagonizing a variety of pathogenic bacteria (including *S. aureus*), fungi, parasites, and even viruses (Shang et al., 2020). Berberine not only can exert an antimicrobial effect by regulating host immunity but also has a significant direct antimicrobial effect. Some experimental evidence shows that berberine alone or in combination with other agents showed obvious antimicrobial effects *in vivo* and *in vitro* (Aksoy et al., 2020; Huang et al., 2020; Xie et al., 2020; Bhatia et al., 2021). Berberine even has the potential to inhibit antibiotic-resistant bacteria (Morita et al., 2016; Zhang et al., 2020; Li et al., 2021), which gives it great potential in the development of new antibiotics. There are many studies on the antimicrobial activity of berberine, and it is found that berberine has a variety of antimicrobial effects. A multi-omics study suggests that berberine may interfere with the nucleic acid, cell wall, cell membrane transport, and motility functions of *Escherichia coli* and inhibit its metabolism (Karaosmanoglu et al., 2014). A recent study has shown that berberine can destroy the cell wall structure and cell membrane integrity of methicillin-resistant *Staphylococcus aureus* (MRSA)

and play a synergistic antimicrobial role with clindamycin or rifamycin (Xia et al., 2022). In addition, a few studies have suggested other possible antimicrobial mechanisms of berberine, including the inhibition of biofilm formation, protein synthesis, and bacterial division (Boberek et al., 2010; Li et al., 2011). However, the pathway and potential targets of berberine causing these antibacterial effects are unclear. A more clear direction is needed to further study the complex antimicrobial molecular mechanism of berberine.

Analyzing the expression changes of specific genes in microorganisms is a common method to explain the antimicrobial effect of berberine. The intervention on gene expression level (including transcription and protein synthesis) may be indirect, so it is difficult to explain the antimicrobial mechanism of berberine. Metabolites are the final products of gene expression, and the metabolic alterations represent the exact physiological state of microorganisms (Dorries et al., 2014). Thus, the response of microorganisms to a given antibiotic stress at the metabolic level can help us better understand the antibacterial mechanisms. Several studies have used metabolomics technology to study the antimicrobial mechanism of antibiotics (Dorries et al., 2014; Schelli et al., 2017; Vemula et al., 2017) and natural products (Hussein et al., 2020; Shen et al., 2020; Tang et al., 2021; Chen et al., 2022). However, we have not read any report on the antimicrobial mechanism of berberine based on metabolomics. In this study, berberine hydrochloride (BBR) was used as the representative form of berberine, and we attempted to explore a new perspective of antimicrobial mechanism of berberine by using metabolomics technology. Two untargeted metabolomics techniques, namely, gas chromatography-mass spectrometry (GC-MS) and liquid chromatography-mass spectrometry (LC-MS), were combined to explore the antimicrobial mechanism of BBR against *S. aureus* through extensive screening of metabolic markers and analysis of related metabolic pathways.

MATERIALS AND METHODS

Reagents, Bacterial Strain, and Culture Conditions

The BBR (HPLC \geq 98%) and vancomycin (potency \geq 900 μ g/mg) were purchased from Desite Bio-Tech Co., Ltd. (Chengdu, CHN) and Solarbio Bio-Tech Co., Ltd. (Beijing, CHN), respectively, and were dissolved in sterilized ultra-pure water before use. The reagents used in the preparation of culture medium were purchased from Aoboxing Bio-Tech Co., Ltd. (Beijing, CHN). The standard strain *S. aureus* ATCC 25923 was

purchased from the Biobw Culture Collection (Beijing, CHN). Before use, the strain was subcultured onto nutrient agar plates for 24 h at 37°C. Then, the single colony was selected and coated on a nutritious agar plate to grow for 7 h, and the culture would be used as a “seed” to cultivate working bacteria culture (WBC) for subsequent experiments. For the preparation of WBC, the “seed” was inoculated into the broth medium (composed of 1% tryptone, 0.3% beef extract powder, and 0.5% sodium chloride, pH ~ 7.4) with an initial inoculation dose of 10^7 CFU/ml and then cultured with shaking at 37°C and 120 rpm for ~2.5 h to enter the logarithmic growth phase ($OD_{600} \sim 0.3$).

MIC and MBC Test

The MIC value was determined by the improved broth dilution method to improve the test sensitivity (Surre et al., 2018). A small amount of phenol red (0.018 g/L) and glucose (0.5 %) were added to the broth for the test (containing 1% tryptone, 0.1% beef extract powder, 0.5% sodium chloride, pH ~ 7.4). The basic principle of the test is that bacteria grow to produce acid by fermenting glucose, which makes the broth turn yellow from the original red color. The operation method is similar to that of the traditional broth dilution method except that color change and turbidity change are combined as the basis for judging whether the bacteria grow or not. Generally speaking, the phenol red-containing broth added with a certain concentration of BBR was diluted in a series of gradients and used for the culture of *S. aureus* ($\sim 10^8$ CFU/ml) at 37°C. The lowest BBR concentration without visible color change and turbidity change within 24 h was MIC. The bacterial cultures exposed to different concentrations of berberine for 24 h were coated on nutrient agar plates and cultured at 37°C for 24 h. The MBC was determined by the lowest berberine concentration without bacterial growth.

Antibacterial Effect Test

The WBC ($OD_{600} \sim 0.3$) was diluted with the same volume of broth medium containing BBR to give an approximate starting inoculum of 10^8 CFU/ml and to obtain final BBR concentrations of $1/4 \times \text{MIC}$, $3/8 \times \text{MIC}$, $1/2 \times \text{MIC}$, or MIC. The control culture was added with the same volume of broth medium without BBR. The cultures were incubated further for 8 h, and cell growth was monitored spectrophotometrically ($OD_{600\text{nm}}$ at 1 h intervals). Time kill tests of the above BBR concentrations were assessed by counting CFU (Lobritz et al., 2015). WBC was incubated in different concentrations of BBR at 37°C for 30 min. Bacterial cells were collected by centrifugation and washed two times with 0.85% sterile saline and then stained for 15 min using Live/Dead BacLight bacterial viability kit (Invitrogen, Eugene, OR, USA) according to the manufacturer's instructions and imaged by Image Xpress Micro Confocal (Molecular Devices LLC, Sunnyvale, CA).

Cultivation of Metabolic Samples

The BBR concentration ($3/8 \times \text{MIC}$, 19 µg/ml) and exposure time (1 h) for the treatment of metabolic samples were determined by the result of time kill tests. The culture conditions were the same as the antibacterial effect test. Therefore, metabolic samples (group T1) were collected at the 1-h time point after

being exposed to 19 µg/ml BBR. Two control groups (without BBR addition) collected at zero time point were treated as the initial control group (C0) and those collected 1 h later were treated as the growth control group (C1).

Intracellular Metabolites Extraction

Intracellular metabolites were extracted using cold methanol and chloroform (Stipetic et al., 2016). Briefly, after co-incubation with or without BBR, 80 ml of bacterial culture from each biological sample (six biological replicates for each group) was collected. The bacterial cells were harvested by 4°C cryogenic centrifugation at 6,000 rpm for 10 min, followed by cold phosphate buffer saline (PBS) washes. A total of 1 ml cold methanol:water (4:1, v/v) and 200 µl of chloroform were added to the cell pellet, and the mixtures were vortexed. After that, cells were broken up with an ultrasonic homogenizer (3 min, 500 W), and 20 µl of L-2-chlorophenylalanine (0.3 mg/ml) was added as the internal standard. Then, the mixture was extracted by ultrasonic for 20 min in ice-water bath and then centrifuged at 4°C (13,000 rpm) for 10 min. Finally, 200 µl of the supernatant for GC-MS (or 400 µl for LC-MS) was dried in a freeze concentration centrifugal dryer. Quality control sample (QC) was prepared by mixing an aliquot of all samples to be a pooled sample.

Untargeted Metabolomics Analyses

A Thermo Trace 1310/TSQ 9000 GC/MSD System was used for GC-MS analysis. DB-5MS fused-silica capillary column (30 m \times 0.25 mm \times 0.25 µm) was utilized to separate the derivative metabolites. For LC-MS analysis, the freeze-dried samples were re-extracted and analyzed by a Nexera UPLC system coupled with Q Exactive quadrupole-orbitrap mass spectrometer equipped with heated electrospray ionization (ESI) source. An ACQUITY UPLC HSS T3 column (1.8 µm, 2.1 \times

TABLE 1 | Classification statistics of identified metabolites.

Super Class of metabolites	GC-MS	LC-MS	Total
Lipids and lipid-like molecules	62	637	698
Organic acids and derivatives	76	384	460
Organoheterocyclic compounds	38	265	303
Organic oxygen compounds	56	227	283
Benzenoids	31	195	226
Phenylpropanoids and polyketides	13	111	124
Nucleosides, nucleotides, and analogs	15	77	92
Organic nitrogen compounds	12	30	42
Organosulfur compounds	0	25	25
Hydrocarbons	1	17	18
Alkaloids and derivatives	1	11	12
Homogeneous non-metal compounds	3	2	5
Organohalogen compounds	0	4	4
Lignans, neolignans and related compounds	0	2	2
Organic 1,3-dipolar compounds	0	1	1
Organometallic compounds	0	1	1
Unclassified	61	1,465	1,526

100 mm) was employed in both positive and negative modes. Metabolome analysis was performed by Lu-Ming Biotech Co. Ltd. (Shanghai, China) [see details in the supporting information (Supplementary Text 1)].

Metabolome Data Processing

The MS-DIAL software was used to preprocess GC-MS data. Metabolite characterization is based on the LUG database (a self-built untargeted database of GC-MS from Lu-Ming Bio). All peak signal intensities in each sample were segmented and normalized according to the internal standards with RSD > 0.3 after screening. LC-MS data were processed by software Progenesis QI V2.3. Main parameters of 5 ppm precursor tolerance, 10 ppm product tolerance, and 5% production threshold were applied. Compound identification was based on the precise mass-to-charge ratio (m/z), secondary fragments, and isotopic distribution using HMDB, Lipidmaps (V2.3), Metlin, EMD, PMDB, and self-built databases to do qualitative analysis. Peaks with a missing value (ion intensity = 0) in more than 50% of groups were removed. Zero value was replaced by half of the minimum value. Compounds with resulting scores below 36 (out of 60) points were deemed to be inaccurate and removed.

Statistical Analyses

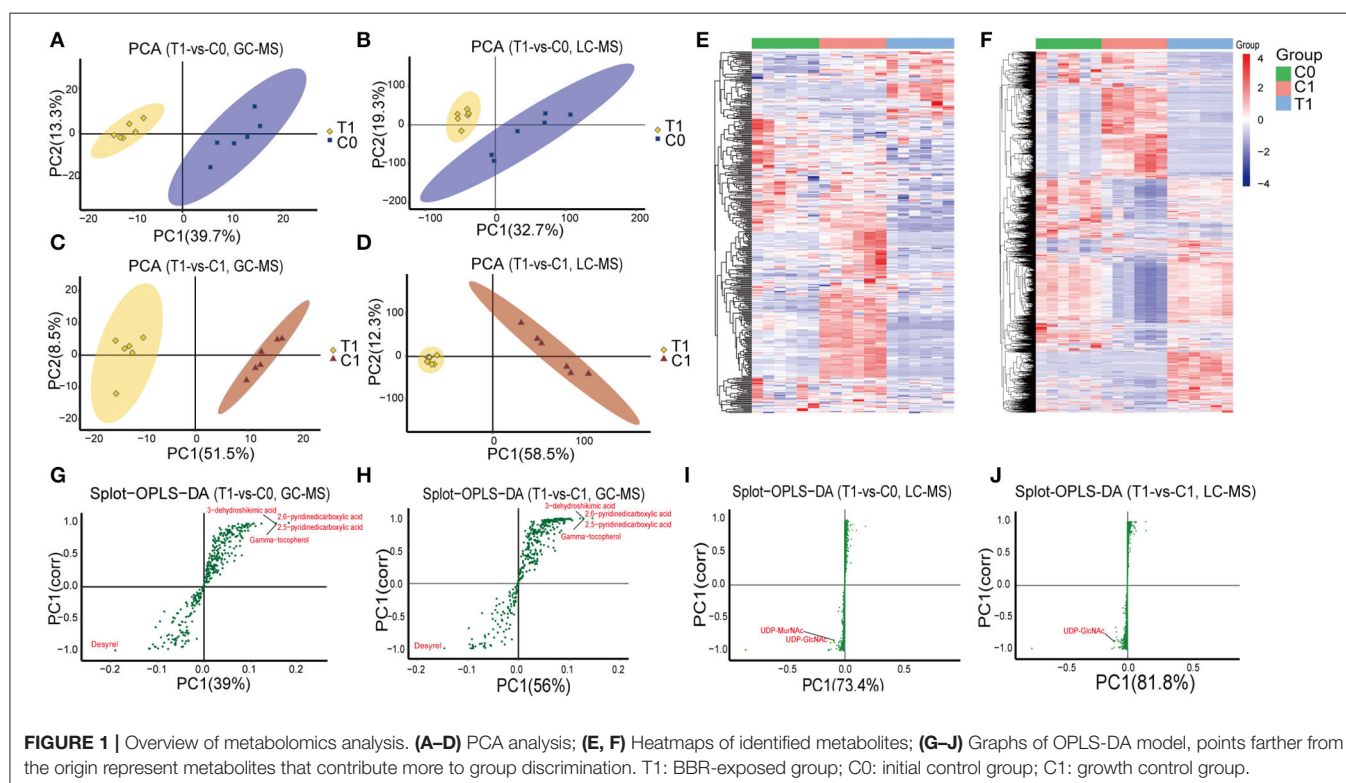
The data matrix of the metabolome was imported in R to carry out principle component analysis (PCA) and orthogonal partial least-squares-discriminant analysis (OPLS-DA). To prevent overfitting, 7-fold cross-validation and 200 response permutation testing (RPT) were carried out to evaluate the quality of

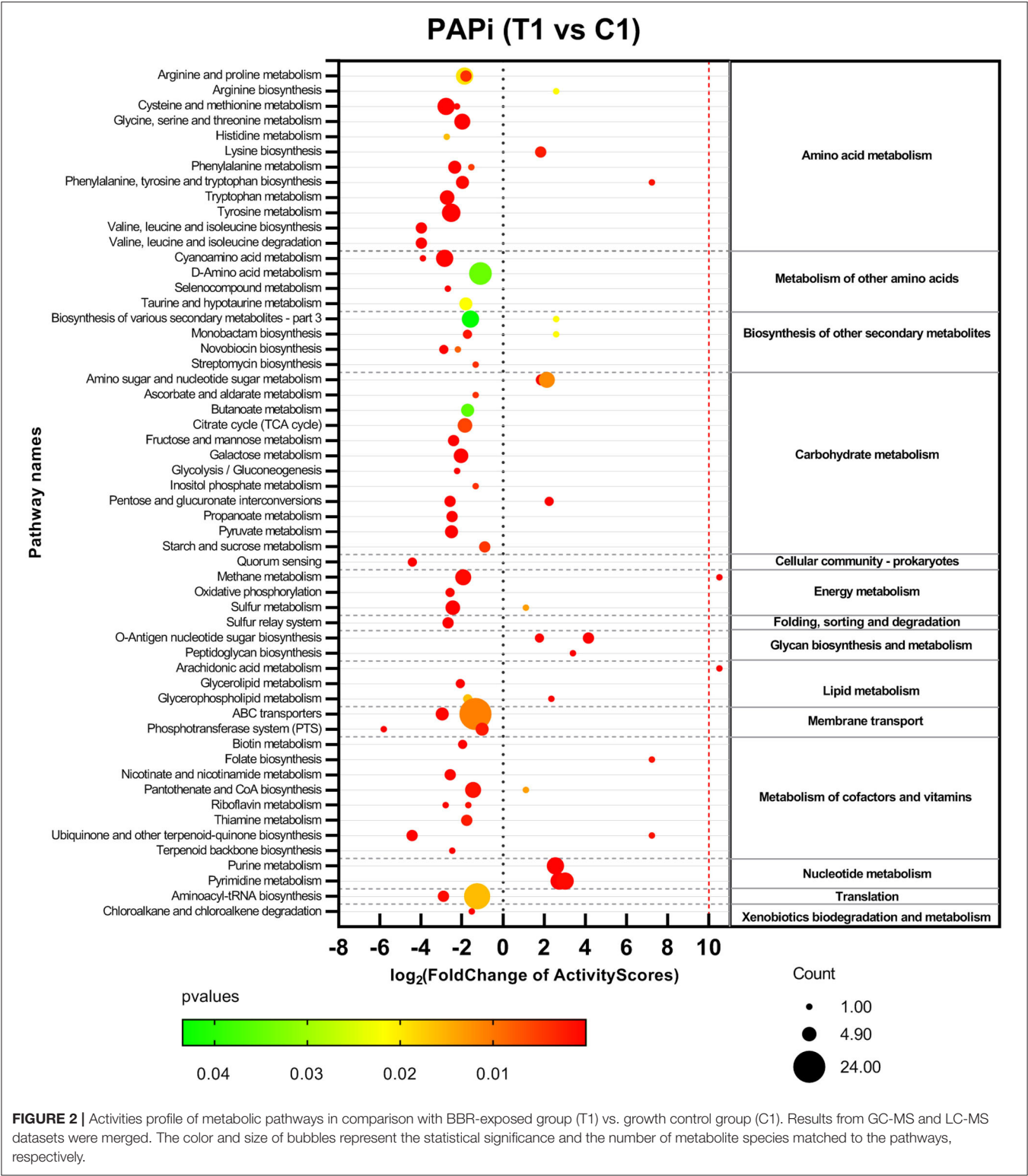
the OPLS-DA models. Variable importance of projection (VIP) values obtained from the OPLS-DA model were used to rank the overall contribution of each variable to group discrimination. A two-tailed Student's T -test was further used to verify whether the metabolites of difference between the two groups were significant. P -value adjustment was performed using the Benjamini-Hochberg method (false discovery rate). Heatmaps (hierarchical clustering) were plotted by <http://www.bioinformatics.com.cn>, a free online platform for data analysis and visualization. Metabolomics datasets and metabolic pathway activities were correlated using the pathway activity profiling (PAPi) algorithm (Aggio, 2014). Only the significant metabolites (VIP > 1, FC > 2, $P < 0.05$ and adj. $P < 0.05$) were analyzed by the PAPi_1.8.0 package in R.

RESULTS

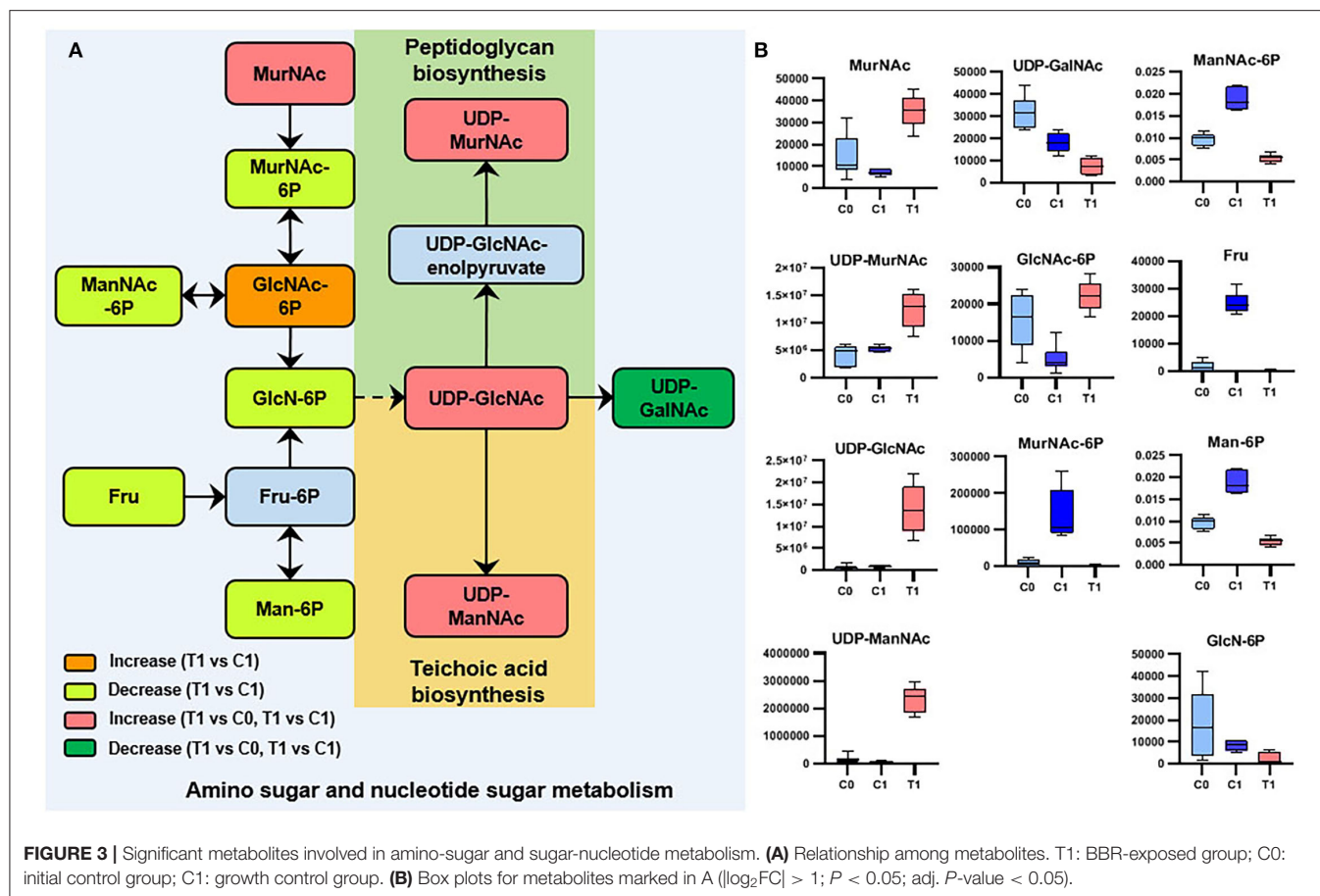
Activity of BBR Against *S. aureus*

The MIC value of BBR against *S. aureus* strain ATCC 25923 was 51 $\mu\text{g/ml}$, and the MBC value was two times the value of MIC (102 $\mu\text{g/ml}$). When combined with vancomycin, BBR of $1/2 \times \text{MIC}$ (25.5 $\mu\text{g/ml}$) halved the MIC value (2 $\mu\text{g/ml}$) of vancomycin against *S. aureus* strain ATCC 25923 (Supplementary Figure 1). Fluorescent staining of live and dead bacterial cells showed that BBR had a significant inhibitory effect on the survival of *S. aureus* (Supplementary Figure 2). BBR inhibited the growth of *S. aureus* in a concentration-dependent manner. No obvious growth trend was observed in *S. aureus* exposed to MIC and $1/2 \times \text{MIC}$ of BBR, while moderate inhibition





and mild inhibition were mediated by $3/8 \times \text{MIC}$ and $1/4 \times \text{MIC}$, respectively (Supplementary Figure 3A). Based on the results of time-kill test (Supplementary Figure 3B), BBR concentration and exposure time for the treatment of metabolic samples were determined. The exposure time of 1 h was chosen because BBR had shown obvious bactericidal activity at this time (Supplementary Figure 3B); $3/8 \times \text{MIC}$ ($19 \mu\text{g/ml}$) was a suitable exposure concentration to minimize cell death at the 1-h



time point and to achieve an obvious bacteriostatic effect at later time points (Supplementary Figure 3B).

Metabolite Profiles

A total of 368 and 3,454 putative metabolites were identified, respectively, from GC-MS and LC-MS datasets. They were divided into 16 super classes including 2,296 classified metabolites and 1,526 unclassified metabolites (Table 1). PCA reviewed a significant separation between controls [initial control (C0) and growth control (C1)] and BBR-exposed group (T1) (Figures 1A–D). A pair of heatmaps demonstrated the characteristic profiles of T1 group (Figures 1E,F). OPLS-DA models showed the importance of each metabolite on group discrimination (Figures 1G–J). Model parameters indicated the excellent prediction ability of the models (Supplementary Table 1), and no overfitting was found (Supplementary Table 1, Supplementary Figure 4).

Key Metabolic Pathways Affected by BBR

Metabolomics datasets and metabolic pathway activities were correlated using PAPI analysis. As compared with control groups, the activities of most metabolic pathways in the T1 group were downregulated (Figure 2, Supplementary Figure 5). The upregulated metabolic pathways were mainly nucleic acid metabolism, amino sugar, and nucleotide sugar metabolism, as

well as glycan biosynthesis and metabolism. Similar trends can be seen in the volcanic maps (Supplementary Figure 6). The enhancement of nucleic acid metabolism activity involved the accumulation of nucleotide metabolites (Supplementary Figure 6). The upregulation of amino sugars, nucleotide sugars metabolism, and downstream glycan biosynthesis involved the accumulation of precursor metabolites of glycan biosynthesis, mainly UDP-N-acetylmuramate (UDP-MurNAc), UDP-N-acetylglucosamine (UDP-GlcNAc), and UDP-N-acetyl-D-mannosamine (UDP-ManNAc) (Figure 3).

The Metabolites of Cell Wall Biosynthesis Were Disturbed

We analyzed the potential biological functions of the top five metabolites sorted by VIP values and the related metabolites (Table 2, Supplementary Figure 7). UDP-GlcNAc (a precursor of peptidoglycan and teichoic acid) was one of the VIP-top five metabolites in the LC-MS dataset and was significantly upregulated in the T1 group [$\log_2\text{FC} = 4.6$ (4.0)]. Six other significant metabolites involved in peptidoglycan biosynthesis were identified (Table 2), and their relationships are shown in Figure 4. Downregulated D-alanyl-D-alanine (D-Ala-D-Ala) [$\log_2\text{FC} = -2.4$ (−3.6)]

TABLE 2 | The main molecular markers in BBR-exposed *S. aureus*.

Metabolites	Database	Classification	VIP [T1-vs.-C0 (C1)]	Log ₂ FC [T1-vs.-C0 (C1)]	Main Pathways/Functions
Desyrel	GC-MS	Phenylpiperazines	3.6 (2.8)	8.9 [#] (8.9)*	unknown
2,5-pyridinedicarboxylic acid	GC-MS	Pyridinecarboxylic acids	3.5 (2.8)	−8.3 [#] (−9.0)*	Stress resistance
2,6-pyridinedicarboxylic acid	GC-MS	Pyridinecarboxylic acids	3.5 (2.8)	−8.3 [#] (−9.0)*	Stress resistance
Gamma-tocopherol	GC-MS	Tocopherols	3.0 (2.5)	−6.0 [#] (−6.9)*	Lipid antioxidant
3-dehydroshikimate	GC-MS	Cyclohexenones	3.0 (2.5)	−5.9 [#] (−6.9)*	Shikimate pathway
2',2'-Dimethyl(pyrano-5',6':3:4)-1,5-dihydroxy-6-methoxy-10-methylacridone	LC-MS	Acridones	83.0 (75.7)	12.3 [#] (14.1)*	Unknown
UDP-GlcNAc	LC-MS	Pyrimidine nucleotide sugars	11.9 (10.7)	4.6 [#] (4.0)*	Peptidoglycan and teichoic acid biosynthesis
Gravacridonediol methyl ether	LC-MS	Acridones	11.4 (10.4)	14.6 [#] (16.3)*	Unknown
UDP-MurNAc	LC-MS	Pyrimidine nucleotide sugars	9.1 (7.7)	1.5 [#] (1.2)*	Peptidoglycan and teichoic acid biosynthesis
CDP-ribitol	LC-MS	Nucleotide-alditol	6.7 (6.8)	1.5 [#] (2.2)*	Teichoic acid biosynthesis
UDP-ManNAc	LC-MS	Pyrimidine nucleotide sugars	5.0 (4.7)	4.0 [#] (5.1)*	Teichoic acid biosynthesis
CDP-glycerol	LC-MS	Glycerophospholipids	4.2 (3.9)	2.4 [#] (2.3)*	Teichoic acid biosynthesis
D-Ala-D-Ala	LC-MS	Dipeptides	3.0 (4.8)	−2.4 [#] (−3.6)*	Peptidoglycan biosynthesis
L-Glutamine	GC-MS	Amino acids	1.7 (1.7)	2.1 [#] (3.4)*	Peptidoglycan biosynthesis
Glycine	GC-MS	Amino acids	1.4 (1.3)	−1.9 [#] (−2.0)*	Peptidoglycan biosynthesis
L-Alanine	GC-MS	Amino acids	1.4 (1.5)	−1.4 [#] (−2.7)*	Peptidoglycan biosynthesis
Chorismate	LC-MS	Dicarboxylic acids and derivatives	1.2 (1.1)	6.3 [#] (7.2)*	Shikimate pathway/Phenylalanine, tyrosine and tryptophan biosynthesis/Folate biosynthesis
PHOOA-PE	LC-MS	Oxidized glycerophospholipids	1.2 (1.1)	32.5 [#] (32.5)*	Marker of lipid peroxidation
Farnesyl-PP	LC-MS	Sesquiterpenoids	0.3 (0.3)	−29.5 (−29.3)*	Staphyloxanthin and peptidoglycan biosynthesis

* Statistically significant ($P < 0.05$, adj. P -value < 0.05) for berberine-exposed (T1) group compared with initial control (C0) group.

[#] Statistically significant ($P < 0.05$, adj. P -value < 0.05) for T1 group compared with growth control (C1) group.

restricts the upstream part of peptidoglycan biosynthesis pathway. Farnesyl diphosphate (farnesyl-PP), the precursor metabolite of undecaprenyl pyrophosphate (Und-PP) in the peptidoglycan biosynthesis pathway, was found to be decreased below the detection threshold in the T1 group, while it was detected in all the 12 samples of the control groups [$\log_2\text{FC} = -29.5 (-29.3)$]. L-alanine [$\log_2\text{FC} = -1.4 (-2.7)$] and glycine [$\log_2\text{FC} = -1.9 (-2.0)$] were downregulated, while L-glutamine was accumulated [$\log_2\text{FC} = 2.1 (3.4)$]. The precursors of teichoic acid biosynthesis (UDP-GlcNAc, UDP-ManNAc, CDP-ribitol, and CDP-glycerol) were also accumulated significantly (Table 2, Supplementary Figure 7).

The Metabolites Related to Stress Resistance and Antioxidant Activity Were Significantly Downregulated

The VIP-top five metabolites in GC-MS dataset were desyrel, 2,5-pyridinedicarboxylic acid, 2,6-pyridinedicarboxylic acid, gamma-tocopherol, and 3-dehydroshikimate (Table 2, Supplementary Figure 7). 2,5-pyridinedicarboxylic acid [$\log_2\text{FC} = -8.3 (-9.0)$] and 2,6-pyridinedicarboxylic acid [$\log_2\text{FC} = -8.3 (-9.0)$] were significantly decreased after BBR treatment. They belong to pyridine dicarboxylic acid, which is known to be abundant in bacterial spores and endows spores with stress resistance (Setlow, 2007; Ramirez-Guadiana et al., 2017). Gamma-tocopherol was downregulated in the T1 group

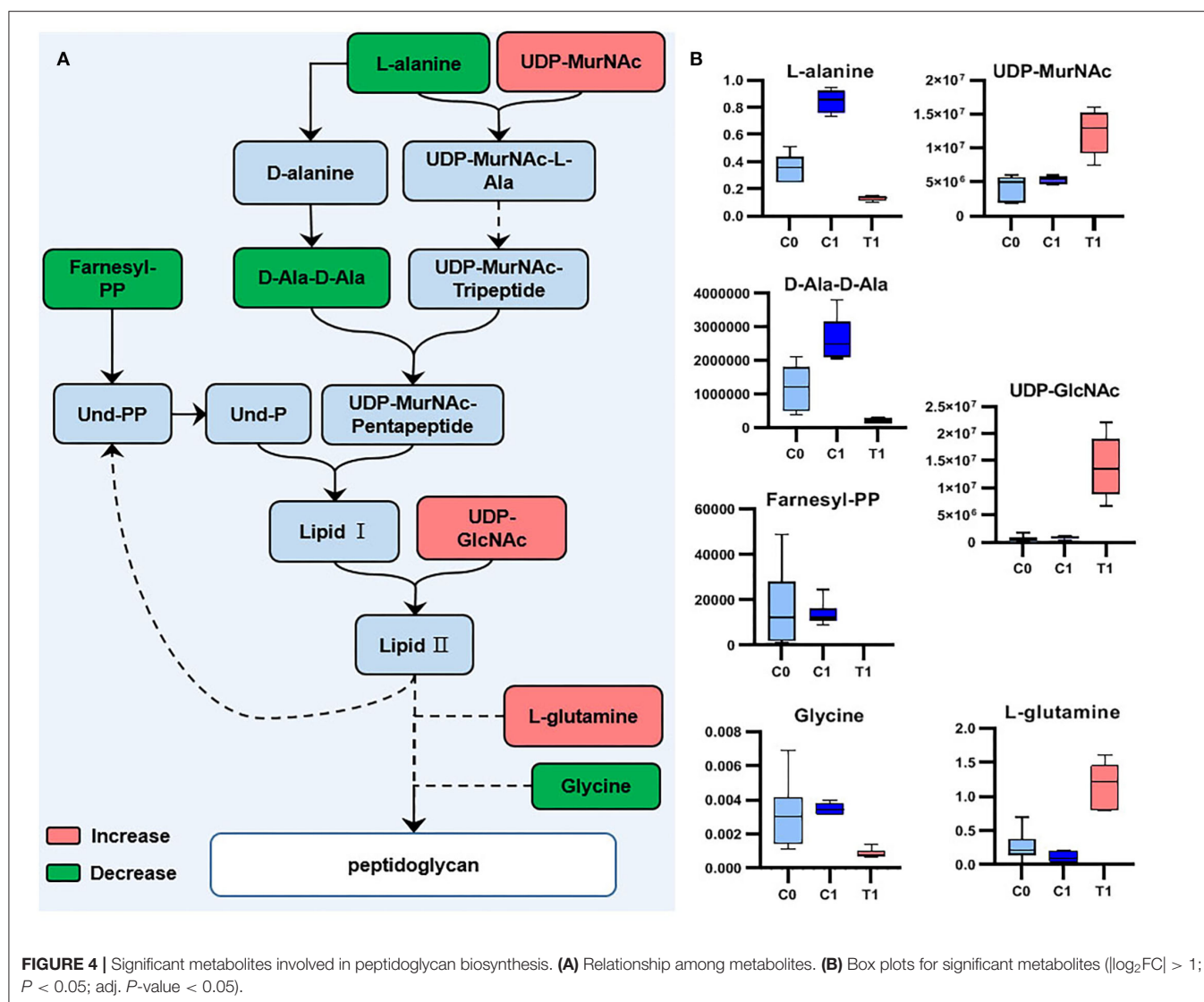


FIGURE 4 | Significant metabolites involved in peptidoglycan biosynthesis. **(A)** Relationship among metabolites. **(B)** Box plots for significant metabolites ($|\log_2FC| > 1$; $P < 0.05$; adj. P -value < 0.05).

$[\log_2FC = -6.0 (-6.9)]$, which is known as a lipid vitamin and acts as an antioxidant (Kim et al., 2012). The decreased farnesyl-PP in the T1 group, as the precursor of Und-PP, is also the precursor of staphyloxanthin (another important antioxidant in *S. aureus*). The oxidized glycerol phospholipid (PHOOA-PE) was not detected in the control groups, but was accumulated in the T1 group ($\log_2FC = 32.5$).

The Metabolites Involved in the Shikimate Pathway and Biosynthesis of Aromatic Amino Acids Were Disturbed

The two metabolites involved in the shikimate pathway, 3-dehydroshikimate [$\log_2FC = -5.9 (-6.9)$] and chorismate [$\log_2FC = 6.3 (7.2)$], showed opposite regulatory trends. L-phenylalanine, L-tyrosine, and L-tryptophan, which were synthesized using chorismate as precursors, were downregulated (Figure 5).

DISCUSSION

According to the existing research, the antibacterial effect of berberine can be generally summarized as “multi-effect” (Karaosmanoglu et al., 2014). Berberine can inhibit the formation of biofilm (Zhang et al., 2020; Bhatia et al., 2021; Xu et al., 2021), destroy the cell wall and cell membrane (Karaosmanoglu et al., 2014; Zhang et al., 2020; Xia et al., 2022), inhibit bacterial cell division (Domadia et al., 2008), inhibit nucleic acid and protein synthesis (Du et al., 2020), and inhibit bacterial adhesion (Kang et al., 2015), etc.

This study revealed that BBR inhibited most of the metabolic activities of amino acid metabolism, carbon metabolism, and energy metabolism in *S. aureus*, while the accumulation of nucleotide metabolites suggested that the synthesis of downstream nucleic acid macromolecules may be inhibited (Figure 2). The metabolic changes in these pathways support the inhibitory effect of berberine on bacterial growth proposed

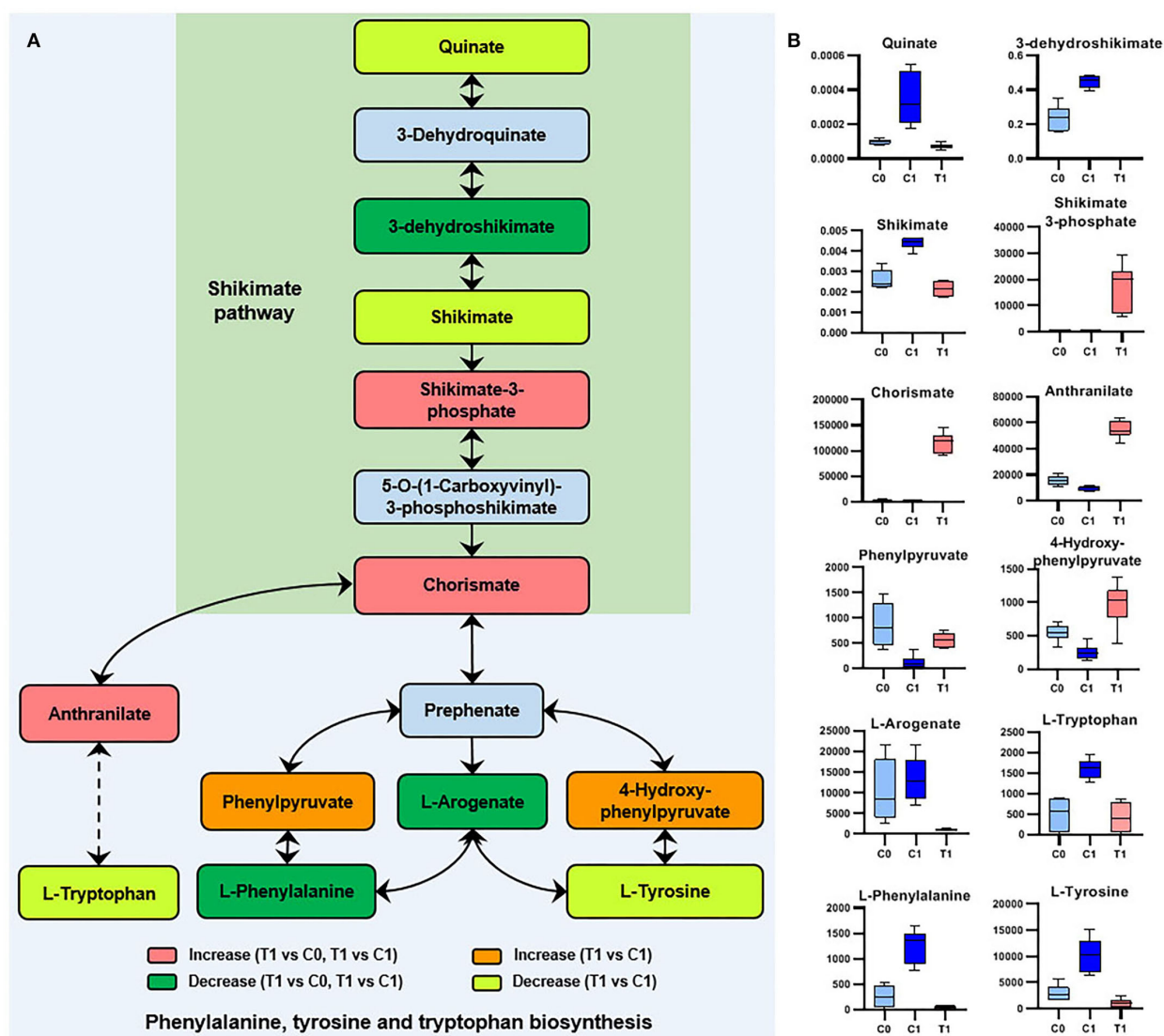


FIGURE 5 | Significant metabolites involved in phenylalanine, tyrosine, and tryptophan biosynthesis. **(A)** Relationship among metabolites. T1: BBR-exposed group; C0: initial control group; C1: growth control group. **(B)** Box plots for metabolites marked in A (|log2FC| > 1; P < 0.05; adj. P-value < 0.05).

by previous studies. However, these metabolic changes are not the unique antimicrobial properties of berberine, as exposure to other antibiotics also causes a general perturbation of bacterial metabolism (Dorries et al., 2014). Berberine and its derivatives inhibit bacterial division by inhibiting the cell division protein FtsZ (Boberek et al., 2010; Sun et al., 2014). Although the results of this study cannot directly verify the target of BBR inhibiting bacterial cell division, the extensive changes in bacterial metabolism caused by BBR may be the result of complex physiological regulation indirectly caused by the inhibition of bacterial cell division and other possible antibacterial activities of BBR.

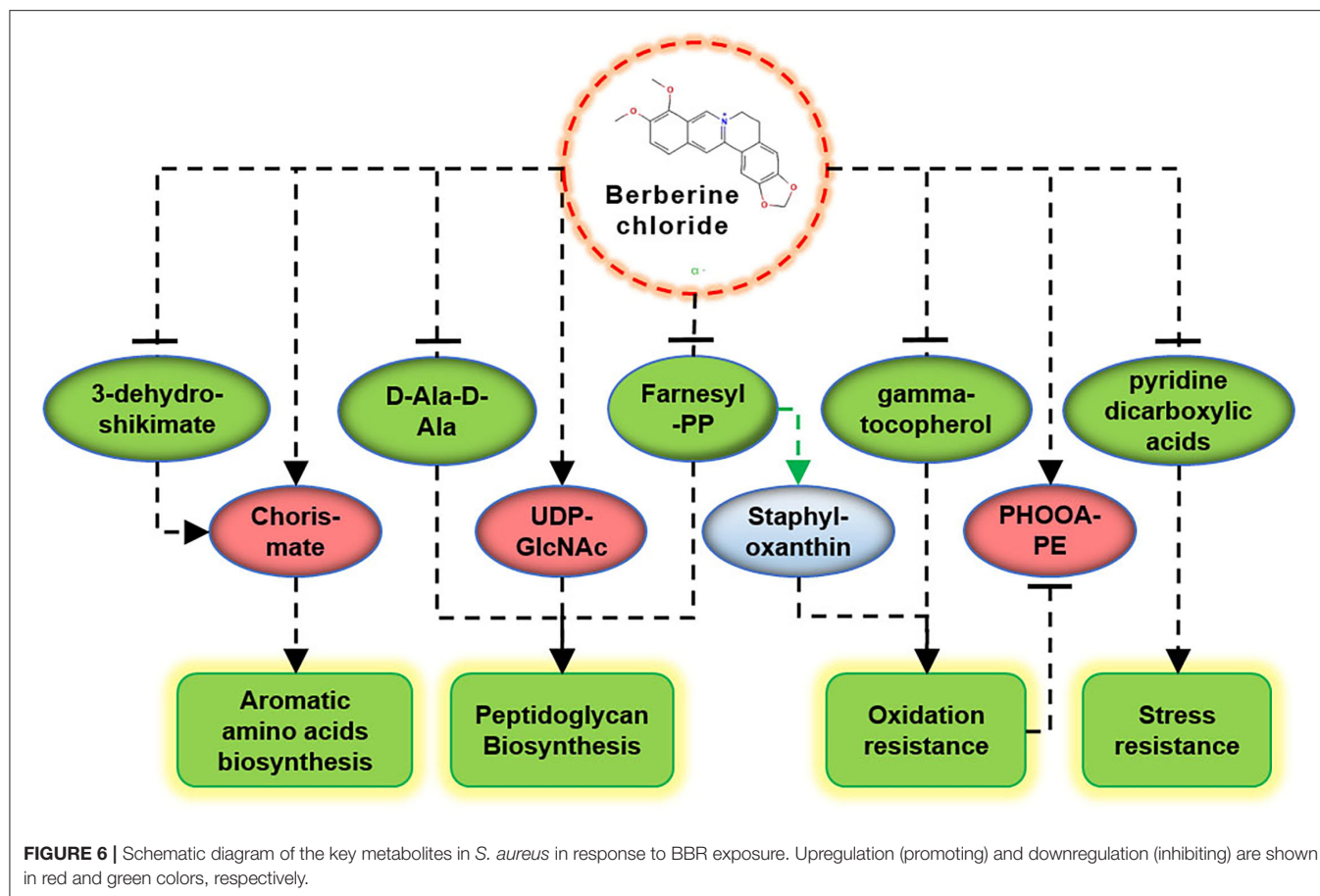
The main metabolic markers screened in this study provide a new perspective for exploring the antibacterial mechanism of BBR, as follows.

Shikimate Pathway

The end product of the shikimate pathway (chorismate) was accumulated (Figure 5), indicating a disturbance in the biosynthesis of downstream aromatic amino acids and folate. In contrast, the intermediate metabolite (3-dehydroshikimate) of the shikimate pathway was significantly downregulated by BBR (Figure 5). Since being essential in bacteria and fungi, but absent from mammals, the shikimate pathway was suggested to be an antimicrobial target (Sadaka et al., 2018). Therefore, it is worthwhile to further study the interference mechanism of BBR on the bacterial shikimate pathway.

Antioxidant Capacity

Bactericidal antibiotics cause bacterial death due to oxidative damage by stimulating the generation of reactive oxygen species



(ROS) (Kohanski et al., 2007), which is also applicable to the action mode of BBR (Du et al., 2020). In this study, some evidence suggests that BBR reduces the antioxidant capacity of *S. aureus*, such as the reduction of gamma-tocopherol and farnesyl-PP, and the accumulation of PHOOA-PE (Figure 6). Gamma-tocopherol reacts with ROS and protects unsaturated fatty acids from oxidation (Kim et al., 2012). Farnesyl-PP is a precursor metabolite of staphyloxanthin that acts as an antioxidant to protect *S. aureus* from being killed by ROS released by leukocytes (Clauditz et al., 2006). The downregulation of gamma-tocopherol and farnesyl-PP means the decrease in antioxidant capacity, and as a result, the oxidized glycerophospholipid (PHOOA-PE) was accumulated in the cells of *S. aureus*. Staphyloxanthin is the main pigment in *S. aureus*, and its accumulation is inhibited by BBR (Supplementary Figure 8). In addition, based on the transcriptome data of our related study (unpublished), the transcription levels of genes involved in staphyloxanthin biosynthesis were also downregulated by BBR (Supplementary Figure 9). The targeted perturbation of staphyloxanthin is expected to restore the sensitivity of drug-resistant strains to traditional antibiotics (Garcia-Fernandez et al., 2017; Hui et al., 2020). Therefore, the attractive potential of BBR to inhibit staphyloxanthin synthesis is another direction worthy of further study.

The synthesis of farnesyl-PP is regulated by other upstream metabolic pathways (Lan et al., 2010). Since BBR interferes with most of the metabolic activities of *S. aureus*, its effect on

the synthesis of farnesyl-PP is complex. As a key precursor metabolite that likes the biosynthesis of staphyloxanthin and peptidoglycan, farnesyl PP affects the abilities of antioxidation and cell wall synthesis, both of which are critical to the survival of *S. aureus*.

Cell Wall Synthesis

A recent study found that berberine can damage the cell walls of MRSA, but the mechanism is unknown (Xia et al., 2022). According to the metabolic responses of *S. aureus* to antibiotics with known targets, the precursor metabolites upstream would accumulate, while the level of metabolites downstream of the inhibited metabolic targets would decrease (Schelli et al., 2017; Vemula et al., 2017). In this study, besides farnesyl PP, the change of other metabolites also demonstrated that BBR act by impairing bacterial cell wall synthesis. The accumulation of precursor metabolites related to cell wall synthesis, such as UDP-GlcNAc, CDP-ribitol and CDP-glycerol, indicated that the downstream synthesis pathways of peptidoglycan and teichoic acid were inhibited. The level of D-Ala-D-Ala was significantly decreased, suggesting the inhibition of BBR to the early stage of peptidoglycan biosynthesis. The synthetic pathway of D-Ala-D-Ala is one of the targets of the cell wall-targeting antibiotics, such as D-cycloserine and D-boroalanine, which act through the inhibition of D-Ala-D-Ala-ligase (Vemula et al., 2017). Whether BBR has the same target as these two antibiotics needs further

verification. Since BBR has synergistic antibacterial effects with other antibiotics such as clindamycin, rifamycin (Xia et al., 2022), and ampicillin (Dziedzic et al., 2015), and we confirmed the synergistic antibacterial effect of BBR combined with vancomycin (which also targets the synthesis of peptidoglycan) (Supplementary Figure 1), its inhibitory effect on the synthesis of peptidoglycan is an interesting discovery and has important value for further study.

Prospects

Some of the metabolites identified in this study, such as the pyridine dicarboxylic acids, have unclear metabolic pathways in *S. aureus*. Pyridine dicarboxylic acid is present in the spores of spore-producing bacteria in high concentrations and endorses the spores with stress-resistant properties (Setlow, 2007). The genes of dihydro-pyridine dicarboxylate synthases and reductase had been annotated in the genome of MRSA, and they were considered to have potential interactions with the penicillin-resistant binding protein (PBP2a) (Yuan et al., 2010). However, the properties of the substrates of these enzymes remain controversial (Devenish et al., 2010; Karsten et al., 2018). It is worth mentioning that gamma-tocopherol can be synthesized in plants and algae with farnesyl-PP as a precursor (56), although no study on its biosynthesis in *S. aureus* has been retrieved. It is predicted that the average number of metabolites of *S. aureus* ranges from more than 1,000 to more than 2,000, with a maximum of 4,416 (Renz and Drager, 2021). Among the more than 3,000 metabolites identified in this study, a considerable part of them should be products of unknown metabolic pathways, in addition to substances absorbed from the culture environment. As metabolic databases become richer, the number of metabolites accurately identified will increase. Therefore, the revelation of unknown metabolic pathways in the future will help us to deeply understand the complexity and intrinsic relationship of antibiotic effects on bacterial metabolism. In addition, when there is a clear research direction or determined metabolic pathway (as suggested in this study), the application of targeted metabolomics and other technologies that can accurately verify the specific antibacterial effect will further promote the research on the antibacterial mechanism of natural products such as BBR.

CONCLUSION

The key metabolic markers suggest that BBR plays antibacterial activities against *S. aureus* ATCC 25923 by inhibiting the cell wall biosynthesis, promoting oxidative damage, reducing stress resistance, and inhibiting the synthesis of aromatic amino acids (Figure 6). These results provide new directions of peptidoglycan biosynthesis, staphyloxanthin synthesis, and shikimate pathway to study the antibacterial molecular mechanism of BBR and help to promote its application in the field of anti-infective medicine.

DATA AVAILABILITY STATEMENT

The original contributions presented in the study are included in the article/Supplementary Material, further inquiries can be directed to the corresponding author/s.

AUTHOR CONTRIBUTIONS

SW, KY, and NY conducted the experiments. SW, YH, and JN performed data analysis. SW and YG wrote the manuscript. SW and WD reviewed, edited the manuscript, and acquired funding. All authors made significant contributions to this article and have read and agreed to the final manuscript.

FUNDING

This study was supported by the Sichuan Science and Technology Program (No. 2021YJ0112) and the Chengdu University of TCM Science Foundation (BSH2019010). The authors declare that this study received funding from Science and Technology Department of Sichuan Province and Chengdu University of TCM. The funders were not involved in the study design, collection, analysis, interpretation of data, the writing of this article or the decision to submit it for publication.

ACKNOWLEDGMENTS

We would like to thank the Lu-Ming Biotech Co., Ltd. (Shanghai, China) for the sample detecting services. We also thank Yi-li Wang from the Innovative Institute of Chinese Medicine and Pharmacy, Chengdu University of Traditional Chinese Medicine, for her gracious assistance in the imaging technique of fluorescent staining.

SUPPLEMENTARY MATERIAL

The Supplementary Material for this article can be found online at: <https://www.frontiersin.org/articles/10.3389/fmicb.2022.917414/full#supplementary-material>

Supplementary Text 1 | Details for untargeted metabolomics analyses.

Supplementary Figure 1 | MIC test of BBR combined with vancomycin against *S. aureus* ATCC 25923.

Supplementary Figure 2 | The effect of BBR on survival of *S. aureus* ATCC 25923.

Supplementary Figure 3 | Growth curves (A) and the results of time kill tests (B) for *S. aureus* ATCC 25923 in the presence (1/4MIC, 3/8MIC, 1/2MIC or MIC) or absence (control) of berberine.

Supplementary Figure 4 | Result of RPT.

Supplementary Figure 5 | Activities change profile of metabolic pathways in comparison with berberine-exposed group (T1) vs. initial control group (C0).

Supplementary Figure 6 | Volcano plots showing the trends of metabolites detected in the major metabolic pathways.

Supplementary Figure 7 | Box plots for the major metabolic markers in *S. aureus* ATCC 25923 following berberine-exposure (T1) compared with non-exposed controls (C0, C1).

Supplementary Figure 8 | Effect of BBR on pigment accumulation of *S. aureus* ATCC 25923.

Supplementary Figure 9 | Expression profile of genes involved in staphyloxanthin biosynthesis in *S. aureus* ATCC 25923 responsive to berberine-exposure.

Supplementary Table 1 | Parameters of OPLS-DA and RPT test.

REFERENCES

- Aggio, R. B. (2014). Pathway activity profiling (PAPi): a tool for metabolic pathway analysis. *Methods Mol. Biol.* 1152, 233–250. doi: 10.1007/978-1-4939-0563-8_14
- Aksoy, C. S., Avci, F. G., Ugurel, O. M., Atas, B., Sayar, N. A., and Sariyar Akbulut, B. (2020). Potentiating the activity of berberine for *Staphylococcus aureus* in a combinatorial treatment with thymol. *Microb. Pathog.* 149, 104542. doi: 10.1016/j.micpath.2020.104542
- Anitha, P., Anbarasu, A., and Ramaiah, S. (2016). Gene network analysis reveals the association of important functional partners involved in antibiotic resistance: a report on an important pathogenic bacterium *Staphylococcus aureus*. *Gene* 575(2 Pt 1), 253–263. doi: 10.1016/j.gene.2015.08.068
- Bhatia, E., Sharma, S., Jadhav, K., and Banerjee, R. (2021). Combinatorial liposomes of berberine and curcumin inhibit biofilm formation and intracellular methicillin resistant *Staphylococcus aureus* infections and associated inflammation. *J. Mater. Chem. B* 9, 864–875. doi: 10.1039/d0tb02036b
- Boberek, J. M., Stach, J., and Good, L. (2010). Genetic evidence for inhibition of bacterial division protein FtsZ by berberine. *PLoS ONE* 5:e13745. doi: 10.1371/journal.pone.0013745
- Chen, J., Zhang, J., Zhu, L., Qian, C., Tian, H., Zhao, Z., et al. (2022). Antibacterial activity of the essential oil from litsea cubeba against cutibacterium acnes and the investigations of its potential mechanism by gas chromatography-mass spectrometry metabolomics. *Front. Microbiol.* 13:823845. doi: 10.3389/fmicb.2022.823845
- Clauditz, A., Resch, A., Wieland, K. P., Peschel, A., and Gotz, F. (2006). Staphyloxanthin plays a role in the fitness of *Staphylococcus aureus* and its ability to cope with oxidative stress. *Infect. Immun.* 74, 4950–4953. doi: 10.1128/IAI.00204-06
- Devenish, S. R., Blunt, J. W., and Gerrard, J. A. (2010). NMR studies uncover alternate substrates for dihydrodipicolinate synthase and suggest that dihydrodipicolinate reductase is also a dehydratase. *J. Med. Chem.* 53, 4808–4812. doi: 10.1021/jm100349s
- Domadia, P. N., Bhunia, A., Sivaraman, J., Swarup, S., and Dasgupta, D. (2008). Berberine targets assembly of *Escherichia coli* cell division protein FtsZ. *Biochemistry* 47, 3225–3234. doi: 10.1021/bi7018546
- Dorries, K., Schlueter, R., and Lalk, M. (2014). Impact of antibiotics with various target sites on the metabolome of *Staphylococcus aureus*. *Antimicrob. Agents Chemother.* 58, 7151–7163. doi: 10.1128/AAC.03104-14
- Du, G. F., Le, Y. J., Sun, X., Yang, X. Y., and He, Q. Y. (2020). Proteomic investigation into the action mechanism of berberine against *Streptococcus pyogenes*. *J. Proteomics* 215, 103666. doi: 10.1016/j.jprot.2020.103666
- Dziedzic, A., Wojtyczka, R. D., and Kubina, R. (2015). Inhibition of oral streptococci growth induced by the complementary action of berberine chloride and antibacterial compounds. *Molecules* 20, 13705–13724. doi: 10.3390/molecules200813705
- Garcia-Fernandez, E., Koch, G., Wagner, R. M., Fekete, A., Stengel, S. T., Schneider, J., et al. (2017). Membrane microdomain disassembly inhibits MRSA antibiotic resistance. *Cell* 171, 1354–1367 e1320. doi: 10.1016/j.cell.2017.10.012
- Herrmann, J., Lukežić, T., Kling, A., Baumann, S., Hüttel, S., Petković, H., et al. (2016). Strategies for the discovery and development of new antibiotics from natural products: three case studies. *Curr. Top. Microbiol. Immunol.* 398, 339–363. doi: 10.1007/82_2016_498
- Huang, X., Wang, P., Li, T., Tian, X., Guo, W., Xu, B., et al. (2020). Self-assemblies based on traditional medicine berberine and cinnamic acid for adhesion-induced inhibition multidrug-resistant *Staphylococcus aureus*. *ACS Appl. Mater. Interfaces* 12, 227–237. doi: 10.1021/acsami.9b17722
- Hui, J., Dong, P. T., Liang, L., Mandal, T., Li, J., Ulloa, E. R., et al. (2020). Photo-disassembly of membrane microdomains revives conventional antibiotics against MRSA. *Adv. Sci.* 7, 1903117. doi: 10.1002/adv.201903117
- Hussein, M., Karas, J. A., Schneider-Futschik, E. K., Chen, F., Swarbrick, J., Paulin, O. K. A., et al. (2020). The killing mechanism of teixobactin against methicillin-resistant *Staphylococcus aureus*: an untargeted metabolomics study. *mSystems* 5:e00077–20. doi: 10.1128/mSystems.00077-20
- Imenshahidi, M., and Hosseinzadeh, H. (2016). Berberis vulgaris and berberine: an update review. *Phytother. Res.* 30, 1745–1764. doi: 10.1002/ptr.5693
- Kang, S., Li, Z., Yin, Z., Jia, R., Song, X., Li, L., et al. (2015). The antibacterial mechanism of berberine against *Actinobacillus pleuropneumoniae*. *Nat. Prod. Res.* 29, 2203–2206. doi: 10.1080/14786419.2014.1001388
- Karaosmanoglu, K., Sayar, N. A., Kurnaz, I. A., and Akbulut, B. S. (2014). Assessment of berberine as a multi-target antimicrobial: a multi-omics study for drug discovery and repositioning. *OMICS* 18, 42–53. doi: 10.1089/omi.2013.0100
- Karsten, W. E., Nimmo, S. A., Liu, J., and Chooback, L. (2018). Identification of 2, 3-dihydrodipicolinate as the product of the dihydrodipicolinate synthase reaction from *Escherichia coli*. *Arch. Biochem. Biophys.* 653, 50–62. doi: 10.1016/j.abb.2018.06.011
- Kim, S., Lee, E. H., Kim, S. H., Lee, S., and Lim, S. J. (2012). Comparison of three tocopherol analogs as an inhibitor of production of proinflammatory mediators in macrophages. *J. Pharmacol. Sci.* 118, 237–244. doi: 10.1254/jphs.11152fp
- Kohanski, M. A., Dwyer, D. J., Hayete, B., Lawrence, C. A., and Collins, J. J. (2007). A common mechanism of cellular death induced by bactericidal antibiotics. *Cell* 130, 797–810. doi: 10.1016/j.cell.2007.06.049
- Kokoska, L., Kloucek, P., Leuner, O., and Novy, P. (2019). Plant-derived products as antibacterial and antifungal agents in human health care. *Curr. Med. Chem.* 26, 5501–5541. doi: 10.2174/0929867325666180831144344
- Lan, L., Cheng, A., Dunman, P. M., Missiakas, D., and He, C. (2010). Golden pigment production and virulence gene expression are affected by metabolisms in *Staphylococcus aureus*. *J. Bacteriol.* 192, 3068–3077. doi: 10.1128/JB.00928-09
- Li, X., Song, Y., Wang, L., Kang, G., Wang, P., Yin, H., et al. (2021). A potential combination therapy of berberine hydrochloride with antibiotics against multidrug-resistant *Acinetobacter baumannii*. *Front. Cell. Infect. Microbiol.* 11:660431. doi: 10.3389/fcimb.2021.660431
- Li, Z., Garner, A. L., Gloeckner, C., Janda, K. D., and Carlow, C. K. (2011). Targeting the Wolbachia cell division protein FtsZ as a new approach for antifilarial therapy. *PLoS Negl. Trop. Dis.* 5:e1411. doi: 10.1371/journal.pntd.0001411
- Lobritz, M. A., Belenky, P., Porter, C. B., Gutierrez, A., Yang, J. H., Schwarz, E. G., et al. (2015). Antibiotic efficacy is linked to bacterial cellular respiration. *Proc. Natl. Acad. Sci. U. S. A.* 112, 8173–8180. doi: 10.1073/pnas.1509743112
- Miryal, S. K., Basu, S., Naha, A., Debroy, R., Ramaiah, S., Anbarasu, A., et al. (2021). Identification of bioactive natural compounds as efficient inhibitors against *Mycobacterium tuberculosis* protein-targets: a molecular docking and molecular dynamics simulation study. *J. Mol. Liq.* 341, 117340. doi: 10.1016/j.molliq.2021.117340
- Miryal, S. K., Basu, S., Naha, A., Debroy, R., Ramaiah, S., Anbarasu, A., et al. (2022). Datasets comprising the quality validations of simulated protein-ligand complexes and SYBYL docking scores of bioactive natural compounds as inhibitors of *Mycobacterium tuberculosis* protein-targets. *Data in Brief* 42, 108146. doi: 10.1016/j.dib.2022.108146
- Morita, Y., Nakashima, K., Nishino, K., Kotani, K., Tomida, J., Inoue, M., et al. (2016). Berberine is a novel type efflux inhibitor which attenuates the MexXY-mediated aminoglycoside resistance in *Pseudomonas aeruginosa*. *Front. Microbiol.* 7:1223. doi: 10.3389/fmicb.2016.01223
- Newman, D. J., and Cragg, G. M. (2016). Natural products as sources of new drugs from 1981 to 2014. *J. Nat. Prod.* 79, 629–661. doi: 10.1021/acs.jnatprod.5b01055
- Ragunathan, A., Malathi, K., Ramaiah, S., and Anbarasu, A. (2018). FtsA as a cidal target for *Staphylococcus aureus*: molecular docking and dynamics studies. *J. Cell. Biochem.* doi: 10.1002/jcb.28049
- Ramirez-Guadiana, F. H., Meeske, A. J., Rodrigues, C. D. A., Barajas-Ornelas, R. D. C., Kruse, A. C., and Rudner, D. Z. (2017). A two-step transport pathway allows the mother cell to nurture the developing spore in *Bacillus subtilis*. *PLoS Genet.* 13:e1007015. doi: 10.1371/journal.pgen.1007015
- Renz, A., and Dräger, A. (2021). Curating and comparing 114 strain-specific genome-scale metabolic models of *Staphylococcus aureus*. *NPJ Syst. Biol. Appl.* 7, 30. doi: 10.1038/s41540-021-00188-4
- Sadaka, C., Ellsworth, E., Hansen, P. R., Ewin, R., Damborg, P., and Watts, J. L. (2018). Review on abyssomicins: inhibitors of the chorismate pathway and folate biosynthesis. *Molecules* 23, 1371. doi: 10.3390/molecules23061371
- Schelli, K., Zhong, F., and Zhu, J. (2017). Comparative metabolomics revealing *Staphylococcus aureus* metabolic response to different antibiotics. *Microb. Biotechnol.* 10, 1764–1774. doi: 10.1111/1751-7915.12839
- Setlow, P. (2007). I will survive: DNA protection in bacterial spores. *Trends Microbiol.* 15, 172–180. doi: 10.1016/j.tim.2007.02.004
- Shang, X. F., Yang, C. J., Morris-Natschke, S. L., Li, J. C., Yin, X. D., Liu, Y. Q., et al. (2020). Biologically active isoquinoline alkaloids covering 2014–2018. *Med. Res. Rev.* 40, 2212–2289. doi: 10.1002/med.21703
- Shen, F., Ge, C., and Yuan, P. (2020). Metabolomics study reveals inhibition and metabolic dysregulation in *Staphylococcus aureus* Planktonic

- cells and biofilms induced by Carnosol. *Front. Microbiol.* 11:538572. doi: 10.3389/fmicb.2020.538572
- Stipetic, L. H., Dalby, M. J., Davies, R. L., Morton, F. R., Ramage, G., and Burgess, K. E. (2016). A novel metabolomic approach used for the comparison of *Staphylococcus aureus* planktonic cells and biofilm samples. *Metabolomics* 12:75. doi: 10.1007/s11306-016-1002-0
- Sun, N., Chan, F. Y., Lu, Y. J., Neves, M. A., Lui, H. K., Wang, Y., et al. (2014). Rational design of berberine-based FtsZ inhibitors with broad-spectrum antibacterial activity. *PLoS ONE* 9:e97514. doi: 10.1371/journal.pone.0097514
- Surre, J., Canard, I., Bourne-Branchu, P., Courbiere, E., Franceschi, C., Chatellier, S., et al. (2018). Enhanced detection of carbapenemase-producing Enterobacteriaceae by an optimized phenol red assay. *Diagn. Microbiol. Infect. Dis.* 90, 11–17. doi: 10.1016/j.diagmicrobio.2017.09.005
- Tang, C., Chen, J., Zhou, Y., Ding, P., He, G., Zhang, L., et al. (2021). Exploring antimicrobial mechanism of essential oil of *Amomum villosum* Lour through metabolomics based on gas chromatography-mass spectrometry in methicillin-resistant *Staphylococcus aureus*. *Microbiol. Res.* 242, 126608. doi: 10.1016/j.micres.2020.126608
- Vemula, H., Ayon, N. J., Burton, A., and Gutheil, W. G. (2017). Antibiotic effects on methicillin-resistant *Staphylococcus aureus* cytoplasmic peptidoglycan intermediate levels and evidence for potential metabolite level regulatory loops. *Antimicrob. Agents Chemother.* 61, e02253-16. doi: 10.1128/AAC.02253-16
- Xia, S., Ma, L., Wang, G., Yang, J., Zhang, M., Wang, X., et al. (2022). *In vitro* antimicrobial activity and the mechanism of berberine against methicillin-resistant *Staphylococcus aureus* isolated from bloodstream infection patients. *Infect. Drug Resist.* 15, 1933–1944. doi: 10.2147/idr.s357077
- Xie, Y., Liu, X., and Zhou, P. (2020). *In vitro* antifungal effects of berberine against *Candida* spp. In Planktonic and biofilm conditions. *Drug Des. Devel. Ther.* 14, 87–101. doi: 10.2147/dddt.s230857
- Xu, C., Wang, F., Huang, F., Yang, M., He, D., and Deng, L. (2021). Targeting effect of berberine on type I fimbriae of *Salmonella Typhimurium* and its effective inhibition of biofilm. *Appl. Microbiol. Biotechnol.* 105, 1563–1573. doi: 10.1007/s00253-021-11116-1
- Yuan, W. W., Yang, J., Wang, D. M., Hu, Z., and Zhu, J. M. (2010). Screening of proteins interacting with PBP2a in methicillin-resistant *Staphylococcus aureus*. *Acta Acad. Med. Militaris Tertiae* 32, 749–753. doi: 10.16016/j.1000-5404.2010.08.009
- Zhang, X., Sun, X., Wu, J., Wu, Y., Wang, Y., Hu, X., et al. (2020). Berberine damages the cell surface of methicillin-resistant *Staphylococcus aureus*. *Front. Microbiol.* 11:621. doi: 10.3389/fmicb.2020.00621

Conflict of Interest: JN was employed by Guangdong Meilikang Bio-Sciences Ltd.

The remaining authors declare that the research was conducted in the absence of any commercial or financial relationships that could be construed as a potential conflict of interest.

Publisher's Note: All claims expressed in this article are solely those of the authors and do not necessarily represent those of their affiliated organizations, or those of the publisher, the editors and the reviewers. Any product that may be evaluated in this article, or claim that may be made by its manufacturer, is not guaranteed or endorsed by the publisher.

Copyright © 2022 Wu, Yang, Hong, Gong, Ni, Yang and Ding. This is an open-access article distributed under the terms of the Creative Commons Attribution License (CC BY). The use, distribution or reproduction in other forums is permitted, provided the original author(s) and the copyright owner(s) are credited and that the original publication in this journal is cited, in accordance with accepted academic practice. No use, distribution or reproduction is permitted which does not comply with these terms.



OPEN ACCESS

EDITED BY

Vijay Soni,
NewYork-Presbyterian, United States

REVIEWED BY

Hyungjin Eoh,
University of Southern California,
United States
Yesha Patel,
Cornell University, United States

*CORRESPONDENCE

Ian A. Lewis
ian.lewis2@ucalgary.ca

†These authors have contributed
equally to this work and share first
authorship

SPECIALTY SECTION

This article was submitted to
Antimicrobials, Resistance and
Chemotherapy,
a section of the journal
Frontiers in Microbiology

RECEIVED 30 May 2022

ACCEPTED 27 June 2022

PUBLISHED 22 July 2022

CITATION

Mapar M, Rydzak T, Groves RA and
Lewis IA (2022) Biomarker enrichment
medium: A defined medium for
metabolomic analysis of microbial
pathogens.
Front. Microbiol. 13:957158.
doi: 10.3389/fmicb.2022.957158

COPYRIGHT

© 2022 Mapar, Rydzak, Groves and
Lewis. This is an open-access article
distributed under the terms of the
[Creative Commons Attribution License](#)
(CC BY). The use, distribution or
reproduction in other forums is
permitted, provided the original
author(s) and the copyright owner(s)
are credited and that the original
publication in this journal is cited, in
accordance with accepted academic
practice. No use, distribution or
reproduction is permitted which does
not comply with these terms.

Biomarker enrichment medium: A defined medium for metabolomic analysis of microbial pathogens

Maryam Mapar[†], Thomas Rydzak[†], Ryan A. Groves and
Ian A. Lewis^{*}

Department of Biological Science, University of Calgary, Calgary, AB, Canada

Microbes have diverse metabolic capabilities and differences in these phenotypes are critical for differentiating strains, species, and broader taxa of microorganisms. Recent advances in liquid chromatography-mass spectrometry (LC-MS) allow researchers to track the complex combinations of molecules that are taken up by each cell type and to quantify the rates that individual metabolites enter or exit the cells. This metabolomics-based approach allows complex metabolic phenotypes to be captured in a single assay, enables computational models of microbial metabolism to be constructed, and can serve as a diagnostic approach for clinical microbiology. Unfortunately, metabolic phenotypes are directly affected by the molecular composition of the culture medium and many traditional media are subject to molecular-level heterogeneity. Herein, we show that commercially sourced Mueller Hinton (MH) medium, a Clinical and Laboratory Standards Institute (CLSI) approved medium for clinical microbiology, has significant lot-to-lot and supplier-to-supplier variability in the concentrations of individual nutrients. We show that this variability does not affect microbial growth rates but does affect the metabolic phenotypes observed *in vitro*—including metabolic phenotypes that distinguish six common pathogens. To address this, we used a combination of isotope-labeling, substrate exclusion, and nutritional supplementation experiments using Roswell Park Memorial Institute (RPMI) medium to identify the specific nutrients used by the microbes to produce diagnostic biomarkers, and to formulate a Biomarker Enrichment Medium (BEM) as an alternative to complex undefined media for metabolomics research, clinical diagnostics, antibiotic susceptibility testing, and other applications where the analysis of stable microbial metabolic phenotypes is important.

KEYWORDS

biomarker enrichment medium, Mueller Hinton, metabolomics, LC-MS, biomarkers

Introduction

Microbial phenotypes are dictated not only by their inherent metabolic capabilities (dictated by genes and protein expression), but also by their nutritional environment. The effect of medium composition on biological phenotypes [i.e., growth rates and biomass (Mah et al., 1967; Letort and Juillard, 2001; Zhang et al., 2009; Texeira et al., 2015; Machado et al., 2019; Sanchez-Rosario and Johnson, 2021)], and bioproduct yields [i.e., exopolysaccharides, proteins, biofuels (DeBell, 1979; Grobбен et al., 1998; Torino et al., 2005; Islam et al., 2013; Khan et al., 2013; Verbeke et al., 2017)] is well-documented. Nutritional availability can not only affect cell growth, but can direct metabolism toward the production of certain bioproducts.

Significant biological insights can be gained by quantifying the rates at which molecules are consumed and secreted by cells (Teusink et al., 2006). These boundary fluxes can be used to systematically screen isolates for auxotrophies (Levering et al., 2016; Basile et al., 2020), construct computational networks to understand cellular metabolism and nutrient-product relationships (Steuer, 2007; Copeland et al., 2012), optimize bioproduct yields and rates (Laiglecia et al., 2013; Joshi et al., 2017), and differentiate species and antimicrobial susceptibilities for diagnostics (Rydzak et al., 2022). With the evolution of high-resolution liquid chromatography-mass spectrometry (LC-MS), there has been an increasing emphasis on capturing a broad range of molecular targets for boundary flux analysis. These new approaches now capture a large transect in central carbon metabolism, allowing us to better understand intracellular metabolomic phenotypes.

One of the challenges in quantifying metabolic boundary fluxes is that microbial phenotypes are sensitive to medium composition. These minor variations in nutrients can dramatically affect the metabolic phenotype observed *in vitro* (Sánchez et al., 2000; McGillicuddy et al., 2018). This is particularly problematic when microbial phenotypes are being used for diagnostic purposes that require reproducible quantification of limited biomarker sets. This reproducibility can be impacted when using complex medium. While the production of complex medium is well-standardized by suppliers, it does contain many chemical species in unknown proportions derived from biological sources (i.e., yeast or beef extract, casein hydrolysate, etc.). Although the bulk composition of these media with respect to lipids, proteins, and nutrients is stable enough to maintain consistent growth, the specific concentrations of nutrients present in these media are not well-controlled.

Herein, we show that commercially sourced Mueller Hinton (MH) medium, a CLSI approved medium for clinical

microbiology, has significant lot-to-lot and supplier-to-supplier variability in the concentrations of individual nutrients. To demonstrate that this variability directly translates into instability in metabolic phenotypes, we employed a previously published metabolic preference assay (MPA) that is capable of differentiating common bloodstream pathogens and testing their antibiotic susceptibility *in vitro* following a short 4 h incubation (Rydzak et al., 2022). Specifically, as little as six biomarkers including arabinol, urocanate, succinate, xanthine, mevalonate and N¹,N¹²-diacetylspermine can differentiate six common bloodstream pathogens (*Candida albicans*, *Klebsiella pneumoniae*, *Escherichia coli*, *Pseudomonas aeruginosa*, *Staphylococcus aureus*, and *Enterococcus faecalis*). While variability in metabolomic phenotypes on different lots of media was encountered during the rapid clinical assay for bloodstream infections (BSI), this is a generalized problem in any metabolomic assay that seeks to collect metabolomic phenotypes using a boundary flux approach. To address this, we developed a defined, complex medium, derived from nutrient-rich Roswell Park Memorial Institute (RPMI) medium, that supports the growth of pathogens, restores the metabolic biomarkers used to differentiate six common bloodstream infection species, and allows for antibiotic susceptibility testing (AST). Using a combination of isotope-labeling, substrate exclusion, and nutritional supplementation experiments, we identified the specific nutrients used by the microbes in the production of these biomarkers, as well as the minimal complement of nutrients needed to support their growth *in vitro*. We propose this newly formulated Biomarker Enrichment Medium (BEM) as an alternative to complex undefined media for metabolomics research, clinical diagnostics, and other applications where the analysis of stable microbial metabolic phenotypes is important.

Results

Batches of Mueller Hinton medium differ in nutritional composition

To assess variability in MH medium, non-cation adjusted MH medium (MH I) and cation adjusted MH medium (MH II), from two different suppliers (BD and Fluka Analytical; See Materials and Methods), was analyzed using untargeted ultra high-pressure liquid chromatography-mass spectrometry (UHPLC-MS). One way ANOVA identified variability in 359 features when using the stringent cut-offs ($p < 1 \times 10^{-5}$) between the 8 batches of MH medium tested (Figure 1A; Source Data File 1). Even lot-to-lot variability of both MH I and MH II was observed from the same suppliers. Targeted UHPLC-MS analysis identified

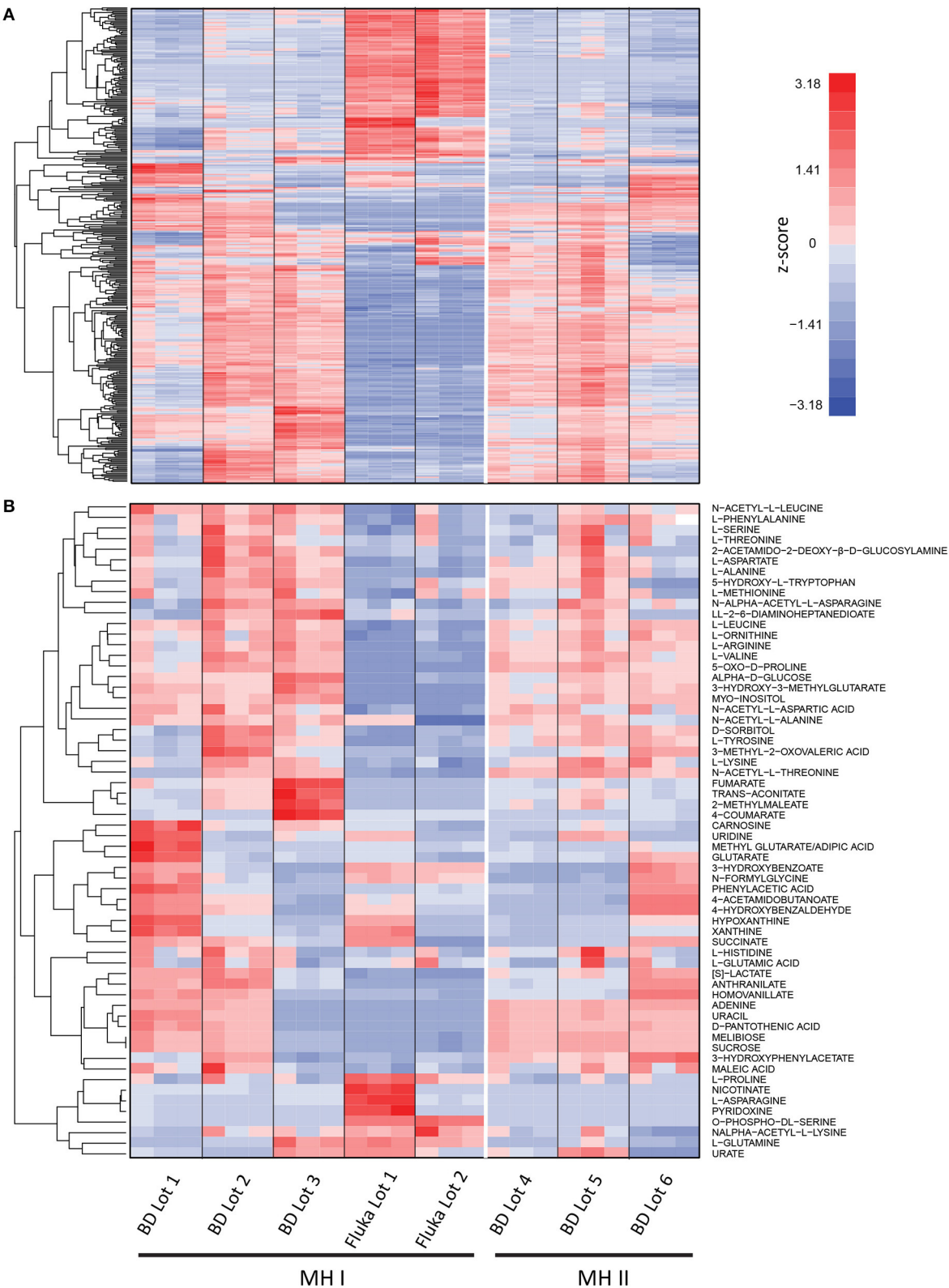


FIGURE 1
Mass spectrometry analysis of different lots and suppliers of Mueller Hinton (MH I) and cation adjusted Mueller Hinton (MH II) medium. **(A)** Untargeted analysis identified significant differences ($p < 1 \times 10^{-5}$) in 359 features were observed in at least one lot of medium ($n = 3$). **(B)** Targeted UHPLC-MS analysis identified variability in concentrations of many common microbial nutrients, including various amino acids, nucleotides, and sugars. Signal intensities are shown as z-scores (i.e., mean centered, variance stabilized signal intensities). See [Source Data File 1](#).

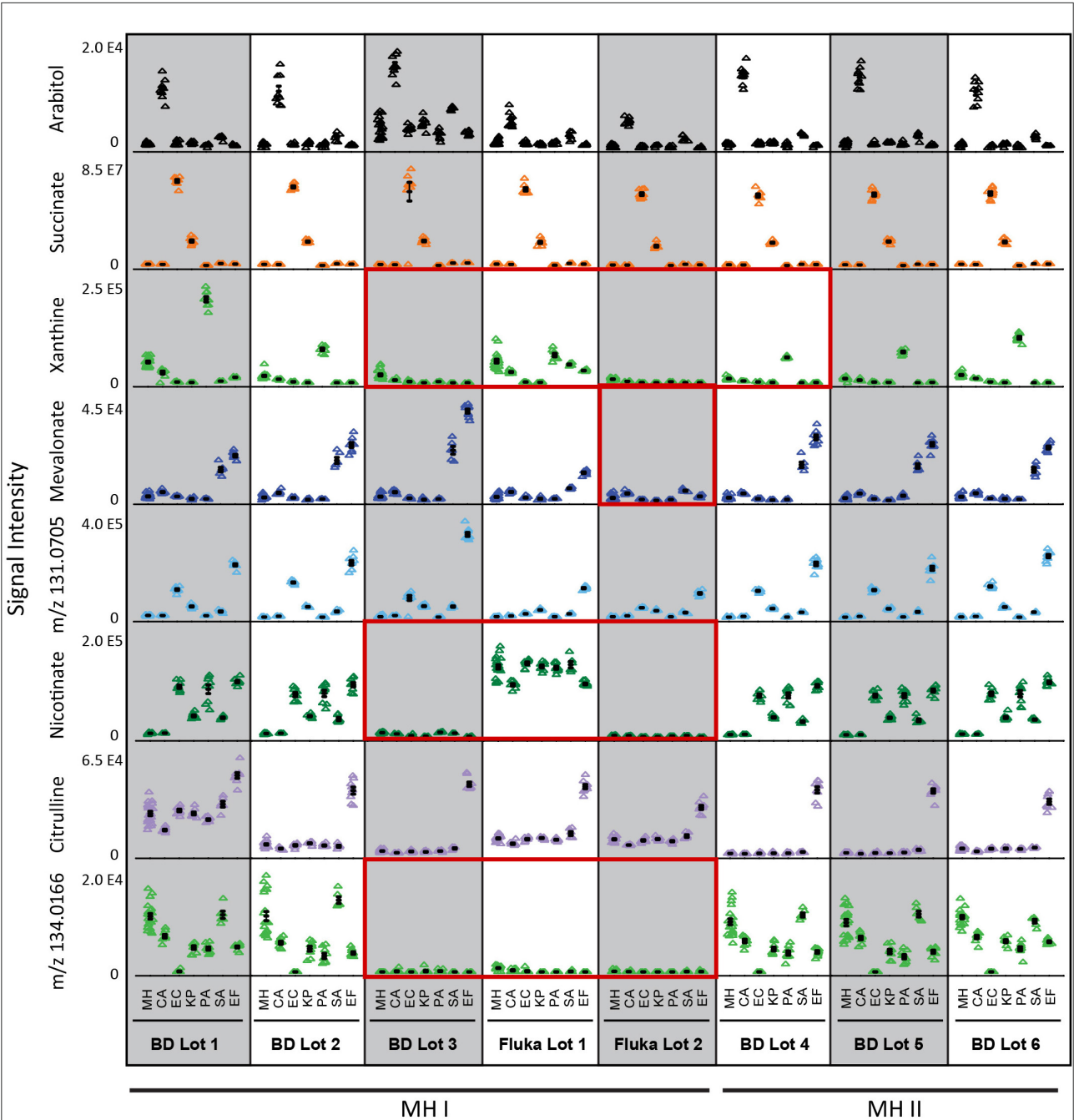


FIGURE 2
Differential biomarker production used to differentiate the six common species responsible for bloodstream infections incubated in different batches of MH medium. Three of the eight batches studies (BD Lot 3, and Fluka Lots 1 and 2) showed greatest inconsistencies with regards to species-specific production of xanthine, nicotinate, and mevalonate (Fluka Lot 2 only), and initial medium levels of unassigned marker with *m/z* 134.0166 (Source Data File 2). Key biomarkers that are affected by certain lots of media have been highlighted in red boxes. MH, Mueller Hinton medium; CA, *Candida albicans*; KP, *Klebsiella pneumoniae*; EC, *Escherichia coli*; PA, *Pseudomonas aeruginosa*; SA, *Staphylococcus aureus*; EF, *Enterococcus faecalis*. Data represents *n* = 9 biological replicates.

variability in concentrations of many common microbial nutrients, including various amino acids, nucleotides, and sugars (Figure 1B; Source Data File 1). This lot-to-lot nutritional

variability was unsurprising given that MH medium is composed of undefined components including beef extract and casein hydrolysate.

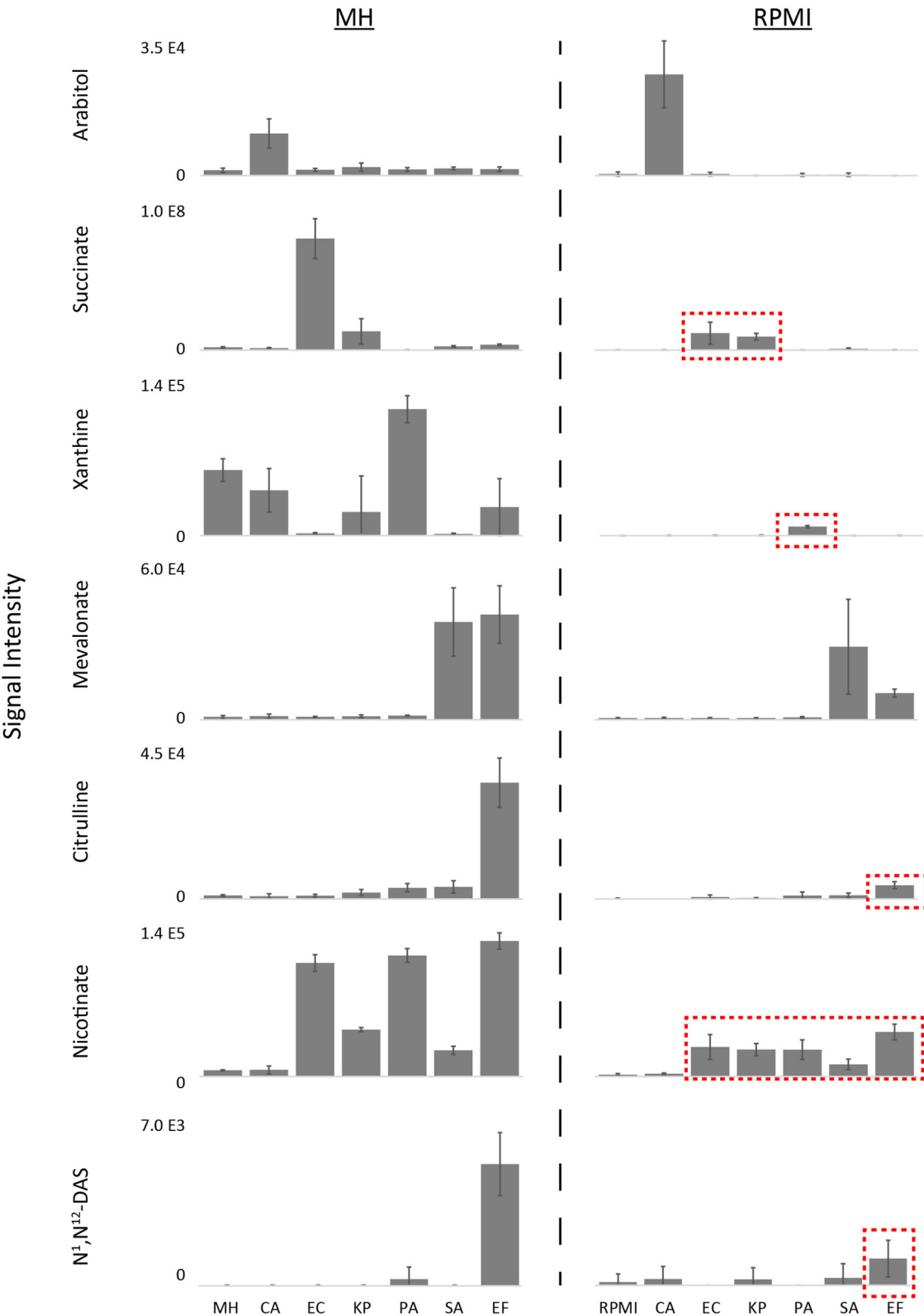
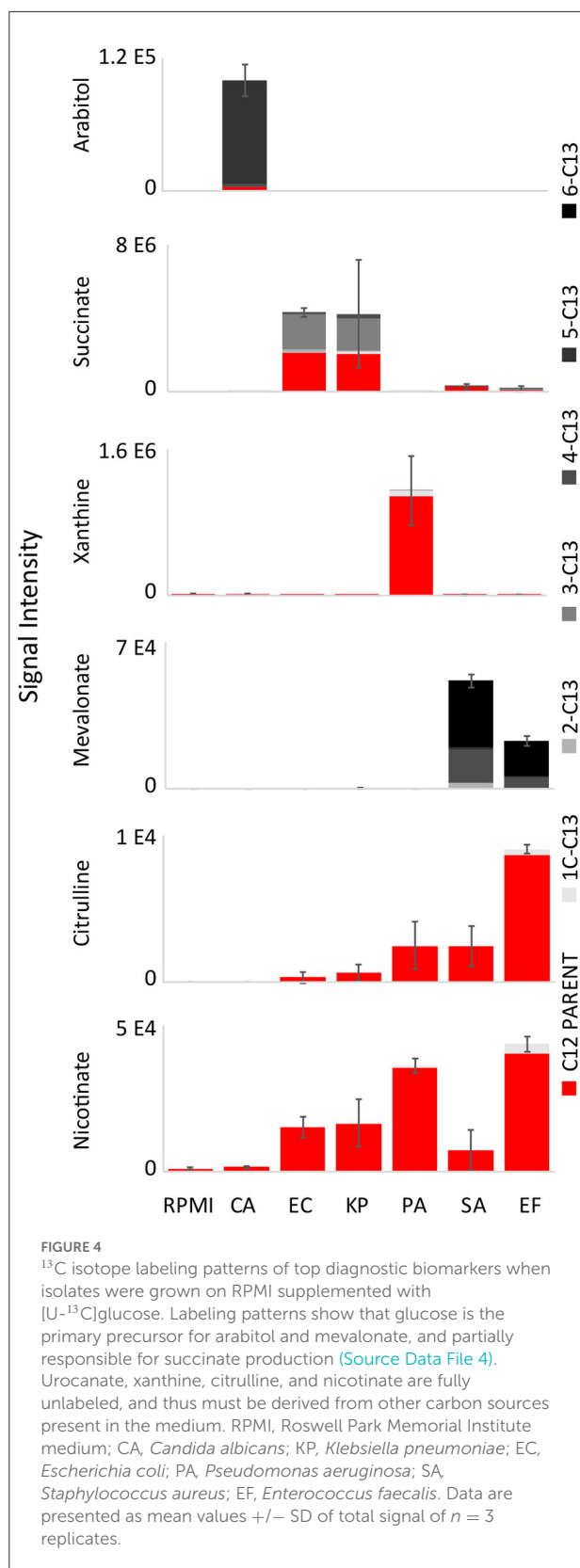


FIGURE 3 Differential biomarker production of pathogens incubated in MH vs. RPMI medium. While most production biomarkers were observed on MH and RPMI, levels of succinate, xanthine, citrulline, and nicotinate were significantly lower on RPMI, and N¹,N¹²-diacetylspermine production on RPMI did not meet diagnostic thresholds (Source Data File 3). Key biomarkers that are affected by medium have been highlighted in red boxes. MH, Mueller Hinton medium; RPMI, Roswell Park Memorial Institute medium; CA, *Candida albicans*; KP, *Klebsiella pneumoniae*; EC, *Escherichia coli*; PA, *Pseudomonas aeruginosa*; SA, *Staphylococcus aureus*; EF, *Enterococcus faecalis*. Data are presented as mean values \pm SD of $n = 4$ replicates.

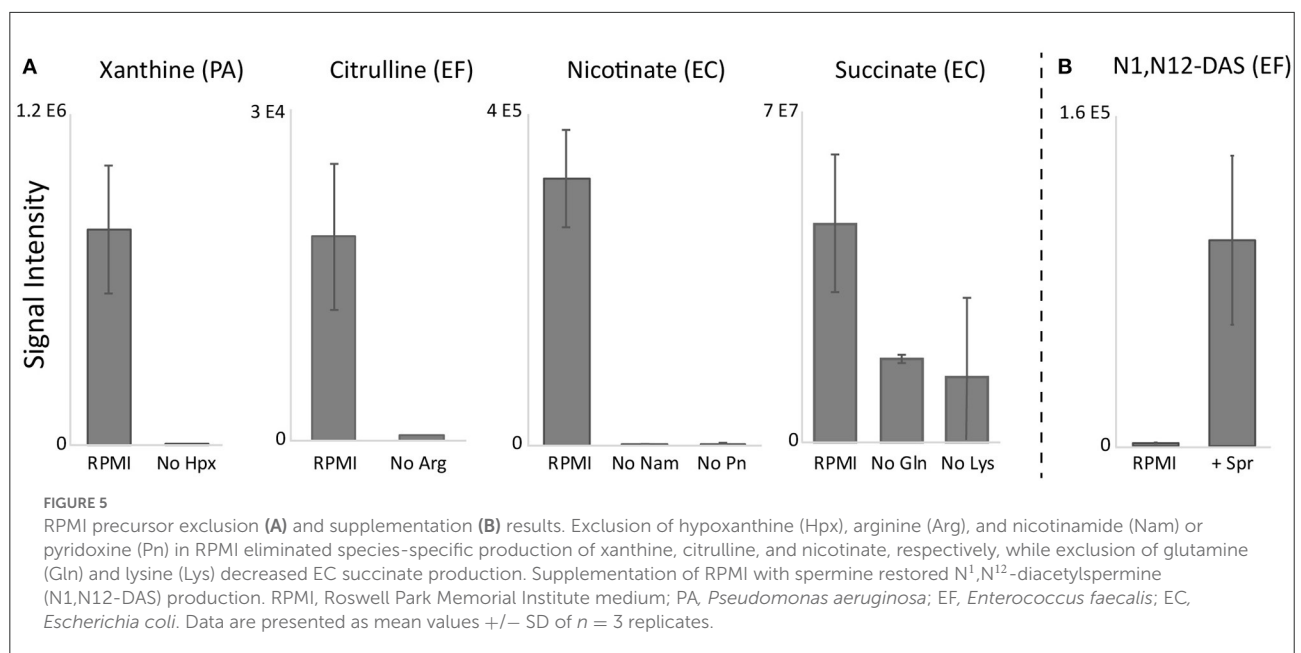


Differences in metabolomic phenotypes are observed on different batches of medium

To determine if this nutritional variability affects microbial metabolic boundary fluxes, six prevalent pathogens responsible for BSIs (*Candida albicans*, CA; *Klebsiella pneumoniae*, KP; *Escherichia coli*, EC; *Pseudomonas aeruginosa*, PA; *Staphylococcus aureus*, SA; and *Enterococcus faecalis*, EF) were incubated for 4 h on each lot of MH medium and previously identified biomarkers used to differentiate these species were measured by targeted UHPLC-MS (Figure 2, Source Data File 2) (Rydzak et al., 2022). In some cases, the production of biomarkers in inoculated vs. non-inoculated medium was sufficient to differentiate these pathogens in all batches of medium. These include arabitol production by CA, succinate production by EC and KP. However, batch-dependent variability was also observed in many cases where species-specific biomarker production did not exceed that of MH non-inoculated controls. This was true for (i) mevalonate production in Fluka Lot 2 for SA and EF, (ii) xanthine production in BD Lot 3 and Fluka Lots 1 and 2 for PA, and (iii) nicotinate production in BD Lot 3 and Fluka Lots 1 and 2 for EC, KP, PA, SA, and EF. Notably, non-inoculated MH control nicotinate levels were much higher in Fluka Lot 1 than in all other lots. This was also true for citrulline in BD Lot 1. Lastly, the concentration of the unassigned marker with m/z 134.0166 was negligible in BD Lot 3 and Fluka Lots 1 and 2, and thus consumption by CA, EC, KP, PA, and EF was not observed in these lots. Given that all samples were incubated on the same day and analyzed on the MS concurrently, we can rule out that this variance is due to differences in processing or MS response factors. These discrepancies in lot-to-lot biomarker changes demonstrate the need for the use of a more standardized medium to ensure consistency when performing metabolomic studies.

Biomarker production levels are lower on defined RPMI vs. MH

Using a defined medium that is not subject to potential variations in beef or casein sources or downstream production steps is critical for inter-laboratory standardization. We therefore substituted the MH medium with nutrient-rich defined RPMI medium (Supplementary Table 1) to evaluate growth and biomarker production of the six prevalent BSI pathogens tested above. Unsurprisingly, the levels of key nutrients were different between MH medium (BD Lot 1) and RPMI (Supplementary Figure 1, Source Data File 1). Notably, levels of most amino acids, with the exception



of glutamine, asparagine, and cysteine, were higher in MH vs. RPMI, whereas glucose and select vitamins were higher in RPMI. While all six microorganisms tested grew on both media, growth was generally poorer on RPMI when compared to MH (Supplementary Figure 2). Furthermore, while most production biomarkers (i.e., arabinol, succinate, xanthine, mevalonate, citrulline, and nicotinate) were still suitable for species differentiation on RPMI, levels of succinate, xanthine, citrulline, and nicotinate were on average 7.5-fold lower when the respective species that produced these markers were grown on RPMI (Figure 3, Source Data File 3). These decreased levels in key biomarkers can have significant impacts on diagnostic accuracy when performing MS/MS fragmentation using less sensitive clinical triple quadrupole mass spectrometers (Groves et al., 2022). Moreover, production of N¹,N¹²-diacetylspermine—used for identification of EF—was so low on RPMI that it did not meet diagnostic thresholds. The limited production of key biomarkers in RPMI warranted further investigation to identify which medium precursors are responsible for their production in order to potentially improve their levels.

[U-¹³C]glucose is not a precursor for many biomarkers

To determine if key biomarkers are coming from glucose or other medium components, glucose-free RPMI was supplemented with uniformly labeled [U-¹³C]glucose. The ¹³C isotope labeling patterns of top diagnostic biomarkers (excluding N¹,N¹²-diacetylspermine) were analyzed using

UHPLC-MS (Figure 4, Source Data File 4). Surprisingly, fully unlabeled isotopologues were minimal for arabinol (80% fully ¹³C labeled, and 20% fully unlabeled) and negligible for mevalonate (62% fully ¹³C labeled and 30% ¹³C₄ labeled), implying that glucose is the primary precursor for these two biomarkers. Succinate was 45% ¹³C₃ labeled and 49% fully unlabeled. This indicates that a portion of succinate is derived from glucose flowing into the TCA cycle, while the remainder is derived from other precursors. Urocanate, xanthine, citrulline, and nicotinate were fully unlabeled, and thus must be derived from other carbon sources present in the medium.

Biomarkers were eliminated when precursors were excluded

To identify likely precursors for biomarkers that did not predominantly come from glucose (i.e., citrulline, xanthine, nicotinate, and succinate) we excluded the individual amino acids and other putative precursors found in RPMI and assessed the effect on these four biomarkers. We took a two-pronged approach for these experiments: we both randomly screened individual exclusion of the majority of amino acids found in RPMI (Source Data File 5), and investigated pathways that could provide insights into which substrates could be contributing to biomarker production (Wishart et al., 2018; Karp et al., 2019). While it was difficult to identify which precursors could be partially responsible for the additional succinate production, precursors for other biomarkers could be deduced from metabolic pathways. For example, xanthine could potentially be derived from hypoxanthine—a component

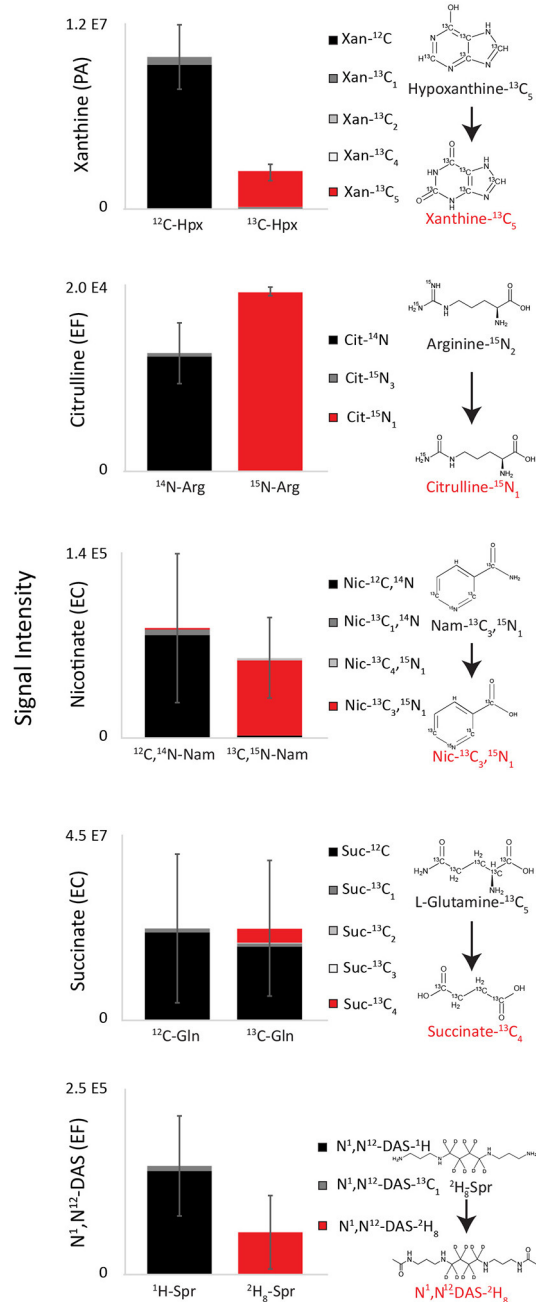


FIGURE 6
Labeling patterns of top diagnostic biomarkers when isolates were grown on RPMI supplemented with putative precursors. Species-specific xanthine, citrulline, nicotinate, and N^1,N^{12} -diacetylspermine were all >95% labeled when labeled substrates were used, demonstrating that that hypoxanthine, arginine, nicotinamide, and spermine are direct medium precursors for xanthine, citrulline, nicotinate, and N^1,N^{12} -diacetylspermine (Source Data File 6). EC cultured in RPMI with unlabeled glucose and uniformly labeled L-glutamine- $^{13}C_5$ was 80% fully ^{12}C labeled and 15% fully $^{13}C_4$ labeled, demonstrating that it is mostly synthesized from glucose, although glutamine partially contributes to its
(Continued)

FIGURE 6

production as well. Hpx, Hypoxanthine; Arg, arginine; Nam, nicotinamide; Gln, glutamine; Spr, spermine; PA, *Pseudomonas aeruginosa*; EF, *Enterococcus faecalis*; EC, *Escherichia coli*. Data are presented as mean values \pm SD of $n = 3$ replicates.

of RPMI—via xanthine oxidase (EC:1.17.3.2) which is present in the adenine dinucleotide salvage pathway (Bortolotti et al., 2021). Citrulline has been proposed to be formed from arginine via nitric-oxide synthase (EC:1.14.13.39) or indirectly via the urea cycle (Marletta, 1993). Nicotinate could be derived from nicotinamide, also present in RPMI, via nicotinamidase (EC:3.5.1.19) present in the nicotinamide adenine dinucleotide salvage pathway (Berger et al., 2004). Indeed, exclusion of hypoxanthine in PA cultures, arginine in EF cultures, and nicotinamide in EC (and other) cultures eliminated production of citrulline, xanthine, and nicotinate, respectively (Figure 5A, Source Data File 5). Notably, exclusion of pyridoxine, a known co-enzyme used in aminotransferase reactions (Feldman and Gunsalus, 1950; Gunsalus and Tonzetich, 1952) in EC cultures also eliminated nicotinate production. Lastly, screening of amino acid exclusions revealed that exclusion of both glutamine and lysine decreased succinate production in EC cultures. Given that N^1,N^{12} -diacetylspermine production was negligible in RPMI for EF cultures, we suspected that the precursor for this biomarker may be absent in RPMI. Through pathway analysis, we hypothesized that spermine supplementation could restore N^1,N^{12} -diacetylspermine secretion in EF cultures (Pegg, 2008). Indeed, supplementation of RPMI with spermine not only restored N^1,N^{12} -diacetylspermine production by EF, but also resulted in N^1,N^{12} -diacetylspermine production in EC and KP cultures (Figure 5B, Source Data File 5).

Non-glucose biomarker precursors were confirmed using labeled precursors

To further confirm species-specific biomarker precursors identified in precursor exclusion experiments, unlabeled precursors were substituted with labeled analogs in RPMI medium (Figure 6, Source Data File 6). Resulting species-specific xanthine, citrulline, nicotinate, and N^1,N^{12} -diacetylspermine were all >95% labeled when labeled substrates were used. Specifically, reduction of uniformly labeled hypoxanthine- $^{13}C_5$ in PA cultures resulted in uniformly labeled xanthine- $^{13}C_5$. Deamination of arginine (Guanido- $^{15}N_2$) in EF cultures resulted in citrulline- $^{15}N_1$. Substitution of the terminal amine with a hydroxide of nicotinamide-2,6,7- $^{13}C_3$ -(pyridyl- ^{15}N) resulted in nicotinate-2,6,7- $^{13}C_3$ -(pyridyl- ^{15}N). This data suggests that hypoxanthine, arginine, and nicotinamide

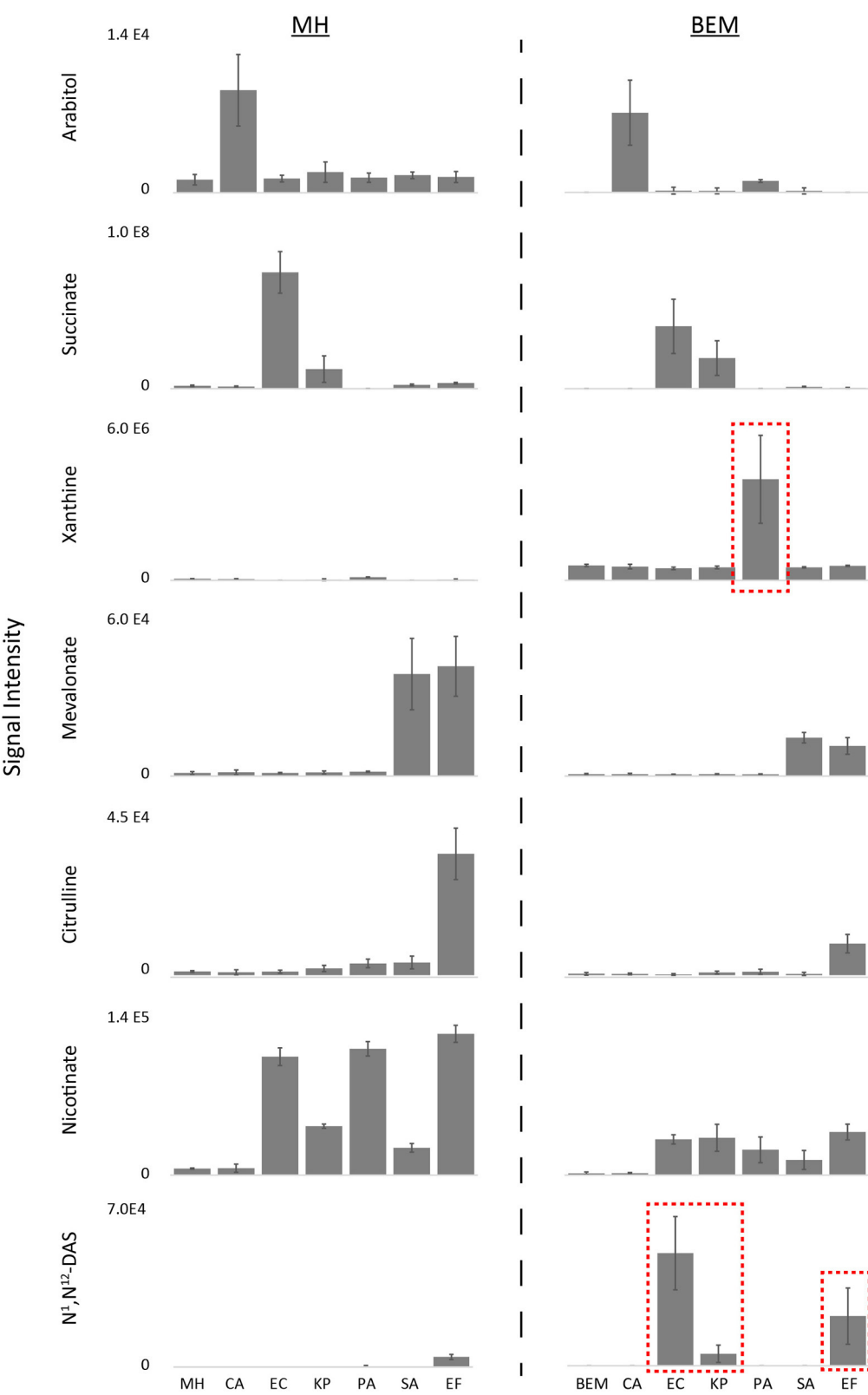


FIGURE 7
Differential biomarker production of pathogens incubated in MH vs. defined BEM medium. Metabolic phenotypes of MH were reproduced in BEM. Notably, supplementation of hypoxanthine in BEM improved PA xanthine levels and addition of spermine resulted in improved N¹,N¹²-diacetylspermine production by EF, as well as EC and KP (Source Data File 3). Key biomarkers that are affected by medium have been highlighted in red boxes. MH, Mueller Hinton medium; BEM, Biomarker Enrichment Medium; CA, *Candida albicans*; KP, *Klebsiella pneumoniae*; EC, *Escherichia coli*; PA, *Pseudomonas aeruginosa*; SA, *Staphylococcus aureus*; EF, *Enterococcus faecalis*. Data are presented as mean values \pm SD of $n = 3$ replicates.

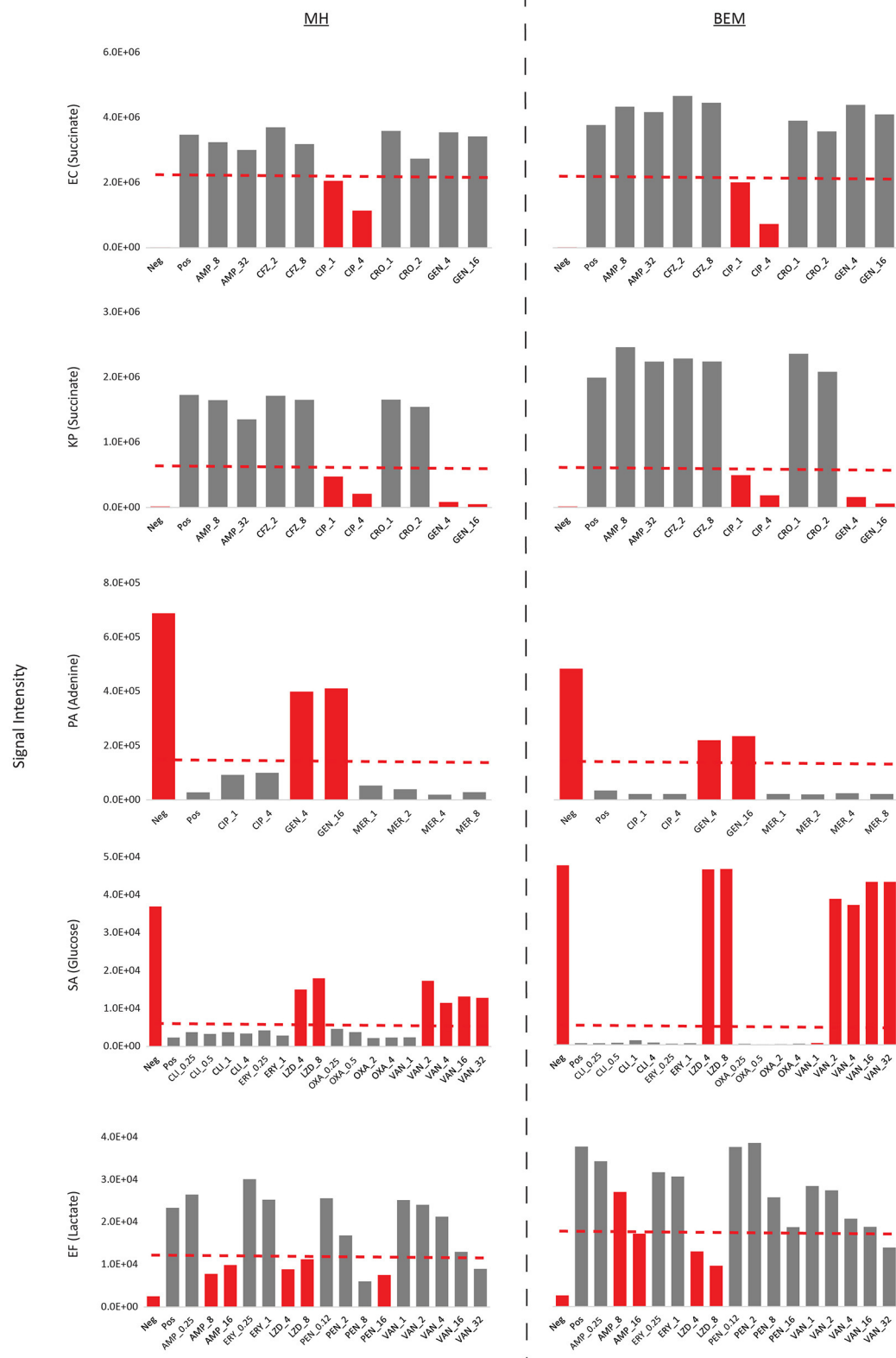


FIGURE 8

Antibiotic susceptibility validation on BEM and MH II using metabolic inhibition profiles. Metabolic inhibition of select biomarkers in response to antibiotics were tested on bacterial isolates with known microdilution or Vitek2 AST profiles. Inhibition of biomarker production/consumption were in general agreement with microbroth dilution/Vitek2 calls, correctly identifying sensitive (gray bars) and resistant strains (red bars). Furthermore, changes in biomarker levels in both media were comparable. Sensitive vs. resistant threshold cutoffs are indicated in dashed red lines. Concentrations in antibiotics are provided as $\mu\text{g/mL}$. Neg, uninoculated medium control; Pos, inoculated control with no added antibiotics; AMP, ampicillin; CFZ, ceftazolin; CIP, ciprofloxacin; CRO, ceftriaxone; GEN, gentamicin; MER, meropenem; CLI, clindamycin; ERY, erythromycin; LDZ, linezolid; OXA, oxacillin; VAN, vancomycin; PEN, benzylpenicillin.

are direct medium precursors for xanthine, citrulline, and nicotinate, respectively. Similarly, deacetylation of spermine-(butyl-d8) tetrahydrochloride resulted in N¹,N¹²-diacetylspermine (butyl-d8). Succinate produced by EC cultured in RPMI with unlabeled glucose and uniformly labeled L-glutamine-¹³C₅ was 80% fully ¹²C labeled and 15% fully ¹³C₄ labeled. This result confirms that succinate is mostly synthesized from glucose, although glutamine partially contributes to its production as well.

Chemically defined biomarker enrichment medium restored pathogen metabolic phenotypes to those that were originally observed in Mueller Hinton

Our ultimate objective was to develop a reproducible defined medium allowing for pathogen growth and that enabled the production of the key biomarkers originally observable in MH medium (Rydzak et al., 2022). Using defined RPMI as our basal medium, and integrating the additional precursors needed for select biomarkers, we developed a modified, defined Biomarker Enrichment Medium (BEM; Supplementary Table 1). A number of critical modifications were made to RPMI to generate BEM (see Supplementary Table 1 for all modifications). (1) Medium was supplemented with additional amino acids that were found in MH and not present in RPMI. (2) Concentrations of many amino acids were increased to more closely resemble those found in MH medium. (3) Trace metals and nucleosides were also added to potentially promote growth of a wider array of species. (4) Catalase was added to promote the viability of species that produce hydrogen peroxide (ex. *Streptococcus pneumoniae*). (5) Albumax (a lipid-rich bovine serum albumin formulation), which is commonly added to RPMI as a substitute for human serum, was eliminated to ensure that BEM is fully defined. (6) While sucrose was added in addition to glucose, concentrations of total sugars was kept low (i.e., 5-fold hexose equivalents lower than original RPMI) to promote metabolism of amino acids and other components during the short, 4 h incubation period. (7) BEM was supplemented with spermine and concentrations of other identified precursors (with the exception of nicotinamide) were increased.

Our final BEM medium sustained growth of all six pathogen tested ($n = 3$). While growth of EC, KP, and SA was best on MH, potentially due to a richer nutrient composition, growth of these species was comparable on RPMI and BEM (Supplementary Figure 2). CA and EF grew similarly on all three media (except one EF isolate on MH), while PA grew well on MH and BEM, but not on RPMI. More importantly, our defined BEM produced the necessary diagnostic biomarkers originally identified in MH medium (Figure 7, Source Data File 3). While strictly glucose-derived biomarkers (arabitol and mevalonate)

were lower on BEM than MH and RPMI (1.3 and 3.3-fold lower for CA arabitol production and 2.6 and 2.0-fold lower for SA/EF mevalonate production, respectively), they were still significantly higher than the signals from other cultures (≥ 7.0 -fold higher for arabitol and ≥ 16.4 -fold higher for mevalonate), and thus had sufficient diagnostic power. EC and KP succinate production was comparable to MH and 2.2 to 3.5-fold higher than that observed in RPMI, potentially due to higher glutamine and lysine concentrations. Nicotinate production by EC, KP, PA, SA, and EF was almost identical to that of RPMI, which was unsurprising, given that nicotinamide concentrations were the same in both media. While EF citrulline concentrations were 3.9-fold lower in BEM when compared to MH, increasing arginine concentrations increased citrulline concentrations by 2.2-fold when compared to RPMI. Most importantly, supplementation of hypoxanthine in BEM increased PA xanthine levels by 33 and 467-fold when compared to MH and RPMI, respectively. Similarly, addition of spermine restored N¹,N¹²-diacetylspermine production by EF, production that was almost absent in RPMI. Notably, addition of spermine also resulted in N¹,N¹²-diacetylspermine production by EC and KP. However, EF can still be differentiated from EC and KP by the absence of succinate production.

Biomarker patterns for antibiotic susceptibility testing using BEM and clinically approved MH medium are comparable

To ensure that BEM is suitable for antibiotic susceptibility testing (AST), we measured the metabolic inhibition of select biomarkers in response to commonly prescribed antibiotics on bacterial isolates with known microdilution or Vitek2 AST profiles using a rapid MS/MS assay (see Methods; Source Data File 8, Figure 8). Inhibition of succinate production, adenine consumption, glucose consumption, and lactate production were used to assess antibiotic efficacy on EC and KP, PA, SA, and EF, respectively, on both BEM and CLSI approved MH II. For EC, KP, PA, and SA, inhibition of biomarker production/consumption not only identified sensitive (gray bars) and resistant strains (red bars) accurately in agreement with microbroth dilution methods (or Vitek2 for SA) in both media, but changes in biomarker levels in both media were comparable. Furthermore, sensitive vs. resistant threshold cutoffs (dashed red lines) for these species could be set at identical levels when species are incubated on either BEM or MH II. Some discrepancies between metabolic inhibition assay (MIA) results and Vitek2 results were observed for EF. Specifically, the MIA on MH II identified EF as sensitive to 8 µg/mL of benzylpenicillin and 32 µg/mL of vancomycin, contradicting Vitek2 results. Similarly, the MIA

on TM identified EF as resistant to 8 µg/mL of ampicillin and sensitive to 32 µg/mL of vancomycin in contradiction to Vitek2 results. Minor adjustments in cation levels may address these discrepancies. However, one serial dilution differences between platforms are generally acceptable by regulatory bodies (Food Administration, 2007). Ideally, MIA results should be compared to microbroth dilution results. While identical sensitive vs. resistant threshold cutoffs could be used for most species on both media, these thresholds needed to be re-calibrated for each medium with respect to lactate production levels for EF. This may be attributed to small changes in growth and/or metabolism on each medium for EF. Nevertheless, we show here that BEM is not only effective at identifying species based on metabolic patterns, but also that it can be effectively used to differentiate sensitive vs. resistant strains based on metabolic inhibition profiles of select metabolites and that these profiles are comparable to those of MH II medium.

Discussion

In this study, we showed that batches of clinical MH have significant lot-to-lot variability in their small molecule composition. This variability, in turn, had a direct impact on the metabolic phenotypes observed across a broad range of opportunistic pathogens when cultured *in vitro*. Moreover, these changes had a significant impact on our ability to differentiate these pathogens using metabolomics approaches. To address this, we developed a defined biomarker enrichment medium (BEM) that was specifically tuned for enhancing the diagnostic metabolic phenotypes of bloodstream pathogens and to enable robust to lot-to-lot reproducibility of these phenotypes.

Although we developed BEM with clinical applications in mind, our observations about the instability of metabolic phenotypes elicited by undefined media and our strategy for resolving these problems are generalizable to a broad range of other metabolomics-based applications. Metabolomics is emerging as a mainstream microbiology tool that is seeing increasing use in clinical diagnostics (Kennedy et al., 2018), metabolic engineering (Dromms and Styczynski, 2012), and is becoming a key tool for unraveling complex host-microbe dynamics (Han et al., 2010). The variability in metabolic phenotypes that we observed here could negatively affect any of these applications and may have a direct impact on our ability to reproduce metabolomic studies lab-to-lab. The strategy we introduce here (substrate exclusion, isotope tracing, and mass spectrometry-based metabolic analyses) for identifying substrate-product relationships, and enriching desirable phenotypes, is broadly applicable to any *in vitro* culture system and may help researchers develop other specialized media to ensure their experiments can be replicated by other groups.

In addition to stabilizing metabolic phenotypes, developing defined growth media has a range of other benefits. For instance, many efforts have gone into developing defined media in order to sustain growth of microorganisms (Cocaign-Bousquet et al., 1995; Letort and Juillard, 2001; Zhang et al., 2009), improve downstream purification steps of industrially valuable secreted proteins [ex. bacteriocins; (Mah et al., 1967; Pingitore et al., 2009; Khan et al., 2013)], and enable the analysis of secreted compounds [ex. exopolysaccharides; (Grobbs et al., 1998; Torino et al., 2005)]. The nutrient composition of a defined medium also influences production of secreted compounds. For example, vitamins and osmolites have been shown to impact growth and bacteriocin production in *Lactobacillus salivarius*, adenine and lactose can stimulate exopolysaccharide production in *Lactobacillus helveticus*, higher CaCl₂ and low magnesium concentrations improved bioethanol yields in *Clostridium thermocellum*, and pentose sugars can inhibit growth and biofuel yields (Torino et al., 2005; Pingitore et al., 2009); Vera (Pingitore et al., 2009; Girardello et al., 2012b; Islam et al., 2013; Sander et al., 2015; Verbeke et al., 2017). Medium cation concentrations of different MH agar brands can also influence antibiotic susceptibility results (Girardello et al., 2012a). Furthermore, the cleaner matrix of chemically defined medium can also improve the resolution of mass spectrometry analysis (Texeira et al., 2015). In summary, chemically defined media have a range of benefits beyond metabolism that warrant consideration in any large-scale studies.

One important caveat to the findings reported here is that the significant media-related variability we observed in metabolic phenotypes may not necessarily translate to more traditional clinical microbiology assays. MH is a Clinical and Laboratory Standards Institute (CLSI) approved medium for growth of pathogens and has a multi-decade track record as the gold standard media for clinical microbiology (Clinical and Laboratory Standards Institute, 2022). The distinction between our findings and this previously established efficacy is attributable to the difference between the two approaches: metabolomics monitors the concentrations of individual nutrients, whereas clinical assays generally track microbial growth. Since microbes can satisfy their biomass and energetic needs using a variety of precursors (Koch, 2005), minor variations in the levels of individual nutrients will not necessarily be reflected in altered *in vitro* growth rates.

In conclusion, we have shown that undefined media can be an unstable foundation for biomarker discovery, clinical diagnostics, and other metabolism-based microbiology assays where reproducibility is paramount. We show that our specifically engineered BEM reduces batch-to-batch variation and optimizes our target metabolic phenotypes. We recommend that future metabolomics-based studies carefully consider chemical composition of the growth media.

Materials and methods

Bacterial strains, cultivation, and sample preparation

Candida albicans, *Klebsiella pneumoniae*, *Escherichia coli*, *Pseudomonas aeruginosa*, *Staphylococcus aureus*, and *Enterococcus faecalis* used in for biomarker identification experiments were recovered from patient blood culture samples and provided as cryo stocks by Alberta Precision Laboratories (APL) and approved by the Conjoint Regional Ethics Board (REB # 16-2457 and REB#17-1525, UC). Isolates used for antibiotic susceptibility testing (AST) with known antibiotic susceptibility profiles were obtained from the Center for Disease Control (EC SAMN04014991, KP SAMN04014967, PA SAMN04014936) or from the American Type Culture Collection (SA ATCC BAA-1708, EF ATCC 51575). Antibiotic susceptibility profiles of ATCC strains were determined using the Vitek2 (BioMérieux) according to manufacturer protocols. All strains were cultured in a humidified incubator (Heracell VIOS 250i Tri-Gas Incubator, Thermo Scientific, Waltham, Mass. USA) under a 5% CO₂ and 21% O₂ atmosphere. Cryo stocks were first revived on Mueller Hinton agar plates overnight. Colonies were then scraped off the plate and diluted to a 0.5 McFarland (OD₆₀₀ ~ 0.15 or ~7.5 × 10⁷ CFU/mL) in respective medium (see below), and incubated for 4 h as described previously (Rydzak et al., 2022). Cultures were then centrifuged for 10 min for 4,000 g at 4°C to remove cells. Supernatant was removed, mixed 1:1 with 100% LC-MS grade methanol, and frozen at −80°C for further processing. Upon thawing, samples were centrifuged again for 10 min at 4,000 g at 4°C to remove any protein precipitate and supernatants were diluted 1:10 with 50% LC-MS grade methanol and analyzed using UHPLC-MS.

Chemicals and medium preparation

All chemicals were obtained from Sigma-Aldrich (St. Louis, Mo. USA), VWR (Radnor, Pa. USA), or Fisher Scientific (Waltham, Mass. USA) unless otherwise specified. To study the lot-to-lot variability in MH, different lots of media was sourced from BD (Becton, Dickinson, and Co) and Fluka Analytical. These include MH I from BD (BD lots 1-3; 1025007, 8119710, 9127956), MH I from Fluka Analytical (Fluka Lot 1-2; BCBG7588V, BCBM5081V), and MH II from BD (BD Lot 4-6; 8095574, 8190586, 9044411). Each medium was prepared according to the recipe specified on the bottle, autoclaved for 20 min at 121°C, and stored at 4°C. RPMI 1640 was supplemented with 25 mM HEPES, 100 μM hypoxanthine, and 2.5 g/L Albumax II [see [Supplementary Table 1](#) for full recipe; (Lewis et al., 2014)] and filter sterilized (pore size, 0.2 μm; Millipore, Billerica, MA). Final Biomarker Enrichment Medium composition is also provided in [Supplementary Table 1](#). Catalase

was added to medium on the same day as experiments were performed, and medium was filter sterilized.

To investigate which biomarkers were derived from glucose, RPMI 1640 medium with no glucose (MP Biomedicals, 1646854) was supplemented with uniformly labeled [U-¹³C]glucose purchased from Cambridge Isotope Laboratories (catalog number: CLM-1396-50). To identify likely precursors for biomarkers that did not predominantly come from glucose (i.e., citrulline, xanthine, nicotinate, and succinate) we screened the effect of exclusion of individual amino acids and other putative precursors found in RPMI on the production of these four biomarkers. RPMI was made according to the recipe in [Supplementary Table 1](#) and amino acids and other putative precursors/cofactors (nicotinamide, hypoxanthine, pyridoxine) were excluded individually.

To verify species-specific biomarker precursors, L-arginine, nicotinamide, spermine, L-glutamine, and hypoxanthine in RPMI were individually replaced with labeled analogs. Arginine-HCl (Guanido-¹⁵N₂) (catalog number: NLM-395-1), hypoxanthine (¹³C₅) (catalog number: CLM-8042-0.1MG), and L-glutamine (¹³C₅) (catalog number: CNLM-1275-H-0.5) were purchased from Cambridge Isotope Laboratories. Spermine-(butyl-d₈) tetrahydrochloride (catalog number: 705330-5MG) was purchased from Sigma-Aldrich. Finally, nicotinamide-2,6,7-¹³C₃-(pyridyl-¹⁵N) (catalog number: 809799-1MG) was purchased from Millipore Sigma.

Growth measurements

Growth curves were performed in 96-well-plates incubated inside a spectrophotometer (Multiskan Go, Thermo Scientific) at 37°C for 24 h. Turbidity was measured every hour at 600 nm. Optical density values were adjusted to a 1 cm pathlength by multiplying the net change in OD₆₀₀ by a conversion factor of 4.6. Given that growth curves were performed for 24 h, evaporation occurring in the wells near the edge of the 96-well-plate could affect optical density. To avoid this technical error, all the wells near the edges were filled with non-inoculated medium, and only central wells were inoculated.

UHPLC-MS

All metabolomics data were acquired at the Calgary Metabolomics Research Facility (CMRF) as previously described (Rydzak et al., 2022). Briefly, chromatography was performed using hydrophilic interaction liquid chromatography (HILIC) with changing gradients of 20 mM ammonium formate at pH 3.0 in LC-MS grade water (Solvent A) and 0.1% formic acid (% v/v) in LC-MS grade acetonitrile (Solvent B) on a Thermo Fisher Scientific Vanquish UHPLC platform. The flow rate used in all analyses was 600 μL/min and the sample injection volume was 2 μL. Samples were analyzed in both negative (−2,000 V)

and positive mode (+3,000 V) on a Thermo Scientific Q Exactive™ HF (Thermo Scientific) mass spectrometer using full scan acquisitions (50–750 m/z) with a 240,000 resolving power, an automatic gain control target of 3×10^6 , and a maximum injection time of 200 ms. Data for antibiotic susceptibility testing validation were acquired on a TSQ Altis Triple Quadrupole (Thermo Scientific) mass spectrometer operating in selected reaction monitoring (SRM) mode using flow injection analysis. Samples were run at a flow rate of 1.5 mL/min using 60/40 LC-MS grade acetonitrile/water (%v/v) with 0.1% formic acid (%v/v) running isocratically with a method duration of 0.65 mins. Samples were run in positive (+3,000V) and negative (−2,500V) ion mode using the following SRM transitions with their respective collision energies (CE): adenine $[M+H]^+$ 136 $m/z \rightarrow$ 119 m/z (23V CE), lactate $[M-H]^-$ 89 $m/z \rightarrow$ 43 m/z (12V CE), succinate $[M-H]^-$ 117 $m/z \rightarrow$ 73 m/z (11V CE), and glucose $[M+Cl]^-$ 215 $m/z \rightarrow$ 35 m/z (11V CE).

Computational methods

All MS analyses were conducted in MAVEN (EI-MAVEN v0.12.0) (Melamud et al., 2010). Untargeted analysis of different batches of MH medium was performed with the peak picking function in EI-MAVEN v0.12.0 with a 10 ppm m/z window and a minimum peak intensity set to 50,000. Targeted peak assignments were based on the Mass Spectrometry Metabolite Library of Standards (MSMLS, IROA Technologies) as previously described (Groves et al., 2022). Statistical analyses were conducted using the R statistical software platform (R Core Team, 2022) using in-house software tools previously published [<https://zenodo.org/record/6403220#.YkYXoi9730o>; (Rydzak et al., 2022)].

Data availability statement

The original contributions presented in the study are included in the article/Supplementary Material, further inquiries can be directed to the corresponding author/s.

Author contributions

MM, TR, RG, and IL designed the experiments. MM and TR performed experiments. RG, MM, and TR collected and interpreted mass spectrometry data. TR, MM, and IL wrote the manuscript. All authors contributed to the article and approved the submitted version.

Funding

This work was supported by Genome Canada's 2016 Genomics Application Partnership Program (GAPP) award

and the 2017 Large Scale Applied Research Project (LSARP) competition, administered through Genome Alberta. This work was made possible in part by a research collaboration agreement with Thermo Fisher. IL was supported by an Alberta Innovates Translational Health Chair. TR was supported by an Eyes High Postdoctoral Fellowship from the University of Calgary. Metabolomics data were acquired at the Calgary Metabolomics Research Facility, which was supported by the International Microbiome Center and the Canada Foundation for Innovation (CFI-JELF 34986). This research was funded by a Genome Canada GAPP award, which is intended to enable the commercialization of research findings.

Conflict of interest

IL and TR have submitted a patent (International Application Number CA2019051351) describing substrate-product relationships used to identify pathogens.

The remaining authors declare that the research was conducted in the absence of any commercial or financial relationships that could be construed as a potential conflict of interest.

Publisher's note

All claims expressed in this article are solely those of the authors and do not necessarily represent those of their affiliated organizations, or those of the publisher, the editors and the reviewers. Any product that may be evaluated in this article, or claim that may be made by its manufacturer, is not guaranteed or endorsed by the publisher.

Supplementary material

The Supplementary Material for this article can be found online at: <https://www.frontiersin.org/articles/10.3389/fmicb.2022.957158/full#supplementary-material>

SUPPLEMENTARY FIGURE 1

Comparison of MH and RPMI medium components. Levels of most amino acids, with the exception of glutamine, asparagine, and cysteine, were higher in MH vs. RPMI, whereas glucose and select vitamins were higher in RPMI.

SUPPLEMENTARY FIGURE 2

Growth rates on MH, RPMI, and BEM medium. Biological replicates ($n = 3$; red, blue and gray lines) of *Candida albicans* (CA), *Klebsiella pneumoniae* (KP), *Escherichia coli* (EC), *Pseudomonas aeruginosa* (PA), *Staphylococcus aureus* (SA), *Enterococcus faecalis* (EF), and *Streptococcus pneumoniae* (SP) were grown for 24 h.

SUPPLEMENTARY TABLE 1

Composition of RPMI and BEM.

References

- Basile, A., Campanaro, S., Kovalovszki, A., Zampieri, G., Rossi, A., Angelidaki, I., et al. (2020). Revealing metabolic mechanisms of interaction in the anaerobic digestion microbiome by flux balance analysis. *Metab. Eng.* 62, 138–149. doi: 10.1016/j.ymben.2020.08.013
- Berger, F., Ramirez-Hernández, M. A. H., and Ziegler, M. (2004). The new life of a centenarian: signalling functions of NAD (P). *Trends Biochem. Sci.* 29, 111–118. doi: 10.1016/j.tibs.2004.01.007
- Bortolotti, M., Polito, L., Battelli, M. G., and Bolognesi, A. (2021). Xanthine oxidoreductase: One enzyme for multiple physiological tasks. *Redox Biology* 41, 101882. doi: 10.1016/j.redox.2021.101882
- Clinical and Laboratory Standards Institute. (2022). *M100: Performance Standards for Antimicrobial Susceptibility Testing*, 32nd Edn. p. 1–362.
- Cocaign-Bousquet, M., Garrigues, C., Novak, L., Lindley, N., and Loublere, P. (1995). Rational development of a simple synthetic medium for the sustained growth of *Lactococcus lactis*. *J. Appl. Bacteriol.* 79, 108–116. doi: 10.1111/j.1365-2672.1995.tb03131.x
- Copeland, W. B., Bartley, B. A., Chandran, D., Galdzicki, M., Kim, K. H., Sleight, S. C., et al. (2012). Computational tools for metabolic engineering. *Metab. Eng.* 14, 270–280. doi: 10.1016/j.ymben.2012.03.001
- DeBell, R. M. (1979). Production of exotoxin A by *Pseudomonas aeruginosa* in a chemically defined medium. *Infect. Immun.* 24, 132–138. doi: 10.1128/iai.24.1.132-138.1979
- Dromms, R. A., and Styczynski, M. P. (2012). Systematic applications of metabolomics in metabolic engineering. *Metabolites* 2, 1090–1122. doi: 10.3390/metabo2041090
- Feldman, L. I., and Gunsalus, I. C. (1950). The occurrence of a wide variety of transaminases in bacteria. *J. Biol. Chem.* 187, 821–830. doi: 10.1016/S0021-9258(18)56228-1
- Food and Administration, D. (2007). *Antimicrobial Susceptibility Test (AST) Systems—Class II Special Controls Guidance for Industry and FDA*. Silver Spring, MD: Food and Drug Administration.
- Girardello, R., Bispo, P. J., Yamanaka, T. M., and Gales, A. C. (2012a). Cation concentration variability of four distinct mueller-hinton agar brands influences polymyxin B susceptibility results. *J. Clin. Microbiol.* 50, 2414–2418. doi: 10.1128/JCM.06686-11
- Girardello, R., Bispo, P. J. M., Yamanaka, T. M., and Gales, A. C. (2012b). Cation concentration variability of four distinct mueller-hinton agar brands influences polymyxin B Susceptibility results. *J. Clin. Microbiol.* 50, 2414–2418. doi: 10.1128/JCM.06686-11
- Grobben, G. J., Chin-Joe, I., Kitzen, V. A., Boels, I. C., Boer, F., Sikkema, J., et al. (1998). Enhancement of exopolysaccharide production by *Lactobacillus delbrueckii* subsp. *bulgaricus* NCFB 2772 with a simplified defined medium. *Appl. Environ. Microbiol.* 64, 1333–1337. doi: 10.1128/AEM.64.4.1333-1337.1998
- Groves, R. A., Mapar, M., Aburashed, R., Ponce, L. F., Bishop, S. L., Rydzak, T., et al. (2022). Methods for quantifying the metabolic boundary fluxes of cell cultures in large cohorts by high-resolution hydrophilic liquid chromatography mass spectrometry. *Anal. Chem.* 94, 8874–8882. doi: 10.1021/acs.analchem.2c00078
- Gunsalus, C. F., and Tonzetich, J. (1952). Transaminases for pyridoxamine and purines. *Nature* 170, 162–162. doi: 10.1038/170162a0
- Han, J., Antunes, L. C. M., Finlay, B. B., and Borchers, C. H. (2010). Metabolomics: towards understanding host–microbe interactions. *Future Microbiol.* 5, 153–161. doi: 10.2217/fmb.09.132
- Islam, R., Özmihçi, S., Cicek, N., Sparling, R., and Levin, D. B. (2013). Enhanced cellulose fermentation and end-product synthesis by *Clostridium thermocellum* with varied nutrient compositions under carbon-excess conditions. *Biomass Bioenergy* 48, 213–223. doi: 10.1016/j.biombioe.2012.11.010
- Joshi, C. J., Peebles, C. A., and Prasad, A. (2017). Modeling and analysis of flux distribution and bioproduct formation in *Synechocystis* sp. PCC 6803 using a new genome-scale metabolic reconstruction. *Algal Res.* 27, 295–310. doi: 10.1016/j.algal.2017.09.013
- Karp, P. D., Billington, R., Caspi, R., Fulcher, C. A., Latendresse, M., Kothari, A., et al. (2019). The BioCyc collection of microbial genomes and metabolic pathways. *Brief. Bioinform.* 20, 1085–1093. doi: 10.1093/bib/bbx085
- Kennedy, A. D., Wittmann, B. M., Evans, A. M., Miller, L. A., Toal, D. R., Loneragan, S., et al. (2018). Metabolomics in the clinic: a review of the shared and unique features of untargeted metabolomics for clinical research and clinical testing. *J. Mass Spectrom.* 53, 1143–1154. doi: 10.1002/jms.4292
- Khan, H., Flint, S., and Yu, P. L. (2013). Development of a chemically defined medium for the production of enterolysin A from *Enterococcus faecalis* B 9510. *J. Appl. Microbiol.* 114, 1092–1102. doi: 10.1111/jam.12115
- Koch, A. L. (2005). Bacterial choices for the consumption of multiple resources for current and future needs. *Microb. Ecol.* 49, 183–197. doi: 10.1007/s00248-003-1053-4
- Laiglecia, J. I., Estrada, V. G., Vidal Vidal, R., Florencio, F. J., Guerrero, M. G., and Diaz, M. S. (2013). Dynamic flux balance analysis of a genetic engineered cyanobacterium for ethanol production: parameter estimation. *Chem. Eng. Trans.* 32, 955–960. doi: 10.3303/CET1332160
- Letort, C., and Juillard, V. (2001). Development of a minimal chemically-defined medium for the exponential growth of *Streptococcus thermophilus*. *J. Appl. Microbiol.* 91, 1023–1029. doi: 10.1046/j.1365-2672.2001.01469.x
- Levering, J., Fiedler, T., Sieg, A., van Grinsven, K. W., Hering, S., Veith, N., et al. (2016). Genome-scale reconstruction of the *Streptococcus pyogenes* M49 metabolic network reveals growth requirements and indicates potential drug targets. *J. Biotechnol.* 232, 25–37. doi: 10.1016/j.jbiotec.2016.01.035
- Lewis, I. A., Wacker, M., Olszewski, K. L., Cobbold, S. A., Baska, K. S., Tan, A., et al. (2014). Metabolic QTL analysis links chloroquine resistance in *Plasmodium falciparum* to impaired hemoglobin catabolism. *PLoS Genet.* 10, e1004085. doi: 10.1371/journal.pgen.1004085
- Machado, H., Weng, L. L., Dillon, N., Seif, Y., Holland, M., Pekar, J. E., et al. (2019). Strain-specific metabolic requirements revealed by a defined minimal medium for systems analyses of *Staphylococcus aureus*. *Appl. Environ. Microb.* 85, e01773–e01719. doi: 10.1128/AEM.01773-19
- Mah, R. A., Fung, D. Y., and Morse, S. A. (1967). Nutritional requirements of *Staphylococcus aureus* S-6. *Appl. Microbiol.* 15, 866–870. doi: 10.1128/am.15.4.866-870.1967
- Marletta, M. A. (1993). Nitric oxide synthase structure and mechanism. *J. Biol. Chem.* 268, 12231–12234. doi: 10.1016/S0021-9258(18)31375-9
- McGillicuddy, N., Floris, P., Albrecht, S., and Bones, J. (2018). Examining the sources of variability in cell culture media used for biopharmaceutical production. *Biotechnol. Lett.* 40, 5–21. doi: 10.1007/s10529-017-2437-8
- Melamud, E., Vastag, L., and Rabinowitz, J. D. (2010). Metabolomic analysis and visualization engine for LC-MS data. *Anal. Chem.* 82, 9818–9826. doi: 10.1021/ac1021166
- Pegg, A. E. (2008). Spermidine/spermine-N1-acetyltransferase: a key metabolic regulator. *Am. J. Physiol. Endocrin. Metab.* 294, E995–E1010. doi: 10.1152/ajpendo.90217.2008
- Pingitore, E. P. V., Hebert, E. M. M., Sesma, F., and Nader-Macias, M. E.-M. E. (2009). Influence of vitamins and osmolytes on growth and bacteriocin production by *Lactobacillus salivarius* CRL 1328 in a chemically defined medium. *Can. J. Microbiol.* 55, 304–310. doi: 10.1139/W08-092
- R Core Team. (2022). *R: A language and environment for statistical computing*. R Foundation for Statistical Computing, Vienna, Austria. Available online at: <https://www.R-project.org/> (accessed March 10, 2022).
- Rydzak, T., Groves, R. A., Zhang, R., Aburashed, R., Pushpker, R., Mapar, M., et al. (2022). Metabolic preference assay for rapid diagnosis of bloodstream infections. *Nat. Commun.* 13, 1–12. doi: 10.1038/s41467-022-30048-6
- Sánchez, S., Martínez, M. E., and Espinola, F. (2000). Biomass production and biochemical variability of the marine microalga *Isochrysis galbana* in relation to culture medium. *Biochem. Eng. J.* 6, 13–18. doi: 10.1016/S1369-703X(00)00071-1
- Sanchez-Rosario, Y., and Johnson, M. D. L. (2021). Media matters, examining historical and modern *Streptococcus pneumoniae* growth media and the experiments they affect. *Front. Cell. Infect. Microbiol.* 11, 613623. doi: 10.3389/fcimb.2021.613623
- Sander, K., Wilson, C. M., Rodriguez, M., Klingeman, D. M., Rydzak, T., Davison, B. H., et al. (2015). *Clostridium thermocellum* DSM 1313 transcriptional responses to redox perturbation. *Biotechnol. Biofuels* 8, 211. doi: 10.1186/s13068-015-0394-9
- Steuer, R. (2007). Computational approaches to the topology, stability and dynamics of metabolic networks. *Phytochemistry* 68, 2139–2151. doi: 10.1016/j.phytochem.2007.04.041
- Teusink, B., Wiersma, A., Molenaar, D., Francke, C., De Vos, W. M., Siezen, R. J., et al. (2006). Analysis of growth of *Lactobacillus plantarum* WCFS1 on a complex medium using a genome-scale metabolic model. *J. Biol. Chem.* 281, 40041–40048. doi: 10.1074/jbc.M606263200

- Texeira, E., Checa, J., Rial, A., Chabalgoity, J. A., and Suárez, N. (2015). A new chemically defined medium for cultivation of *Streptococcus pneumoniae* Serotype 1. *J. Biotech Res.* 6, 54. Available online at: <https://btsjournals.sharepoint.com/Documents/2015v6p54-62.pdf>
- Torino, M., Hebert, E., Mozzi, F., and Font de Valdez, G. (2005). Growth and exopolysaccharide production by *Lactobacillus helveticus* ATCC 15807 in an adenine-supplemented chemically defined medium. *J. Appl. Microbiol.* 99, 1123–1129. doi: 10.1111/j.1365-2672.2005.02701.x
- Verbeke, T. J., Giannone, R. J., Klingeman, D. M., Engle, N. L., Rydzak, T., Guss, A. M., et al. (2017). Pentose sugars inhibit metabolism and increase expression of an AgrD-type cyclic pentapeptide in *Clostridium thermocellum*. *Sci. Rep.* 7, 1–11. doi: 10.1038/srep43355
- Wishart, D. S., Feunang, Y. D., Marcu, A., Guo, A. C., Liang, K., Vázquez-Fresno, R., et al. (2018). HMDB 4.0: the human metabolome database for 2018. *Nucleic Acids Res.* 46, D608–D617. doi: 10.1093/nar/gkx1089
- Zhang, G., Mills, D. A., and Block, D. E. (2009). Development of chemically defined media supporting high-cell-density growth of *lactococci*, *enterococci*, and *streptococci*. *Appl. Environ. Microbiol.* 75, 1080–1087. doi: 10.1128/AEM.01416-08



OPEN ACCESS

EDITED BY

Vijay Soni,
NewYork-Presbyterian, United States

REVIEWED BY

Nimi Vashi,
Memorial Sloan Kettering Cancer
Center, United States
Neelam Oswal,
Hackensack Meridian Health Center
for Discovery and Innovation,
United States

*CORRESPONDENCE

Ian A. Lewis
ian.lewis2@ucalgary.ca

SPECIALTY SECTION

This article was submitted to
Antimicrobials, Resistance
and Chemotherapy,
a section of the journal
Frontiers in Microbiology

RECEIVED 01 June 2022

ACCEPTED 11 July 2022

PUBLISHED 13 September 2022

CITATION

Mohammadi M, Bishop SL,
Aburashed R, Luqman S, Groves RA,
Bihan DG, Rydzak T and Lewis IA
(2022) Microbial containment device:
A platform for comprehensive analysis
of microbial metabolism without
sample preparation.
Front. Microbiol. 13:958785.
doi: 10.3389/fmicb.2022.958785

COPYRIGHT

© 2022 Mohammadi, Bishop,
Aburashed, Luqman, Groves, Bihan,
Rydzak and Lewis. This is an
open-access article distributed under
the terms of the [Creative Commons
Attribution License \(CC BY\)](https://creativecommons.org/licenses/by/4.0/). The use,
distribution or reproduction in other
forums is permitted, provided the
original author(s) and the copyright
owner(s) are credited and that the
original publication in this journal is
cited, in accordance with accepted
academic practice. No use, distribution
or reproduction is permitted which
does not comply with these terms.

Microbial containment device: A platform for comprehensive analysis of microbial metabolism without sample preparation

Mehdi Mohammadi^{1,2}, Stephanie L. Bishop¹,
Raied Aburashed², Saad Luqman², Ryan A. Groves¹,
Dominique G. Bihan¹, Thomas Rydzak¹ and Ian A. Lewis^{1*}

¹Department of Biological Sciences, University of Calgary, Calgary, AB, Canada, ²Department of Biomedical Engineering, University of Calgary, Calgary, AB, Canada

Metabolomics is a mainstream strategy for investigating microbial metabolism. One emerging application of metabolomics is the systematic quantification of metabolic boundary fluxes – the rates at which metabolites flow into and out of cultured cells. Metabolic boundary fluxes can capture complex metabolic phenotypes in a rapid assay, allow computational models to be built that predict the behavior of cultured organisms, and are an emerging strategy for clinical diagnostics. One advantage of quantifying metabolic boundary fluxes rather than intracellular metabolite levels is that it requires minimal sample processing. Whereas traditional intracellular analyses require a multi-step process involving extraction, centrifugation, and solvent exchange, boundary fluxes can be measured by simply analyzing the soluble components of the culture medium. To further simplify boundary flux analyses, we developed a custom 96-well sampling system—the Microbial Containment Device (MCD)—that allows water-soluble metabolites to diffuse from a microbial culture well into a bacteria-free analytical well via a semi-permeable membrane. The MCD was designed to be compatible with the autosamplers present in commercial liquid chromatography-mass spectrometry systems, allowing metabolic fluxes to be analyzed with minimal sample handling. Herein, we describe the design, evaluation, and performance testing of the MCD relative to traditional culture methods. We illustrate the utility of this platform, by quantifying the unique boundary fluxes of four bacterial species and demonstrate antibiotic-induced perturbations in their metabolic activity. We propose the use of the MCD for enabling single-step metabolomics sample preparation for microbial identification, antimicrobial susceptibility testing, and other metabolic boundary flux applications where traditional sample preparation methods are impractical.

KEYWORDS

metabolomics, antibiotic susceptibility testing (AST), metabolic boundary fluxes, liquid chromatography-mass spectrometry, metabolic preference assay, bacteria identification, fabrication

Introduction

Metabolomics is a mainstream strategy for understanding complex biological processes and mapping the molecular underpinnings of disease (Kell and Oliver, 2016; Pinu et al., 2019). Liquid chromatography-mass spectrometry (LC-MS) has emerged as the main platform for performing these analyses and increasing technological advances have allowed LC-MS to capture ever broader transects of the metabolome (Metz et al., 2007; Lu et al., 2017; Cui et al., 2018). Over the past several years, there has been an increasing emphasis on developing high-sensitivity LC-MS methods that capture the largest possible range of metabolites present in a given sample (Monge et al., 2019; Araujo-León et al., 2020). While these sensitivity-focused methods have enabled researchers to characterize astonishing chemical diversity in a wide range of organisms, these methods are difficult to implement in large-scale studies due to their use of long gradients and due to difficulties in conducting stable quantitative analyses over large-scale studies.

Recently, there has been increasing interest in establishing quantitatively robust metabolomics assays that can be applied to large-scale cohort studies (Zheng et al., 2018; Cao et al., 2020). One of the most promising approaches is tracking metabolic boundary fluxes—the rates at which metabolites are consumed or produced by *in vitro* cell cultures—to map intracellular metabolic activities (Orth et al., 2010; Pinu and Villas-Boas, 2017; Hui et al., 2020). Quantifying the rates that molecules are secreted or consumed can provide extensive insight into cellular function, the activity of metabolic networks (Liang et al., 2011; Hollinshead et al., 2014), and nutritional dependencies of diverse organisms (Orth et al., 2010). This emerging strategy is useful because it is quantitatively robust, can be applied to large-scale cohorts, and can rapidly capture phenotypic information about microbes, such as their species and antibiotic susceptibility profiles (Rydzak et al., 2022). In summary, measuring microbial boundary fluxes provides a robust mechanism for understanding the metabolism of cultured organisms. Notably, LC-MS methods that quantify these fluxes are a powerful emerging strategy in clinical diagnostics (Rydzak et al., 2022), improving biofuels production (Hollinshead et al., 2014; Bideaux et al., 2016), decoding microbiome interactions (Antoniewicz, 2020), understanding microbial community interactions (Khandelwal et al., 2013; Perez-Garcia et al., 2016), and enabling microbial engineering projects (Munro and Kell, 2021).

One of the primary advantages of studying microbes via their metabolic boundary fluxes is its simplicity. The metabolites that are consumed or secreted by *in vitro* cultures are generally water soluble, relatively abundant, and less chemically diverse than intracellular metabolites (Groves et al., 2022). Moreover, they are accessible via relatively simple sample preparation workflows that separate cells from the metabolites present in the culture medium (Pinu and Villas-Boas, 2017). These analyses

could be further simplified if they were coupled to a device that physically separated the cells from the metabolite. To achieve this, we developed the Microbial Containment Device (MCD), a novel two-chamber sampling platform that separates microbial specimens in one chamber from a sterile analytical chamber via a semipermeable membrane. The primary goal of the MCD is to enable microbial boundary flux analyses via a single-step metabolomics sample processing method that minimizes human error, helps prevent sample cross-contamination, and minimizes technical error across large-scale cohorts. The MCD uses a similar design strategy to the commercial Transwell® (Corning) device, but it addresses two shortcomings of the Transwell® for use in high-throughput microbial metabolomics studies: (1) the pore size of the Transwell® (0.4 μm) allows some bacteria to pass through the membrane and (2) the high cost of the Transwell® is incompatible with the needs of large-scale metabolomics studies. To demonstrate the applicability of the MCD in replacing a traditional microbial culture workflow, we used the MCD to differentiate four bacteria species (*Escherichia coli*, *Klebsiella pneumoniae*, *Enterococcus faecalis*, and *Staphylococcus aureus*) and measure their antibiotic susceptibility profiles. Our data show that the MCD can (1) accurately reproduce traditional microbial culture workflows; (2) allow the user to analyze samples with no additional sample preparation steps once samples are loaded into the device; (3) facilitate pathogen identification (ID) and empirically measure antibiotic susceptibility profiles of these pathogens; and (4) maintain a sterile mass spectrometry analysis chamber. In summary, we introduce this tool as a simple device for enabling large-scale metabolomics projects where the emphasis is on quantifying metabolic boundary fluxes.

Materials and methods

Design principle of the microbial containment device

The MCD is a plastic insert that fits into a standard-format 96-well microplate. The MCD has 96 sampling inserts and the bottom of each is enclosed, with a 0.2- μm semi-permeable membrane. When the MCD is inserted into a 96-well microplate, the membrane creates a lower microbial growth chamber and upper analytical chamber. Media components, including small molecules such as metabolites, can freely diffuse through the membrane between the upper and the lower compartments (Figures 1A,B). The MCD is compatible with LC instrumentation that handles 96-well plates (e.g., Thermo Scientific™ Vanquish™ UHPLC system), and the MCD insert was designed to allow the Vanquish LC sampling needle to extract samples from the top of the MCD without piercing the membrane to enable simplified sample preparation for large cohort studies (Figure 1D).

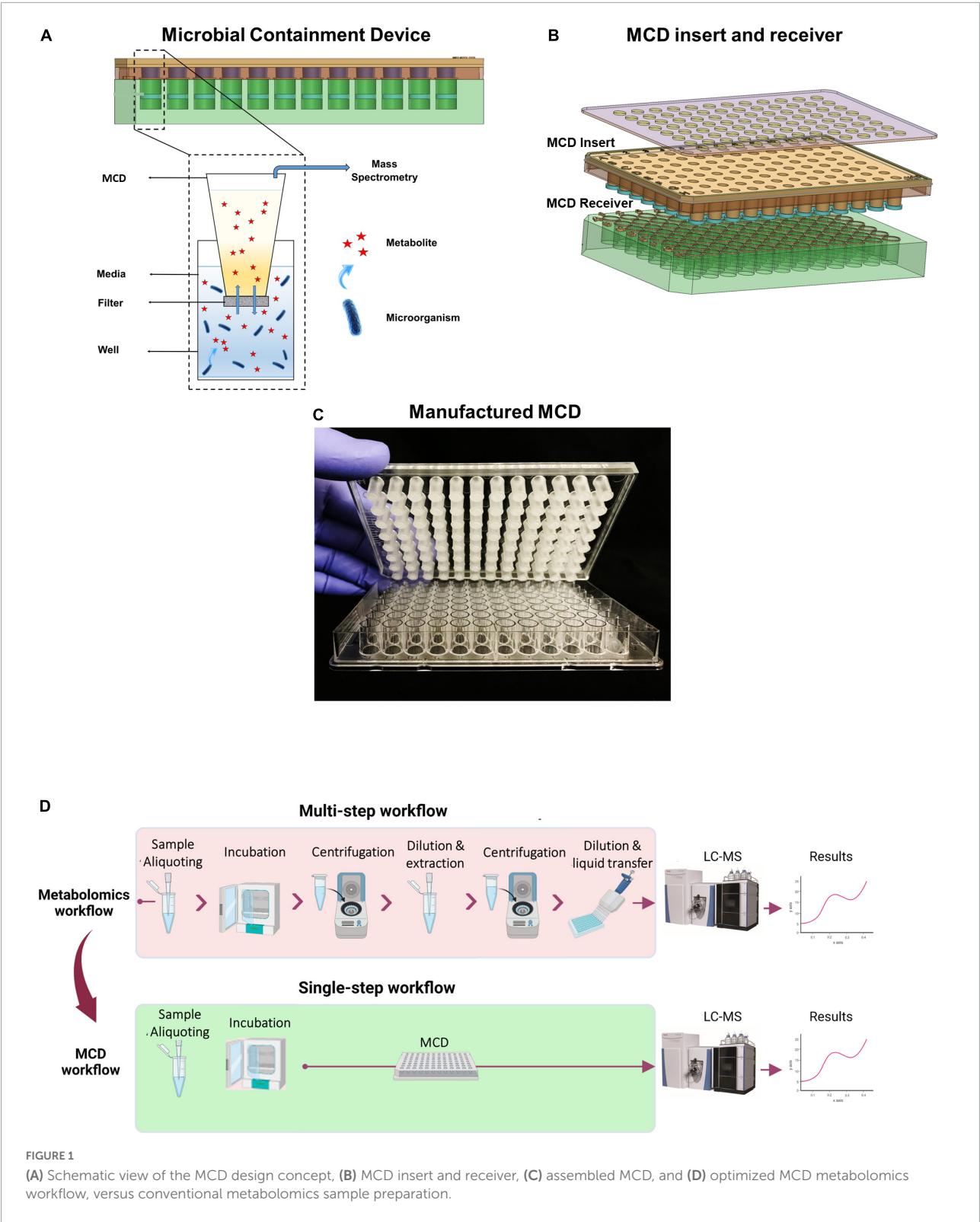


FIGURE 1
(A) Schematic view of the MCD design concept, (B) MCD insert and receiver, (C) assembled MCD, and (D) optimized MCD metabolomics workflow, versus conventional metabolomics sample preparation.

Fabrication of the microbial containment device

We used a rapid prototyping workflow to design, fabricate, and test the MCD. We used Fusion 360 software to design the MCD and performed 3D printing with high temp resin and a Form 3 SLA 3D printer (Formlabs, Boston, MA, United States). We then post-washed the 3D printed component in an isopropyl alcohol bath to dissolve liquid resin followed by post-curing using 405 nm light along with a heating system (based on the Formlabs manufacturing instructions for high temperature resin¹). A Universal Laser Systems VLS3.60DT² (Canadian Engravers Supply, Mississauga, ON, Canada) was used to cut the filter and double-sided tape for filter assembly. We used an Anprolene AN74j ethylene oxide gas sterilization machine (Andersen Sterilizers, Inc., Haw River, NC, United States) to sterilize the prototype MCD before testing and validation. After we performed proof-of-concept testing and validation of the device, we designed a custom mold for the injection molding and mass manufacturing processes. This required us to develop a new semi-automatic machine and assembly technique for polycarbonate filter (0.2 μm pore size) assembly in our lab. We also developed a Quality Control (QC) procedure (including visual testing, clinical testing, and validation) to ensure repeatability and reliability of the manufactured MCD. Commercial MCD platforms can be ordered from Fluidome, Inc.³ (Calgary, AB, Canada). All steps of development are shown in [Supplementary Figure 1](#).

Numerical simulation

To optimize the MCD design, we computationally modeled the metabolite diffusion and dynamic changes of metabolite concentration over time within the proposed device. We used COMSOL Multiphysics software⁴, a finite element simulation platform that spans all simulation steps from model design and geometries, selection of appropriate material and physics, solving, and postprocessing results, to simulate the diffusion rate in the MCD. For this study, we created a 3D model for one well where the bottom well geometry was 7 mm diameter \times 4 mm height, and the top well geometry was 4 mm diameter \times 4 mm height. We considered a filter membrane with 10% porosity on the interface of both top and bottom wells (porosity is the percent of the total surface area occupied by the pores) based on the polycarbonate filter membrane specification datasheet. For the boundary condition for this

study, we assumed initial concentrations of 0 and 2 mM on the top and bottom wells, respectively (as 2 mM meets or exceeds the instrumental upper limit of quantification for most metabolites of interest). We considered the ambient pressure and temperature to be 100 kPa and 310 K, respectively, and water as the liquid material. Furthermore, we considered free tetrahedral mesh (extra fine), including 149,756 mesh elements, in this study. We used the transport of diluted species physics and a time-dependent study to monitor the concentration change over 6 h on the top and bottom of a single 3D well. The dynamic change of concentration was simulated in the 3D model over the cross-sectional surface and over the centerline of the well from bottom to top. Additionally, to ensure that the size of mesh and number of mesh elements had no impact on our result, we ran the mesh dependency test. The purpose of the mesh dependency test is to determine the correct mesh size (ranging from coarse to extra fine mesh) that leads to a consistent result (in this case, the diffusion rate of metabolites) in the simulation. This means that the simulation result remains independent from the mesh size. After running the simulation and gradually increasing the mesh density, we determined that free tetrahedral mesh (extra fine), including 149,756 mesh elements, produced the most consistent result for our simulation.

Strains, growth, and sample preparation

Bacterial strains were grown on BD BBLTM Mueller Hinton II Broth (BD Biosciences; VWR, Edmonton, AB, Canada), prepared as per the manufacturer's instructions. The Mueller Hinton broth was autoclaved at 121.5°C for 20 min (Primus Sterilizer, Omaha, NE, United States) and cooled to room temperature. The prepared medium was stored at 4°C. Mueller Hinton (MH) agar plates were prepared in the same way but with supplementation of 1% agar before autoclaving.

Different bacterial strains including *Escherichia coli* (EC 1, 2, 3, 4), *Klebsiella pneumoniae* (KP 1, 2, 3, 4), *Enterococcus faecalis* (EF 1, 2, 3), and *Staphylococcus aureus* (SA 1, 2, 3, 4) were purchased from the American Type Culture Collection (ATCC) or provided by the Center for Disease Control (CDC) (see [Table 1](#)).

Bacteria were incubated overnight (36.5°C, 5% CO₂ and 17.5% O₂) on Mueller Hinton (MH) agar plates prior to experiments, and 17.5% O₂. All experiments were performed in the Thermo 1,300 Series A2 biosafety cabinet. To create initial stock solutions, we picked a bacterial colony from an agar plate and diluted it in 4 mL saline to reach 0.5 McFarland ($\sim 7.5 \times 10^6$ CFU/mL). Optical density values at 600 nm (OD₆₀₀) were measured in a microplate reader (Thermo ScientificTM MultiskanTM GO).

1 www.formlabs.com

2 www.ulsinc.com

3 www.fluidome.ca

4 www.comsol.com

TABLE 1 Organism names and strains used in this study.

Sample name	Organism name	Strain	Sample name	Organism name	Strain
EC (1)	<i>E. coli</i>	ATCC 25922	KP (1)	<i>K. pneumoniae</i>	ATCC 700603
EC (2)	<i>E. coli</i>	BAA-196	KP (2)	<i>K. pneumoniae</i>	ATCC BAA-1705
EC (3)	<i>E. coli</i>	SAMN04014854	KP (3)	<i>K. pneumoniae</i>	SAMN04014953
EC (4)	<i>E. coli</i>	SAMN04014978	KP (4)	<i>K. pneumoniae</i>	SAMN04014954
SA (1)	<i>S. aureus</i>	ATCC 25923	EF (1)	<i>E. faecalis</i>	ATCC 29212
SA (2)	<i>S. aureus</i>	ATCC 43300	EF (2)	<i>E. faecalis</i>	ATCC 51299
SA (3)	<i>S. aureus</i>	ATCC BAA-976	EF (3)	<i>E. faecalis</i>	ATCC 19433
SA (4)	<i>S. aureus</i>	ATCC BAA-977			

Experimental workflow

Antibiotic panels containing cefazolin (CFZ; 2, 8 μ M), gentamicin (GEN; 4, 8 μ M), ampicillin (AMP; 8, 32 μ M), ciprofloxacin (CIP; 1, 4 μ M), ceftriaxone (CRO; 1, 2 μ M), and meropenem (MER; 1, 2, 4, 8 μ M) at Clinical and Laboratory Standards Institute (CLSI) breakpoint concentrations were made by adding the antibiotic solution to each well of a 96-well plate and drying the plates for 4 h in the biosafety cabinet.

Conventional metabolomics workflow

270 μ l MH medium was added to each well of the MCD receiver (96-well plate). Wells were inoculated using 30 μ l of bacterial suspension (0.5 McFarland). The plate was sealed using a gas permeable sealer (rayon, 139.7 μ m pore size; VWR) and incubated at 36.5°C, 5% CO₂ and 17.5% O₂. After 4 h, a 10 μ l aliquot from each well was diluted with 90 μ l 50% methanol (Thermo Scientific™ Optima™ LC/MS grade reagent)/50% water (v/v; Optima LC/MS grade reagent) in a 96-well PCR plate (VWR 96-well Real-Time PCR skirted plate). The plate was centrifuged at 4,000 rpm for 10 min (Thermo Scientific™ Sorvall™ Legend™ XTR centrifuge). Subsequently, 70 μ l of the supernatant was transferred to a new 96-well sampling plate (Greiner Bio-One Masterblock, 0.5 mL V-bottom, sterile; Monroe, NC, United States) and diluted with 70 μ l 50% methanol for a total sample dilution of 1:20 from the starting concentration. The samples were analyzed via LC-MS.

Microbial containment device workflow

The following workflow was used to compare the results from the MCD to the conventional metabolomics workflow. However, the MCD is designed to be used with the Thermo Scientific™ Vanquish™ Charger Module to enable the optimized workflow, as shown in [Figure 1D](#). 220 μ l MH medium was added to each well of the MCD receiver (96-well plate). Wells were inoculated using 30 μ l of bacterial suspension (0.5 McFarland). The MCD insert was placed into the MCD receiver followed by transferring 50 μ l MH medium to each MCD insert ([Figure 1](#)). The MCD was then sealed using a gas permeable sealer (rayon, 139.7 μ m pore size; VWR). Samples from the MCD were then incubated, extracted, and analyzed following the conditions described above.

Metabolomics analysis and data visualization

Ultra-high-performance liquid chromatography-mass spectrometry

All metabolomics testing and characterization steps were carried out in the Calgary Metabolomics Research Facility (CMRF). Our methods have been described elsewhere ([Groves et al., 2022](#); [Rydzak et al., 2022](#)). Briefly, we used a Vanquish UHPLC platform coupled to a Thermo Scientific™ Q Exactive™ HF Hybrid Quadrupole-Orbitrap™ mass spectrometer. Metabolites were resolved via hydrophilic interaction liquid chromatography (HILIC; 100 mm \times 2.1 mm Thermo Scientific™ Synchronis™ LC column 2.1 μ m particle size). A 600 μ l/min binary gradient consisting of 20 mM ammonium formate at pH 3.0 in LC-MS grade water (Solvent A; Optima LC/MS reagent) and 0.1% formic acid (% v/v) in LC-MS grade acetonitrile (Solvent B; Optima LC/MS reagent) was used as a mobile phase. Metabolites were eluted using a 15-min gradient. Samples were ionized via electrospray ionization (positive mode for tyramine and negative mode for all other metabolites) with the auxiliary gas of 15 (arbitrary units), sweep gas of 2 (arbitrary units), sheath gas of 35 (arbitrary units), auxiliary gas temperature of 300°C, spray voltage of -2000 V, and capillary temperature of 275°C. Data were acquired in full scan mode (50–750 m/z) with a 240,000 resolving power, an automatic gain control target of $3e^6$, and a maximum injection time of 200 ms. All standards were purchased from Sigma-Aldrich (CAS Numbers: Mevalonate—1255502-07-8; Succinate—6106-21-4; Tyramine—51-67-2; Urocanate—104-98-3) and used to verify the biomarkers described in [Rydzak et al. \(2022\)](#). Raw MS data were converted to mzXML file format using MSConvert GUI software ([Chambers et al., 2012](#)) and analyzed using MAVEN (EL-MAVEN v0.12.0) ([Melamud et al., 2010](#)).

Statistical analysis

All experiments were replicated with three biological replicates and three technical replicates for each treatment and we used GraphPad Prism 9 software ([Skinner, 2018](#)) to calculate

the statistical differences between treatments using one-way ANOVA with *post hoc* Tukey correction, where $*p < 0.05$; $**p < 0.01$; $***p < 0.001$; and $****p < 0.0001$. All the statistical methods for finding microbial biomarkers were reported in our previous study (Rydzak et al., 2022).

Results

Diffusion characterization (empirical testing)

The primary function of the MCD is to separate microbes in the lower growth chamber from the upper analytical chamber but allows microbial metabolites to freely diffuse between the two chambers. To assess the efficacy of the prototyped MCD, we conducted a series of diffusion assays and quantified the kinetics of diffusion between lower and upper wells. Two parameters affecting diffusion equilibrium timelines were analyzed: (1) the volume of liquid in the MCD insert and (2) the concentration of metabolites in the MCD receiver. We used succinate as a representative small molecule metabolite for this study since its size, cross-sectional area, and chemical properties are broadly representative of soluble metabolites found in microbial growth media; 250 μ l of succinate solutions at varying concentrations (2, 0.2, and 0.02 mM) was introduced into the MCD receiver (bottom well). Then, 50, 75, or 100 μ l of water was added to the MCD insert (top well). Samples were incubated for 4 h and aliquots were then taken from each MCD insert, diluted 20-fold with 50% methanol, and succinate concentrations were measured by UHPLC-MS (Figures 2A–C). The results demonstrated that succinate freely diffused from the bottom to top wells. As expected, larger volumes in the top well slowed equilibrium timelines, whereas increasing metabolite concentration in the bottom wells accelerated diffusion. When succinate was prepared at a 2 mM concentration in the bottom well, we observed $\sim 10\times$ faster diffusion than comparable wells prepared at 0.2 mM. These data demonstrated that our prototype enabled the diffusion of metabolites between the upper and lower wells and that diffusion rates followed the expected behaviors.

Diffusion characterization (numerical simulation)

A critical consideration in conducting metabolomics experiments in the MCD is the time required for a microbe to reach equilibrium between the lower and upper wells. We used COMSOL Multiphysics software to conduct a numerical simulation of diffusion and to quantify the diffusion rate between 0 and 6 h for molecules dissolved in liquids in an aqueous (water) solution. Since samples were taken within a

1 mm distance from the filter membrane of the MCD insert during empirical testing, we considered this same sampling zone for evaluation of the diffusion rate in the MCD for the numerical simulation. The 3D schematic showing the diffusion of metabolites in one well including the MCD receiver and insert along the centerline is shown in Figure 2D. After running the 2D and 3D simulations, the gradient of concentration over the cross-sectional surface of the model for 0, 1, 2, 3, and 4 h are shown in Figure 2E. The gradient of concentration for the 3D model at 4 h is also shown in Figure 2E. Figure 2F illustrates the concentration change for metabolites in both the MCD receiver and insert over the center line from 0 to 6 h. These simulations showed that both the MCD insert and receiver reach equilibrium conditions within 4 h in the sampling zone, which is in agreement with empirical testing using 2 mM succinate in the bottom well and 50 μ l water in the upper. Based on these simulations, we determined that sampling time points of 4 h or longer are sufficient for high-abundance metabolites to reach equilibrium.

Sterility testing

One critical function of the MCD is to grow microbes in the lower chamber to ensure that they cannot traverse into the upper chamber where they could potentially contaminate the LC-MS hardware. To evaluate the efficacy of our membrane in separating the growth and the analytical chambers, we conducted a series of contamination (bottom-to-top) sterility tests using *E. coli*. For bottom-to-top sterility testing, 250 μ l of MH medium containing either *E. coli* or *K. pneumoniae* (OD₆₀₀ 0.01) was loaded into the MCD receiver. The MCD insert was placed on top of the MCD receiver and 100 μ l of MH broth was added to each well of the MCD insert. Optical density measurements after 8 h on the MCD receiver were much higher than the MCD insert (Figures 3A,B, respectively) suggesting that it effectively contained the bacteria in the MCD receiver. To further ensure sterility of the analytical chamber (upper well), samples were streaked on agar plates and incubated overnight. No growth was observed on agar plates streaked with inoculum from the upper analytical chamber (Figures 3C,D), demonstrating that the MCD membrane successfully separated the microbial chamber (MCD receiver) and the analytical chamber (MCD insert). This analysis was repeated using both *S. aureus* and *E. faecalis*, and no bacterial growth was observed in the upper analytical chamber (Supplementary Figure 2).

Species identification using metabolites

One obvious application of the MCD is in quantifying microbial boundary fluxes, which were recently shown to be

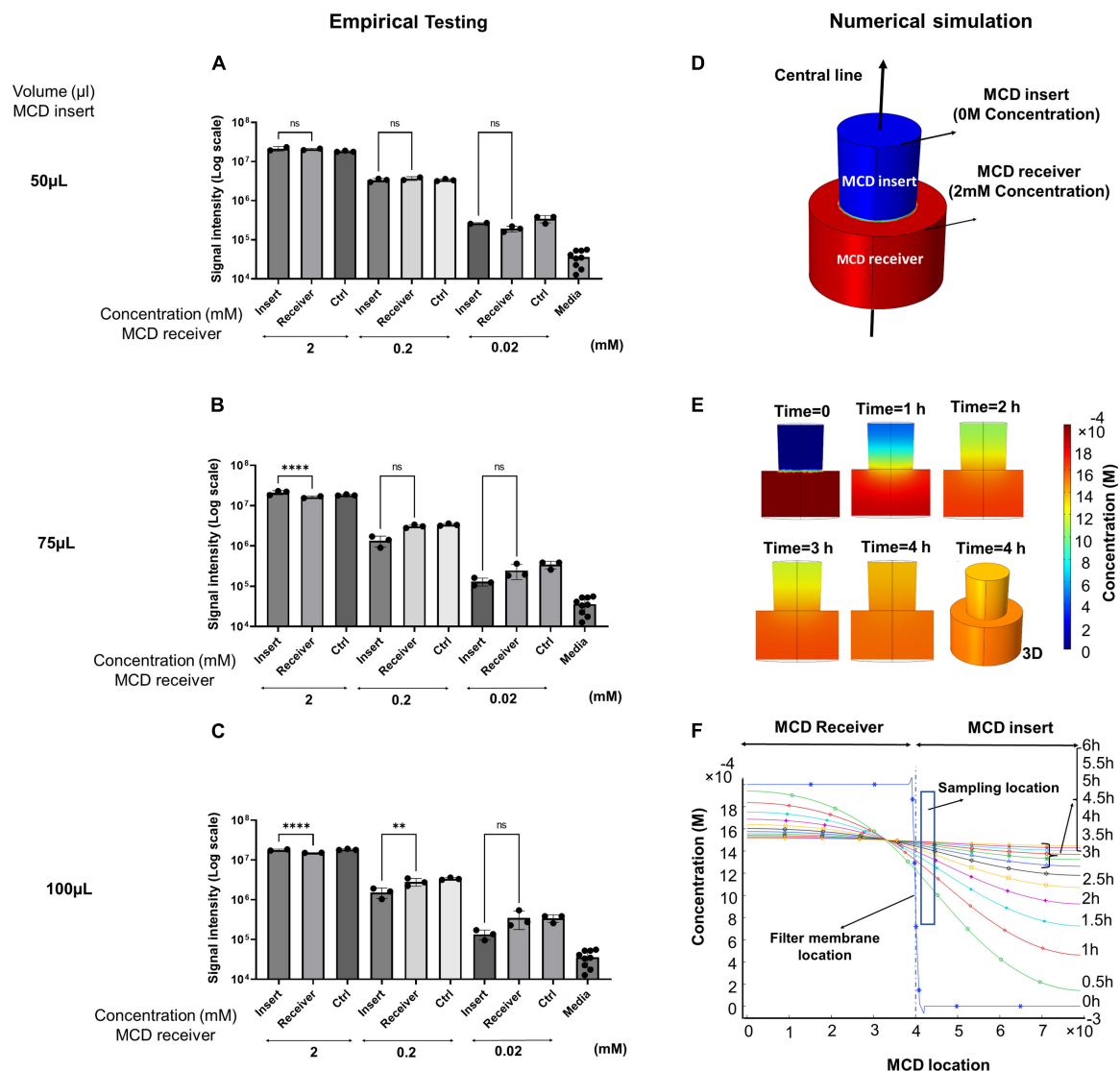


FIGURE 2

(A–C) Empirical versus (D–F) simulated diffusion kinetics of succinate dissolved in water in the MCD device. Succinate was added to the MCD receiver (bottom well) and the effects of initial succinate concentration (2, 0.2, and 0.02 mM) and insert aqueous volume (upper well) (50, 75, and 100 µL) on the final concentrations of succinate observed after 4 h at 37°C. Succinate signal intensities for MCD insert versus receiver (A) 50 µL insert aqueous volume, (B) 75 µL insert aqueous volume, and (C) 100 µL insert aqueous volume. (D) A 3D model of metabolite concentrations in the MCD was constructed and (E) metabolite diffusion was computed over a 4-h incubation. (F) Metabolite concentrations observed across a vertical transect of sampling points in the MCD crossing from the bottom of the receiver, through the membrane, and to the top of the insert are shown across a time point ranging from 0 to 6 h. For bar graphs, ** $p < 0.01$ and **** $p < 0.0001$.

an effective strategy for differentiating bloodstream pathogens (Rydzak et al., 2022). To illustrate the utility of the MCD, we inoculated MCD plates with four bloodstream pathogens (*E. coli*, *K. pneumoniae*, *E. faecalis*, and *S. aureus*; three to four unique isolates per species) and analyzed the analytical chamber for the presence of diagnostic biomarkers following a 4-h incubation. It has been reported previously (Rydzak et al., 2022) that both *E. coli* and *K. pneumoniae* produce succinate, but *K. pneumoniae* also produces urocanate. Similarly, both *S. aureus* and *E. faecalis* produce mevalonate, but *E. faecalis*

also produces tyramine. Thus, quantifying succinate, urocanate, mevalonate, and tyramine are sufficient for differentiating these species. As anticipated, microbes incubated in the MCD were differentiable based on these biomarker patterns. Significant succinate production was observed in *E. coli* and *K. pneumoniae* cultures (Figure 4A), and urocanate production was uniquely observed in the *K. pneumoniae* cultures (Figure 4B). Similarly, we observed significant mevalonate production in *S. aureus* and *E. faecalis* cultures (Figure 4C), but tyramine production was only observed in *E. faecalis* cultures (Figure 4D). Furthermore,

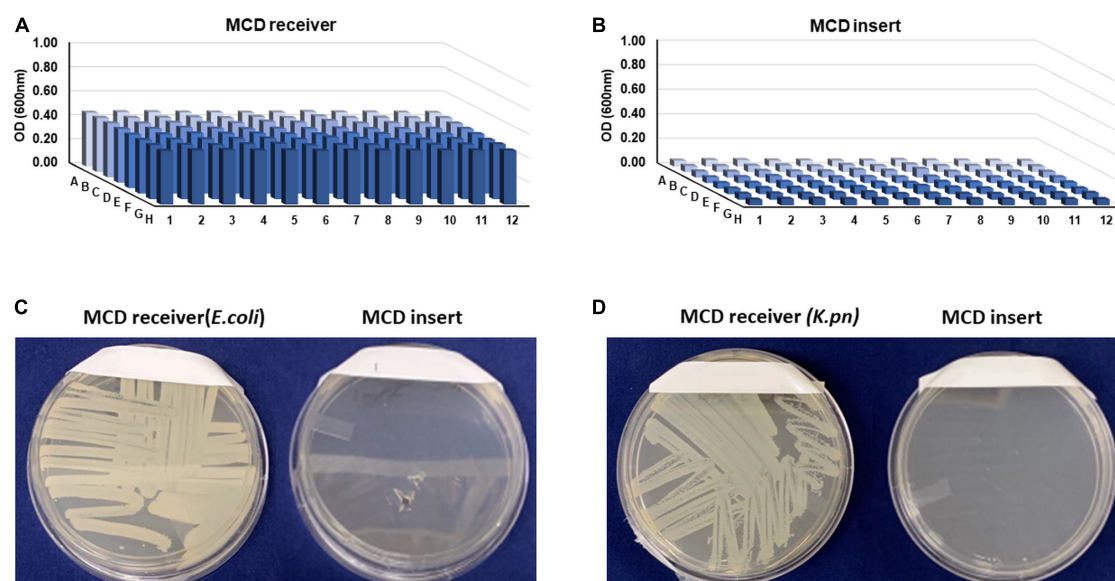


FIGURE 3

Sterility testing of the MCD insert (upper, analytical chamber) following an 8-h incubation of the MCD receiver seeded with bacteria. Bacterial cell densities (OD_{600}) in the MCD receiver (A) and MCD insert (B) show that growth only took place in the receiver and not the insert. To further validate sterility of the insert, the MCD receiver and insert samples were streaked on agar plates and incubated overnight (C,D).

biomarker intensities observed in the MCD were comparable to those observed via the conventional metabolomics method (Figure 5). In summary, the MCD enables boundary flux analyses and microbes grown in the MCD produce diagnostic markers at levels that are comparable to those observed via conventional sample preparation methods.

Antibiotic susceptibility testing

Recently, Rydzak et al. (2022) showed that antibiotic-sensitive microbes have significant perturbations in their metabolic boundary fluxes when exposed to antibiotics, whereas antimicrobial resistant strains have a minimal metabolic response to antibiotic exposure. They showed that these perturbations can be used to determine the minimal inhibitory concentrations of antibiotics. To assess the applicability of the MCD for antibiotic susceptibility testing (AST), *E. coli* strains ($n = 3$; each with a distinct susceptibility profile as described in Supplementary Figure 3) were incubated with a panel of antibiotics containing cefazolin (CFZ), gentamycin (GEN), ampicillin (AMP), ciprofloxacin (CIP), and meropenem (MER) at CLSI breakpoint concentrations as described in the section “Materials and methods.” The sensitivity profiles of each strain were known based on their ATCC strain information (Supplementary Figure 4). These phenotypes were verified using the MCD by measuring optical density (OD_{600}) after a 4-h incubation in our antibiotic panel (Supplementary Figure 4). As expected, the MCD-based growth matched the

patterns expected based on the ATCC literature for each strain (Figure 6). Antibiotic-induced perturbations in the metabolic activity of each microbe were then assessed using both the MCD and conventional metabolomics methods. LC-MS analyses showed that antibiotic exposure inhibited succinate production in antibiotic-sensitive strains but not in antibiotic-resistant strains. Moreover, the pattern of inhibition followed the known resistance profiles for each strain. Furthermore, the overall intensity of succinate signals observed via the MCD corresponded to the patterns observed via the conventional metabolomics workflow (Figure 6). In summary, MCD-based analyses of boundary fluxes enable antibiotic susceptibility profiles to be determined.

Discussion

In this study, we showed that a simple consumable device, the MCD, enabled us to characterize the metabolic boundary fluxes of microbial cultures via a streamlined sample preparation procedure. We demonstrated that: (1) metabolites produced by microbes diffused freely through the MCD membrane over a 4 h incubation; (2) the membrane maintains the sterility of upper wells in the device; and (3) this tool can be used to both identify microbial species and empirically measure antibiotic susceptibility profiles. In summary, this study shows that the MCD functions as a tool for single-step metabolomics experiments and *in vitro* metabolic assays.

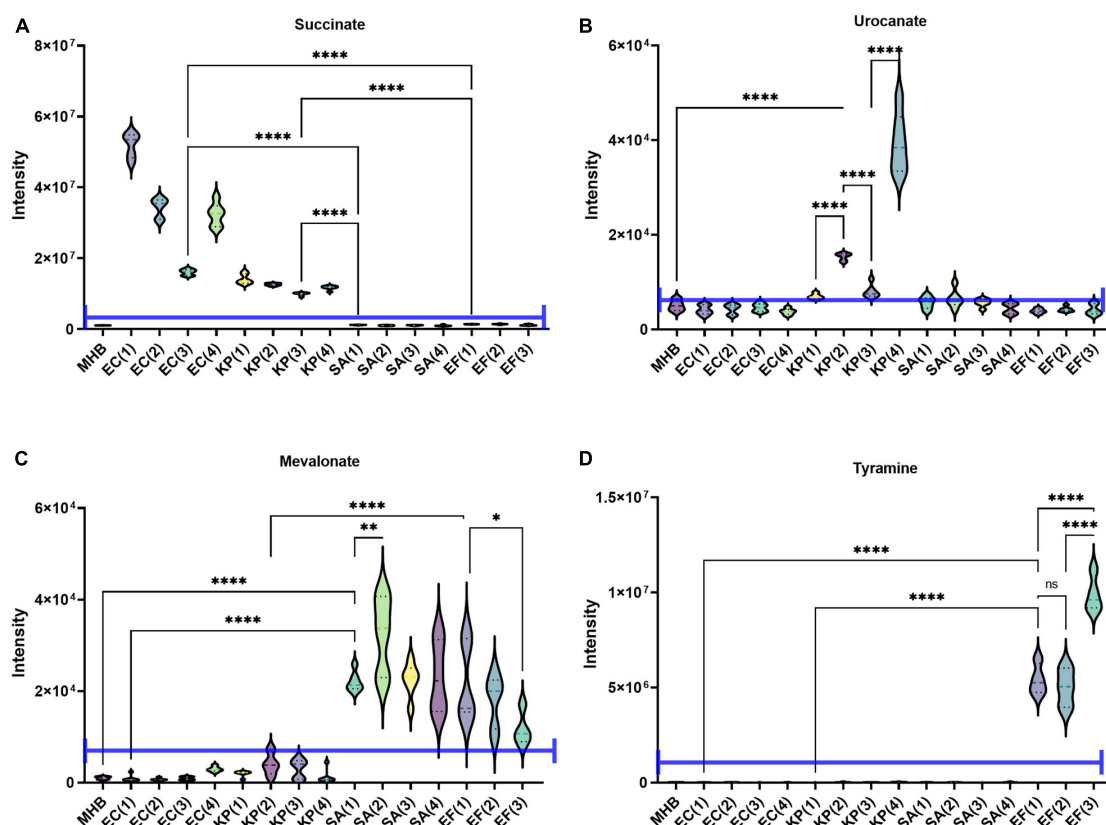


FIGURE 4

Demonstration of the MCD as a platform for identifying microbes via their metabolic boundary fluxes. *Escherichia coli* (EC 1, 2, 3, 4), *Klebsiella pneumoniae* (KP 1, 2, 3, 4), *Enterococcus faecalis* (EF 1, 2, 3), and *Staphylococcus aureus* (SA 1, 2, 3, 4) were identified based on the intensity of (A) succinate, (B) urocanate, (C) mevalonate, and (D) tyramine signals observed in the MCD insert following a 4 h incubation. The purple line in each plot shows the signal intensity threshold for each biomarker used to distinguish the four species. * $p < 0.05$; ** $p < 0.01$; **** $p < 0.0001$.

Although we illustrated the use of this tool in the context of microbial diagnostics, this concept is broadly applicable to any metabolomics study where the objective is to quantify the metabolic boundary fluxes of *in vitro* cell cultures. This wider range of applications includes biofuel production studies, such as for quantifying butyric acid and other products of fermentation by *Clostridium acetobutylicum* (Jang et al., 2013; Liu et al., 2019) and for studying the microbial bioconversion of plant polymers such as pectin and lignocellulose to biofuels (Kuivanen et al., 2019; Lu et al., 2022). The MCD could also provide a useful vehicle for systematically screening large gene knockout libraries in microbial engineering projects (Porokhin et al., 2021). Although the MCD was evaluated here in the context of bacterial metabolism, we anticipate it could be readily adapted to studying mammalian cell culture models (Allen et al., 2003; Zukunft et al., 2018; Lagziel et al., 2019; Wright Muelas et al., 2020), biomarker discovery (Tolstikov et al., 2020), pharmaceutical lead screening (Tomita et al., 2018), environmental monitoring (Lankadurai et al., 2013), microbiology (Ye et al., 2022), plant biology (Kumar et al., 2017), and food chemistry (Cevallos-Cevallos et al., 2009).

Limitations

Although the MCD may simplify metabolomics studies for a wide range of studies, it has some obvious limitations that warrant consideration. One important point is that the diffusion rates of metabolites limit the minimum sampling times possible on this platform. Our data show that small water-soluble metabolites take ~ 4 h to reach equilibrium, which precludes the use of the MCD in studying transient phenotypes. In addition, diffusion rates are directly affected by molecular size. Although larger molecules (e.g., lipoproteins, albumin, enzymes, and antibodies) may freely pass through the MCD filter, the longer incubation times needed to equilibrate these large molecules (Nikaide and Rosenberg, 1981) may make them unsuitable for study in the MCD. This will be particularly problematic for high flux biological model systems (e.g., quickly dividing cells that are grown at high density). Gas availability in the microbial growth chamber may also be problematic in high flux systems. Although microbial growth rates observed with and without the MCD receiver suggest O_2/CO_2 availability was not a growth-limiting factor in this study, the semi-permeable membrane

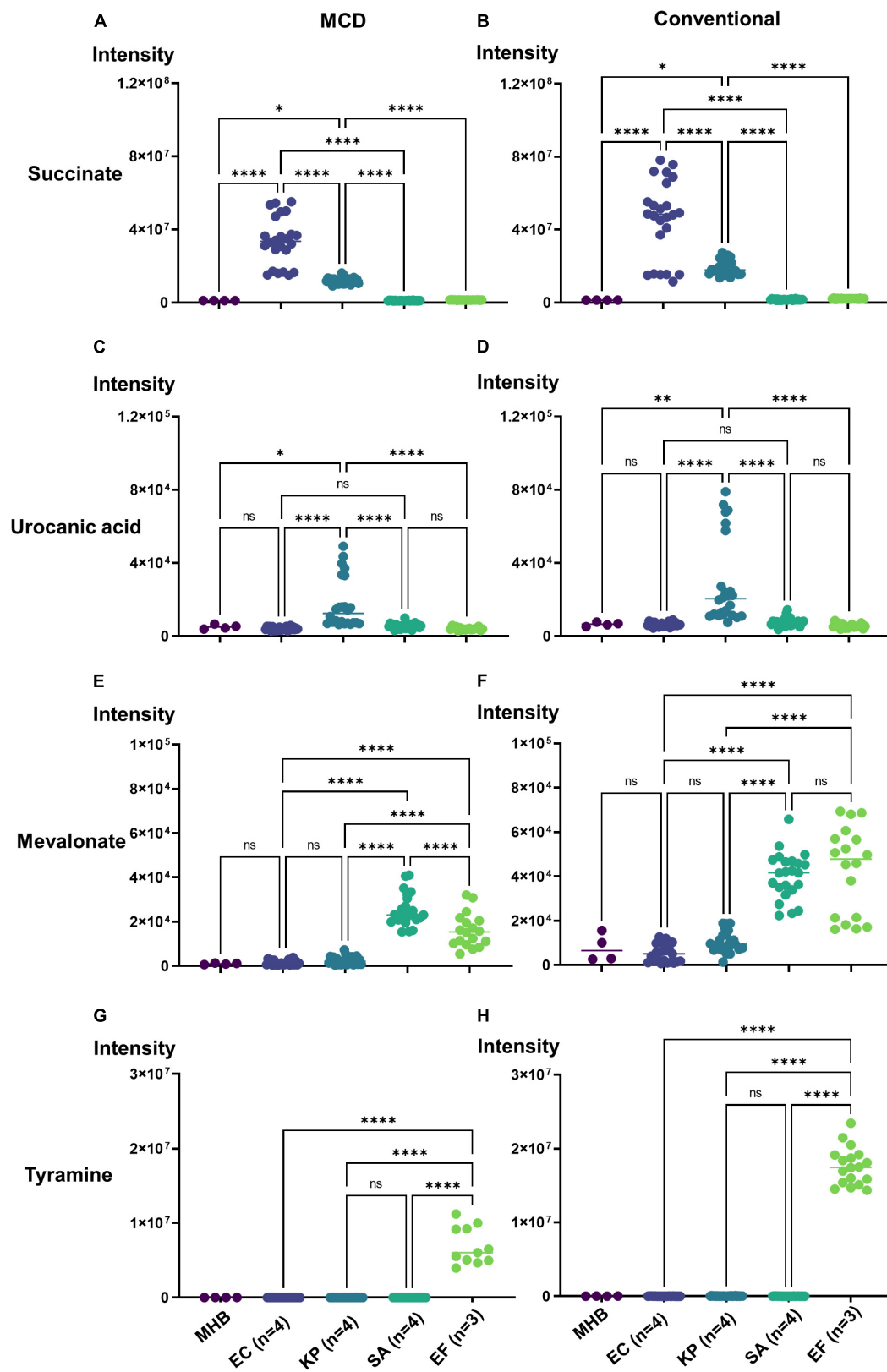


FIGURE 5

Bacteria identification using the MCD (A,C,E,G) versus the a conventional metabolomics workflow (B,D,F,H) for EC ($n = 4$), KP ($n = 4$), EF ($n = 3$), and SA ($n = 4$), strains. For all plots, * $p < 0.05$; ** $p < 0.01$; and **** $p < 0.0001$.

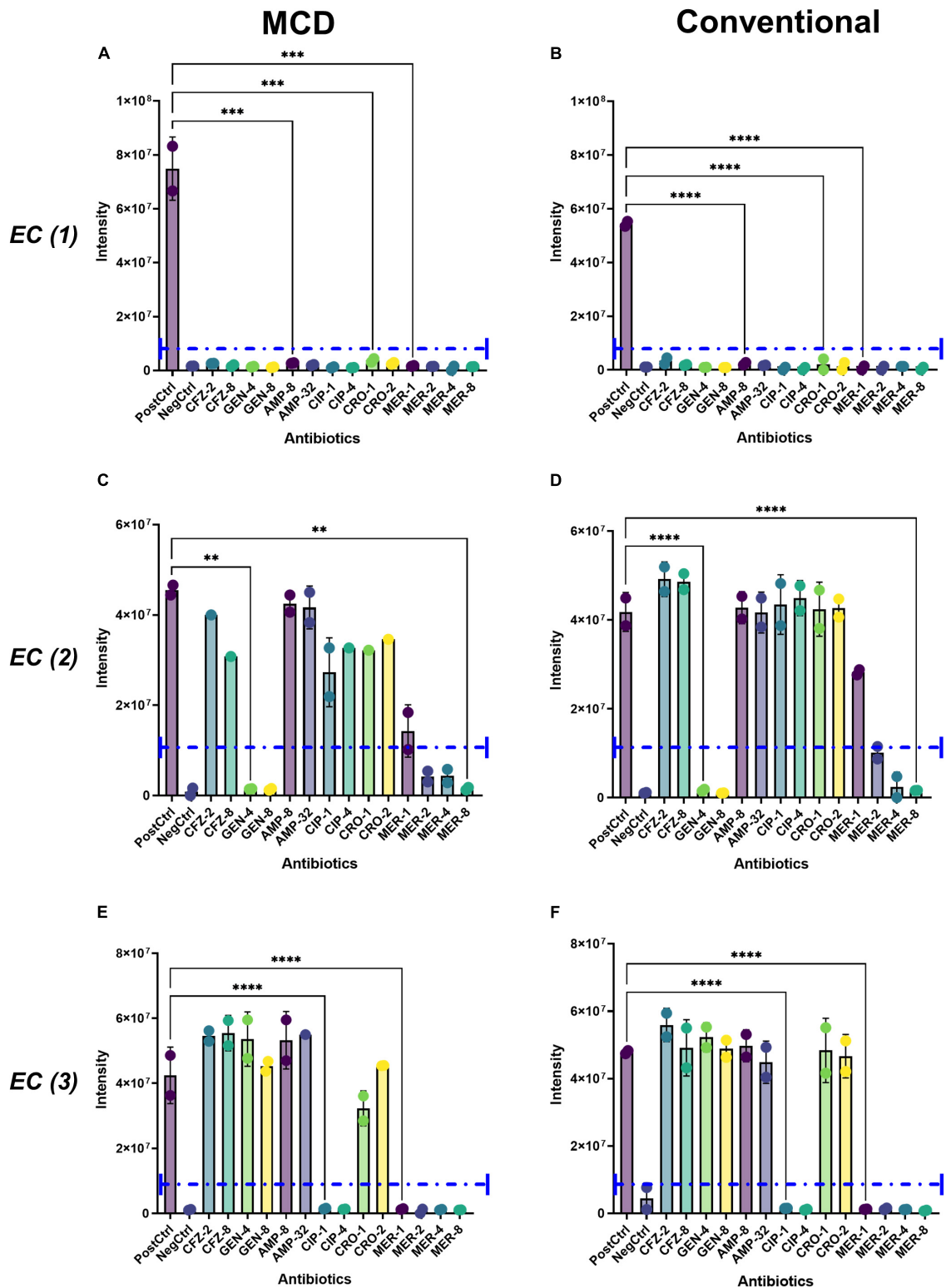


FIGURE 6
Demonstration of the MCD as a platform for antibiotic susceptibility testing. The metabolic activity of *E. coli* (EC, 1, 2, 3) was analyzed when cells were grown in a panel of antibiotics including cefazolin (CFZ 2, 8 μ M), gentamicin (GEN 4, 8 μ M), ciprofloxacin (CIP 1, 4 μ M), ceftriaxone (CRO 1, 2 μ M), and meropenem (MER 1, 2, 4, 8 μ M). Boundary fluxes were quantified via LC-MS using both the (A,C,E) MCD and (B,D,F) conventional metabolomics workflows. The purple dotted line in each plot shows the signal intensity threshold considered as biomarker production. For all plots, ** $p < 0.01$, *** $p < 0.001$, and **** $p < 0.0001$.

used in the MCD will slow gas diffusion to the lower well and may affect some model systems. Another consideration that may affect the use of the MCD is the suspension state of the cells. The experiments herein illustrate diffusion times linked to uniformly suspended cells; adherent or sedimented cells will have longer equilibrium timelines since cellular metabolism will be concentrated at the bottom of the MCD receiver.

In summary, we introduce here a simple consumable device that enables metabolic boundary fluxes to be studied via a streamlined sample handling procedure. We illustrate the utility of the MCD platform for microbial identification and antibiotic susceptibility testing and propose its applicability to a wide range of studies.

Data availability statement

All of the data used in this article are available on request from the authors.

Author contributions

MM, TR, and IAL designed the experiments. MM designed, manufactured, and assembled the MCD and conducted the microbial growth, identification, and antibiotic susceptibility testing assays. MM, RA, and SL characterized the MCD. MM, RAG, and DGB collected mass spectrometry data. MM, SLB, TR, and IAL wrote the manuscript. All authors have read and approved the final version of the manuscript.

Funding

This work was supported by a Genomics Application Partnership Program award from Genome Canada (10019200), Genome Alberta (10021232), Canadian Institute of Health Research (10020019), and the 2017 Large Scale Applied Research Project competition. This work was made possible in part by a

research collaboration agreement with Thermo Fisher Scientific. IAL was supported by an Alberta Innovates Translational Health Chair (10010625). TR was supported by an Eyes High Postdoctoral Fellowship from the University of Calgary (10011121). Metabolomics data were acquired at the Calgary Metabolomics Research Facility, which is supported by the International Microbiome Centre and the Canada Foundation for Innovation (CFI-JELF 34986).

Conflict of interest

This research was funded in part by a Genome Canada GAPP award, which is intended to enable the commercialization of research findings. MM and SLB have started a company, Fluidome, Inc. to commercialize the MCD platform described herein.

The remaining authors declare that the research was conducted in the absence of any commercial or financial relationships that could be construed as a potential conflict of interest.

Publisher's note

All claims expressed in this article are solely those of the authors and do not necessarily represent those of their affiliated organizations, or those of the publisher, the editors and the reviewers. Any product that may be evaluated in this article, or claim that may be made by its manufacturer, is not guaranteed or endorsed by the publisher.

Supplementary material

The Supplementary Material for this article can be found online at: <https://www.frontiersin.org/articles/10.3389/fmicb.2022.958785/full#supplementary-material>

References

- Allen, J., Davey, H. M., Broadhurst, D., Heald, J. K., Rowland, J. J., Oliver, S. G., et al. (2003). High-throughput classification of yeast mutants for functional genomics using metabolic footprinting. *Nat. Biotechnol.* 21, 692–696. doi: 10.1038/nbt823
- Antoniewicz, M. R. (2020). A guide to deciphering microbial interactions and metabolic fluxes in microbiome communities. *Curr. Opin. Biotechnol.* 64, 230–237. doi: 10.1016/j.copbio.2020.07.001
- Araujo-León, J. A., Ortiz-Andrade, R., Vera-Sánchez, R. A., Oney-Montalvo, J. E., Coral-Martínez, T. I., and Cantillo-Ciau, Z. (2020). Development and optimization of a high sensitivity LC-MS/MS method for the determination of hesperidin and naringenin in rat plasma: pharmacokinetic approach. *Molecules* 25:4241. doi: 10.3390/molecules25184241
- Bideaux, C., Montheard, J., Cameleyre, X., Molina-Jouve, C., and Alfenore, S. (2016). Metabolic flux analysis model for optimizing xylose conversion into ethanol by the natural C5-fermenting yeast *Candida shehatae*. *Appl. Microbiol. Biotechnol.* 100, 1489–1499. doi: 10.1007/s00253-015-7085-0
- Cao, G., Song, Z., Hong, Y., Yang, Z., Song, Y., Chen, Z., et al. (2020). Large-scale targeted metabolomics method for metabolite profiling of human samples. *Anal. Chim. Acta* 1125, 144–151. doi: 10.1016/j.aca.2020.05.053

- Cevallos-Cevallos, J. M., Reyes-De-Corcuera, J. I., Etxeberria, E., Danyluk, M. D., and Rodrick, G. E. (2009). Metabolomic analysis in food science: a review. *Trends Food Sci. Technol.* 20, 557–566. doi: 10.1016/j.tifs.2009.07.002
- Chambers, M. C., Maclean, B., Burke, R., Amodei, D., Ruderman, D. L., Neumann, S., et al. (2012). A cross-platform toolkit for mass spectrometry and proteomics. *Nat. Biotechnol.* 30, 918–920. doi: 10.1038/nbt.2377
- Chhabra, M. (2021). “Chapter 6 – Biological therapeutic modalities,” in *Translational Biotechnology*, ed. Y. Hasija (London: Academic Press). doi: 10.1016/B978-0-12-821972-0.00015-0
- Cui, L., Lu, H., and Lee, Y. H. (2018). Challenges and emergent solutions for LC-MS/MS based untargeted metabolomics in diseases. *Mass Spectrom. Rev.* 37, 772–792. doi: 10.1002/mas.21562
- Groves, R. A., Mapar, M., Aburashed, R., Ponce, L. F., Bishop, S. L., Rydzak, T., et al. (2022). Method for quantifying the metabolic boundary fluxes of cell cultures in large cohorts by high resolution hydrophilic liquid chromatography mass spectrometry. *bioRxiv [Preprint]* 2022.04.25.489416. doi: 10.1021/acs.analchem.2c00078
- Hollinshead, W., He, L., and Tang, Y. J. (2014). Biofuel production: an odyssey from metabolic engineering to fermentation scale-up. *Front. Microbiol.* 5:344. doi: 10.3389/fmicb.2014.00344
- Hui, S., Cowan, A. J., Zeng, X., Yang, L., Teslaa, T., Li, X., et al. (2020). Quantitative fluxomics of circulating metabolites. *Cell. Metab.* 32, 676.e4–688.e4. doi: 10.1016/j.cmet.2020.07.013
- Jang, Y.-S., Woo, H. M., Im, J. A., Kim, I. H., and Lee, S. Y. (2013). Metabolic engineering of *Clostridium acetobutylicum* for enhanced production of butyric acid. *Appl. Microbiol. Biotechnol.* 97, 9355–9363. doi: 10.1007/s00253-013-5161-x
- Kell, D. B., and Oliver, S. G. (2016). The metabolome 18 years on: a concept comes of age. *Metabolomics* 12:148. doi: 10.1007/s11306-016-1108-4
- Khandelwal, R. A., Olivier, B. G., Röling, W. F. M., Teusink, B., and Bruggeman, F. J. (2013). Community flux balance analysis for microbial consortia at balanced growth. *PLoS One* 8:e64567. doi: 10.1371/journal.pone.0064567
- Kuivanen, J., Biz, A., and Richard, P. (2019). Microbial hexuronate catabolism in biotechnology. *AMB Express* 9:16. doi: 10.1186/s13568-019-0737-1
- Kumar, R., Bohra, A., Pandey, A. K., Pandey, M. K., and Kumar, A. (2017). Metabolomics for plant improvement: status and prospects. *Front. Plant Sci.* 8:1302. doi: 10.3389/fpls.2017.01302
- Lagziel, S., Lee, W. D., and Shlomi, T. (2019). Studying metabolic flux adaptations in cancer through integrated experimental-computational approaches. *BMC Biol.* 17:51. doi: 10.1186/s12915-019-0669-x
- Lankadurai, B. P., Nagato, E. G., and Simpson, M. J. (2013). Environmental metabolomics: an emerging approach to study organism responses to environmental stressors. *Environ. Rev.* 21, 180–205. doi: 10.1139/er-2013-0011
- Liang, C., Liebecke, M., Schwarz, R., Zühlke, D., Fuchs, S., Menschner, L., et al. (2011). Staphylococcus aureus physiological growth limitations: insights from flux calculations built on proteomics and external metabolite data. *Proteomics* 11, 1915–1935. doi: 10.1002/pmic.201000151
- Liu, H., Zhang, J., Yuan, J., Jiang, X., Jiang, L., Zhao, G., et al. (2019). Omics-based analyses revealed metabolic responses of *Clostridium acetobutylicum* to lignocellulose-derived inhibitors furfural, formic acid and phenol stress for butanol fermentation. *Biotechnol. Biofuels* 12, 101–101. doi: 10.1186/s13068-019-1440-9
- Lu, H., Yadav, V., Zhong, M., Bilal, M., Taherzadeh, M. J., and Iqbal, H. M. N. (2022). Bioengineered microbial platforms for biomass-derived biofuel production – A review. *Chemosphere* 288:132528. doi: 10.1016/j.chemosphere.2021.132528
- Lu, W., Su, X., Klein, M. S., Lewis, I. A., Fiehn, O., and Rabinowitz, J. D. (2017). Metabolite measurement: pitfalls to avoid and practices to follow. *Annu. Rev. Biochem.* 86, 277–304. doi: 10.1146/annurev-biochem-061516-044952
- Melamud, E., Vastag, L., and Rabinowitz, J. D. (2010). Metabolomic analysis and visualization engine for LC-MS data. *Anal. Chem.* 82, 9818–9826. doi: 10.1021/ac1021166
- Metz, T. O., Zhang, Q., Page, J. S., Shen, Y., Callister, S. J., Jacobs, J. M., (2007). The future of liquid chromatography-mass spectrometry (LC-MS) in metabolic profiling and metabolomic studies for biomarker discovery. *Biomarkers Med.* 1, 159–185. doi: 10.2217/17520363.1.1.159
- Monge, M. E., Dodds, J. N., Baker, E. S., Edison, A. S., and Fernández, F. M. (2019). Challenges in identifying the dark molecules of life. *Annu. Rev. Anal. Chem.* 12, 177–199. doi: 10.1146/annurev-anchem-061318-114959
- Munro, L. J., and Kell, D. B. (2021). Intelligent host engineering for metabolic flux optimisation in biotechnology. *Biochem. J.* 478, 3685–3721. doi: 10.1042/BCJ20210535
- Nikaido, H., and Rosenberg, E. Y. (1981). Effect on solute size on diffusion rates through the transmembrane pores of the outer membrane of *Escherichia coli*. *J. Gen. Physiol.* 77, 121–135. doi: 10.1085/jgp.77.2.121
- Orth, J. D., Thiele, I., and Palsson, B. O. (2010). What is flux balance analysis? *Nat. Biotechnol.* 28, 245–248. doi: 10.1038/nbt.1614
- Perez-Garcia, O., Lear, G., and Singhal, N. (2016). Metabolic network modeling of microbial interactions in natural and engineered environmental systems. *Front. Microbiol.* 7:673. doi: 10.3389/fmicb.2016.00673
- Pinu, F. R., Goldansaz, S. A., and Jaine, J. (2019). Translational metabolomics: current challenges and future opportunities. *Metabolites* 9:108. doi: 10.3390/metabo9060108
- Pinu, F. R., and Villas-Boas, S. G. (2017). Extracellular microbial metabolomics: the state of the art. *Metabolites* 7:43.
- Porokhin, V., Amin, S. A., Nicks, T. B., Gopinathan, V. E., Nair, N. U., and Hassoun, S. (2021). Analysis of metabolic network disruption in engineered microbial hosts due to enzyme promiscuity. *Metab. Eng. Commun.* 12:e00170. doi: 10.1016/j.mec.2021.e00170
- Rydzak, T., Groves, R. A., Zhang, R., Aburashed, R., Pushpker, R., Mapar, M., et al. (2022). Metabolic preference assay for rapid diagnosis of bloodstream infections. *Nat. Commun.* 13:2332. doi: 10.1038/s41467-022-30048-6
- Skinner, J. (2018). Statistics for Immunologists. *Curr. Protoc. Immunol.* 122, 54–54. doi: 10.1002/cpim.54
- Tolstikov, V., Moser, A. J., Sarangarajan, R., Narain, N. R., and Kiebish, M. A. (2020). Current status of metabolomic biomarker discovery: impact of study design and demographic characteristics. *Metabolites* 10:224. doi: 10.3390/metabo10060224
- Tomita, R., Todoroki, K., Hayama, T., Yoshida, H., Fujioka, T., Nakashima, M., et al. (2018). Assessment of anticancer drug effects on pancreatic cancer cells under glucose-depleted conditions using intracellular and extracellular amino acid metabolomics. *Biol. Pharmaceutical Bull.* 41, 220–228. doi: 10.1248/bpb.b17-00746
- Wright Muelas, M., Roberts, I., Mughal, F., O’hagan, S., Day, P. J., and Kell, D. B. (2020). An untargeted metabolomics strategy to measure differences in metabolite uptake and excretion by mammalian cell lines. *Metabolomics* 16:107. doi: 10.1007/s11306-020-01725-8
- Ye, D., Li, X., Shen, J., and Xia, X. (2022). Microbial metabolomics: from novel technologies to diversified applications. *Trac Trends Anal. Chem.* 148:116540. doi: 10.1016/j.trac.2022.116540
- Zheng, J., Mandal, R., and Wishart, D. S. (2018). A sensitive, high-throughput LC-MS/MS method for measuring catecholamines in low volume serum. *Anal. Chim. Acta* 1037, 159–167. doi: 10.1016/j.aca.2018.01.021
- Zukunft, S., Prehn, C., Röhring, C., Möller, G., Hrabi De Angelis, M., Adamski, J., et al. (2018). High-throughput extraction and quantification method for targeted metabolomics in murine tissues. *Metab. Off. J. Metab. Soc.* 14, 18–18. doi: 10.1007/s11306-017-1312-x



OPEN ACCESS

EDITED BY

Zhe Wang,
Shanghai Jiao Tong University, China

REVIEWED BY

Hongcai Zhang,
Shanghai Jiao Tong University, China
Benhai Xiong,
Institute of Animal Sciences (CAAS), China

*CORRESPONDENCE

Linshu Jiang
linshujiangbua@163.com
Jinjin Tong
tongjinjin0451@163.com

†These authors have contributed equally to
this work

SPECIALTY SECTION

This article was submitted to
Antimicrobials, Resistance and
Chemotherapy,
a section of the journal
Frontiers in Microbiology

RECEIVED 22 May 2022

ACCEPTED 24 August 2022

PUBLISHED 20 September 2022

CITATION

Zhang H, Wang Z, Yao H, Jiang L and
Tong J (2022) Intramammary infusion of
matrine-chitosan hydrogels for treating
subclinical bovine mastitis —effects on milk
microbiome and metabolites.
Front. Microbiol. 13:950231.
doi: 10.3389/fmicb.2022.950231

COPYRIGHT

© 2022 Zhang, Wang, Yao, Jiang and Tong.
This is an open-access article distributed
under the terms of the [Creative Commons
Attribution License \(CC BY\)](https://creativecommons.org/licenses/by/4.0/). The use,
distribution or reproduction in other
forums is permitted, provided the original
author(s) and the copyright owner(s) are
credited and that the original publication in
this journal is cited, in accordance with
accepted academic practice. No use,
distribution or reproduction is permitted
which does not comply with these terms.

Intramammary infusion of matrine-chitosan hydrogels for treating subclinical bovine mastitis —effects on milk microbiome and metabolites

Hua Zhang[†], Ziyue Wang[†], Hua Yao, Linshu Jiang* and
Jinjin Tong*

Animal Science and Technology College, Beijing University of Agriculture, Beijing, China

Background: Bovine metabolism undergoes significant changes during subclinical mastitis, but the relevant molecular mechanisms have not been elucidated. In this study we investigated the changes in milk microbiota and metabolites after intramammary infusion of matrine-chitosan hydrogels (MCHs) in cows with subclinical mastitis.

Methods: Infusions were continued for 7 days, and milk samples were collected on days 1 and 7 for microbiome analysis by 16S rRNA gene sequencing and metabolite profiling by liquid chromatography-mass spectrometry.

Results: MCHs significantly decreased the somatic cell count on day 7 compared to day 1, and the Simpson index indicated that microbial diversity was significantly lower on day 7. The relative abundance of *Aerococcus*, *Corynebacterium_1*, *Staphylococcus* and *Firmicutes* was significantly decreased on day 7, while Proteobacteria increased. In the milk samples, we identified 74 differentially expressed metabolites. The MCHs infusion group had the most significantly upregulated metabolites including sphingolipids, glycerophospholipids, flavonoids and fatty acyls. The mammary gland metabolic pathways identified after MCHs treatment were consistent with the known antimicrobial and anti-inflammatory properties of matrine that are associated with glycerophospholipid metabolism and the sphingolipid metabolic signaling pathways.

Conclusion: These insights into the immunoregulatory mechanisms and the corresponding biological responses to matrine demonstrate its potential activity in mitigating the harmful effects of bovine mastitis.

KEYWORDS

matrine-chitosan hydrogels, inflammatory factors, mammary gland, immunity, microbiome, metabolomics

Introduction

The udder microbiota plays an important role in the host-pathogen interactions of the innate and adaptive immune system. This is especially true of pathogens that trigger inflammation that is detrimental to mammary tissue and bovine physiology (Gao et al., 2017; Derakhshani et al., 2018). Mastitis is an inflammation of the udder most commonly from bacterial infection, and the pathological changes not only affect milk quality but also quantity (Gao et al., 2017). The increasing demand for animal protein has led to a substantial increase in the use of antibiotics in food animal production (Guillaume et al., 2016). This can exacerbate antimicrobial resistance, which is a global concern for treating human as well as farm animal diseases. Developing an effective drug for mastitis that is safe for use in food animals and for which no resistance exists in the microbial population would be highly desirable for the worldwide dairy industry.

Matrine is a polycyclic alkaloid isolated from the plant, *Sophora flavescens*, that has been used in Chinese traditional medicine because of its anticancer, anti-inflammatory, cardioprotective, and opioid effects (Xiaofei et al., 2018). Previous research (Feng et al., 2018) found that matrine inhibited the virulence of *Staphylococcus aureus*, one of the main causes of mastitis. Matrine attenuated the lipopolysaccharide-induced immune response by downregulating IL-1 and IL-17 and inhibiting production of the proinflammatory compound, malondialdehyde, reducing inflammation and oxidative stress, and enhancing CCR7 expression (Zhou et al., 2017; Sun et al., 2018a). Chitosan is a natural polymer produced by acetylation and enzymatic cleavage of chitin, the most abundant animal polysaccharide in nature (Zhang et al., 2019). The applications for chitosan have continued to increase because of its biocompatibility and ease of chemical modification, together with its anti-inflammatory, antimicrobial, cholesterol-lowering, immunomodulatory, and antitumor properties (Feng et al., 2018). Chitosan can be beneficial at the cellular or molecular level (Sun et al., 2018b), by reducing intracellular material leakage and triggering an antimicrobial response to enhance the therapeutic effects of mastitis treatment. Chitosan can be formulated to be injectable at room temperature, but change into a biodegradable hydrogel at body temperature (Chenite et al., 2000). It has been used in drug formulations and delivery vehicles for decades; However, the influence of matrine and chitosan on the udders of dairy cows has received little research attention. Therefore, it is worthwhile to explore the effectiveness of intramammary infusion

of matrine-loaded chitosan hydrogels (MCHs) on the udders of dairy cows with mastitis in terms of positively changing the microbial population and metabolic profile of milk. We hypothesized that intramammary infusion of MCHs would favor the growth of beneficial microorganisms and cause a shift in diversity of the milk microbiota in normal udder quarters.

DNA sequencing has become routine for many labs and the advanced software and bioinformatics databases available have created great opportunities for studying pathogenic mechanisms (Oikonomou et al., 2014; Falentin et al., 2016). By understanding the host's responses to microbial attack, we expected to be able to identify the most effective targets for antimicrobial intervention, to develop new treatments for bovine mastitis and to find sensitive biomarkers for early detection and diagnosis. Metabolomics can also be used for quantitative measurement of the metabolic state of milk, including the biomarkers of lactation (Sun et al., 2017), the variation in metabolites associated with mastitis (Tong et al., 2019), and the changes in metabolism after antibacterial therapy (Junza et al., 2016). Little is known about the changes in milk metabolites in response to MCHs treatment of mastitis; Therefore, one of the goals of this study was to obtain detailed information on the effect of matrine delivery by chitosan hydrogel infusion into bovine mammary glands on milk microbiota and metabolites. We investigated the effect of MCHs on subclinical-mastitis and the relationship between milk microbiota diversity and metabolite profiles, to probe the mechanisms of the antibacterial benefits of matrine and chitosan for mastitis. The results can be provided new knowledge for the development of novel, safe and effective prophylactic, and therapeutic compounds for dairy cow operations.

Materials and methods

Preparation of matrine-loaded chitosan hydrogels

Matrine (98% purity) was purchased from Sigma-Aldrich Corp. (St. Louis, MO, United States), and chitosan was purchased from Shanghai Sunny Biotech Co., Ltd., Shanghai, China. All solutions were prepared with nonpyrogenic products and materials under aseptic conditions in a laminar flow hood. The procedures were like those of Lanct et al. (2017) and Jt et al. (2022). Matrine (0.05 g) and chitosan (4 g) were added to 95 ml of deionized water and heated at 37°C until the chitosan dissolved to form matrine-loaded chitosan complexes. Ten ml of matrine-chitosan and 5 ml of 4% hydroxyethyl cellulose (2:1 ratio) were put into disposable plastic dishes (60 mm diameter) and mixed thoroughly. The water used was nonpyrogenic with <0.005 endotoxin units/mL (Lonza, Walkersville, MD). For intramammary infusion, plastic syringes were filled with 10 ml of MCHs, sealed and stored at room temperature.

Abbreviations: MCHs, Matrine-chitosan hydrogels; PCA Principal component analysis; OPLS-DA, Orthogonal partial least squares discriminant analysis; KEGG, Kyoto Encyclopedia of Genes and Genomes; M, Metabolism; HD, Human diseases; EIP, Environmental information processing; OS, Organismal systems; GIP, Genetic information processing; SCC, Somatic cell counts; CMT, California mastitis rapid detection reagent; RDP, Ribosomal database project; OTUs, Operational taxonomic units.

TABLE 1 Components and nutritional analysis of the total mixed rations (dry matter basis, $n=6$).

Item	Content (%)
Alfalfa hay	13.34
Leymus chinensis	11.20
Corn	15.73
Whole cottonseed	3.19
Maize silage	28.57
DDGS	2.99
Steam-flaked corn	7.16
Soybean meal	11.53
Cottonseed meal	3.87
Premix ¹	1.96
NaCl	0.46
Total	100.00
Nutrient levels	
NEL/(MJ/kg) ²	7.26
EE	4.97
CP	17.35
NDF	30.8
ADF	16.5
Ca	0.74
P	0.41

¹One kg of premix contained the following: Cu 1,230 mg, Zn 4,950 mg, Mn 1760 mg, I 50 mg, Se 61 mg, VA 230000 IU, VD 350000 IU, VE 1000 IU.

²NEL was a calculated value; the other nutrient levels were measured values.

Animals and experimental design

Animals selected in this study were provided by the Beijing Sunlow Livestock Dairy Farming Center (Beijing, China), our animal protocols were reviewed and accepted by the Animal Care Committee of Beijing University of Agriculture (BUA2021056, Beijing, China) in concordance with the guidelines for the use of bovines in research studies of the SSTCC (The State Science and Technology Commission of the P.R. of China, 2017). Samples of untreated milk ($n=580$) were received from commercial dairies in Beijing from June to August 2021 with the California mastitis rapid detection reagent (CMT). Twelve mid-lactation cows with high somatic cell counts (SCC, average 360,000 cells/ml) indicative of subclinical-mastitis were selected according to milk yield and parity. There were few initial differences in milk yield (24.2 ± 2.7 kg/d), DIM (127 ± 14.4 d), parity (2.3 ± 0.2), or body weight (BW; 726 ± 27 kg). The cows were fed a standard basal diet (Table 1) with free access to water, and were kept in a tie-stall barn. They received intramammary infusions either MCHs or CON (ceftiofur hydrochloride, 125 mg, Zoetis, Florham Park, NJ, United States) after each milking, twice daily (7 AM and 7 PM) for 7 days. Milk samples were collected on the first day (D1) and the last injection day (D7) and totaled 15 ml per animal, with about equal volumes from each lactating udder quarter. The milk samples were cleaned and sterilized by hand after discarding the first three milkings. SCCs were determined using an automatic cell counter (DeLaval International AB, Tumba, Sweden), and the

remaining milk was stored in liquid nitrogen for later analysis. At the end of the experimental period, all cows were returned to the herd after veterinary examination ensured they were healthy.

Isolation of bacterial DNA and sequencing of 16S rRNA genes

Bacterial DNA was isolated from milk using a Power Soil DNA isolation kit (Qiagen, United Kingdom) as previously described by Tong et al. (2019). DNA concentration and 260/280 ratio were measured with a NanoDrop 1,000 spectrophotometer (Nanodrop Technologies, United States), and integrity was visualized by running DNA aliquots on an agarose gel. The V1-V2 region of the 16S rRNA gene was PCR-amplified with a GeneAmp 9,700 (ABI, United States) using forward (5'-CGTATCGCCT-CCCTCGCGCCATCAG-3') and reverse (5'-CTA-TGCGCCTTGCCAGCCCCGCTCAG-3') primers that incorporated adaptors and barcodes (Tong et al., 2019). Amplicons of about 450bp were selected and combined in equal concentrations (Li Y. et al., 2018), then electrophoresed and extracted from the gel with GeneJET (Thermo-Fisher, Waltham, MA, United States). Paired-end libraries were prepared by Majorbio Bio-Pharm (Shanghai, China). Bacterial rRNA genes were sequenced with Illumina HiSeq (Illumina, United States) to obtain paired-end reads of 300 base pairs. All raw sequence data were uploaded to NCBI (#SRP254162).

Analytical bioinformatics of milk microbiota

Analyses were conducted with FLASH version 1.2.11 and quantitative insights into microbial ecology (QIIME) version 1.9.1. These programs gave data like that published by Tong et al. (2019). Sequences were assigned to taxa by BLASTing the ribosomal database project (RDP) dbase using a 97% identity cut-off. Operational taxonomic units (OTUs) were normalized to relative abundance and bacterial composition was determined by Majorbio I-Sanger. Within-sample diversity (α -diversity) was measured as bacterial community enrichment (ACE and Chao indices) and diversity (Shannon and Simpson indices) was measured in a stochastic subset of the OTUs. Between-sample microbial diversity (β -diversity) was determined by phylogenetically-based, weighted UniFrac distances (Lozupone and Knight, 2005). A more detailed picture of the diversity of the most abundant evolutionary clades in the bovine microbiota was obtained by filtering the OTUs to yield those with a relative abundance of $\geq 1\%$ for at least one sample.

Milk metabolome determination

Milk samples were assessed by Majorbio Bio-Pharm using the LC-MS AB Sciex Triple TOF 5600TM (AB SCIEX,

United States) according to published procedures (Tong et al., 2019). The liquid chromatography conditions were like those of a previous study (Wang et al., 2019). Quality controls were run by combining milk samples and injecting them periodically during experimental measurements. The results were analyzed with XCMS (ver. 3.4.4). The retention times, MZ, observations, and peak intensities were normalized with Excel. The differentially expressed metabolites were analyzed with the public database¹ on the Majorbio I-Sanger platform² and the KEGG pathway software for differential metabolite profiles.³

Multivariate statistics

Comparisons were validated by Student's *t*, and $p < 0.05$ was defined as significant. Hierarchical clustering was conducted using the Bray–Curtis similarity index and the unweighted pair-group method with arithmetic averages. The SPSS software v.21.0 (IBM, Armonk, NY) was used. The α -diversity indices were given as mean \pm SD. A $p < 0.05$ was considered statistically significant, and a $p < 0.10$ suggested a trend. Principal component analysis and orthogonal partial least-squares-discriminant analysis (OPLS-DA) were carried out to show the metabolism changes among the experimental groups after mean centering and unit variance scaling. Parameters with variable importance in projection (VIP) values >1.0 were allowed for group discriminant testing. Our OPLS-DA model was confirmed by 7-fold permutation testing. Significantly different metabolites among groups were assessed and identified by Wilcoxon rank-sum tests.

1 https://metlin.scripps.edu/landing_page.php?pgcontent=mainPage

2 <https://cloud.majorbio.com>

3 <https://www.metaboanalyst.ca>

Results

Effect of matrine-chitosan hydrogels on milk yield and milk composition

Compared with D1, the milk yield, the yield of milk fat ($p = 0.03$), protein ($p = 0.04$), lactose ($p = 0.04$), and energy-corrected milk (ECM; $p = 0.01$) content all significantly increased by D7 (Table 2). MCHs significantly decreased the SCC on D7 compared to D1 ($p < 0.01$). However, there were no differences among the percentages of lactose, fat, and protein ($p > 0.05$). Similar results were found in CON group.

Diversity and relative numbers of milk microbiota

A total of 950,855 high-quality sequences from 24 samples passed quality control and were used for testing. The sequences averaged 460 bp, and there was greater than 99 % depth coverage; Therefore, the amount of data was sufficient to show differences in all bacterial species. The α -diversity indices of the microbiota are shown in Table 3. Although ACE showed a tendency to decrease, no difference was observed in the Chao indices, which were all representative of bacterial community richness in MCH group. Moreover, the Simpson index showed that the bacterial diversity at D7 was significantly higher than at D1 ($P < 0.05$) in both groups, and there was an overall tendency toward decrease ($p = 0.06$), but this was variable and depended on whether the calculations were based on abundance or biomass. No significant differences were seen among the groups for the other α -diversities. The PCA scores showed clear differences between MCH group and CON group on D1 and D7 milk samples (Figure 1). Principal components one and two were found to account for 22.07 and 16.4% of the variation, respectively.

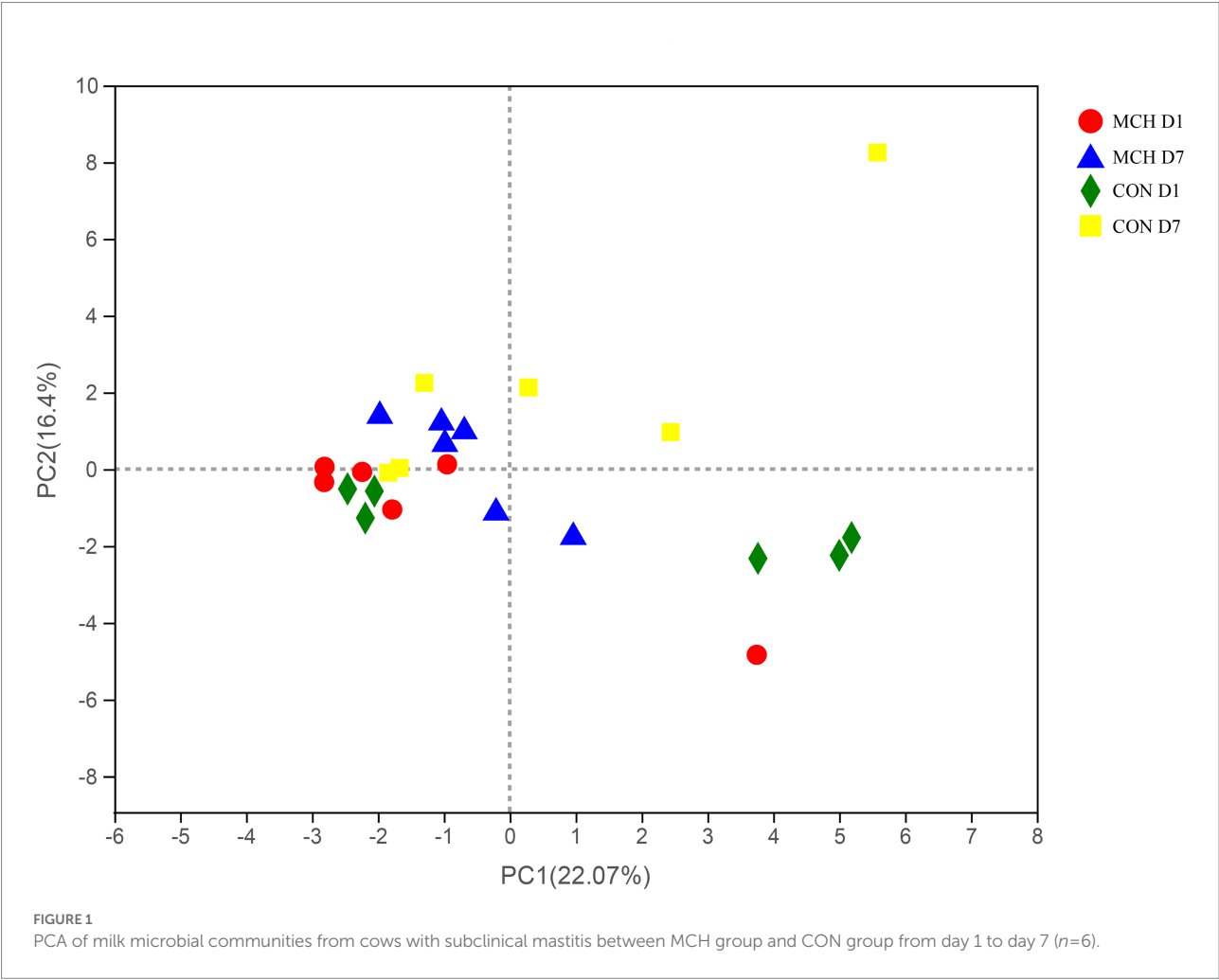
TABLE 2 Comparisons of milk yield and composition after intramammary treatment with matrine-loaded chitosan hydrogel ($n = 6$).

Yield and composition	MCH				CON			
	D1	D7	SEM	<i>P</i> -value	D1	D7	SEM	<i>P</i> -value
Yield								
Milk yield (kg/day)	25.2	34.27	2.67	0.03	23.17	29.93	2.81	0.05
ECM ¹ (kg/day)	27.3	39.2	2.18	0.01	24.10	32.35	3.16	0.05
Lactose (kg/day)	1.17	1.67	0.17	0.04	1.09	1.57	0.17	0.04
Fat (kg/day)	0.97	1.4	0.07	<0.01	0.85	1.14	0.12	0.05
Protein (kg/day)	0.8	1.23	0.14	0.04	0.68	0.96	0.09	0.04
Composition								
Lactose (%)	4.59	4.82	0.17	0.25	4.58	5.26	0.29	0.05
Fat (%)	3.87	4.13	0.28	0.41	3.62	3.83	0.17	0.23
Protein (%)	3.12	3.53	0.2	0.08	2.95	3.21	0.09	0.04
Fat: protein	1.17	1.17	0.09	0.99	1.23	1.20	0.07	0.60
SCC ($\times 10^4$ cells/ml)	35.4	10.7	3.6	<0.01	37.59	15.25	2.33	<0.01

TABLE 3 Alpha diversity indices for milk microbiota.

Item	MCH			CON		
	D 1	D 7	P-value	D 1	D 7	P-value
ACE	1769.86 ± 189.07	1211.79 ± 196.29	0.08	1659.6 ± 257.01	1,096 ± 597.53	0.06
Chao	1675.43 ± 201.72	1176.47 ± 196.24	0.11	1439.50 ± 437.05	1025.4 ± 573.23	0.19
Simpson	0.19 ± 0.07	0.47 ± 0.09	0.05*	0.15 ± 0.12	0.37 ± 0.24	0.07
Shannon	3.35 ± 0.52	1.92 ± 0.36	0.06	3.53 ± 0.82	2.22 ± 0.90	0.03*
Coverage	0.99 ± 0.01	0.99 ± 0.02	0.57	0.99 ± 0.01	0.99 ± 0.01	0.14

**p* < 0.05.

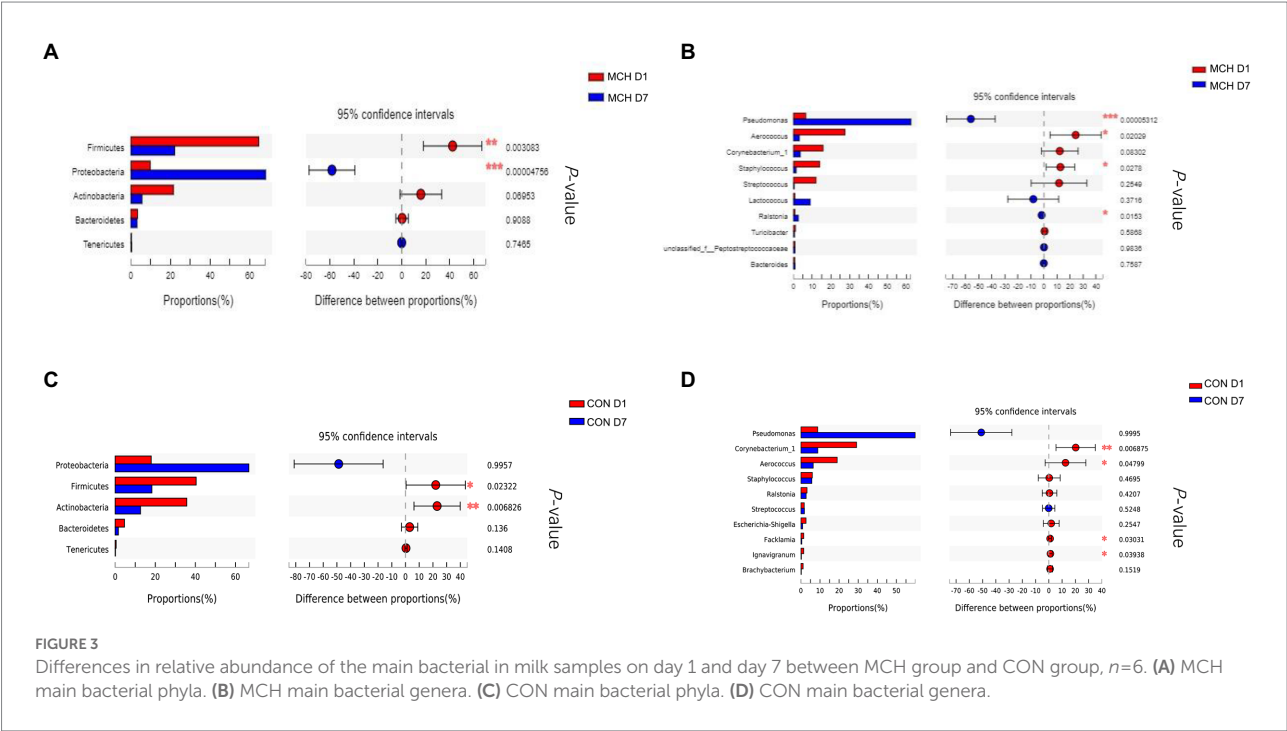
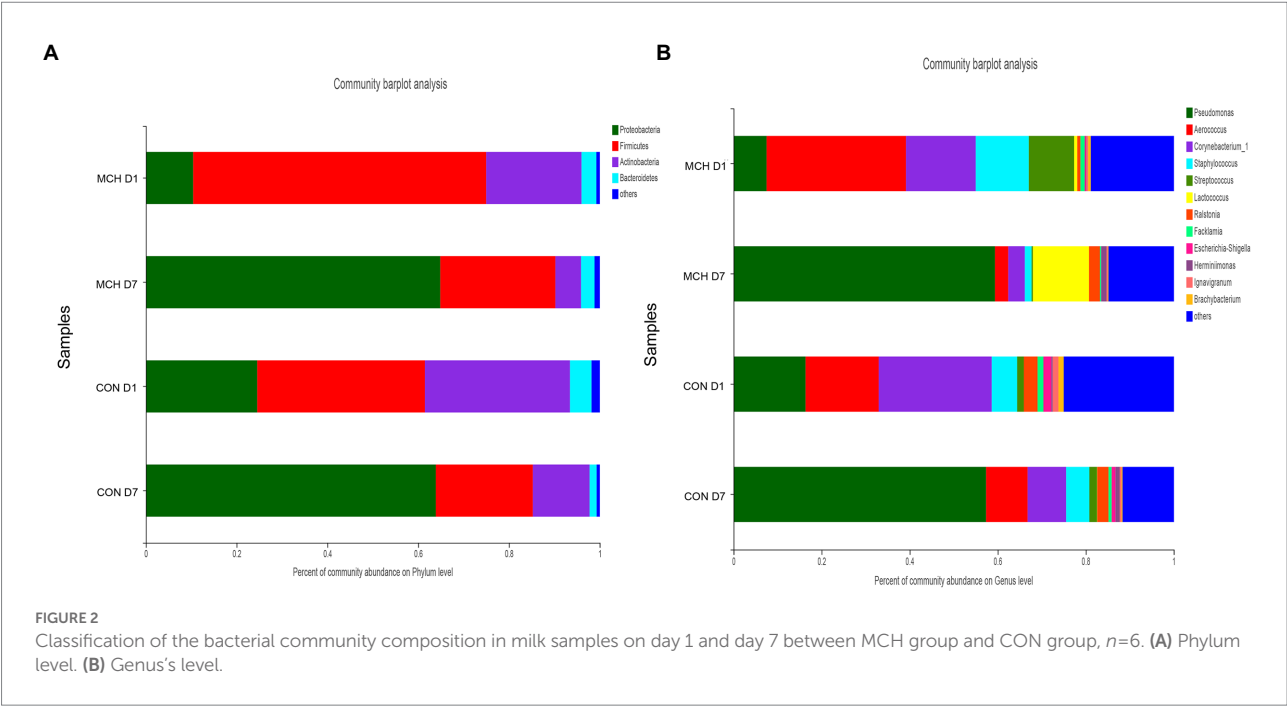


In MCH group, the taxonomic changes in milk samples from day 1 to day 7 were determined. *Proteobacteria*, *Firmicutes*, *Actinobacteria* and *Bacteroidetes* were the three predominant phyla (Figure 2A). Taxa with a relative abundance of 1 % in at least one sample were identified, and the 10 most abundant genera are presented (Figure 2B). The abundance of *Firmicutes* was extremely significantly decreased on day 7 (*p*=0.01), whereas the numbers of *Proteobacteria* increased (*p*=0.01; Figure 3A). On day 7, there was a significantly lower abundance of *Aerococcus* (*p*=0.01), *Corynebacterium_1* (*p*=0.08) and *Staphylococcus* (*p*=0.03). In contrast, the relative abundances of *Pseudomonas*

(*p*=0.01) and *Ralstonia* (*p*=0.02) were significantly increased (Figure 3B). Meanwhile, the same tendency was observed in the CON group (Figures 3C,D).

Identification and comparison of milk metabolites

A non-targeted metabolome method was used to evaluate milk metabolites after MCHs and ceftiofur hydrochloride treatment. Reproducible metabolite data profiles were



obtained and differences between two groups on D1 and D7 were characterized using VIP metrics from OPLS-DA. Seventy-four milk metabolite signals were obtained that were significantly different between MCH-treated and untreated cows ($VIP > 1$ and $p < 0.05$; Table 4), the CON group milk metabolite in Supplementary Table 1. They consisted mainly

of sphingolipids, oxanes, glycerophospholipids, flavonoids, and fatty acyls. Milk from animals receiving MCHs for 7 days had higher levels of steroids and steroid derivatives, prenol lipids, oxanes, macrolides and analogues, hydroxy acids and derivatives, carboxylic acids and derivatives, benzene, and substituted derivatives than milk on D1.

TABLE 4 Milk metabolites on day 1 compared to day 7 of MCH treatment (n=6).

Metabolite	M/Z	Retention time	Mass error	VIP	FC(d1/d7)	P-value	Trend
Steroids and steroid derivatives							
12b-hydroxy-5b-cholanoic acid	418.35	9.43	1.12	4.42	0.48	0.01	↑
Pregnanetriolone	349.24	8.8	−0.06	1.79	0.43	0.026	↑
Aginocide progenin	814.46	2.51	−2.8	1.02	0.04	<0.01	↑
Sphingolipids							
SM(d18:0/24:1(15Z))	859.7	13.36	5.06	1.58	3,208,275,862	<0.01	↓
SM(d18:1/23:0)	845.68	12.95	5.27	2.26	11748.6	<0.01	↓
SM(d18:1/22:1(13Z))	829.65	11.92	4.59	1.72	369.77	<0.01	↓
SM(d18:0/22:1(13Z))	831.66	12.73	4.91	4.9	212.45	<0.01	↓
Glucosylceramide (d18:1/16:0)	744.57	11	3.44	1.89	34.01	<0.01	↓
Galactosylceramide (d18:1/14:0)	706.51	10.5	3.07	1.29	27.94	<0.01	↓
Glucosylceramide (d18:1/25:0)	790.69	14.01	−0.89	3.78	21.09	<0.01	↓
stearoyl sphingomyelin	775.6	11.48	4.77	1.32	19.61	<0.01	↓
N-hexadecanoylsphinganine-1-phosphocholine	749.58	11.16	2.57	2.76	16.13	<0.01	↓
Galabiosylceramide (d18:1/16:0)	906.62	10.86	5.8	1.9	9.04	<0.01	↓
SM(d18:0/14:0)	721.55	10.62	3.35	2.94	7.99	<0.01	↓
SM(d18:0/16:1(9Z))	747.57	10.92	4.52	6.89	3.62	<0.01	↓
N-Glycoloylganglioside GM2	708.61	12.75	−0.87	9.56	2.38	<0.01	↓
SM(d18:1/14:0)	719.54	10.42	3.7	5.12	2.34	<0.01	↓
Arabicacerebroside	776.55	10.75	−6.85	1.95	1.49	<0.01	↓
Ganglioside GM1 (d18:1/18:1(11Z))	772.43	4.33	−7.63	1	0.28	0.02	↑
nLc6Cer	696.82	3.25	−1.78	2.36	0.09	<0.01	↑
Prenol lipids							
Hodulose VI	819.43	2.96	−3.62	1.42	0.05	0.01	↑
Oxanes							
D-1,5-anhydrofructose	325.11	0.78	−0.78	1.1	0.78	<0.01	↑
Organo-oxygen compounds							
3,4,5-trihydroxy-6-(2-hydroxyethoxy)oxane-2-carboxylic acid	475.13	0.7	−1.46	1.13	2.62	<0.01	↓
N6-galacturonyl-L-lysine	357.11	2.4	8.9	2.54	1.56	0.02	↓
Lactulose	365.11	0.62	1.53	6.7	0.56	<0.01	↑
Macrolides and analogues							
Pectenotoxin 7	909.37	2.45	−1.88	1.95	0.1	<0.01	↑
31-O-demethylacrolimus	810.44	0.75	−1.37	1.15	0.03	<0.01	↑
Indoles and derivatives							
Indole-3-carboxylic acid-O-sulfate	240	2.27	−1	3.13	1.74	<0.01	↓
Hydroxy acids and derivatives							
2-hydroxy-3-methoxyestrone	442.35	9.08	1.05	2.9	0.43	0.01	↑
Glycerophospholipids							
PE (15:0/22:0)	806.6	11.84	5.06	2.5	48.31	<0.01	↓
PE (14:0/22:0)	792.58	11.45	8.49	1.14	15.03	<0.01	↓
PS (DiMe (11,3)/MonoMe (11,5))	880.54	12.16	2.74	1.21	8.01	<0.01	↓
PE (15:0/24:1(15Z))	832.61	11.77	5.01	4.77	6.11	<0.01	↓
lysoPC (6:0)	400.17	3.01	−1.21	2.04	5.51	<0.01	↓
PE (16:0/16:0)	736.52	10.42	2.96	2.16	2.26	<0.01	↓
PS (18:0/18:1(9Z))	810.53	11.5	5.99	2.68	2.12	<0.01	↓
PE (18:2(9Z,12Z)/18:1(11Z))	786.53	12.04	4.76	7.92	1.99	<0.01	↓
PE (15:0/16:0)	722.5	10.33	5.04	3.2	1.85	<0.01	↓
PE (15:0/14:0)	694.47	9.94	3.99	1.33	1.72	<0.01	↓

(Continued)

TABLE 4 (Continued)

Metabolite	M/Z	Retention time	Mass error	VIP	FC(d1/d7)	P-value	Trend
PE (15:0/22:1(13Z))	804.58	11.24	5.01	4	1.67	<0.01	↓
PS (16:0/18:0)	784.52	11.45	7.51	3.58	1.63	<0.01	↓
LysoPE (0:0/18:2(9Z,12Z))	476.28	7.75	−0.17	1.66	1.53	0.05	↓
PE (18:1(9Z)/16:0)	718.54	11.44	0.48	1.83	1.5	0.03	↓
PE (15:0/20:2(11Z,14Z))	774.53	10.37	4.68	1.03	1.39	0.02	↓
LysoPE (16:0/0:0)	452.28	8.32	0.26	1.84	1.36	0.01	↓
PS (15:0/24:1(15Z))	830.6	11.21	4.84	1.71	1.3	0.02	↓
LysoPC (18:1(9Z))	566.35	8.31	0.06	3.94	0.68	0.01	↑
LysoPC (18:2(9Z,12Z))	564.33	7.79	−1.16	5.06	0.56	0.01	↑
LysoPC (16:1(9Z)/0:0)	538.32	7.58	1.76	1.12	0.55	0.02	↑
LysoPE (20:3(11Z,14Z,17Z)/0:0)	502.29	8.11	0.14	1.65	0.5	0.02	↑
PC (18:2(9Z,12Z)/P-18:0)	814.6	11.07	4.43	1.18	0.47	0.01	↑
LysoPE (20:4(5Z,8Z,11Z,14Z)/0:0)	500.28	7.8	−0.15	3.45	0.41	<0.01	↑
LysoPE (18:2(9Z,12Z)/0:0)	478.29	7.77	2	2.75	0.35	<0.01	↑
LysoPC (18:1(11Z))	522.36	8.2	0.69	4.22	0.31	<0.01	↑
LysoPE (0:0/22:5(7Z,10Z,13Z,16Z,19Z))	562.27	5.39	−0.86	1.06	0.3	<0.01	↑
1-Linoleoylglycerophosphocholine	520.34	7.69	0.61	4.27	0.17	0.01	↑
1-(8Z,11Z,14Z-eicosatrienoyl)-glycero-3-phosphate	502.29	7.7	−0.01	1.27	0.14	<0.01	↑
LysoPC (P-18:0)	552.37	8.59	0.37	1.31	0.09	<0.01	↑
TG (16:1(9Z)/16:1(9Z)/16:1(9Z))	845.68	13.12	−9.94	3.56	1607.82	<0.01	↓
MG (0:0/16:0/0:0)	365.25	8.94	−0.54	3.43	0.53	0.027	↑
Flavonoids							
Menthosides	723.2	0.7	4.79	4.57	2.69	<0.01	↓
Isoscoparin 2'-(6-(E)-ferulylglucoside)	781.2	0.84	−0.3	2.37	1.31	0.02	↓
Kaempferol 3-(2'-rhamnosylgalactoside)	777.16	0.7	−1.93	4.24	0.49	<0.01	↑
7-rhamnosides							
Licorice glycoside C1	765.18	0.64	0.82	2.27	0.19	<0.01	↑
Fatty Acyls							
cis-uvariamicin IB	627.48	11.55	2.27	1.32	1268.67	<0.01	↓
3,4-dimethyl-5-pentyl-2-furanpentadecanoic acid	857.68	12.57	−9.88	1.54	130.24	<0.01	↓
15-hydroxyeicosanoic acid	698.63	13.78	−0.76	4.76	11.33	<0.01	↓
2-hydroxyhexadecanoic acid	271.23	8.73	0.84	2.08	0.47	0.01	↑
3-hydroxyhexadecanoyl carnitine	416.34	8.99	2.02	2.15	0.43	0.01	↑
Aminocaproic acid	132.1	1.17	0.75	1.42	0.04	<0.01	↑
Carboxylic acids and derivatives							
Tyrosyl-Isoleucine	293.15	2.31	−0.33	1.53	0.22	<0.01	↑
L-Phenylalanine	164.07	1.71	0.73	1.03	0.09	<0.01	↑
Benzene and substituted derivatives							
fluvoxamino acid	360.15	0.86	−8.35	2.72	0.53	<0.01	↑

PCA and OPLS-DA were employed to evaluate the differences in metabolomes. The PCA scores showed clear differences between D1 and D7 milk samples (Figure 4A). Principal components one and two were found to account for 15.6 and 20% of the variation, respectively. The variables for assessing OPLS-DA model quality are shown as validation plots (Figure 4B). The Q2 value of the OPLS-DA model was −0.18, and the R2Y value was 0.21. Q2 represents a model's

prediction ability and the closer these three indicators are to 1, the more stable and reliable it is. The OPLS-DA data confirmed that the two groups had significantly different types and levels of metabolites (Figure 4C). OPLS-DA model integrity is shown by validation plots. The D7 metabolite profiles were significantly different from those of D1 indicating that the PCA and OPLS-DA results were valid for assessing variations in milk metabolomes between the 2 days.

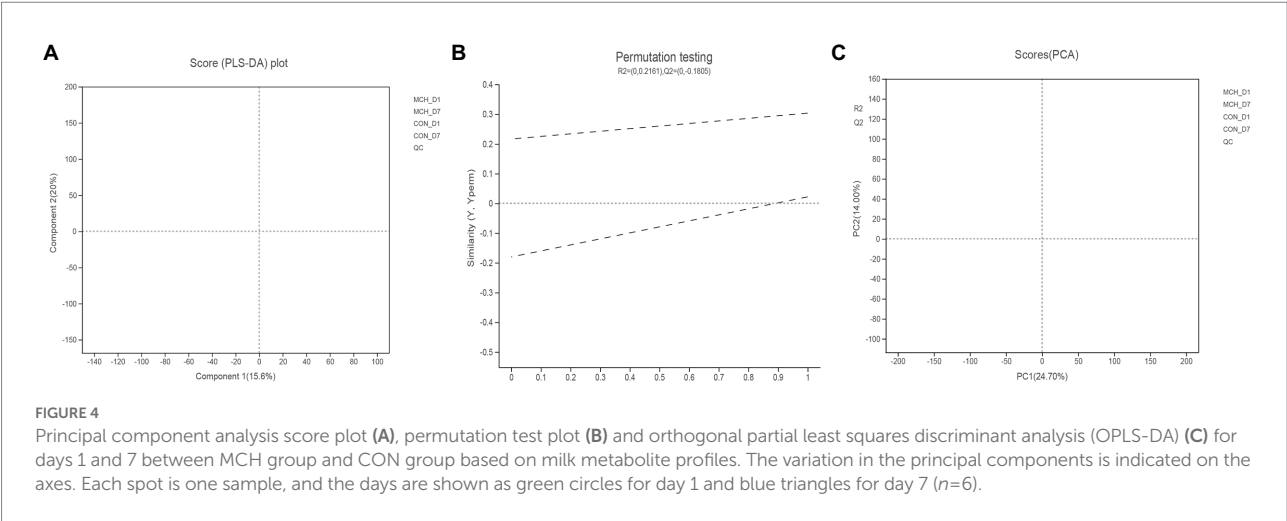


TABLE 5 Differences in metabolites enriched from specific pathways in milk of dairy cows receiving MCH infusions (7days, $n=6$).

Metabolic pathway	Metabolite
Sphingolipid metabolism (10)	Galabiosylceramide (d18:1/16:0); SM(d18:1/22:1(13Z)); SM(d18:0/22:1(13Z)); Glucosylceramide (d18:1/16:0); SM(d18:0/16:1(9Z)); Glucosylceramide (d18:1/25:0); SM(d18:0/24:1(15Z)); Galactosylceramide (d18:1/14:0); SM(d18:0/14:0); SM(d18:1/23:0)
Sphingolipid signaling pathway (6)	SM(d18:1/22:1(13Z)); SM(d18:0/22:1(13Z)); SM(d18:0/16:1(9Z)); SM(d18:0/24:1(15Z)); SM(d18:0/14:0); SM(d18:1/23:0)
Glycerophospholipid metabolism (3)	PE(14:0/24:1(15Z)); LysoPC(20:4(8Z,11Z,14Z,17Z)); PC(15:0/16:0)
Choline metabolism in cancer (2)	LysoPC(20:4(8Z,11Z,14Z,17Z)); PC(15:0/16:0)
Retrograde endocannabinoid signaling (2)	PE (14:0/24:1(15Z)); PC (15:0/16:0)
Pathogenic Escherichia coli infection (1)	PE (14:0/24:1(15Z))
Autophagy – other (1)	PE (14:0/24:1(15Z))
Glycosylphosphatidylinositol (GPI)- anchor biosynthesis (1)	PE (14:0/24:1(15Z))
Autophagy – animal (1)	PE (14:0/24:1(15Z))

Differences in metabolites resulting from changes in metabolic pathways

Comparison of metabolite levels relative to changes in pathway activation from MCHs treatment on D1 to D7 was performed using the Kyoto Encyclopedia of Genes and Genomes

(KEGG) for determining enrichment of pathways involved in metabolite production (Table 5; Figure 5). Enrichment analysis showed that sphingolipid metabolism, the sphingolipid signaling pathway, glycerophospholipid metabolism and ABC transporters, were significantly affected by MCHs infusion. Pathway topology analysis (Figure 6; $p < 0.05$) revealed eight key pathways enriched between days 1 and 7. They included sphingolipid, phenylalanine, glycerophospholipid, starch and sucrose metabolism, synthesis of phenylalanine, tyrosine and tryptophan and linoleic acid metabolism. For the CON group, the enrichment of pathways analysis was shown in Supplementary Figure 1.

Discussion

The results of this study revealed that matrine-chitosan hydrogel markedly decreased SCCs after 7 days of treatment. Although we did not observe any changes in bacterial community richness by the Chao indices, the Shannon index showed a significant decrease in bacterial diversity. On D7, the relative abundance of Firmicutes was significantly decreased, and that of Proteobacteria was significantly increased compared to levels on D1. It has been reported that the richness and diversity of the milk microbiome reflects the health of cows and the functional performance of their organs (Mohammed et al., 2014; Schokker et al., 2015; Blanco et al., 2016). Matrine has antibacterial and anti-inflammatory properties and has been commonly used to treat bovine mastitis, but its efficacy is still unproven (Oliveira and Ruegg, 2014). That is why we chose to test the plant-derived compound, matrine, as an intramammary treatment loaded into chitosan hydrogels to see if it would alter the milk microbiota and improve mammary gland function.

Measurement of the number of somatic cells in milk is an internationally recognized test for the detection of mastitis. A SCC of more than 200,000 per ml is evidence of disease (Kovac et al., 2007). Recent investigations have shown that the milk microbiota of dairy cows is usually closely associated with the SCC

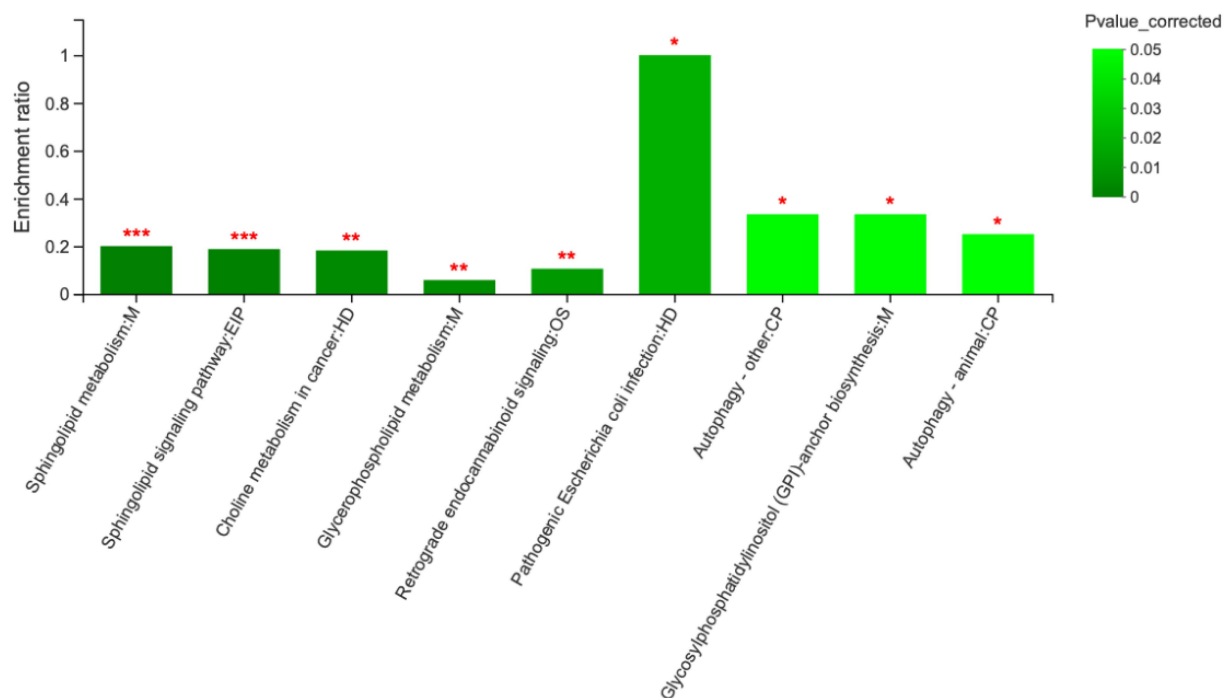


FIGURE 5

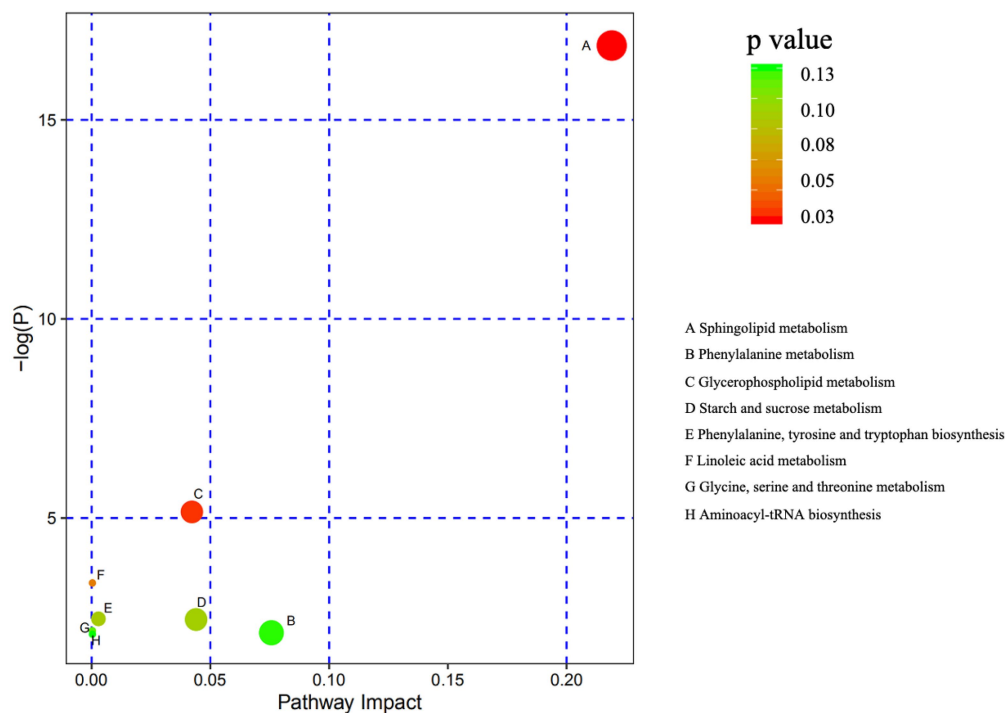
Metabolic pathway enrichment analysis between day 1 and day 7. M, EIP, HD, OS and CP are the names of the metabolic pathways in KEGG annotation. M, metabolism; EIP, environmental information processing; HD, human diseases; OS, organismal systems; CP, cellular processes ($n=6$). *** $p < 0.001$, ** $p < 0.01$, and * $p < 0.05$.

(Oikonomou et al., 2014; Vanderhaeghen et al., 2014). This suggests that modulation of the udder ecosystem through the microbiota could help to maintain homeostasis and enhance the mammary gland's defenses. Consistent with these reports, we observed that the udder SCC was significantly increased in mastitis caused by common pathogens like staphylococci, but was markedly decreased after perfusion of the udder with matrine-chitosan hydrogel. This is in line with previous studies showing that chitosan hydrogels decreased the SCC in milk from dairy cows (Lanct et al., 2017). The therapeutic synergy achieved by loading the chitosan hydrogel with matrine suggests potential applications in mastitis protection and treatment. The mechanism by which the milk microbiota influences inflammatory and immune responses to decrease the SCC needs further investigation.

The next generation of high-throughput DNA sequencing methods together with updated bioinformatics software is now being used for the in-depth assessment of microbial communities to elucidate how bacterial activity and metabolites affect human and animal health (Catozzi et al., 2017). We found that the microbial diversity in milk was dramatically decreased after 1 week of intramammary infusion of matrine-chitosan hydrogels. The relative abundance of Proteobacteria was significantly increased, while staphylococcus decreased significantly. Staphylococci are recognized as one of the most prevalent mastitis pathogens, accounting for about 70% of the cases (Gao et al., 2017). Moreover, it has been reported that Proteobacteria were significantly more

abundant in healthy cows than in those with mastitis (Catozzi et al., 2017). Previous studies also showed that the numbers of Proteobacteria after non-antibiotic hydrogel treatment increased significantly (Bhatt, 2012), indicating that hydrogel therapy can effectively return the milk microbial environment to normal diversity and defend against disease. Our investigation provides mechanistic insights into how the microbiota respond to MCHs that may help in the development of novel prophylactic and therapeutic products as alternatives to antibiotics in dairy cows. Our data are also important for understanding how the regulation of biosynthesis by milk microbiota influences udder health and defense against mastitis. The milk microbiota is usually closely associated with the SCC (Oikonomou et al., 2014; Vanderhaeghen et al., 2014) suggesting that the udder microbiota is important in modulation of the udder ecosystem, maintenance of homeostasis, and resistance of the mammary gland to infections (Barkema et al., 2006; Rainard and Pascal, 2017).

Metabolomics is a comparatively new research method that has been widely used in the detection of mastitis in recent years due to its more comprehensive test results. Previous studies suggested that metabolomics could provide a more complete understanding of an animal's physiology and biochemistry (Zhao et al., 2014). The metabolomics data from this study highlight the potential function of matrine-chitosan hydrogels in modulating the metabolite levels, which were enriched in sphingolipid metabolic pathways, phenylalanine, glycerophospholipid, and



starch and sucrose metabolism. A previous report suggested that sphingolipid metabolites acted as signaling molecules to regulate a diverse group of cellular processes, particularly those related to immunity, inflammation, and inflammatory disorders (Maceyka and Spiegel, 2014). We speculate that this activity might be associated with the decrease in SCC caused by infusion of matrine-chitosan hydrogels. The metabolic differences we observed gave us further insights into how MCHs affects metabolite levels after mastitis treatment. The data showed that alterations in the milk metabolome could be used to reveal the therapeutic mechanism of matrine therapy for mastitis treatment and in the recovery of milk production in dairy cows.

We found significant changes in the concentrations of sphingolipids, glycerolipids, fatty acyls, glycerophospholipids, and organo-oxygen compounds from D1 to D7. Sphingolipids are major components of cell membranes and are widely involved in important processes such as cell aging and apoptosis (Thomas et al., 2016). Glycerolipids (Li N. et al., 2018) and fatty acyls (Kagan et al., 2017) are both important components of cell membranes. Previous research found that bacterial invasion could induce inflammatory reactions accompanied by apoptosis and cause oxidative damage during breast development (Turk, 2017). The reduction in sphingolipids, glycerolipids, and fatty acyls seen in this study indicates that apoptosis caused by inflammatory reactions may have been lessened. The decrease of organo-oxygen compounds suggests that the oxidative damage caused by inflammatory reactions may also have been reduced. The metabolites were enriched in sphingolipid and glycerophospholipids, which are both related to apoptotic pathways

(Gao et al., 2016, 2018). We conclude that MCHs can inhibit apoptosis by blocking oxidative damage, thereby reducing inflammatory changes to the udder.

It is worth noting that L-phenylalanine was involved in many pathways that were significantly changed in this study (Table 3). L-phenylalanine is an essential amino acid as well as a precursor for the commercial synthesis of antiviral and anticancer drugs. It can also be a marker of inflammatory reactions and affect the body's immune response (Turk, 2017). Here, the content of L-phenylalanine was significantly increased on day 7, which means that the immune defenses in the mammary gland may have been effectively strengthened. In a previous study, Strasser et al. (2016) found that tryptophan and phenylalanine were used in the body to synthesize serotonin, L-DOPA derivatives and 5, 6, 7, 8-tetrahydrobiopterin (BH4), which compounds can affect the severity of inflammation. In the study of Smith et al. (2018), tyrosine and phenylalanine participated in the regulation of TLR4 signaling pathways, thereby influencing the degree of inflammation. Phenylalanine also is part of the glycolytic and liposynthetic pathways (Waisbren et al., 2007; Obianom et al., 2019). It has been reported that phenylalanine deficiency can severely affect protein metabolism in the breast and compromise the health of the organ (Shibata et al., 1992). Phenylalanine is an essential amino acid in milk and is also the precursor of tyrosine, which is one of the main amino acids in milk (Rezaei et al., 2016). We know that untreated bovine mastitis results in reduced milk fat and milk protein content; therefore, the increase in L-phenylalanine by MCHs infusion could be effective in restoring normal milk production during lactation.

The milk metabolites induced by MCHs were found to have an intimate relationship with sphingolipid and glycerophospholipid metabolism. A previous study suggested that the sphingolipid metabolic pathways participate in a variety of immune-related signal transductions, inflammation, and inflammatory disorders (Maceyka and Spiegel, 2014). The sphingolipid metabolic pathways have many functions, such as regulating cell adhesion and cellular immunity, activating cancer repressors, regulating apoptosis, and modulating immune function and the inflammatory response (Maceyka and Spiegel, 2014). We speculate that this activity might be associated with the decrease in SCC caused by MCHs. Brice and Cowart (2011) showed that an imbalance in the pathway for sphingolipid metabolism caused ketosis, mastitis, and metritis in cows. It has been proved that sphingolipid metabolites, especially ceramide and sphingosine-1-phosphate, can regulate a variety of biochemical processes important in immunological and inflammatory diseases (Maceyka and Spiegel, 2014). In the present study, we found that MCHs significantly regulated sphingolipid pathways to reduce inflammation; thus, it is reasonable to believe that MCHs could effectively treat bovine mastitis.

Despite the documented health-promoting properties of matrine and chitosan, scientific evidence for the efficacy of MCHs in dairy cows is limited. Our study affords many useful insights, but the mechanism of MCH's effect on immune regulation still requires further study. Another limitation relates to the mechanistic links involved in the observed significant changes in the microbiota and biomarker metabolites as a result of MCHs infusion that need further exploration to be clearly understood. Previous studies suggested that the antimicrobial activity of chitosan stimulated the innate immune response and hastened involution of the mammary gland (Lanct et al., 2017). It is not known whether matrine-chitosan complexes could be used in the circulation to regulate the immune system and inhibit inflammation, but our data indicate that future research in this area is strongly warranted.

Conclusion

Our data indicate that matrine-chitosan hydrogels significantly decrease the somatic cell counts and affect the structures of bacterial communities in the udder, especially the relative abundances of *Corynebacterium_1*, *Aerococcus*, and *Staphylococcus*. Our findings show significant changes in metabolites and metabolic pathways as a result of intramammary MCHs infusion, and some of the 74 resulting milk metabolites may be used as indicators of the response to MCHs treatment. The results from the milk metabolic pathway analysis are promising for the investigation of matrine-chitosan's antimicrobial and anti-inflammatory properties that are closely associated with sphingolipid and glycerophospholipid metabolism. These insights into the complex mechanisms and corresponding biological responses highlight the beneficial action of matrine-chitosan hydrogels and justify continued investigations to identify the immunoregulatory mechanisms for treatment of mastitis in dairy cows.

Data availability statement

The datasets presented in this study can be found in online repositories. The names of the repository/repositories and accession number(s) can be found at: NCBI-SRP254162.

Ethics statement

The animal study was reviewed and approved by Animal Care Committee of Beijing University of Agriculture.

Author contributions

JT, ZW, and LJ developed hypothesis, conceived the project, and responsible for all data, figures, and text. JT, HZ, and ZW performed the experiments. ZW and HY conducted data analysis. JT and ZW wrote the manuscript. JT, HZ, and LJ revised the paper. All authors contributed to the article and approved the submitted version.

Funding

This study was funded by the Project of the National Natural Science Foundation of China (Grant No. 31802091). JT thanks the Beijing University Youth Talent Science Foundation and R&D Program of Beijing Municipal Education Commission (KM202210020006).

Acknowledgments

The authors thank the dairy barn staff for taking care of the cows, especially Kangkang Chu for providing technical assistance. The authors are grateful to Shihui Wen, from Shanghai Majorbio Bio-pharm Technology Co., Ltd., for her assistant of the multivariate statistics analysis.

Conflict of interest

The authors declare that the research was conducted in the absence of any commercial or financial relationships that could be construed as a potential conflict of interest.

Publisher's note

All claims expressed in this article are solely those of the authors and do not necessarily represent those of

their affiliated organizations, or those of the publisher, the editors and the reviewers. Any product that may be evaluated in this article, or claim that may be made by its manufacturer, is not guaranteed or endorsed by the publisher.

References

- Barkema, H. W., Schukken, Y. H., and Zadoks, R. N. (2006). Invited review: the role of cow, pathogen, and treatment regimen in the therapeutic success of bovine *Staphylococcus aureus* mastitis. *J. Dairy Sci.* 89, 1877–1895. doi: 10.3168/jds.S0022-0302(06)72256-1
- Bhatt, S. K. (2012). Bacteriological profile and ANTIBIOGRAM of neonatal septicemia. *Nati. J. Commun. Med.* 3, 371–374. doi: 10.1007/s12098-012-0911-9
- Blanco, G., Junza, A., Segarra, D., Barbosa, J., and Barron, D. (2016). Wildlife contamination with fluoroquinolones from livestock: widespread occurrence of enrofloxacin and marbofloxacin in vultures. *Chemosphere* 144, 1536–1543. doi: 10.1016/j.chemosphere.2015.10.045
- Brice, S. E., and Cowart, L. A. (2011). Sphingolipid metabolism and analysis in metabolic disease. *Adv. Exp. Med. Biol.* 721, 1–17. doi: 10.1007/978-1-4614-0650-1_1
- Catozzi, C., Bonastre, A. S., Francino, O., Lecchi, C., and Ceciliani, F. (2017). The microbiota of water buffalo milk during mastitis. *PLoS One* 12:e0184710. doi: 10.1371/journal.pone.0184710
- Chenite, A., Chaput, C., Wang, D., Combes, C., Buschmann, M. D., Hoemann, C. D., et al. (2000). Novel injectable neutral solutions of chitosan form biodegradable gels in situ. *Biomaterials* 21, 2155–2161. doi: 10.1016/S0142-9612(00)00116-2
- Derakhshani, H., Plazier, J. C., Jeroen, D. B., Barkema Herman, W., and Ehsan, K. (2018). Association of bovine major histocompatibility complex (BoLA) gene polymorphism with colostrum and milk microbiota of dairy cows during the first week of lactation. *Microbiologia* 6:203. doi: 10.1186/s40168-018-0586-1
- Falentin, H., Rault, L., Nicolas, A., Bouchard, D. S., Lassalas, J., Lamberton, P., et al. (2016). Bovine teat microbiome analysis revealed reduced alpha diversity and significant changes in taxonomic profiles in quarters with a history of mastitis. *Front. Microbiol.* 7:480. doi: 10.3389/fmicb.2016.00480
- Feng, F., Wa, M., Luo, H. X., Guan, C. P., and Zhou, X. Z. (2018). Effect of matrine on reducing damage to bovine mammary epithelial cells induced by *Staphylococcus aureus* alpha-hemolysin. *Pol. J. Vet. Sci.* 21, 409–413. doi: 10.24425/122610
- Gao, J., Barkema, H. W., Zhang, L., Liu, G., Deng, Z., Cai, L., et al. (2017). Incidence of clinical mastitis and distribution of pathogens on large Chinese dairy farms. *J. Dairy Sci.* 100, 4797–4806. doi: 10.3168/jds.2016-12334
- Gao, X., Guo, S., Zhang, S., Liu, A., Shi, L., and Zhang, Y. (2018). Matrine attenuates endoplasmic reticulum stress and mitochondrion dysfunction in nonalcoholic fatty liver disease by regulating SERCA pathway. *J. Transl. Med.* 16:319. doi: 10.1186/s12967-018-1685-2
- Gao, D., Wang, Y., Xie, W., Yang, T., Jiang, Y., Guo, Y., et al. (2016). Metabolomics study on the antitumor effect of marine natural compound flexibilide in HCT-116 colon cancer cell line. *J. Chroma. B. Anal. Technol. Biomed. life. Sci.* 1014, 17–23. doi: 10.1016/j.jchromb.2016.01.003
- Guillaume, L., GrHn, Y. T., and Didier, R. (2016). Addressing antimicrobial resistance: an overview of priority actions to prevent suboptimal antimicrobial use in food-animal production. *Front. Microbiol.* 7:2114. doi: 10.3389/fmicb.2016.02114
- Jt, A., Xh, B., Dc, B., Wu, C. B., Hua, Y. B., Bx, C., et al. (2022). A berberine hydrochloride-carboxymethyl chitosan hydrogel protects against *Staphylococcus aureus* infection in a rat mastitis model. *Carbohydr. Polym.* 278, 1–10.
- Junza, A., Minguillon, C., Saurina, J., et al. (2016). Metabolic profile modifications in milk after enrofloxacin administration studied by liquid chromatography coupled with high resolution mass spectrometry. *J. Chromato. A: Including electrop. other sepa. methods.* 1460, 92–99. doi: 10.1016/j.chroma.2016.07.016
- Kagan, V. E., Mao, G., Feng, Q., Angeli, J., Doll, S., Croix, C. S., et al. (2017). Oxidized arachidonic and adrenic PEs navigate cells to ferroptosis. *Nat. Chem. Biol.* 13, 81–90. doi: 10.1038/nchembio.2238
- Kovac, G. U. V. L. K., Popelkova, M. U. V. L. K., Tkacikova, L. U. V. L. K., Burdova, O. U. V. L. K., and Ihnat, O. U. V. L. K. (2007). Interrelationship between somatic cell count and acute phase proteins in serum and Milk of dairy cows. *Acta Vet. Brno* 76, 51–57. doi: 10.2754/AVB200776010051
- Lanct, T. S., Fustier, P., Taherian, A. R., Bisakowski, B., Zhao, X., Lacasse, P., et al. (2017). Effect of intramammary infusion of chitosan hydrogels at drying-off on bovine mammary gland involution. *J. Dairy Sci.* 100, 2269–2281. doi: 10.3168/jds.2016-12087
- Li, Y., Hu, X., Yang, S., Zhou, J., and Hu, D. (2018). Comparison between the fecal bacterial microbiota of healthy and diarrheic captive musk deer. *Front. Microbiol.* 9:300. doi: 10.3389/fmicb.2018.00300
- Li, N., Sancak, Y., Frasar, J., and Atilla-Gokcumen, G. E. (2018). A protective role for Triacylglycerols during apoptosis. *Biochemistry: aca.* 57:72. doi: 10.1021/acs.biochem.7b00975
- Lozupone, C., and Knight, R. (2005). UniFrac: a new phylogenetic method for comparing microbial communities. *Appl. Environ. Microbiol.* 71, 8228–8235. doi: 10.1128/AEM.71.12.8228-8235.2005
- Maceyka, M., and Spiegel, S. (2014). Sphingolipid metabolites in inflammatory disease. *Nature* 510, 58–67. doi: 10.1038/nature13475
- Mohammed, R., Brink, G. E., Stevenson, D. M., Neumann, A. P., Beauchemin, K. A., Suen, G., et al. (2014). Bacterial communities in the rumen of Holstein heifers differ when fed orchardgrass as pasture vs. hay. *Front. Microbiol.* 5:689. doi: 10.3389/fmicb.2014.00689
- Obianom, C., Romanazzi, G., and Sivakumar, D. (2019). Effects of chitosan treatment on avocado postharvest diseases and expression of phenylalanine ammonia-lyase, chitinase and lipoxygenase genes. *Postharvest Biol. Technol.* 147, 214–221. doi: 10.1016/j.postharvbio.2018.10.004
- Oikonomou, G., Bicalho, M. L., Meira, E., Rossi, R. E., Foditsch, C., Machado, V. S., et al. (2014). Microbiota of Cow's Milk; distinguishing healthy, sub-clinically and clinically diseased quarters. *PLoS One* 9:e85904. doi: 10.1371/journal.pone.0085904
- Oliveira, L., and Ruegg, P. L. (2014). Treatments of clinical mastitis occurring in cows on 51 large dairy herds in Wisconsin. *J. Dairy Sci.* 97, 5426–5436. doi: 10.3168/jds.2013-7756
- Rainard, , and Pascal, (2017). Mammary microbiota of dairy ruminants: fact or fiction. *Vet. Res.* 48:25. doi: 10.1186/s13567-017-0429-2
- Rezaei, R., Wu, Z., Hou, Y., Bazer, F. W., and Wu, G. (2016). Amino acids and mammary gland development: nutritional implications for milk production and neonatal growth. *J. Chem. Technol. Biotechnol.* 7:20. doi: 10.1186/s40104-016-0078-8
- Schokker, D., Veninga, G., Vastenhout, S. A., Bossers, A., and Smits, M. A. (2015). Early life microbial colonization of the gut and intestinal development differ between genetically divergent broiler lines. *BMC Genomics* 16:418. doi: 10.1186/s12864-015-1646-6
- Shibata, K., Miyuki, S. H. I. O. T. A. N. I., Michiko, O. N. O. D. E. R. A., and Takeshi, S. U. Z. U. K. I. (1992). Changes in Nicotinamide metabolism by one amino acid deficiency. (I) Threonine-, tryptophan-, aspartic acid-, lysine-, Leucine-, or methionine-free diet. *J. Agri. Chem. Soc. Japan.* 56, 783–787. doi: 10.1271/bbb.56.783
- Smith, T. L., Paul, V. S., Nina, J., Dumont, D. J., and Jane, M. C. (2018). Tie2 signalling through Erk1/2 regulates TLR4 driven inflammation. *Cell. Signal.* 51, 211–221. doi: 10.1016/j.cellsig.2018.08.001
- Strasser, B., Sperner-Unterwieser, B., Fuchs, D., and Gostner, J. M. (2016). Mechanisms of inflammation-associated depression: immune influences on tryptophan and phenylalanine metabolisms. *Curr. Top. Behav. Neurosci.* 31, 95–115. doi: 10.1007/7854_2016_23
- Sun, H. Z., Kai, S., Wu, X. H., Xue, M. Y., Wei, Z. H., Liu, J. X., et al. (2017). Lactation-related metabolic mechanism investigated based on mammary gland metabolomics and 4 biofluids' metabolomics relationships in dairy cows. *BMC Genomics* 18:936. doi: 10.1186/s12864-017-4314-1
- Sun, K., Pengyu, Y., Rong, Z., Yuting, B., and Zijiaoe, G. (2018a). Matrine attenuates D-Galactose-induced aging-related behavior in mice via inhibition of cellular senescence and oxidative stress. *Oxidative Med. Cell. Longev.* 2018, 1–12. doi: 10.1155/2018/7108604
- Sun, M., Tong, J., Zhang, H., Yang, D., Zhang, J., Jiang, L., et al. (2018b). Chitosan: biochemical functions and application in dairy cows. *Chin. J. Anim. Nutri.* 30, 2079–2084. doi: 10.3969/j.issn.1006-267x.2018.06.009
- Thomas, F. C., Mudaliar, M., Tassi, R., Mcneilly, T. N., Burchmore, R., Burgess, K., et al. (2016). Mastitomics, the integrated omics of bovine milk in an experimental model of streptococcus uberis mastitis: 3. *Untarg. metabol. Mol. Biosyst.* 12, 2735–2747. doi: 10.1039/c6mb00289g
- Tong, J., Zhang, H., Zhang, Y., Xiong, B., and Jiang, L. (2019). Microbiome and Metabolome analyses of Milk from dairy cows with subclinical streptococcus Agalactiae mastitis—potential biomarkers. *Front. Microbiol.* 10:2547. doi: 10.3389/fmicb.2019.02547

Supplementary material

The Supplementary material for this article can be found online at: <https://www.frontiersin.org/articles/10.3389/fmicb.2022.950231/full#supplementary-material>

- Turk, R. (2017). The role of oxidative stress and inflammatory response in the pathogenesis of mastitis in dairy cows. *Mljekarstvo*. 67, 91–101. doi: 10.15567/mljekarstvo.2017.0201
- Vanderhaeghen, W., Piepers, S., Leroy, F., Coillie, E. V., Haesebrouck, F., and Vlieghe, S. D. (2014). Invited review: effect, persistence, and virulence of coagulase-negative staphylococcus species associated with ruminant udder health. *J. Dairy Sci.* 97, 5275–5293. doi: 10.3168/jds.2013-7775
- Waisbren, S. E., Noel, K., Fahrbach, K., Cella, C., Frame, D., Dorenbaum, A., et al. (2007). Phenylalanine blood levels and clinical outcomes in phenylketonuria: a systematic literature review and meta-analysis. *Mol. Genet. Metab.* 92, 63–70. doi: 10.1016/j.ymgme.2007.05.006
- Wang, X., Sun, G., Feng, T., Zhang, J., Huang, X., Wang, T., et al. (2019). Sodium oligomannate therapeutically remodels gut microbiota and suppresses gut bacterial amino acids-shaped neuroinflammation to inhibit Alzheimer's disease progression. *Cell Res.* 29, 787–803. doi: 10.1038/s41422-019-0216-x
- Xiaofei, J., Jincheng, G., Yuxiu, , Liu, , et al. (2018). Marine-natural-product development: first discovery of Nortopsentin alkaloids as novel antiviral, anti-phytopathogenic-fungus, and insecticidal agents. *J. Agric. Food Chem.* 66, 4062–4072. doi: 10.1021/acs.jafc.8b00507
- Zhang, H., Tong, J., Zhang, Z., and Jiang, L. (2019). Research Progress on regulatory effect and mechanism of Chitooligosaccharides on immunity and inflammation in animals. *Chin. J. Animal Nutri.* 31, 15–23. doi: 10.3969/j.issn.1006-267x.2019.01.002
- Zhao, S., Zhao, J., Bu, D., Sun, P., Wang, J., and Dong, Z. (2014). Metabolomics analysis reveals large effect of roughage types on rumen microbial metabolic profile in dairy cows. *Lett. Appl. Microbiol.* 59, 79–85. doi: 10.1111/lam.12247
- Zhou, W., Zhao, J., Pan, X., Sun, Y., and Tian, X. (2017). Matrine alleviates lipopolysaccharide-induced intestinal inflammation and oxidative stress via CCR7 signal. *Oncotarget* 8, 11621–11628. doi: 10.18632/oncotarget.14598



OPEN ACCESS

EDITED BY

Zhe Wang,
Shanghai Jiao Tong University, China

REVIEWED BY

Jinxin Zhao,
Monash University,
Australia
Xingchen Bian,
Fudan University,
China

*CORRESPONDENCE

Mingming Yu
yummingming@ouc.edu.cn
Pan Deng
pandeng@suda.edu.cn
Zhihua Lv
lvzhihua@ouc.edu.cn

SPECIALTY SECTION

This article was submitted to
Antimicrobials, Resistance and
Chemotherapy,
a section of the journal
Frontiers in Microbiology

RECEIVED 08 August 2022

ACCEPTED 06 September 2022

PUBLISHED 23 September 2022

CITATION

Zhu S, Zhang J, Song C, Liu Y, Charles O,
Heinrichs MT, Zhihua L, Zhu Y, Sy SKB,
Deng P and Mingming Y (2022)
Metabolomic profiling of polymyxin-B in
combination with meropenem and
sulbactam against multi-drug resistant
Acinetobacter baumannii.
Front. Microbiol. 13:1013934.
doi: 10.3389/fmicb.2022.1013934

COPYRIGHT

© 2022 Zhu, Zhang, Song, Liu, Charles,
Heinrichs, Zhihua, Zhu, Sy, Deng and
Mingming. This is an open-access article
distributed under the terms of the [Creative
Commons Attribution License \(CC BY\)](#). The
use, distribution or reproduction in other
forums is permitted, provided the original
author(s) and the copyright owner(s) are
credited and that the original publication in
this journal is cited, in accordance with
accepted academic practice. No use,
distribution or reproduction is permitted
which does not comply with these terms.

Metabolomic profiling of polymyxin-B in combination with meropenem and sulbactam against multi-drug resistant *Acinetobacter baumannii*

Shixing Zhu¹, Jiayuan Zhang¹, Chu Song¹, Yuwei Liu¹,
Charles Oo², M. Tobias Heinrichs³, Zhihua Lv^{1,4*}, Yuanqi Zhu⁵,
Sherwin K. B. Sy⁶, Pan Deng^{7*} and Mingming Yu^{1,4*}

¹School of Medicine and Pharmacy, Ocean University of China, Qingdao, China, ²SunLife Biopharma, Morris, NJ, United States, ³Department of Pharmaceutics, College of Pharmacy, University of Florida, Gainesville, FL, United States, ⁴Laboratory for Marine Drugs and Bioproducts of Qingdao National Laboratory for Marine Science and Technology, Qingdao, China, ⁵Department of Laboratory Medicine, the Affiliated Hospital of Qingdao University, Qingdao, China, ⁶Department of Statistics, State University of Maringá, Paraná, Brazil, ⁷Department of Pharmaceutical Analysis, College of Pharmaceutical Sciences, Soochow University, Suzhou, China

Empirical therapies using polymyxins combined with other antibiotics are recommended in the treatment of *Acinetobacter baumannii* infections. In the present study, the synergistic activities of polymyxin-B, meropenem, and sulbactam as combination therapy were investigated using metabolomic analysis. The metabolome of *A. baumannii* was investigated after treatment with polymyxin-B alone (2mg/l), meropenem (2mg/l) alone, combination of polymyxin-B/meropenem at their clinical breakpoints, and triple-antibiotic combination of polymyxin-B/meropenem and 4mg/l sulbactam. The triple-antibiotic combination significantly changed the metabolite levels involved in cell outer membrane and cell wall biosynthesis, including fatty acid, glycerophospholipid, lipopolysaccharide, peptidoglycan, and nucleotide within 15min of administration. In contrast, significant changes in metabolome were observed after 1h in sample treated with either meropenem or polymyxin-B alone. After 1h of administration, the double and triple combination therapies significantly disrupted nucleotide and amino acid biosynthesis pathways as well as the central carbon metabolism, including pentose phosphate and glycolysis/gluconeogenesis pathways, and tricarboxylic acid cycle. The addition of sulbactam to polymyxin-B and meropenem combination appeared to be an early disruptor of *A. baumannii* metabolome, which paves the way for further antibiotic penetration into bacteria cells. Combination antibiotics consisting of sulbactam/meropenem/polymyxin-B can effectively confer susceptibility to *A. baumannii* harboring OXA-23 and other drug resistant genes. Metabolomic profiling reveals underlying mechanisms of synergistic effects of polymyxin-B combined with meropenem and sulbactam against multi-drug resistant *A. baumannii*.

KEYWORDS

Acinetobacter baumannii, metabolomics, polymyxin-B, meropenem, synergistic combinations

Introduction

Multi-drug resistant (MDR) pathogens in nosocomial and community-acquired infections are an impending threat to public health. *Acinetobacter baumannii* infections is one of the most prevalent and fatal MDR pathogens often found in wound infection, urinary tract infections, empyema, pneumonia and meningitis (Tacconelli et al., 2018). Polymyxin antibiotics are increasingly being used as last resort against MDR *A. baumannii* infections since 2000s (Li et al., 2006; Poirel et al., 2017). The mechanism of action for polymyxins has been well studied. It was proposed that polymyxins disrupted the outer cell membrane by binding to the negatively charged lipopolysaccharide (LPS), the predominant surface lipid of the outer membrane in Gram-negative bacteria (Jiang et al., 2020; Zhao et al., 2021). However, *A. baumannii* can become highly resistant to polymyxins by incorporating phosphoethanolamine or galactosamine to lipid A structure or through the loss of LPS production (Moffatt et al., 2010; Pelletier et al., 2013; Maifiah et al., 2016; Han et al., 2018; Zhao et al., 2021).

Combination therapies using polymyxins and other antibiotics are recommended to treat MDR pathogens. Among β -lactamase inhibitors, sulbactam has the highest intrinsic bactericidal activity against *A. baumannii* and is usually combined with other antibiotics to treat MDR *A. baumannii* infections (Ripa et al., 1990; Gales et al., 1996; Pei et al., 2012). Previous studies have shown that polymyxin-B combined with meropenem and sulbactam could achieve favorable antibacterial effects against *A. baumannii* (Lenhard et al., 2017; Kulengowski et al., 2019; Menegucci et al., 2019; Fedrigo et al., 2021), but the mechanism for their synergism is yet to be explored. In this paper, we employed metabolomic profiling to elucidate the synergistic mechanism of polymyxin-B when combined with meropenem and sulbactam in the treatment of MDR *A. baumannii*.

Materials and methods

Antibiotics, reagents and bacterial isolates

Polymyxin-B sulfate, meropenem and sulbactam (Shanghai Macklin Biochemical Co. Ltd. Shanghai, China) solutions were prepared according to the guidance from The Clinical and Laboratory Standards Institute (CLSI). Briefly, the stock solutions of polymyxin-B, meropenem and sulbactam (concentration: 5120 mg/l for all three antibiotics) were dissolved in dimethyl

sulfoxide (DMSO). The final DMSO concentration in the culture medium was less than 1/1000 (v/v). Working solutions were prepared in Milli-Q water (Millipore, North Rye, Australia) and filtered before use. Three *A. baumannii* clinical strains were isolated from patients at the Affiliated Hospital of Qingdao University in 2020 and grown in cation-adjusted Mueller-Hinton broth (CAMHB; Land Bridge, Beijing, China). *E. coli* ATCC 25922 and *A. baumannii* ATCC 19606 were used as a quality control strain for antimicrobial susceptibility tests. The isolate carries several known resistant genes (Table 1).

Susceptibility testing

A checkerboard assay with the typical broth microdilution was used to determine the susceptibility profile of each clinical isolate to the three drugs either alone or in combination, according to CLSI guidelines (CLSI, 2020). Susceptibility determination was conducted in triplicate for each of the *A. baumannii* isolates in a sterile 96-well microdilution plate. A standard inoculum size of 0.5 McFarland was prepared and read using a nephelometer (bioMérieux, Marcy l'Etoile, France); the resulting inoculum was diluted into each well to achieve a final concentration of 5×10^5 cfu/ml. The prepared plate was incubated at $35 \pm 2^\circ\text{C}$ for 20 h. The concentration ranges of polymyxin-B and meropenem alone and in combination were 1 to 64 mg/l and 1 to 128 mg/l, respectively.

TABLE 1 Drug resistance genes of *Acinetobacter baumannii* isolates.

Affected antibiotics	Genes		
	Isolate F	Isolate 13	Isolate 20
Streptogramin b	<i>msr(E)</i>	<i>msr(E)</i>	<i>msr(E)</i>
Tetracycline	<i>tet(B)</i>	<i>tet(B)</i>	<i>tet(B)</i>
Folate pathway antagonist	<i>sul2</i>	<i>sul1</i>	<i>sul1</i>
Aminoglycoside	<i>armA</i> ; <i>aph(3'')-Ib</i> ; <i>aph(6)-IId</i> ; <i>aph(3)-Ia</i> ;	<i>armA</i> ; <i>aac(6)-Ib3</i> ; <i>aac(6'')-Ib-cr</i> ; <i>aph(3'')-Ib</i> ;	<i>armA</i> ; <i>aadA1</i> ; <i>aph(6)-Id</i> ; <i>aph(3')-Ia</i> ; <i>aph(3'')-b</i> ;
		<i>aph(6)-Id</i>	<i>aac(6'')-b-cr</i> ;
			<i>aac(6'')-Ib3</i>
Macrolide	<i>msr(E)</i> ; <i>mph(E)</i>	<i>msr(E)</i> ; <i>mph(E)</i>	<i>msr(E)</i> ; <i>mph(E)</i>
Beta-lactam	<i>blaOXA-23</i> ;	<i>blaOXA-23</i> ;	<i>blaOXA-23</i> ;
	<i>blaADC-25</i> ;	<i>blaADC-25</i> ;	<i>blaADC-25</i> ;
	<i>blaTEM-1D</i> ;	<i>blaTEM-1D</i> ;	<i>blaOXA-66</i>
	<i>blaOXA-66</i>	<i>blaOXA-66</i>	

The concentration of sulbactam was fixed at 4 mg/l for the combination test, since ampicillin/sulbactam susceptible breakpoint is $\leq 8/4$ mg/l (CLSI, 2020). Note that the triple-antibiotic combination in this context refers to sulbactam/meropenem/polymyxin-B.

Based on the results of the checkerboard assay, the fractional inhibitory concentration index (FICI) was calculated according to the following equation to classify the antimicrobial synergy of the combination,

$$\text{FICI} = \frac{\text{MIC of antibiotic1 in combination}}{\text{MIC of antibiotic1 alone}} + \frac{\text{MIC of antibiotic2 in combination}}{\text{MIC of antibiotic2 alone}} + \frac{\text{MIC of antibiotic3 in combination}}{\text{MIC of antibiotic3 alone}}$$

When FICI is ≤ 0.5 , the two drugs are considered synergistic; FICI $> 0.5-1$ is additive; $> 1-2$ indicates indifference; and ≥ 2 is antagonistic (Hall et al., 1983).

Bacterial culture

Based on the susceptibility testing result, an *A. baumannii* isolate was selected for metabolomic profiling. This isolate was cultured on a nutrient agar plate from the frozen stock (-80°C) and incubated at 37°C . For the overnight culture, a single colony of *A. baumannii* was inoculated into 15 ml CAMHB and the content was incubated in a shaking water bath at 180 rpm and 37°C . To get sufficient cell number, the bacterial culture was grown to an optical density (OD_{600}) of approximate 0.5 to achieve a starting inoculum at around 10^8 CFU (colony forming units)/mL during an early exponential growth phase (Maifiah et al., 2017). The concentrations of polymyxin-B, meropenem and sulbactam were chosen based on their clinical breakpoints. Bacterial culture was treated with polymyxin-B (2 mg/l) and meropenem (2 mg/l) as both monotherapy and the combination of the two drugs (P + M, 2 mg/l + 2 mg/l, respectively), and the combination with sulbactam (P + M + S, 2 mg/l + 2 mg/l + 4 mg/l, respectively). Bacteria cultured without any antibiotic served as control. Five biological replicates were prepared for each treatment.

Preparation of cellular metabolite extracts

Cellular metabolites of *A. baumannii* were extracted using previously reported method (Maifiah et al., 2016). Briefly, samples were centrifuged at $3,220 \times g$ at 4°C for 20 min; the supernatant was discarded; and the bacterial pellets were washed twice with 1 ml of cold saline. Next, 500 μl of cold chloroform-methanol-water (CMW; 1,3:1, v/v/v) solution containing the internal standards, 3-[(3-cholamidopropyl)-

dimethylammonio]-1-propanesulfonate (CHAPS), N-cyclohexyl-3-aminopropanesulfonic acid (CAPS), piperazine-N,N'-bis(2-ethanesulfonic acid; PIPES), and Tris at 1 μM , was added. The samples were flash frozen in liquid nitrogen, thawed on ice, and vortexed to release the intracellular metabolites. The samples were centrifuged for 10 min at $3,220 \times g$ at 4°C to remove cell debris, and then 300 μl of the supernatants was added to 1.5 ml Eppendorf tubes. After centrifugation at $14,000 \times g$ at 4°C for 10 min, 200 μl of supernatant was transferred into injection vials for bioanalysis. Quality control (QC) samples were obtained by pooling the samples and extracted as described above.

LC-MS analysis

The LC-MS method was based on a previously reported method with modifications (Maifiah et al., 2017; Ribera et al., 2019; Zhao et al., 2021). Samples were analyzed by liquid chromatography-high resolution mass spectrometry (LC-MS) equipped with an Ultimate 3,000 ultra-high-performance liquid chromatography (UHPLC) system (Thermo Scientific, CA, United States) and Q-Exactive Orbitrap mass spectrometer (Thermo Scientific, CA, USA) operated in both positive and negative electrospray ionization (ESI) modes (polarity switching) at a resolution of 35,000 with a detection range of m/z 50 to 1,000 Da. The separation was performed on a HILIC column (2.1×100 mm, 1.7 μm , ACE 1.7 HILIC-A, United Kingdom) coupled with a guard column (ACE UHPLC Pre-column filter) operated at 40°C . The mobile phase which consisted of 10 mM ammonium carbonate in water (solvent A) and acetonitrile (solvent B) was delivered at a flow rate of 0.3 ml/min. The elution mode with an overall duration of 29 min started from 80% B transitioning to 20% B at 15 min, followed by a wash with 5% B for 3 min at 18 min, and a final re-equilibration for 8 min with 80% B. The injection volume was 10 μl .

Data processing, bioinformatics and statistical analyses

The raw data file obtained from the LC-MS was processed and analyzed by Progenesis QI program (Waters). Briefly, the workflow was established for importing data, automatic alignment, peak selection based on minimum intensity of 50,000, and subsequently identifying these metabolites. Metabolites were characterized by LC retention time and accurate m/z value. The maximum retention time shift for peak alignment was limited to 0.2 min and the mass tolerance was 5 ppm. Metabolite intensities were normalized by the sum, followed by \log_{10} -transformation and auto scaling (mean-centered divided by standard deviation) of individual values. Statistical analysis was performed using MetaboAnalyst 5.0 web portal.¹ Principal component analysis

¹ <https://www.metaboanalyst.ca/>

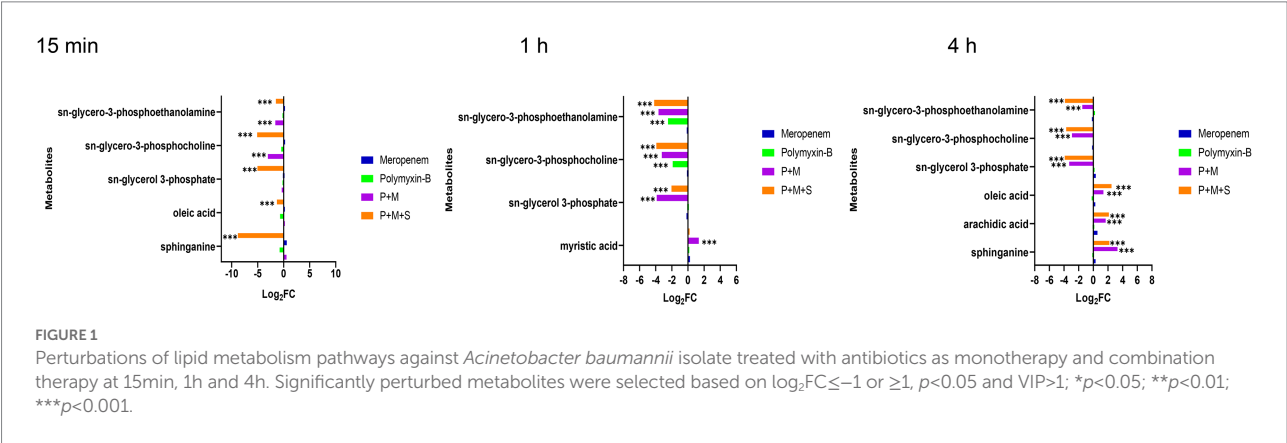


TABLE 2 Minimum inhibitory concentrations of meropenem, polymyxin-B and sulbactam alone or in combination with or without sulbactam (4mg/L) against carbapenem-resistant *Acinetobacter baumannii* isolates and fractional inhibitory concentration index (sulbactam was fixed at 4mg/L).

Strains	MIC (mg/L)							Synergism analysis	
	Monotherapy			Combination therapy					
	Meropenem	Polymyxin-B	Sulbactam	Meropenem/ sulbactam	Polymyxin-B/ sulbactam	Meropenem/ polymyxin-B	Meropenem/ polymyxin-B/ sulbactam	FIC index [‡]	FICI category
<i>E. coli</i> ATCC25922	1	1	32						
<i>A. baumannii</i> F	>128	8	>64	>128/4	8/4	8/2	2/2/4	0.3281	Synergism
13	64	16	>64	64/4	16/4	8/2	2/2/4	0.2188	Synergism
20	32	8	>64	32/4	8/4	2/2	≤1/2/4	0.3438	Synergism

MIC, minimum inhibitory concentration; FIC, fractional inhibitory concentration.[†]FIC index was computed using the reduced MICs of meropenem, polymyxin-B and sulbactam in the triple-antibiotic combination relative to meropenem, polymyxin-B and sulbactam monotherapies. CLSI breakpoints for interpretation of polymyxin-B MIC results: ≤2 mg/l (intermediate), >2 mg/l (resistant); and meropenem MIC results: ≤2 mg/l (susceptible), 4 mg/l (intermediate), and ≥8 mg/l (resistant) for *A. baumannii*.

(PCA) was performed for all treatment groups at each time point (Figure 1). Student's t-test was used to determine metabolites with significantly changed intensity [$p < 0.05$, fold change (FC) ≥ 2 ($\log_2FC \geq 1$ or ≤ -1) and variable important in projection ($VIP > 1$)]. Pathway analysis was performed using KEGG (Kyoto Encyclopedia of Genes and Genomes) and HMDB (The Human Metabolome Database) databases (Maifiah et al., 2017; Ribera et al., 2019; Zhao et al., 2021).

Results

In vitro antimicrobial susceptibility

All three *A. baumannii* isolates carried OXA-23 along with other drug-resistance genes (Table 1) and showed significant drug resistance to sulbactam, polymyxin-B and meropenem (Table 2). The MIC of meropenem alone against these isolates ranged from 32 to >128 mg/l, whereas the MIC of polymyxin-B alone ranged from 8 to 16 mg/l. MIC of sulbactam alone was ≥ 64 mg/l. The

Clinical Laboratory Standards Institute (CLSI) breakpoints were used for the interpretation of polymyxin-B MIC results: ≤2 mg/l (intermediate), >2 mg/l (resistant); and meropenem MIC results: ≤2 mg/l (susceptible), 4 mg/l (intermediate), and ≥8 mg/l (resistant) for *A. baumannii* (CLSI, 2020). These isolates are considered resistant to both meropenem and polymyxin-B. Even though there is no interpretive breakpoint for sulbactam, these isolates can be considered resistant to sulbactam, since the clinical regimens could not sufficiently achieve drug concentration of 64 mg/l in the blood.

The combination of polymyxin-B and meropenem reduced the MIC of polymyxin-B and meropenem to lower than their breakpoints (2 mg/l) in 1/3 strains, and the FICI scores were less than 0.5 for all strains. The addition of 4 mg/l sulbactam to the meropenem/polymyxin-B combination further lowered meropenem MIC values to ≤2 mg/l in all isolates, and the FICI scores of isolate 13 was 0.2188 which was the lowest FICI score of the 3 isolates. Based on the results from *in vitro* antimicrobial susceptibility, isolate 13 was selected for the metabolomic study.

Metabolomic changes in *Acinetobacter baumannii* after treatment with polymyxin-B, meropenem as monotherapy, and in combination with sulbactam

Metabolomic analysis using LC-MS identified a total number of 222 metabolites. The median relative standard deviations (RSD) for metabolites detected in QC samples were less than 10.0%, indicating that the analysis is highly reproducible. A PCA was performed to delineate putative metabolites that contributed to differential effects of drug treatments on *A. baumannii*. In samples treated with drugs for 15 min, clear differences were observed between combination therapy (P + M and P + M + S), monotherapy and control group; significant metabolite alterations were observed in response to P + M and P + M + S (Figure 2A). In contrast, the metabolome of polymyxin-B and meropenem monotherapy groups overlapped with the control group. The heatmap and VIP showed overall changes in metabolite levels and important differential metabolites (VIP > 1), respectively (Figures 2B,C).

A total of 12 significant metabolites whose abundance had changed in the P + M groups at 15 min were identified: 11 metabolites decreased in abundance after exposure to combination therapy, while 1 metabolite exhibited increased levels. For P + M + S group, 28 metabolites were altered at 15 min, of which 24 decreased and 4 increased. After 1 h of treatment, polymyxin-B and meropenem alone induced minor metabolomic changes, while combined drug treatments led to significant alterations (Figure 1); a total number of 25 (2 increased, 23 decreased compared with the control group) and 49 metabolites (6 increased, 43 decreased compared with the control group) were changed in response to P + M and P + M + S treatments, respectively. At 4 h, a total number of 27 (7 increased, 20 decreased compared with the control group) and 30 metabolites (9 increased, 21 decreased compared with the control group) were significantly perturbed by P + M and P + M + S treatments, respectively. All altered metabolites were grouped accordingly to correlate with metabolic pathways, which were assigned to lipids, lipopolysaccharide, amino sugar, peptidoglycan, nucleotide, amino acids, and carbohydrate metabolisms.

Polymyxin-B plus meropenem with or without sulbactam treatment disrupted lipid metabolic pathway in *Acinetobacter baumannii*

Lipid metabolic pathways including glycerophospholipid, fatty acids, and sphingolipid were affected by the combination therapies. The levels of three metabolites including sn-glycerol-3-phosphate, sn-glycerol-3-phosphocholine and sn-glycerol-3-phosphoethanolamine ($\log_2FC = -5.1$ to -1.5), which are important intermediates for membrane structure, were significantly downregulated after the combination treatments at the three time points. In addition, the P + M + S combination remarkably perturbed an intermediate related to sphingolipid pathway which is sphinganine ($\log_2FC = -8.8$ and 2.2) at 15 min and 4 h.

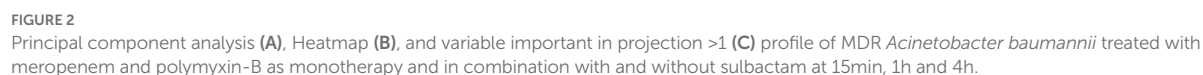
Fatty acid pathway was also significantly affected by the P + M + S treatment. The level of oleic acid was decreased at 15 min but increased after 4 h of treatment, and arachidic acid was remarkably increased at 4 h. Polymyxin-B and meropenem monotherapies did not significantly induce these changes in lipid metabolism within the investigation period (Figure 1).

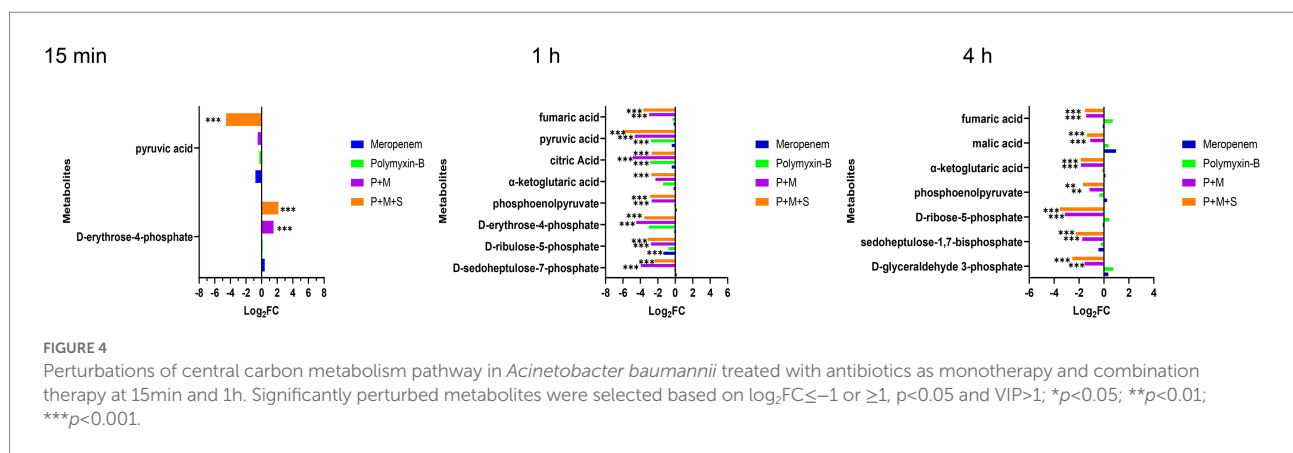
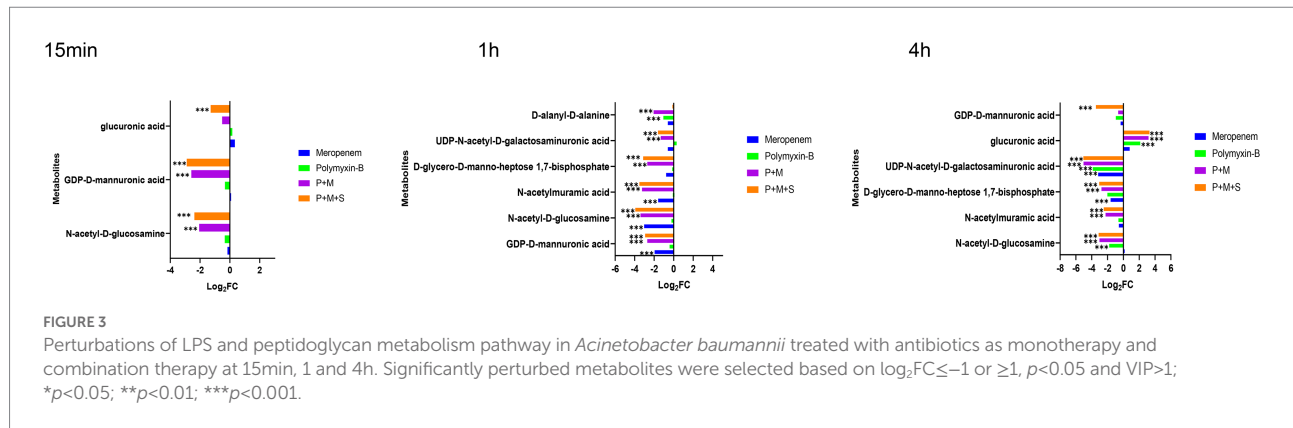
Polymyxin-B plus meropenem with or without sulbactam treatment affect lipopolysaccharide, peptidoglycan and amino sugar metabolisms

Lipopolysaccharide (LPS), peptidoglycan and amino sugar are essential components of the outer membrane of gram-negative bacteria. The levels of intermediate metabolites associated with LPS, peptidoglycan and amino sugar biosynthesis pathways were changed after treatment with combination therapy (Figure 3). The P + M and P + M + S combinations significantly induced changes in the level of N-acetyl-D-glucosamine (GlcNAc) and GDP-D-mannuronic acid (GDP-ManA), which are two important intermediates associated with amino sugar biosynthesis pathway ($\log_2FC = -3.9$ to 2.2) at the three time points. In addition, N-acetylmuramic acid (MurMac), another metabolite related to amino sugar pathway, was perturbed by the combination therapy at 1 h and 4 h ($\log_2FC = -2.5$ to -3.5). Significant downregulations of D-glycero-D-manno-heptose-1,7-bisphosphate and UDP-N-acetyl-D-galactosaminuronic acid (UDP-GalNAc; $\log_2FC = -5.0$ to -1.6) were observed at 1 h and 4 h, which are related to LPS and peptidoglycan pathways, respectively. The level of glucuronic acid was perturbed by P + M + S at 15 min and 4 h. The changes induced by P + M + S treatment were similar to that of P + M group, indicating that sulbactam treatment did not exacerbate metabolite alterations induced by P + M in *A. baumannii*. Compared to the combination therapy, monotherapies of polymyxin-B and meropenem did not perturb the level of metabolites at 15 min. Meropenem alone significantly decreased the levels of GDP-D-mannuronic acid, N-acetyl-D-glucosamine and N-acetylmuramic acid ($\log_2FC = -3.0$ to -1.6) at 1 h, and D-glycero-manno-heptose-1,7-bisphosphate and UDP-N-acetyl-D-galactosaminuronic acid ($\log_2FC = -1.6$ to -3.2) at 4 h. Polymyxin-B alone only changed the levels of N-acetyl-D-glucosamine, UDP-N-acetyl-D-galactosaminuronic acid and glucuronic acid ($\log_2FC = -3.9$ to 2.1) at 4 h. The results showed that combination treatments resulted in a larger metabolomic change compared to monotherapy.

Polymyxin-B plus meropenem with or without sulbactam treatment perturbed central carbon metabolism pathway

After a 15 min treatment, the two-drug combination induced an increase in D-erythrose-4-phosphate ($\log_2FC = 1.5/1.2$) while P + M + S combination also decreased the level of pyruvic acid





($\log_2FC = 1.3$). Meropenem or polymyxin alone did not induce significant changes in the central carbon metabolism pathway. At 1 h and 4 h, the metabolite types and level disorders caused by the combination of P + M and P + M + S were similar (Figure 4). Five metabolites involved in tricarboxylic acid cycle (TCA) pathway including phosphoenolpyruvate, α -ketoglutaric acid, citric acid, fumaric acid and pyruvic acid ($\log_2FC = -5.9$ to 2.7) were significantly downregulated by the two combination treatment groups at 1 h. At the same time, the levels of D-sedoheptulose-7-phosphate, D-ribulose-5-phosphate and D-erythrose-4-phosphate ($\log_2FC = -4.5$ to -2.4), which are three intermediates associated with pentose phosphate pathway (PPP) were also decreased by P + M and P + M + S treatments. In addition, the disruption of another three metabolites associated with PPP including D-glyceraldehyde-3-phosphate, sedoheptulose-1,7-bisphosphate and D-ribose-5-phosphate ($\log_2FC = -3.5$ to -1.5) were also observed at 4 h after either P + M or P + M + S treatments. Among the above metabolites, D-sedoheptulose-7-phosphate and D-ribulose-5-phosphate were also involved in the LPS pathway. After 4 h treatment of either P + M or P + M + S, the altered metabolites involved in TCA cycle were mainly phosphoenolpyruvate, α -ketoglutaric acid, malic acid and fumaric acid ($\log_2FC = -1.9$ to -1.1). For monotherapy, polymyxin-B alone affected the levels of citric acid and pyruvic acid

($\log_2FC = -2.9/-2.8$) at 1 h whereas treatment with meropenem alone was not associated with significant changes in metabolomic profiles.

Polymyxin-B plus meropenem with or without sulbactam treatments altered nucleotide, nicotinate and nicotinamide, amino acid and peptide metabolism pathways

The combination therapy altered both the pyrimidine and purine metabolisms within 15 min of treatment (Figure 5). At the three time points, P + M + S treatment disturbed the equilibrium of thymidine ($\log_2FC = -4.9$ to -1.8) and cytidine diphosphate (CDP, $\log_2FC = 5.6$ to 7.2), two important metabolites associated with pyrimidine metabolism pathway, as well as levels of adenine ($\log_2FC = -5.7$ to -2.7) and 5'-phosphoribosyl-N-formylglycinamide (FGAR, $\log_2FC = 3.3$ to 5.1) which are related to purine metabolism. ADP ($\log_2FC = -4.6$ to -4.3) was significantly downregulated by the triple combination treatment at 15 min and 1 h.

The metabolite disequilibrium caused by P + M was similar in both the affected metabolites and their intensities to that due to

P + M + S. The combination of P + M and P + M + S significantly reduced the level of NAD⁺ ($\log_2FC = -3.9$ to -3.1) at 1 h and 4 h. The P + M + S group induced a change in glutathione (GSH) and L-citrulline ($\log_2FC = -9.7$ to 3.1) at the three time points. For polymyxin-B monotherapy treatment, the levels of thymidine, CDP, ADP, glutathione, NAD⁺ and L-citrulline ($\log_2FC = -7.7$ to 3.3) were altered at 1 h, while at 4 h, the levels of adenine, glutathione, L-citrulline and formiminoglutamic acid ($\log_2FC = -7.7$ to 1.6) were affected. Meropenem alone only affected the levels of thymidine, glutathione and 5'-phosphoribosyl-N-formylglycinamide ($\log_2FC = -2.1$ to 3.6) at 4 h.

Discussion

The World Health Organization lists MDR Gram-negative bacteria as a critical threat to vulnerable patients (Van Duin et al., 2013; Zilberberg et al., 2017). Polymyxins are regarded as a treatment of last resort against life-threatening MDR Gram-negative bacteria, but recent usage pattern of polymyxins has led to increasing resistance of pathogens to polymyxins (Srinivas and Rivard, 2017).

The present study applied metabolomic profiling to investigate the mechanisms underlying the synergistic effects of meropenem/polymyxin-B/sulbactam against MDR *A. baumannii*. These isolates harbor OXA-23, TEM and ADC β -lactamases, which confer resistance to both meropenem and sulbactam. OXA-23, in particular, is not inhibited by sulbactam and is a prevalent

mechanism contributing to sulbactam resistance in diverse *A. baumannii* clinical isolates (Yang et al., 2019). The combination of meropenem and polymyxin-B could significantly reduce the MIC values but only to 8/2 mg/l in two isolates, which are considered resistant to meropenem and intermediate to polymyxin-B. In the third isolate, meropenem/polymyxin-B MICs were 2/2 mg/l. 4 mg/l sulbactam further reduces MIC to $\leq 2/2/4$ mg/l for meropenem/polymyxin-B/sulbactam, resulting in susceptible for meropenem and intermediate for polymyxin-B (CLSI, 2020). The reduction in MIC provides sufficient drug exposure for clinical regimens of meropenem, polymyxin-B and sulbactam to achieve $\geq 90\%$ PTA for their respective pharmacodynamic indices (Martins et al., 2020; Zhu et al., 2022). The metabolomic profiling results revealed that the combination therapy (P + M + S) initially perturbed lipids, LPS and peptidoglycan metabolism therefore impacted the stability of cell membrane and cell wall. This effect was followed by the disturbance of the central carbon metabolism (CCM) and nucleotide metabolism in the cell, which co-occurred with oxidative stress as demonstrated by the depletion of intracellular antioxidant GSH. The sequence of events is summarized in Table 3.

An illustration of affected metabolic pathways is shown in Figure 6. The effect of sulbactam in disrupting metabolic pathways occurred at an earlier time as compared to P + M. Sulbactam effect on *A. baumannii* is accomplished by cell wall disintegration and cell lysis while also acting as a β -lactamase inhibitor (Horii et al., 2002; Lin et al., 2014; Penwell et al., 2015). Meropenem plays a role in cell wall thinning in the

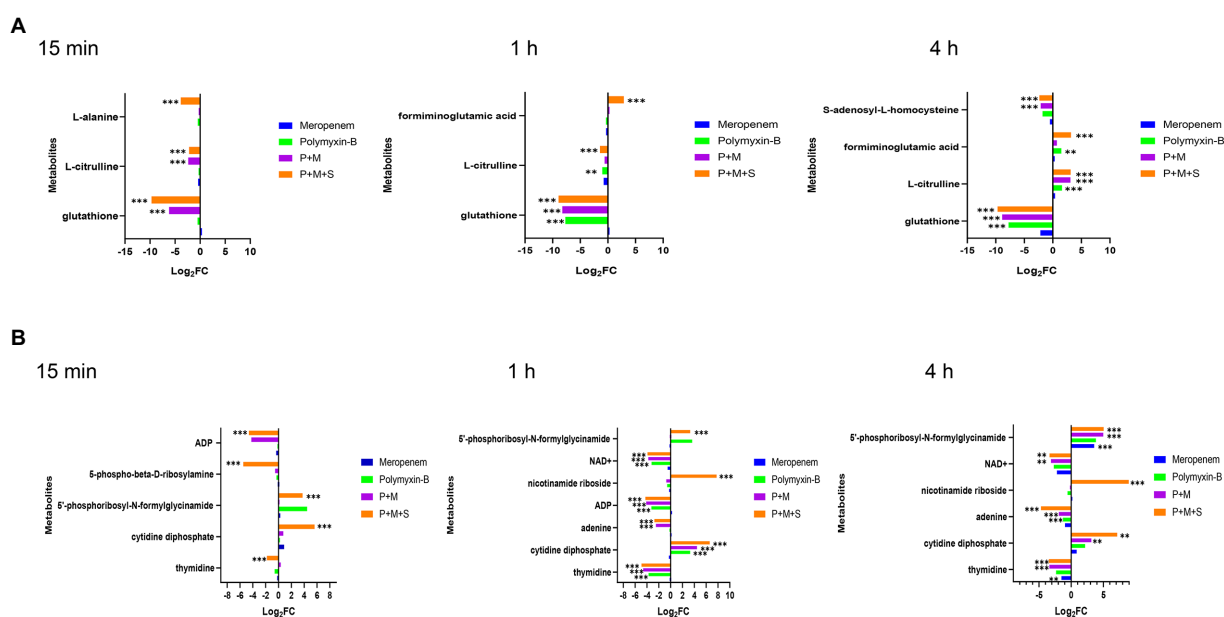


FIGURE 5
Perturbations of amino acid (A) and nucleotide (B) metabolism pathways in *Acinetobacter baumannii* treated with antibiotics as monotherapy and combination therapy at 15min, 1h and 4h. Significantly perturbed metabolites were selected based on $\log_2FC \leq -1$ or ≥ 1 , $p < 0.05$ and $VIP > 1$; * $p < 0.05$; ** $p < 0.01$; *** $p < 0.001$.

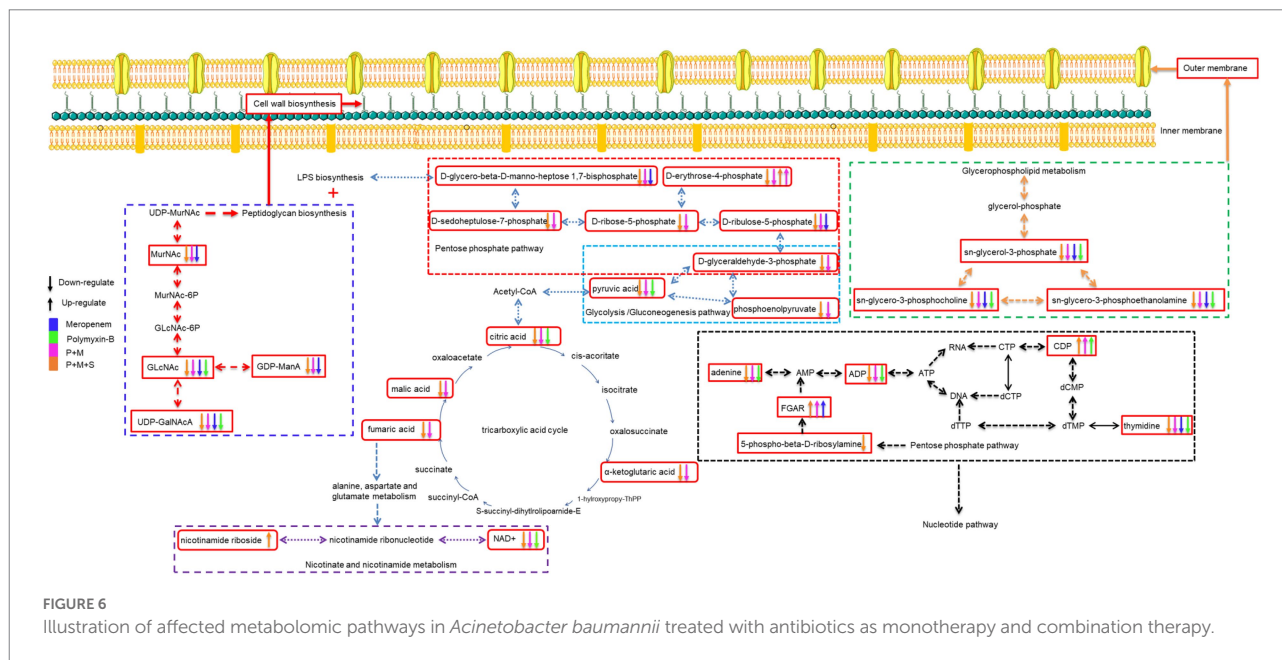
TABLE 3 Sequence of metabolomic changes in *Acinetobacter baumannii* after polymyxin-B and meropenem treatments as monotherapy and in combination with and without sulbactam.

Time	Polymyxin-B/Meropenem/ Sulbactam	Polymyxin-B/Meropenem	Polymyxin-B	Meropenem
15 min	Cell wall synthesis ↓ N-acetyl-D-glucosamine; ↓ GDP-D-mannuronic acid Outer membrane glycerophospholipids ↓ sn-glycerol-3-phosphate; ↓ sn-glycero-3-phosphocholine; ↓ sn-glycero-3-phosphoethanolamine Central carbon metabolism pathway ↑ D-erythrose-4-phosphate; ↓ pyruvic acid Nucleotide, nicotinate and nicotinamide, amino acid and peptide pathway ↓ L-alanine; ↓ L-citrulline; ↓ glutathione; ↓ 5-phospho-beta-D-ribosylamine; ↑ 5'-phosphoribosyl-N-formylglycinamide; ↑ cytidine diphosphate; ↓ thymidine; ↓ ADP	Cell wall synthesis ↓ N-acetyl-D-glucosamine; ↓ GDP-D-mannuronic acid Outer membrane glycerophospholipids ↓ sn-glycero-3-phosphocholine; ↓ sn-glycero-3-phosphoethanolamine Central carbon metabolism pathway ↑ D-erythrose-4-phosphate Nucleotide, nicotinate and nicotinamide, amino acid and peptide pathway ↓ L-alanine; ↓ L-citrulline; ↓ glutathione; ↓ ADP	Cell wall synthesis NA Outer membrane glycerophospholipids NA Central carbon metabolism pathway NA Nucleotide, nicotinate and nicotinamide, amino acid and peptide pathway NA	Cell wall synthesis NA Outer membrane glycerophospholipids NA Central carbon metabolism pathway NA Nucleotide, nicotinate and nicotinamide, amino acid and peptide pathway NA
1 h	Cell wall synthesis ↓ N-acetyl-D-glucosamine; ↓ N-acetylmuramic acid; ↓ GDP-D-mannuronic acid; ↓ UDP-N-acetyl-D-galactosaminuronic acid; ↓ D-glycero-beta-D-manno-heptose 1,7-bisphosphate Outer membrane glycerophospholipids ↓ sn-glycerol-3-phosphate; ↓ sn-glycero-3-phosphocholine; ↓ sn-glycero-3-phosphoethanolamine Central carbon metabolism pathway ↓ fumaric acid; ↓ pyruvic acid; ↓ citric acid; ↓ α-ketoglutaric acid; ↓ phosphoenolpyruvate; ↓ D-erythrose-4-phosphate; ↓ D-ribulose-5-phosphate; ↓ D-sedoheptulose-7-phosphate	Cell wall synthesis ↓ N-acetyl-D-glucosamine; ↓ N-acetylmuramic acid; ↓ GDP-D-mannuronic acid; ↓ UDP-N-acetyl-D-galactosaminuronic acid; ↓ D-glycero-beta-D-manno-heptose 1,7-bisphosphate; ↓ D-alanyl-D-alanine Outer membrane glycerophospholipids ↑ myristic acid; ↓ sn-glycerol-3-phosphate; ↓ sn-glycero-3-phosphocholine; ↓ sn-glycero-3-phosphoethanolamine Central carbon metabolism pathway ↓ fumaric acid; ↓ pyruvic acid; ↓ citric acid; ↓ phosphoenolpyruvate; ↓ D-erythrose-4-phosphate; ↓ D-ribulose-5-phosphate; ↓ D-sedoheptulose-7-phosphate	Cell wall synthesis NA Outer membrane glycerophospholipids ↓ sn-glycerol-3-phosphate; ↓ sn-glycero-3-phosphocholine; ↓ sn-glycero-3-phosphoethanolamine Central carbon metabolism pathway ↓ pyruvic acid; ↓ citric acid	Cell wall synthesis ↓ N-acetyl-D-glucosamine; ↓ GDP-D-mannuronic acid; ↓ N-acetylmuramic acid Outer membrane glycerophospholipids ↓ sn-glycerol-3-phosphate; ↓ sn-glycero-3-phosphocholine; ↓ sn-glycero-3-phosphoethanolamine Central carbon metabolism pathway ↓ D-ribulose-5-phosphate

(Continued)

TABLE 3 (Continued)

Time	Polymyxin-B/Meropenem/ Sulbactam	Polymyxin-B/Meropenem	Polymyxin-B	Meropenem
4h	Nucleotide, nicotinate and nicotinamide, amino acid and peptide pathway ↑ formiminoglutamic acid; ↓ L-citrulline; ↓ glutathione; ↓ NAD+; ↓ thymidine; ↑ 5'-phosphoribosyl-N-formylglycinamide; ↑ nicotinamide riboside; ↓ ADP; ↓ adenine; ↑ cytidine diphosphate	Nucleotide, nicotinate and nicotinamide, amino acid and peptide pathway ↓ glutathione; ↓ NAD+; ↓ ADP; ↓ adenine; ↓ thymidine; ↑ cytidine diphosphate	Nucleotide, nicotinate and nicotinamide, amino acid and peptide pathway ↓ L-citrulline; ↓ glutathione; ↓ NAD+; ↓ ADP; ↓ thymidine; ↑ cytidine diphosphate	Nucleotide, nicotinate and nicotinamide, amino acid and peptide pathway NA
	Cell wall synthesis ↓ GDP-D-mannuronic acid; ↓ UDP-N-acetyl-D-galactosaminuronic acid; ↓ D-glycero-beta-D-manno-heptose 1,7-bisphosphate; ↓ N-acetylmuramic acid; ↓ N-acetyl-beta-D-glucosamine	Cell wall synthesis ↓ UDP-N-acetyl-D-galactosaminuronic acid; ↓ D-glycero-beta-D-manno-heptose 1,7-bisphosphate; ↓ N-acetylmuramic acid; ↓ N-acetyl-beta-D-glucosamine	Cell wall synthesis ↓ UDP-N-acetyl-D-galactosaminuronic acid; ↓ N-acetyl-beta-D-glucosamine	Cell wall synthesis ↓ UDP-N-acetyl-D-galactosaminuronic acid; ↓ D-glycero-beta-D-manno-heptose 1,7-bisphosphate
	Outer membrane glycerophospholipids ↓ sn-glycerol-3-phosphate; ↓ sn-glycerol-3-phosphocholine; ↓ sn-glycerol-3-phosphoethanolamine	Outer membrane glycerophospholipids ↓ sn-glycerol-3-phosphate; ↓ sn-glycerol-3-phosphocholine; ↓ sn-glycerol-3-phosphoethanolamine	Outer membrane glycerophospholipids NA	Outer membrane glycerophospholipids NA
	Central carbon metabolism pathway ↓ fumaric acid; ↓ maleic acid; ↓ α-ketoglutaric acid; ↓ phosphoenolpyruvate; ↓ D-ribose-5-phosphate; ↓ sedoheptulose-1,7-bisphosphate; ↓ D-glyceraldehyde-3-phosphate	Central carbon metabolism pathway ↓ fumaric acid; ↓ malic acid; ↓ α-ketoglutaric acid; ↓ phosphoenolpyruvate; ↓ D-ribose-5-phosphate; ↓ sedoheptulose-1,7-bisphosphate; ↓ D-glyceraldehyde-3-phosphate	Central carbon metabolism pathway NA	Central carbon metabolism pathway NA
	Nucleotide, nicotinate and nicotinamide, amino acid and peptide pathway ↓ S-adenosyl-L-homocysteine; ↑ L-citrulline; ↑ formiminoglutamic acid; ↓ glutathione; ↓ NAD+; ↑ cytidine diphosphate; ↓ adenine; ↑ 5'-phosphoribosyl-N-formylglycinamide; ↑ nicotinamide riboside; ↓ thymidine	Nucleotide, nicotinate and nicotinamide, amino acid and peptide pathway ↓ S-adenosyl-L-homocysteine; ↑ L-citrulline; ↓ glutathione; ↓ NAD+; ↓ adenine; ↓ thymidine; ↑ cytidine diphosphate; ↑ 5'-phosphoribosyl-N-formylglycinamide	Nucleotide, nicotinate and nicotinamide, amino acid and peptide pathway ↑ formiminoglutamic acid; ↑ L-citrulline; ↓ glutathione; ↓ adenine	Nucleotide, nicotinate and nicotinamide, amino acid and peptide pathway ↑ 5'-phosphoribosyl-N-formylglycinamide; ↓ thymidine



exposed bacteria through its high-affinity binding with penicillin-binding protein, which is a major cell wall synthesis enzyme (Cottagnoud, 2002; Sauvage et al., 2008; Bian et al., 2021). The cell wall of bacteria is mainly composed of lipopolysaccharide and peptidoglycan. The combination consisting of P + M and P + M + S depleted the levels of two important cell wall components that are GlcNAc and MurNAc. The levels of GDP-ManA and UDP-GalNAcA, which are two important intermediates involved in peptidoglycan biosynthesis, were in disequilibrium.

The levels of three metabolites related to pentose phosphate pathway were also affected by P + M and P + M + S: D-ribulose-5-phosphate, D-sedoheptulose-7-phosphate and D-glycero-beta-D-manno-heptose-1,7-bisphosphate; they are precursors of LPS biosynthesis (Maifiah et al., 2017; Hu et al., 2019). This shows that an early effect of sulbactam in disrupting and puncturing cell wall structure is an important contributor to the collapse of cell morphology (Horii et al., 2002). When the integrity and stability of cell membrane are disrupted, the therapeutic pressure can either eradicate the bacteria or prompt the bacteria to increase its defense by enhancing drug resistance mechanisms. Previous comparative metabolomic study evaluated sulbactam/colistin combination (Han et al., 2019a). This study showed that colistin/sulbactam combination decreased amino acid and nucleotide levels more dramatically at 4 h compared with monotherapies of either sulbactam or colistin; cell wall synthesis was also perturbed early on at 1 h by sulbactam.

Polymyxin-B effect on bacterial outer membrane is mediated by an electrostatic interaction with the lipid A of LPS and subsequently affected the stability of cell membrane (Cajal et al., 1996; Clausell et al., 2003; Domingues et al., 2012). Polymyxin-resistance in *A. baumannii* was previously shown to be mediated by LPS deficiency and lipid A modifications as well as a shift in

glycerophospholipid profile that increased the abundance of short-chain lipid, resulting in a significant outer-membrane remodeling (Maifiah et al., 2016). The current study was not designed to compare polymyxin-resistant against polymyxin-susceptible *A. baumannii*. The combination of P + M and P + M + S reduced the levels of some metabolites associate with the synthesis of outer membrane glycerophospholipids including sn-glycerol-3-phosphate, sn-glycerol-3-phosphocholine and sn-glycerol-3-phosphoethanolamine (Zhang and Rock, 2008; Allobawi et al., 2020). Metabolites related to cell wall and outer membrane synthesis had only slight alteration when administered polymyxin-B and meropenem alone. This is likely due to the existing resistance mechanisms already at work in the clinical isolate.

The destruction of cell wall and outer membrane by the combination treatment changed the permeability of the outer membrane, allowing for more antibiotics to enter the bacteria (Nikaido, 2003; Khondker and Rheinstadter, 2020). Previous study showed interaction between transcriptomics and metabolomics in response to polymyxin treatment (Han et al., 2019b). In response to disruption of the outer membrane phospholipids by polymyxin, *P. aeruginosa* increased the biosynthesis of LPS and peptidoglycan to stabilize the damage to its cell envelope. The same feedback mechanism was also observed in *A. baumannii* (Maifiah et al., 2017). Subsequent CCM pathway is recruited to generate metabolic precursors in bacteria (Noor et al., 2010).

With more antibiotics entering the bacteria, the CCM pathway in the bacteria was also affected and many metabolites were in disequilibrium (Figure 4). The CCM is an important pathway that can provide energy; disruption of this pathway affects the bacteria's oxidation and reduction states that can modify precursor metabolites for other metabolic pathways (Gest, 1987; Fuchs et al., 2012; Murima et al., 2014; Wolfe, 2015).

The stability of CCM directly affects the survival of bacteria cells (Lobritz et al., 2015). Twelve key metabolites in CCM were perturbed by the combination of P + M and P + M + S (Figure 4). Among them, fumaric acid is involved in the nicotinate and nicotinamide metabolism. The alterations in fumaric acid levels might lead to the perturbation of NAD⁺ and nicotinamide riboside. NAD⁺ and ADP which are markers of energy metabolism were depleted by P + M and P + M + S combination therapies. Depletion of NAD⁺ is a common strategy to enhance immune-mediated cell death in both prokaryotes and eukaryotes (Wang et al., 2022).

The nucleotide metabolism pathway is essential for energy, lipid and protein biosynthesis (Moffatt and Ashihara, 2002; Armenta-Medina et al., 2014; Zhao et al., 2021). This pathway was perturbed by the P + M + S combination treatment. Many metabolites were depleted including ADP, thymidine, adenine, 5-phospho-beta-D-ribosylamine, FGAR and CDP.

Glutathione as an integral part of cellular redox system is a key indicator of oxidative stress (Smirnova and Oktyabrsky, 2005). The perturbation of amino acid and peptide biosynthesis pathway was observed with the combination of P + M and P + M + S, especially on glutathione levels. The significantly depleted glutathione is consistent with the use of glutathione pool to compensate for antibiotic-induced oxidative damage (Maifiah et al., 2017). This shows that the metabolic balance in bacteria has been broken, thus inhibiting bacterial growth.

In conclusion, our findings were consistent with reported *in vitro* benefits of combination therapy in the treatment of MDR *A. baumannii* (Menegucci et al., 2019). The current study on metabolomic profiling elucidates the salutary effects of combination antimicrobial chemotherapy. The addition of sulbactam to P + M combination appears to be an early disruptor of *A. baumannii* metabolome, which paves the way for further antibiotic penetration into bacteria cells.

References

- Allobawi, R., Ghelani, D. P., and Schneider-Futschik, E. K. (2020). Metabolomic description of Ivacaftor elevating polymyxin B mediated antibacterial activity in cystic fibrosis *Pseudomonas aeruginosa*. *ACS Pharmacol. Transl. Sci.* 3, 433–443. doi: 10.1021/acspstsci.0c00030
- Armenta-Medina, D., Segovia, L., and Perez-Rueda, E. (2014). Comparative genomics of nucleotide metabolism: A tour to the past of the three cellular domains of life. *BMC Genomics* 15:800. doi: 10.1186/1471-2164-15-800
- Bian, X., Liu, X., Feng, M., Bergen, P. J., Li, J., Chen, Y., et al. (2021). Enhanced bacterial killing with colistin/sulbactam combination against carbapenem-resistant *Acinetobacter baumannii*. *Int. J. Antimicrob. Agents* 57:106271. doi: 10.1016/j.jantimicag.2020.106271
- Cajal, Y., Rogers, J., Berg, O. G., and Jain, M. K. (1996). Intermembrane molecular contacts by polymyxin B mediate exchange of phospholipids. *Biochemistry* 35, 299–308. doi: 10.1021/bi9512408
- Clausell, A., Pujol, M., Alsina, M. A., and Cajal, Y. (2003). Influence of polymyxins on the structural dynamics of *Escherichia coli* lipid membranes. *Talanta* 60, 225–234. doi: 10.1016/S0039-9140(03)00078-X
- CLSI (2020). "Performance Standards for Antimicrobial Susceptibility Testing" in *CLSI document M100. 30th Edn.* (Wayne, PA: Clinical and Laboratory Standards Institute).
- Cottagnoud, P. (2002). Cellular and molecular aspects of drugs of the future: meropenem. *Cell. Mol. Life Sci.* 59, 1928–1933. doi: 10.1007/PL00012515
- Domingues, M. M., Inacio, R. G., Raimundo, J. M., Martins, M., Castanho, M. A., and Santos, N. C. (2012). Biophysical characterization of polymyxin B interaction with LPS aggregates and membrane model systems. *Biopolymers* 98, 338–344. doi: 10.1002/bip.22095
- Fedrigo, N. H., Shinohara, D. R., Mazucheli, J., Nishiyama, S. A. B., Carrara-Marroni, F. E., Martins, F. S., et al. (2021). Pharmacodynamic evaluation of suppression of *in vitro* resistance in *Acinetobacter baumannii* strains using polymyxin B-based combination therapy. *Sci. Rep.* 11:11339. doi: 10.1038/s41598-021-90709-2
- Fuchs, T. M., Eisenreich, W., Heesemann, J., and Goebel, W. (2012). Metabolic adaptation of human pathogenic and related nonpathogenic bacteria to extra- and intracellular habitats. *FEMS Microbiol. Rev.* 36, 435–462. doi: 10.1111/j.1574-6976.2011.00301.x
- Gales, A. C., Sader, H. S., Sinto, S., Santos, O. P., and Mendes, C. M. (1996). *In vitro* activity of ampicillin-sulbactam against clinical multiresistant *Acinetobacter baumannii* isolates. *J. Chemother.* 8, 416–419. doi: 10.1179/joc.1996.8.6.416
- Gest, H. (1987). Evolutionary roots of the citric acid cycle in prokaryotes. *Biochem. Soc. Symp.* 54, 3–16.

Data availability statement

All authors listed have made a substantial, direct, and intellectual contribution to the work and approved it for publication.

Author contributions

All authors listed have made a substantial, direct, and intellectual contribution to the work and approved it for publication.

Funding

This study was supported by a grant from Shandong Provincial Natural Science Foundation (ZR2019BC025).

Conflict of interest

The authors declare that the research was conducted in the absence of any commercial or financial relationships that could be construed as a potential conflict of interest.

Publisher's note

All claims expressed in this article are solely those of the authors and do not necessarily represent those of their affiliated organizations, or those of the publisher, the editors and the reviewers. Any product that may be evaluated in this article, or claim that may be made by its manufacturer, is not guaranteed or endorsed by the publisher.

- Hall, M. J., Middleton, R. F., and Westmacott, D. (1983). The fractional inhibitory concentration (FIC) index as a measure of synergy. *J. Antimicrob. Chemother.* 11, 427–433. doi: 10.1093/jac/11.5.427
- Han, M. L., Liu, X. F., Velkov, O., Lin, Y. W., Zhu, Y., Creek, D. J., et al. (2019a). Comparative metabolomics reveals key pathways associated with the synergistic killing of Colistin and Sulbactam combination against multidrug-resistant *Acinetobacter baumannii*. *Front. Pharmacol.* 10:10. doi: 10.3389/fphar.2019.00754
- Han, M. L., Velkov, T., Zhu, Y., Roberts, K. D., Le Brun, A. P., Chow, S. H., et al. (2018). Polymyxin-induced lipid A Deacylation in *Pseudomonas aeruginosa* perturbs Polymyxin penetration and confers high-level resistance. *ACS Chem. Biol.* 13, 121–130. doi: 10.1021/acscchembio.7b00836
- Han, M. L., Zhu, Y., Creek, D. J., Lin, Y. W., Gutu, A. D., Hertzog, P., et al. (2019b). Comparative metabolomics and Transcriptomics reveal multiple pathways associated with Polymyxin killing in *Pseudomonas aeruginosa*. *mSystems* 4:4. doi: 10.1128/mSystems.00149-18
- Hori, T., Mase, K., Suzuki, Y., Kimura, T., Ohta, M., Maekawa, M., et al. (2002). Antibacterial activities of beta-lactamase inhibitors associated with morphological changes of cell wall in helicobacter pylori. *Helicobacter* 7, 39–45. doi: 10.1046/j.1523-5378.2002.00054.x
- Hu, X. Y., Yang, C. H., Wang, P. G., and Zhang, G. L. (2019). ADP-heptose: A new innate immune modulator. *Carbohydr. Res.* 473, 123–128. doi: 10.1016/j.carres.2018.12.011
- Jiang, X., Yang, K., Yuan, B., Han, M., Zhu, Y., Roberts, K. D., et al. (2020). Molecular dynamics simulations informed by membrane lipidomics reveal the structure-interaction relationship of polymyxins with the lipid A-based outer membrane of *Acinetobacter baumannii*. *J. Antimicrob. Chemother.* 75, 3534–3543. doi: 10.1093/jac/dkaa376
- Khondker, A., and Rheinstadter, M. C. (2020). How do bacterial membranes resist polymyxin antibiotics? *Communications Biology* 3:77. doi: 10.1038/s42003-020-0803-x
- Kulengowski, B., Clark, J. A., and Burgess, D. S. (2019). Staggering the administration of polymyxin B and meropenem in time-kill against carbapenem-resistant Enterobacteriaceae exhibiting a wide range of meropenem MICs. *Diagn. Microbiol. Infect. Dis.* 93, 261–264. doi: 10.1016/j.diagmicrobio.2018.09.014
- Lenhard, J. R., Bulitta, J. B., Connell, T. D., King-Lyons, N., Landersdorfer, C. B., Cheah, S. E., et al. (2017). High-intensity meropenem combinations with polymyxin B: new strategies to overcome carbapenem resistance in *Acinetobacter baumannii*. *J. Antimicrob. Chemother.* 72, 153–165. doi: 10.1093/jac/dkw355
- Li, J., Nation, R. L., Turnidge, J. D., Milne, R. W., Coulthard, K., Rayner, C. R., et al. (2006). Colistin: the re-emerging antibiotic for multidrug-resistant gram-negative bacterial infections. *Lancet Infect. Dis.* 6, 589–601. doi: 10.1016/S1473-3099(06)70580-1
- Lin, C. H., Su, S. C., Ho, K. H., Hsu, Y. W., and Lee, K. R. (2014). Bactericidal effect of sulbactam against *Acinetobacter baumannii* ATCC 19606 studied by 2D-DIGE and mass spectrometry. *Int. J. Antimicrob. Agents* 44, 38–46. doi: 10.1016/j.ijantimicag.2014.03.004
- Lobritz, M. A., Belenky, P., Porter, C. B. M., Gutierrez, A., Yang, J. H., Schwarz, E. G., et al. (2015). Antibiotic efficacy is linked to bacterial cellular respiration. *Proc. Natl. Acad. Sci. U. S. A.* 112, 8173–8180. doi: 10.1073/pnas.1509743112
- Maifiah, M. H., Cheah, S. E., Johnson, M. D., Han, M. L., Boyce, J. D., Thamlikitkul, V., et al. (2016). Global metabolic analyses identify key differences in metabolite levels between polymyxin-susceptible and polymyxin-resistant *Acinetobacter baumannii*. *Sci. Rep.* 6:22287. doi: 10.1038/srep22287
- Maifiah, M. H., Creek, D. J., Nation, R. L., Forrest, A., Tsuji, B. T., Velkov, T., et al. (2017). Untargeted metabolomics analysis reveals key pathways responsible for the synergistic killing of colistin and doripenem combination against *Acinetobacter baumannii*. *Sci. Rep.* 7:45527. doi: 10.1038/srep45527
- Martins, F. S., Zhu, P., Heinrichs, M. T., and Sy, S. K. B. (2020). Physiologically based pharmacokinetic-pharmacodynamic evaluation of meropenem plus fosfomycin in paediatrics. *Br. J. Clin. Pharmacol.* 87, 1012–1023. doi: 10.1111/bcp.14456
- Menegucci, T. C., Fedrigo, N. H., Lodi, F. G., Albiero, J., Nishiyama, S. A. B., Mazucheli, J., et al. (2019). Pharmacodynamic effects of Sulbactam/Meropenem/Polymyxin-B combination against extremely drug resistant *Acinetobacter baumannii* using checkerboard information. *Microb. Drug Resist.* 25, 1266–1274. doi: 10.1089/mdr.2018.0283
- Moffatt, B. A., and Ashihara, H. (2002). Purine and pyrimidine nucleotide synthesis and metabolism. *Arabidopsis Book* 1:e0018. doi: 10.1199/tab.0018
- Moffatt, J. H., Harper, M., Harrison, P., Hale, J. D., Vinogradov, E., Seemann, T., et al. (2010). Colistin resistance in *Acinetobacter baumannii* is mediated by complete loss of lipopolysaccharide production. *Antimicrob. Agents Chemother.* 54, 4971–4977. doi: 10.1128/AAC.00834-10
- Murima, P., McKinney, J. D., and Pethe, K. (2014). Targeting bacterial central metabolism for drug development. *Chem. Biol.* 21, 1423–1432. doi: 10.1016/j.chembiol.2014.08.020
- Nikaido, H. (2003). Molecular basis of bacterial outer membrane permeability revisited. *Microbiol. Mol. Biol. Rev.* 67, 593–656. doi: 10.1128/MMBR.67.4.593-656.2003
- Noor, E., Eden, E., Milo, R., and Alon, U. (2010). Central carbon metabolism as a minimal biochemical walk between precursors for biomass and energy. *Mol. Cell* 39, 809–820. doi: 10.1016/j.molcel.2010.08.031
- Pei, G., Mao, Y., and Sun, Y. (2012). In vitro activity of minocycline alone and in combination with cefoperazone-sulbactam against carbapenem-resistant *Acinetobacter baumannii*. *Microb. Drug Resist.* 18, 574–577. doi: 10.1089/mdr.2012.0076
- Pelletier, M. R., Casella, L. G., Jones, J. W., Adams, M. D., Zurawski, D. V., Hazlett, K. R., et al. (2013). Unique structural modifications are present in the lipopolysaccharide from colistin-resistant strains of *Acinetobacter baumannii*. *Antimicrob. Agents Chemother.* 57, 4831–4840. doi: 10.1128/AAC.00865-13
- Penwell, W. F., Shapiro, A. B., Giacobbe, R. A., Gu, R. F., Gao, N., Thresher, J., et al. (2015). Molecular mechanisms of sulbactam antibacterial activity and resistance determinants in *Acinetobacter baumannii*. *Antimicrob. Agents Chemother.* 59, 1680–1689. doi: 10.1128/AAC.04808-14
- Poirel, L., Jayol, A., and Nordmann, P. (2017). Polymyxins: antibacterial activity, susceptibility testing, and resistance mechanisms encoded by plasmids or chromosomes. *Clin. Microbiol. Rev.* 30, 557–596. doi: 10.1128/CMR.00064-16
- Ribera, A., Benavent, E., El-Haj, C., Gomez-Junyent, J., Tubau, F., Rigo-Bonnin, R., et al. (2019). Comparative Antibiofilm efficacy of Meropenem alone and in combination with Colistin in an in vitro Pharmacodynamic model by extended-Spectrum-beta-lactamase-producing *Klebsiella pneumoniae*. *Antimicrob. Agents Chemother.* 63:19. doi: 10.1128/AAC.01230-19
- Ripa, S., Ferrante, L., and Prenna, M. (1990). Pharmacokinetics of sulbactam/ampicillin in humans after intravenous and intramuscular injection. *Chemotherapy* 36, 185–192. doi: 10.1159/000238765
- Sauvage, E., Kerff, F., Terrak, M., Ayala, J. A., and Charlier, P. (2008). The penicillin-binding proteins: structure and role in peptidoglycan biosynthesis. *FEMS Microbiol. Rev.* 32, 234–258. doi: 10.1111/j.1574-6976.2008.00105.x
- Smirnova, G. V., and Oktyabrsky, O. N. (2005). Glutathione in bacteria. *Biochemistry (Mosc)* 70, 1199–1211. doi: 10.1007/s10541-005-0248-3
- Srinivas, P., and Rivard, K. (2017). Polymyxin resistance in gram-negative pathogens. *Curr. Infect. Dis. Rep.* 19:38. doi: 10.1007/s11908-017-0596-3
- Tacconelli, E., Carrara, E., Savoldi, A., Harbarth, S., Mendelson, M., Monnet, D. L., et al. (2018). Discovery, research, and development of new antibiotics: the WHO priority list of antibiotic-resistant bacteria and tuberculosis. *Lancet Infect. Dis.* 18, 318–327. doi: 10.1016/S1473-3099(17)30753-3
- Van Duin, D., Kaye, K. S., Neuner, E. A., and Bonomo, R. A. (2013). Carbapenem-resistant Enterobacteriaceae: a review of treatment and outcomes. *Diagn. Microbiol. Infect. Dis.* 75, 115–120. doi: 10.1016/j.diagmicrobio.2012.11.009
- Wang, M., Ji, Q., Liu, P., and Liu, Y. (2022). NAD(+) depletion and defense in bacteria. *Trends Microbiol.* doi: 10.1016/j.tim.2022.06.002
- Wolfe, A. J. (2015). Glycolysis for microbiome generation. *Microbiol. Spectr.* 3:14. doi: 10.1128/microbiolspec.MBP-0014-2014
- Yang, Y., Xu, Q., Li, T., Fu, Y., Shi, Y., Lan, P., et al. (2019). OXA-23 is a prevalent mechanism contributing to Sulbactam resistance in diverse *Acinetobacter baumannii* clinical strains. *Antimicrob. Agents Chemother.* 63:18. doi: 10.1128/AAC.01676-18
- Zhang, Y. M., and Rock, C. O. (2008). Membrane lipid homeostasis in bacteria. *Nat. Rev. Microbiol.* 6, 222–233. doi: 10.1038/nrmicro1839
- Zhao, J., Han, M. L., Zhu, Y., Lin, Y. W., Wang, Y. W., Lu, J., et al. (2021). Comparative metabolomics reveals key pathways associated with the synergistic activity of polymyxin B and rifampicin combination against multidrug-resistant *Acinetobacter baumannii*. *Biochem. Pharmacol.* 184:114400. doi: 10.1016/j.bcp.2020.114400
- Zhu, S., Zhang, J., Lv, Z., Zhu, P., Oo, C., Yu, M., et al. (2022). Prediction of tissue exposures of Meropenem, Colistin, and Sulbactam in pediatrics using physiologically based pharmacokinetic modeling. *Clin. Pharmacokinet.* doi: 10.1007/s40262-022-01161-y
- Zilberberg, M., Nathanson, B. H., Sulham, K., Fan, W., and Shorr, A. F. (2017). Carbapenem resistance, inappropriate empiric treatment and outcomes among patients hospitalized with Enterobacteriaceae urinary tract infection, pneumonia and sepsis. *BMC Infect. Dis.* 17:279. doi: 10.1186/s12879-017-2383-z



OPEN ACCESS

EDITED BY

Zhe Wang,
Shanghai Jiao Tong University, China

REVIEWED BY

Semanti Ray,
Lerner Research Institute,
Cleveland Clinic,
United States
Mingming Yu,
Ocean University of China, China
Shaohui Wang,
Shanghai Veterinary Research Institute
(CAAS), China

*CORRESPONDENCE

Binghu Fang
fangbh@scau.edu.cn

SPECIALTY SECTION

This article was submitted to
Antimicrobials, Resistance and
Chemotherapy, a section of the journal
Frontiers in Microbiology

RECEIVED 25 September 2022

ACCEPTED 21 October 2022

PUBLISHED 07 November 2022

CITATION

Zhou Y, Yong Y, Zhu C, Yang H and
Fang B (2022) Exogenous D-ribose
promotes gentamicin treatment of several
drug-resistant *Salmonella*.
Front. Microbiol. 13:1053330.
doi: 10.3389/fmicb.2022.1053330

COPYRIGHT

© 2022 Zhou, Yong, Zhu, Yang and Fang.
This is an open-access article distributed
under the terms of the [Creative Commons
Attribution License \(CC BY\)](#). The use,
distribution or reproduction in other
forums is permitted, provided the original
author(s) and the copyright owner(s) are
credited and that the original publication in
this journal is cited, in accordance with
accepted academic practice. No use,
distribution or reproduction is permitted
which does not comply with these terms.

Exogenous D-ribose promotes gentamicin treatment of several drug-resistant *Salmonella*

Yanhong Zhou^{1,2}, Yan Yong³, Chunyang Zhu^{1,2}, Heng Yang^{1,2}
and Binghu Fang^{1,2*}

¹Guangdong Provincial Key Laboratory of Veterinary Pharmaceutics Development and Safety Evaluation, South China Agricultural University, Guangzhou, China, ²National Risk Assessment Laboratory for Antimicrobial Resistance of Animal Origin Bacteria, South China Agricultural University, Guangzhou, China, ³Guangdong Wens Dahuanong Biotechnology Limited Company, Yun Fu, China

The metabolic microenvironment of bacteria impacts drug efficacy. However, the metabolic mechanisms of drug-resistant *Salmonella* spp. remain largely unknown. This study characterized the metabolic mechanism of gentamicin-resistant *Salmonella* Choleraesuis and found that D-ribose increased the gentamicin-mediated killing of this bacteria. Non-targeted metabolomics of homologous gentamicin-susceptible *Salmonella* Choleraesuis (SCH-S) and gentamicin-resistant *S. Choleraesuis* (SCH-R) was performed using UHPLC-Q-TOF MS. The metabolic signature of SCH-R included disrupted central carbon metabolism and energy metabolism, along with dysregulated amino acid and nucleotide metabolism, vitamin and cofactor metabolism, and fatty acid synthesis. D-ribose, the most suppressed metabolite in SCH-R, was shown to strengthen gentamicin efficacy against SCH-R and a clinically isolated multidrug-resistant strain. This metabolite had a similar impact on *Salmonella* Derby and *Salmonella* Typhimurium. D-ribose activates central carbon metabolism including glycolysis, the pentose phosphate pathway (PPP), and the tricarboxylic acid cycle (TCA cycle), increases the abundance of NADH, polarizes the electron transport chain (ETC), and elevates the proton motive force (PMF) of cells, and induces drug uptake and cell death. These findings suggest that central carbon metabolism plays a critical role in the acquisition of gentamicin resistance by *Salmonella*, and that D-ribose may serve as an antibiotic adjuvant for gentamicin treatment of resistant bacterial infections.

KEYWORDS

D-ribose, gentamicin, *Salmonella*, metabolomics, resistance

Introduction

Salmonella spp. is a highly prevalent foodborne pathogen that poses a serious threat to human and animal health, causing >10 million global infections each year (CDC, 2019). The World Health Organization (WHO) has defined *Salmonella* spp. as a “priority pathogen” (WHO, 2017). To date, >2,500 serotypes have been identified (Hendriksen et al.,

2011). One of these, *Salmonella* Choleraesuis (*S. Choleraesuis*), is host adaptive, primarily infecting pigs, causing paratyphoid fever in piglets, and occasionally infecting and causing bacteremia in humans (Chiu et al., 2004; Yang et al., 2012). Human infection most often occurs through exposure to contaminated food or water (Mahon and Fields, 2016). *S. Choleraesuis* is a widely disseminated serotype (Chiu et al., 2004) and is the most common cause of nontyphoid *Salmonella* infection in Thailand (Luk-In et al., 2018). In Europe, the growing number of *S. Choleraesuis* infections among wild boars has attracted research attention (Longo et al., 2019; Papic et al., 2021; Ernholm et al., 2022). In humans, this pathogen has higher invasiveness and is thus a greater health threat than other serotypes (Cohen et al., 1987).

Antibiotics play a critical role in the treatment of bacterial infections. However, antimicrobial resistance caused by improper antibiotic use is becoming a serious threat (Bush et al., 2011), particularly with the emergence of multidrug-resistant strains (Hogberg et al., 2010; Ciorba et al., 2015). In addition to methicillin-resistant *Staphylococcus aureus* (MRSA; Otto, 2013), extended-spectrum β -Lactamase producing *Enterobacteriaceae* (ESBLs; Castanheira et al., 2021), and vancomycin-resistant *Enterococcus* (VRE; Reyes et al., 2016), multidrug-resistant *Salmonella* is also a serious health problem (Tyson et al., 2021). Specifically, multidrug-resistant *S. Choleraesuis* is becoming a crisis for both humans and animals (Chang et al., 2005; Gil Molino et al., 2019). Resistant strains are non-responsive to all antimicrobial agents, including β -lactams, aminoglycosides, bolome reprogramming by metabsulfonamides (Molino et al., 2020). *Mcr-3.1* was also discovered in *S. Choleraesuis*, rendering colistin ineffective (Oransathid et al., 2022). Unfortunately, the development of more complex mechanisms of resistance and the high cost of creating new agents have hindered effective treatment (Breijyeh et al., 2020; Provenzano et al., 2020). Some studies predict that antimicrobial-resistant pathogens will be attributed to 10 million deaths worldwide by 2050 (Castro-Vargas et al., 2020). Thus, there is an urgent need to stop the emergence and spread of antibiotic resistance.

The metabolic state of bacteria affects their susceptibility to antibiotics (Stokes et al., 2019). Bacterial cells embedded in biofilms are particularly tough to eliminate due to the impermeability of biofilms and the reduced metabolic status of the embedded cells (Yin et al., 2019). Persister cells are subpopulations of antibiotic-sensitive bacteria which escape antibiotic killing through metabolic repression (Fisher et al., 2017). In recent years, new strategies have been developed to explore the metabolic mechanisms of bacterial acquired resistance. Metabolomics is the large-scale evaluation of small molecules in cells or tissues which cannot be studied using other methods, including genomics, transcriptomics, and proteomics (Castro-Santos et al., 2015; Johnson et al., 2016). An important feature of metabolomics is that basic metabolic pathways and metabolites are similar between species, while genes, transcripts, and proteins are species specific (Kovac et al., 2013). Hence, metabolomics is a potential tool to explore the acquisition of antimicrobial resistance by bacteria

(Kok et al., 2022). A GC-MS-based metabolomics study on cefoperazone sulbactam (SCF)-resistant *P. aeruginosa* (PA-R_{SCF}) found that the metabolic mechanism for resistance was the inhibition of central carbon metabolism (Chen et al., 2022). Another metabolomics study on *Escherichia coli* carrying the *mcr-1* gene found that *mcr-1*-mediated colistin resistance was associated with a disruption in glycerophospholipid metabolism and LPS biosynthesis as well as the accumulation of the substrate PEA (Li et al., 2019). *Mcr-1*-mediated colistin-resistant *Vibrio alginolyticus*, however, showed reduced central carbon metabolism and membrane potential (Li et al., 2020). These differences may be explained by interspecies differences. While the metabolic mechanism of antibiotic resistant *Edwardsiella tarda* and *Campylobacter jejuni* have also been studied (Cheng et al., 2017; Liu et al., 2019), there are few reports on the metabolic mechanism of antibiotic resistance in *Salmonella* spp.

Aminoglycosides, a class of antibiotics that act by inhibiting protein synthesis, are powerful weapons against multiple pathogens, including *Salmonella* (Poulikakos and Falagas, 2013). Unfortunately, several types of bacteria exhibit resistance to aminoglycosides through enzymatic modifications, efflux pump systems, and genetic mutations that threaten their sustainable utilization (Touati, 2019). Strategies are urgently needed to retain these drugs in the antibacterial arsenal (Bottger and Crich, 2020). Metabolome reprogramming by metabolites is an effective strategy against drug resistance (Peng et al., 2015a). For example, alanine, glucose, and fructose can promote kanamycin-mediated killing of *Edwardsiella tarda*. These metabolites induce NADH through the TCA cycle, which activates the proton motive force (PMF) and enables drug uptake (Peng et al., 2015b). A recent study also reported that glutamine promotes the function of antibiotics against multidrug-resistant bacteria (Zhao et al., 2021). This study analyzed the metabolic spectrum of clinically isolated multidrug-resistant and susceptible *Escherichia coli* and identified glutamine, which was inhibited by drug-resistant bacteria, as a biomarker. Exogenous glutamine promoted the β -lactams-, aminoglycosides-, quinolones- and tetracyclines-induced killing of multidrug-resistant uropathogenic bacteria and enhanced the activity of ampicillin against multidrug-resistant *Klebsiella pneumoniae*, *Pseudomonas aeruginosa*, *Acinetobacter baumannii*, *Edwardsiella tarda*, *Vibrio alginolyticus*, and *Vibrio parahaemolyticus*. These results indicate that metabolome reprogramming may be an effective weapon against drug resistance. The current study sought to investigate whether similar mechanisms can be used to improve the activity of other aminoglycosides, including gentamicin, tobramycin, apramycin, and kanamycin, against antibiotic-resistant *Salmonella* spp.

UHPLC-Q-TOF MS was used to characterize the metabolic profile of gentamicin-susceptible and resistant *S. Choleraesuis* and explore the metabolic mechanisms of gentamicin resistance of SCH-R. Resistance was associated with a disruption in central carbon metabolism, along with dysregulated amino acid and nucleotide metabolism, vitamin and cofactor metabolism, and fatty acid synthesis. In addition, D-ribose, the most suppressed

metabolite in SCH-R, significantly increased the gentamicin-mediated killing of both SCH-R and the wild strain and had a similar effect on multidrug-resistant *Salmonella*. These findings provide new perspectives and strategies for the study and resolution of *Salmonella* resistance mechanisms.

Materials and methods

Chemicals

All antibiotics were purchased from the China Institute of Veterinary Drug Control (Beijing, China). Mueller Hinton (MH) Agar, MH Broth, Tryptic Soy Agar (TSA), Luria-Bertani (LB) broth, MacConkey Agar, and Xylose Lysine Deoxycholate (XLD) Agar were purchased from Guangdong Huankai Microbial Sci & Tech. Co., Ltd. (Guangdong, China). Methanol and acetonitrile (high-performance liquid chromatography grade) were purchased from Thermo Fisher Scientific (Waltham, MA, United States). Ammonium ethoxide and formic acid (high-performance liquid chromatography grade) were purchased from Sigma Aldrich (Missouri, United States).

Bacterial strains and growth conditions

Standard strains of *Escherichia coli* (ATCC25922) and *S. Choleraesuis* (ATCC13312) were purchased from American Type Culture Collection (Manassas, VA, United States). The clinical strains, SR-1 and SR-6 (*S. Derby*), SR-7 (*S. Typhimurium*), and SCH2021 (*S. Choleraesuis*) were isolated from swine farms in South China (Guangdong Province, China). These strains exhibit resistance to most clinical antimicrobials, including β -lactams, aminoglycosides, tetracyclines, and sulfonamides. The minimum inhibitory concentrations (MICs) of antimicrobials against different *Salmonella* strains were determined using the microdilution method (Li et al., 2020). The standard *S. Choleraesuis* (ATCC13312) strain was sequentially propagated with or without drug and drug-resistant bacteria were selected. All bacterial cultures were grown in LB medium at 37°C.

Sample pretreatment

S. Choleraesuis (ATCC13312) was used for non-targeted metabolomics studies. Gentamicin-resistant (SCH-R), and susceptible (SCH-S) bacteria were cultured in LB broth to a late exponential phase. The bacterial suspension (5 ml) was centrifuged at 16,000 g for 10 min at -10°C and the precipitate was washed twice with PBS. The bacteria were collected and quickly quenched in liquid nitrogen to halt metabolism. Methanol/acetonitrile/water (1 ml, 2:2:1, V/V) was added, vortexed for 60 s, and extracted ultrasonically twice at a low temperature. The supernatant was placed at -20°C for 1 h to precipitate the proteins. The samples

were centrifuged at 20,000 g at 4°C for 20 min, and the supernatant was collected, lyophilized, and stored at -80°C .

Non-targeted metabolomic analysis

UHPLC-Q-TOF MS was used to perform the non-targeted metabolomics analysis. Samples were separated on a HILIC column at 25°C with mobile phase A (water +25 mM ammonium acetate +25 mM ammonia) and mobile phase B (acetonitrile). The gradient elution procedure included: 0–1 min, 95% B; 1–14 min, 95–65% B; 14–16 min, 65–40% B; 16–18 min, 40% B; 18–18.1 min, 40–95% B; 18.1–23 min, 95% B. The flow rate was 0.3 ml/min with an injection volume of 2 μl . Electrospray ionization (ESI) was used to monitor the samples in positive and negative ion modes using the following parameters: Ion Source Gas 1 (Gas1)=60, Ion Source Gas 2 (Gas 2)=60, Curtain gas (CUR)=30, source temperature= 600°C , IonSapary Voltage Floating (ISVF)= $\pm 5,500\text{ V}$; TOF MS scan m/z range=60–1,000 Da, product ion scan m/z range=25–1,000 Da, TOF MS scan accumulation time=0.20 s/spectra, and product ion scan accumulation time=0.05 s/spectra. The secondary mass spectrum was obtained by information-dependent acquisition (IDA) and used with a high sensitivity mode as follows: Declustering potential (DP)= $\pm 60\text{ V}$ (positive and negative modes), collaboration energy= $35 \pm 15\text{ EV}$. IDA was set to exclude isotopes within 4 Da and monitor six candidate ions per cycle. Quality control (QC) samples were inserted into the sample queue to monitor and evaluate the stability of the system and ensure data reliability.

Data processing and statistical analysis

Mass spectrometry data were processed using Software Analyst 1.6. The total ion and MRM multi-peak diagrams of the samples were obtained. The mass spectrum peaks detected by each metabolite in different samples were corrected based on the retention time and peak metabolite types. Principal component analysis (PCA), partial least squares discrimination analysis (PLS-DA), orthogonal partial least squares analysis (OPLS-DA), multivariate analysis, and the Student's *t*-test were used to investigate intra- and inter-group differences between the samples and to identify differential metabolites. Using OPLS-DA analysis, differences between groups were preliminarily screened using a Variable Importance in Projection (VIP) score >1 . Univariate statistical analysis was used to verify whether the differential metabolites were significant. Those with multidimensional statistical analysis VIP scores >1 and a univariate statistical analysis *p* value of <0.05 were selected as significantly different. The structure of each metabolite was identified using accurate mass number matching ($<25\text{ ppm}$) and secondary spectrum matching. To comprehensively display the relationship between samples and the differences in the expression patterns of metabolites in different samples, we perform hierarchical

clustering on each group of samples to help us accurately screen marker metabolites. Finally, KEGG pathway analysis and pathway enrichment of differential metabolites were carried out to identify those metabolic pathways with the most significant changes.

Antibiotic bactericidal assays

The antibacterial assay was carried out as described previously (Allison et al., 2011). In brief, bacterial cells were cultured in LB broth to the late exponential phase. After centrifugation at 10,000 g for 5 min, the cells were washed twice with sterile PBS buffer and resuspended to 1×10^6 cfu/ml in M9 minimal media. D-ribose and antibiotics were added, and the culture was incubated at 37°C for 6 h. In all CCCP experiments, the cells were preincubated with 20 μ M CCCP for 5 min before adding metabolites or antibiotics. The remaining inhibitors, bromopyruvate, malonate, and rotenone, were added at the same time as the metabolites or antibiotics. After incubation, 100 μ l of the culture was removed, serially diluted, and plated (20 μ l aliquots) onto LB agar plates. The agar plates were incubated at 37°C for 10–16 h and those with 10–100 colonies were enumerated to determine the number of colony-forming units (cfu). Percent survival was determined by the ratio of cfu obtained from the test and control samples.

Measurement of NADH and NADH dehydrogenase 1 (ND1)

NADH production was determined using a NAD⁺/NADH assay kit (BioAssay Systems, Hayward, CA, United States; Peng et al., 2015b). In brief, bacterial cells were grown to the exponential phase (6 h) in broth, and 1 ml of the culture was collected and centrifuged at 13,000 g for 5 min. The supernatant was discarded, and the pellet was washed three times with PBS. NADH extraction buffer (100 μ l) was added, the extract was heated at 60°C for 5 min, then 20 μ l assay buffer and 100 μ l NAD⁺ extraction buffer were added to neutralize the extract. After centrifugation, NADH was measured in the supernatant according to the manufacturer's instructions. NADH dehydrogenase 1 was assessed using a Microorganism ND1 ELISA kit (Jiangsu MEIMIAN Industrial Co., Ltd., Yancheng China). The exponential phase culture (1 ml) was centrifuged and washed, and the cells were resuspended in 1 ml of PBS. The cells were then disrupted by sonication to obtain a supernatant. ND1 was detected according to the manufacturer's instructions.

Measurement of membrane potential

The membrane potential was examined using a BacLight Bacterial Membrane Potential Kit (Life Technologies, Carlsbad, CA, United States) as previously described (Yong et al., 2021).

Measurement of intracellular gentamicin

Measurement of intracellular gentamicin was determined as previously described (Yong et al., 2021). In brief, bacterial cells were cultured in LB broth until the late exponential phase. After centrifugation, the precipitates were collected and resuspended in 10 ml of M9 minimal media to 1×10^6 cfu/ml with or without antibiotics and D-ribose. The reaction samples were incubated at 37°C for 6 h, and the precipitates were harvested by centrifugation, washed twice with PBS, and resuspended in 1 ml of PBS. The solution was sonicated for 10 min and the insoluble substances were removed by centrifugation. Gentamicin was quantified in the supernatant using a Gentamicin ELISA kit (Shanghai Enzyme-linked Biotechnology Co., Ltd., Shanghai, China).

Quantitative RT-PCR analysis

Bacterial cells were harvested in the exponential phase. The total RNA was extracted according to the manufacturer's instructions using an RNAiso Plus kit (Takara Japan). Reverse transcription-PCR was performed using a Hifair® II 1st Strand cDNA Synthesis Kit (Yeasen, Shanghai China) with 1.5 μ g of total RNA according to the manufacturer's instructions. QRT-PCR was performed with a total volume of 10 μ l liquid including 5 μ l 1x SYBR Green Master Mix (Yeasen, Shanghai China), 1 μ l PCR-grade water, 2 μ l cDNA template, and 1 μ l of each primer pair (0.2 μ M) using a real-time PCR system (BIO-RAD). The specific primers are listed in the Supplementary material (Supplementary Table 1). The cycling parameters were as follows: pre-denaturation at 95°C for 300 s, 40 cycles of 95°C for 10 s, and 60°C for 30 s. The melting curve was obtained from 60–95°C with a calefactive velocity of 0.05°C/s. Differences in gene expression were compared between the experimental and control groups and 16S rRNA was used as the internal reference. The biological repeats were carried out in triplicate.

Results

Metabolic profile of SCH-R

Gentamicin-susceptible *S. Choleraesuis* (ATCC13312, SCH-S) was continuously cultured in LB broth with or without gentamicin to obtain gentamicin-resistant *Salmonella* (SCH-R), and microdilution method was used to detect the MIC of different antimicrobials against SCH-R and clinical isolates (Table 1). A non-targeted metabolomics profile of SCH-S and SCH-R was then determined using UHPLC-Q-TOF MS with eight biological replicates per group. Unsupervised PCA was performed on the ion peaks extracted from each group of samples to obtain the overall difference profile between the groups (Figures 1A,B). To better reflect the differences between samples, OPLS-DA analysis was

TABLE 1 MIC value of different antimicrobials against *Salmonella* ($\mu\text{g/mL}$).

	ATCC13312S (SCH-S)	ATCC13312R (SCH-R)	SCH2021	SR-1	SR-6	SR-7
Gentamicin	0.25	16	16	32	16	32
Tobramycin	0.25	0.25	64	32	32	32
Apramycin	2	2	64	128	256	256
Kanamycin	2	2	256	512	512	512
Spectinomycin	8	8	256	512	512	512
Ampicillin	2	2	32	128	32	32
Amoxicillin/Clavulanic acid	1	1	32	32	32	16
Ceftiofur	0.5	0.5	2	1	0.5	0.5
Ofloxacin	0.03	0.03	4	8	4	8
Enrofloxacin	0.03	0.03	4	4	4	4
Tetracycline	1	1	32	32	16	16
Colistin	0.5	0.5	1	1	1	1
Sulfaisoxazole	4	4	512	512	512	512
Sulfamethoxazole/ Trimethoprim	0.5	0.5	32	32	32	32

performed, and the VIP score was used to help identify differential metabolites. Univariate analysis was also conducted to ensure the reliability of differential metabolites, and those with a VIP score > 1 and a value of $p < 0.05$ were considered significant. A total of 114 differential metabolites were identified in the SCH-S and SCH-R strains in the positive and negative ion modes after the same species were removed, of which 59 were up-regulated and 55 were down-regulated (Supplementary Table 2). The four most abundant of the 114 metabolites were nucleic acids (22%), organic acids (15.8%), carbohydrates (7%), and fatty acyls (7%) (Figure 1C). Hierarchical clustering of differential metabolites was used to show the relationship between samples and help to accurately identify biomarkers with significant significance (Figures 1D,E). These results indicated that the metabolic state of SCH-R was disrupted.

Enriched pathways in SCH-R

To assess the metabolic changes of the drug-resistant bacteria, alterations in metabolite abundance were analyzed using KEGG (<https://www.genome.jp/kegg>). As shown in Figure 2A, 23 pathways were enriched (Supplementary Table 3). The most impacted pathway was oxidative phosphorylation, a series of chemical reactions occurring in the electron transport chain (ETC) (Bald et al., 2017). PMF generated by ETC is shown to promote the internalization of aminoglycosides (Taber et al., 1987). Thus, we speculated that the PMF of SCH-R was suppressed as a result of disturbed oxidative phosphorylation, ultimately mediating the resistance of SCH-R to gentamicin. The increased abundance of NAD^+ in SCH-R cells was also suggestive of PMF suppression (Figure 2B). Key metabolites associated with riboflavin metabolism, alanine, aspartate and glutamate metabolism, arginine biosynthesis, glycolysis/gluconeogenesis, and pentose phosphate pathway were down-regulated, while those

associated with pantothenate and CoA biosynthesis and valine, leucine, and isoleucine biosynthesis were up-regulated (Figure 2B). Of these, the glycolysis/gluconeogenesis and pentose phosphate pathway are involved in central carbon metabolism, which converts nutrients into biomass and energy (Ryan et al., 2021). The central carbon metabolism provided protons through NADH reduction to maintain PMF. Thus, we reasoned that a disturbed central carbon metabolism in SCH-R affected oxidative phosphorylation and thereby suppressed PMF. Additionally, amino acid metabolism fuels central carbon metabolism, which benefits riboflavin metabolism, fatty acid synthesis, and other pathways. These findings suggested that the global metabolism of SCH-R was altered and that disrupted central carbon metabolism may play a key role in mediating SCH-R resistance.

Perturbed central carbon metabolism is associated with lower PMF in SCH-R

To verify whether disturbed central carbon metabolism leads to lower PMF via reduced NADH and thus mediates drug resistance, we began by assessing the PMF of SCH-S and SCH-R. Indeed, SCH-R had lower PMF than SCH-S (Figure 3A). NADH, the basis for maintaining PMF, and the activity of NADH dehydrogenase 1 (ND1), were also significantly lower in SCH-R than in SCH-S (Figures 3B,C). These findings suggest that the ETC of SCH-R is severely altered, which leads to lower PMF. To verify whether central carbon metabolism is disrupted, genes involved in glycolysis, PPP, and TCA cycles were assessed by qRT-PCR. As expected, nearly all genes associated with central carbon metabolism were downregulated in SCH-R (Figures 3D,E). These findings suggested that disrupted central carbon metabolism reduced the PMF of SCH-R, potentially accounting for the gentamicin resistance of these bacteria.

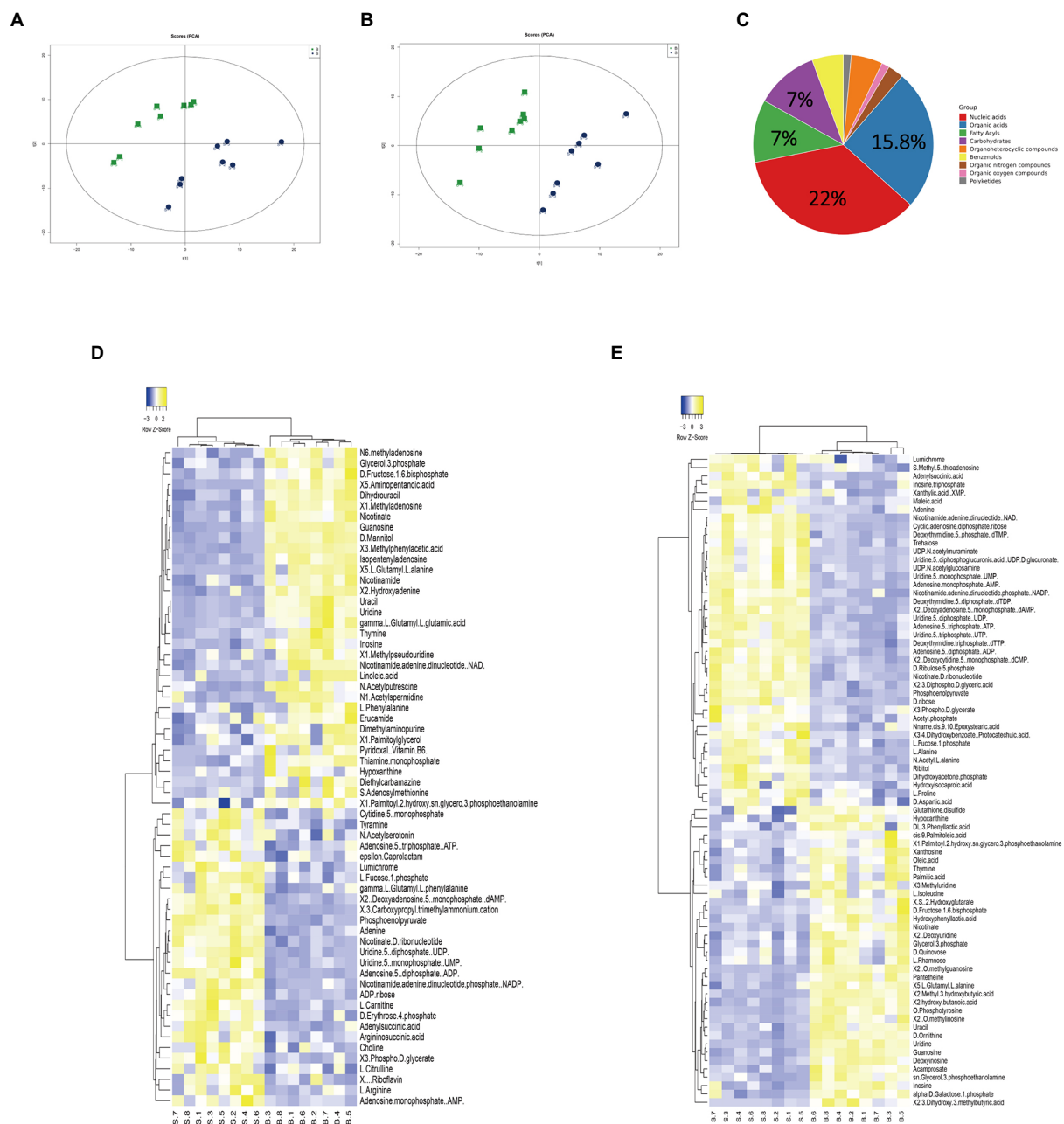


FIGURE 1
Analysis of the SCH-R metabolic profile. **(A)** PCA score of gentamicin-resistant and sensitive *Salmonella* in positive ESI modes. **(B)** PCA score of gentamicin-resistant and sensitive *Salmonella* in negative ESI modes. **(C)** Abundance of different categories of metabolites in SCH-R. **(D)** Cluster analysis of different metabolites in positive ESI modes. **(E)** Cluster analysis of different metabolites in negative ESI modes. "B" represents gentamicin-induced resistant *Salmonella* ATCC13312, "S" represents gentamicin-sensitive *Salmonella* ATCC13312.

D-ribose induces gentamicin against drug-resistant *Salmonella*

Exogenous supplementation to reprogram the metabolome by repressed metabolites can alter the sensitivity of resistant strains (Peng et al., 2015b). Our previous study confirmed that citrulline and glutamine promoted apramycin-mediated killing (Yong et al., 2021). The current study confirmed that exogenous D-ribose, which was

suppressed in SCH-R, enhanced gentamicin-mediated killing in both SCH-R and SCH2021. SCH2021 is a wild *S. Choleraesuis* which confers resistance to gentamicin, tobramycin, apramycin, kanamycin etc. The two gentamicin-resistant strains were co-incubated with or without D-ribose plus gentamicin. In the presence of gentamicin, cell survival declined with increasing doses of D-ribose (Figure 4A). Specifically, in the presence of 1 MIC gentamicin, when 0, 6, 12, 24, or 48 mM D-ribose was added, the cell

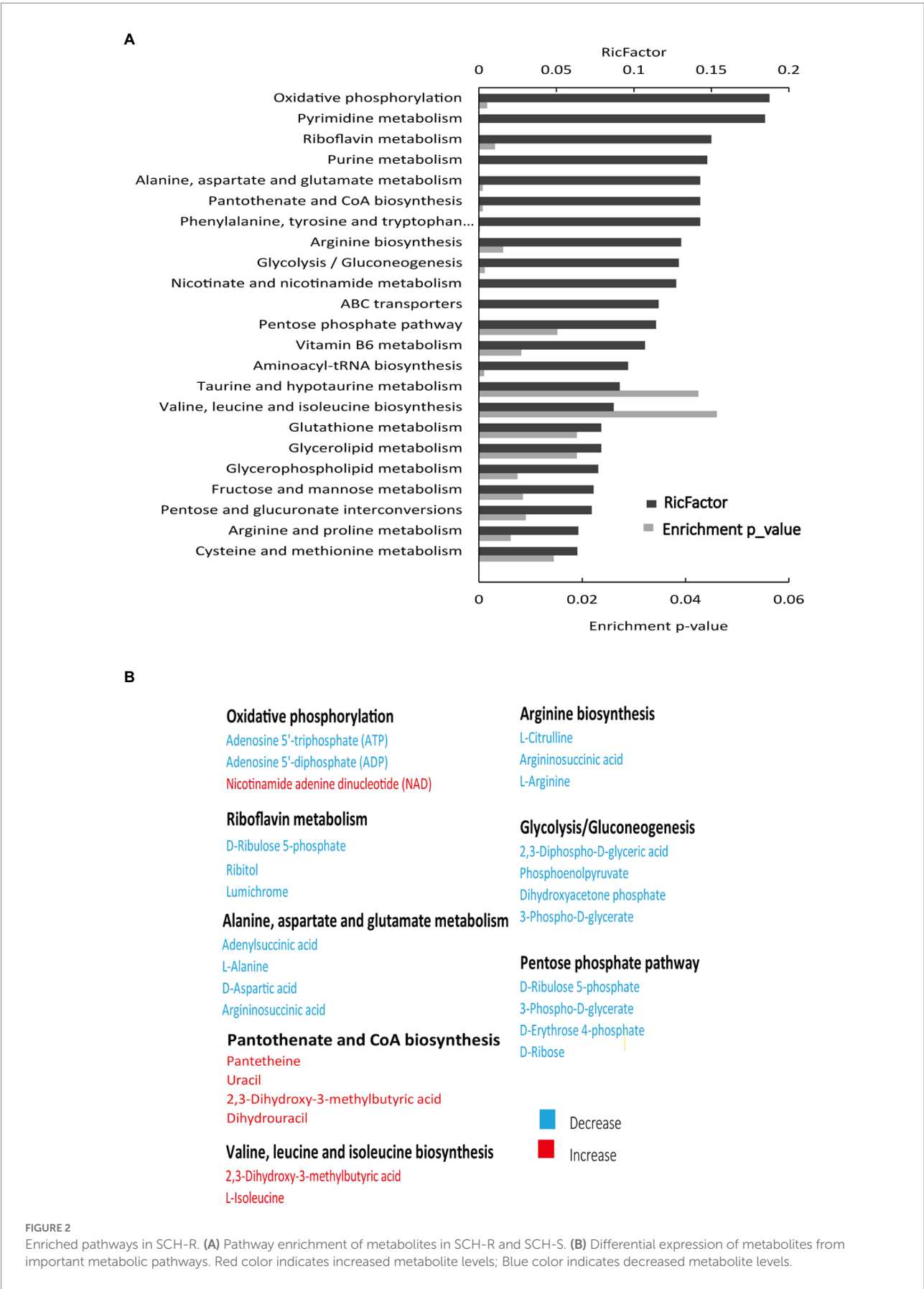


FIGURE 2 Enriched pathways in SCH-R. (A) Pathway enrichment of metabolites in SCH-R and SCH-S. (B) Differential expression of metabolites from important metabolic pathways. Red color indicates increased metabolite levels; Blue color indicates decreased metabolite levels.

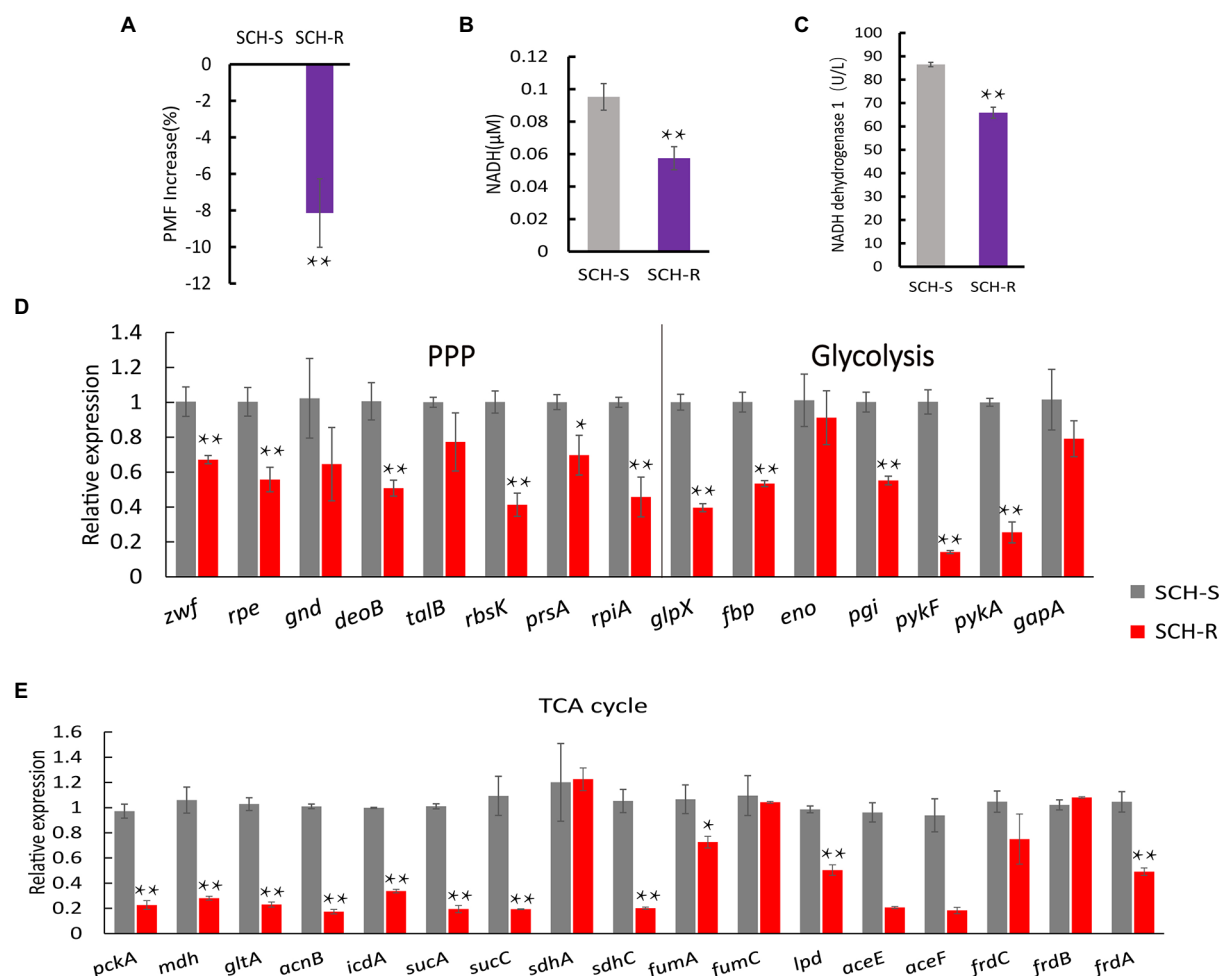


FIGURE 3

SCH-R resistance is mediated by disrupted central carbon metabolism. (A) Variation of the PMF in SCH-R and SCH-S. (B) NADH concentration in SCH-R and SCH-S. (C) Activity of NADH dehydrogenase 1 in SCH-R and SCH-S. (D,E) QRT-PCR for the expression of key genes in central carbon metabolism. *pckA*, phosphoenolpyruvate carboxykinase; *mdh*, malate dehydrogenase; *gltA*, citrate synthase; *acnB*, aconitate hydratase 2; *icdA*, isocitrate dehydrogenase; *sucA*, 2-oxoglutarate dehydrogenase E1 component; *sucC*, succinyl-CoA synthetase beta subunit; *sdhA*, succinate dehydrogenase; *sdhC*, succinate dehydrogenase; *fumA*, fumarate hydratase, class I; *fumC*, fumarate hydratase, class II; *lpd*, dihydrolipoyl dehydrogenase; *aceE*, pyruvate dehydrogenase E1 component; *aceF*, pyruvate dehydrogenase E2 component; *frdC*, fumarate reductase subunit C; *frdB*, fumarate reductase iron-sulfur subunit; *frdA*, fumarate reductase flavoprotein subunit; *zwf*, glucose-6-phosphate dehydrogenase; *rpe*, ribulose-phosphate 3-epimerase; *gnd*, 6-phosphogluconate dehydrogenase; *deoB*, phosphopentomutase; *talB*, transaldolase; *rbsK*, ribokinase; *prsA*, ribose-phosphate pyrophosphokinase; *rpiA*, ribose 5-phosphate isomerase A; *glpX*, fructose-1,6-bisphosphatase II; *fbp*, fructose-1,6-bisphosphatase I; *eno*, phosphopyruvate hydratase; *pgi*, glucose-6-phosphate isomerase; *pykF*, pyruvate kinase; *pykA*, pyruvate kinase; *gapA*, glyceraldehyde 3-phosphate dehydrogenase. Results are displayed as the mean \pm SEM and three biological repeats are carried out. Significant differences are identified (* $p < 0.05$ and ** $p < 0.01$).

survival percentages of SCH-R were 93.46, 88.93, 51.74, 4.69, and 0.56, respectively. Similarly, the cell survival percentages of SCH20221 were 91.50, 89.28, 78.20, 1.41, and 0.071, respectively (Figure 4B). Furthermore, cell survival was gentamicin dose-dependent (Figure 4C; Supplementary Figures S1A–F). D-ribose was also shown to enhance gentamicin-, tobramycin-, and apramycin-mediated killing of multidrug-resistant *S. Choleraesuis*, *S. Typhimurium* and *S. Derby* (Figures 4D–G). These results demonstrated that D-ribose can increase gentamicin-, tobramycin-, and apramycin-mediated killing in drug-resistant *Salmonella*, including multidrug-resistant strains.

Exogenous D-ribose increases PMF-induced uptake of gentamicin

Glucose increases the PMF of *E. coli* and stimulates the uptake of aminoglycosides and induces cell deaths (Allison et al., 2011). To test whether D-ribose can also enhance the PMF of *Salmonella*, cells were cultured in M9 minimal media with or without D-ribose for 6 h and the PMF was assessed using the *BacLight* bacterial membrane potential Kit. The PMF of SCH-R was increased by 8.62, 11.54, and 14.92% in the presence of 12, 24, and 48 mM D-ribose, respectively (Figure 5A). Similar results were observed

using the clinical MDR *Salmonella* SR-7 strain (Figure 5B). To further verify whether elevated PMF can promote drug uptake, an ELISA kit was used to detect the intracellular concentration of gentamicin in the presence of 24 mM D-ribose. The intracellular concentration of gentamicin in SCH-R and clinical *Salmonella* cells increased significantly in the presence of D-ribose (Figure 5C). To verify whether the gentamicin potentiation by D-ribose was result of higher PMF-induced drug uptake and subsequent cell death, PMF was inhibited using the proton ionophore, carbonyl cyanide chlorophenyl hydrazone (CCCP). As expected, CCCP significantly inhibited PMF expression in both the presence and absence of D-ribose (Figures 5A,B), while the intracellular concentration and potentiating effect of gentamicin were declined (Figures 5D,E). These results demonstrated that increased drug uptake induced by D-ribose was responsible for gentamicin killing.

D-ribose activates the ETC

To demonstrate that D-ribose increased PMF by activating ETC. First, the intracellular NADH concentration and NADH dehydrogenase 1 activity of SCH-R were detected. The result showed that both NADH concentration and NADH dehydrogenase 1 activity of SCH-R were elevated by D-ribose in a dose-dependent manner (Figures 6A,B). In addition, rotenone, an ETC inhibitor, abolished D-ribose mediated synergy (Figure 6C). Similar results were obtained using SCH2021 and clinical MDR *Salmonella* (Figures 6A–C). Finally, the expression of ETC-related genes in SCH-R upregulated significantly after adding D-ribose (Figure 6D). These data suggested that D-ribose enhanced PMF by stimulating ETC, and then increased drug uptake, induced cell death ultimately.

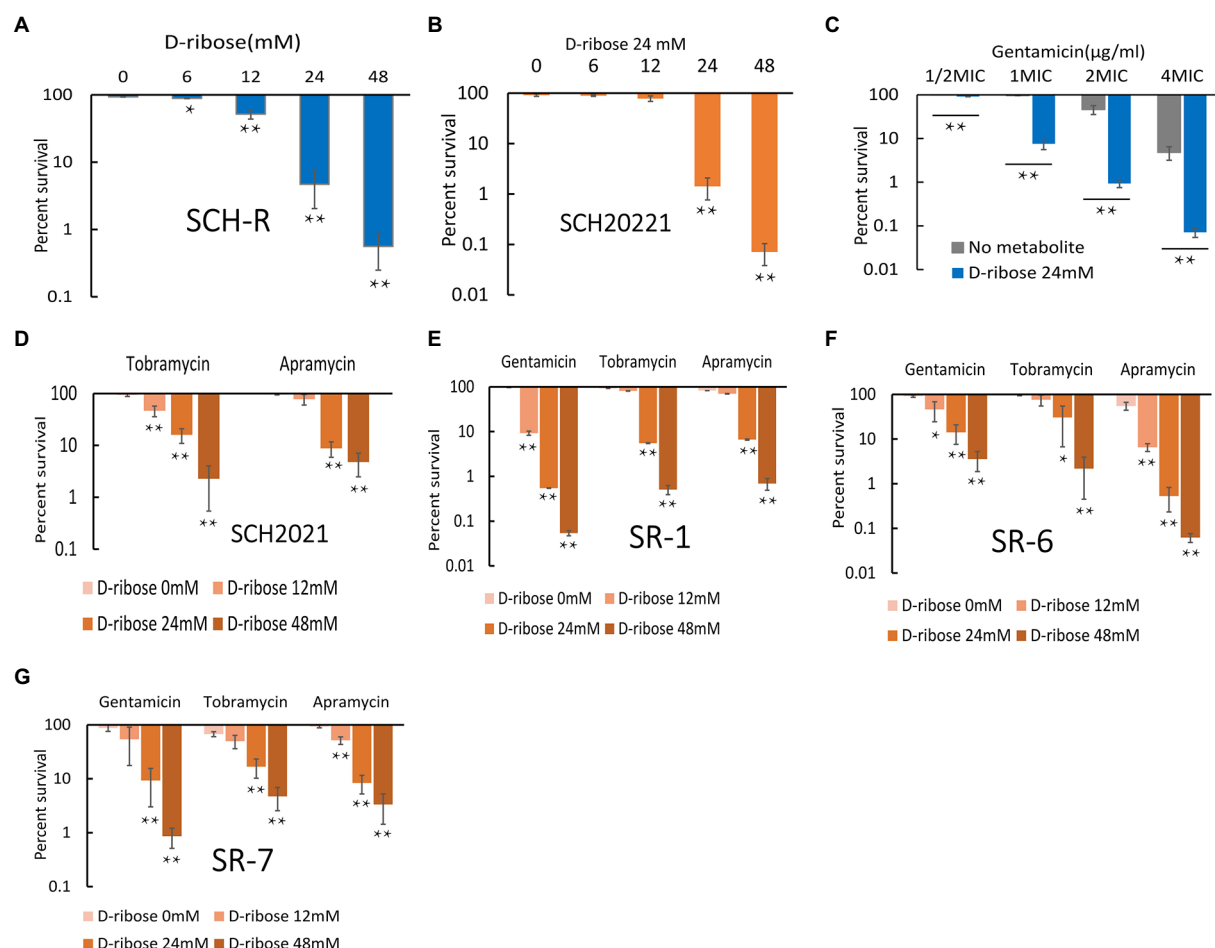


FIGURE 4
Effect of exogenous D-ribose on SCH-R and clinical isolates of drug-resistant *Salmonella*. (A) Percent survival of SCH-R in the presence of 1 MIC gentamicin by D-ribose dose. (B) Percent survival of SCH2021 in the presence of 1 MIC gentamicin by D-ribose dose. (C) Percent survival of SCH-R in the presence of 24 mM D-ribose by gentamicin dose. (D–G) Percent survival of clinical isolates SCH2021 (D), SR-1 (E), SR-6 (F), and SR-7 (G) in the presence of different aminoglycosides (1 MIC) by D-ribose dose. Results are displayed as the mean \pm SEM and three biological repeats are carried out. Significant differences are identified (* p < 0.05 and ** p < 0.01).

Activated central carbon metabolism drives aminoglycoside-mediated killing

We assumed that D-ribose activated central carbon metabolism to promote ETC polarization. First, two TCA cycle inhibitors, bromopyruvate and malonate, were used to verify this. Specifically, bromopyruvate inhibits the E1 subunit of pyruvate dehydrogenase, malonate competitively inhibits succinate dehydrogenase. Cell survival increased as bromopyruvate and malonate concentrations rose (Figures 7A,B). In addition, lower PMF and NADH levels were detected after adding bromopyruvate or malonate (Figures 7C–F). These findings indicated that TCA inhibition eliminated the D-ribose-mediated potential. Furthermore, most genes involved in central carbon metabolism were upregulated by D-ribose (Figure 7G). This indicated that D-ribose was involved in stimulating the central carbon metabolism of drug-resistant bacteria, producing more NADH, polarizing ETC, increasing PMF, and promoting drug uptake and cell death (Figure 8).

Discussion

This study characterized the intracellular metabolic profile of gentamicin-sensitive *S. Choleraesuis*, SCH-S, and the homologous gentamicin-resistant strain, SCH-R. A total of 114 metabolites,

including amino acids, carbohydrates, nucleotides, and their derivatives, in SCH-R changed significantly relative to SCH-S. The pathway enrichment results of this study are similar to those of Peng et al., who used GC–MS to compare the metabolic profiles of kanamycin-sensitive and drug-resistant *Edwardsiella tarda* (Peng et al., 2015b). It is important to note that drug-resistant *S. Choleraesuis* showed broader metabolic fluctuations and enrichment of more metabolic pathways. This may be related to differences between the bacterial species or because more metabolites were identified in the current study.

Results indicated that oxidative phosphorylation was the most impacted pathway. While ATP and ADP levels were diminished, nicotinamide adenine dinucleotide (NAD⁺) production was increased. Oxidative phosphorylation, the pathway by which bacteria produce ATP, involves a series of chemical reactions in the ETC, and an activated ETC is necessary for PMF (Gao et al., 2019). Importantly, PMF is essential for aminoglycoside internalization (Taber et al., 1987). In SCH-R, the reduced production of ATP and ADP and increased production of NAD⁺, indicated that the PMF of SCH-R was affected, a finding confirmed by later experiments (Figure 3B). Carbohydrate metabolism, which involves glycolysis/gluconeogenesis, the pentose phosphate pathway, fructose and mannose metabolism, and pentose and gluconate interconversion, was also seriously disrupted in SCH-R. All PPP metabolites were down-regulated, of which D-ribose, was the most inhibited. Central carbon

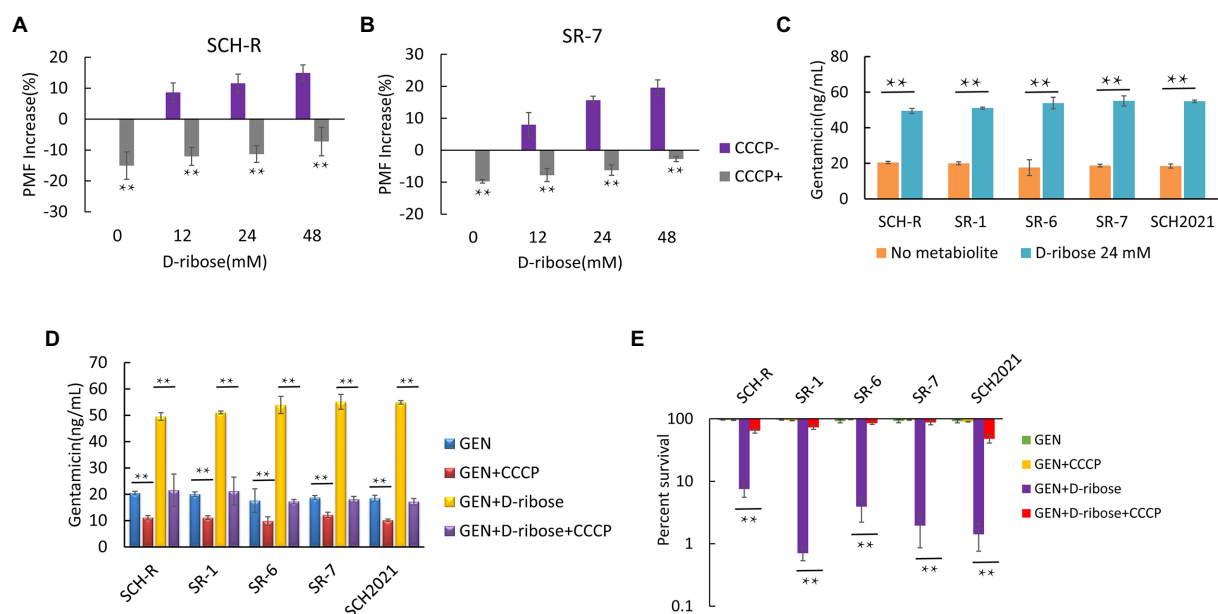


FIGURE 5

Effect of exogenous D-ribose on membrane potential. (A) Variation of PMF in SCH-R by D-ribose dose with or without CCCP. (B) Variation of PMF in SR-7 by D-ribose dose with or without CCCP. (C) Intracellular concentration of gentamicin in SCH-R and clinical isolates in the presence of 24mM D-ribose. (D) Intracellular concentration of gentamicin in SCH-R and clinical isolates in the presence of 24mM D-ribose with or without CCCP. GEN, gentamicin. (E) Percent survival of SCH-R and clinical isolates in the presence or absence of CCCP and 1 MIC gentamicin plus 24mM D-ribose. GEN, gentamicin. Results are displayed as the mean \pm SEM and three biological repeats are carried out. Significant differences are identified (* p < 0.05 and ** p < 0.01).

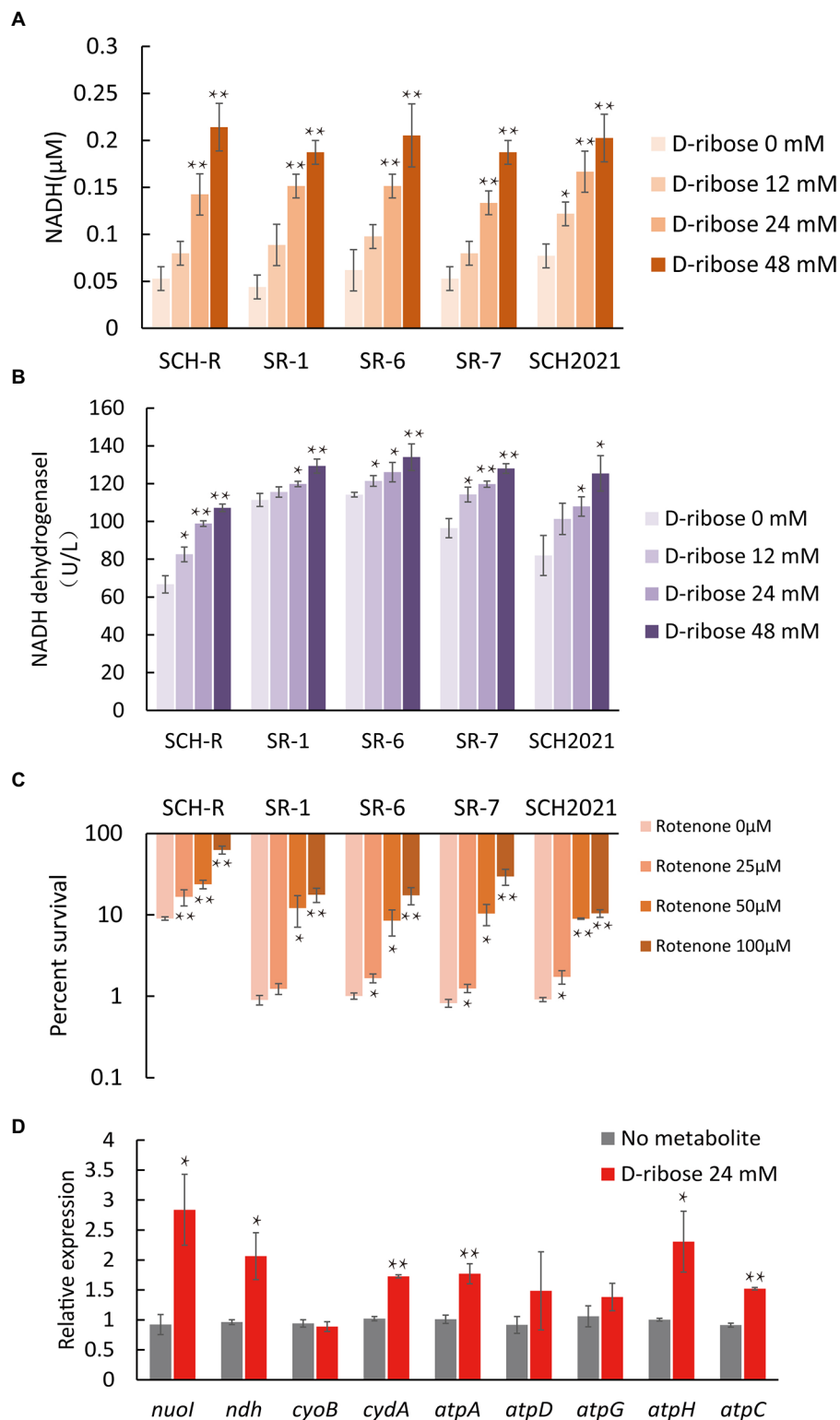


FIGURE 6

Effect of exogenous D-ribose on the electron transport chain. (A) The intracellular NADH concentration of SCH-R and clinical isolates by D-ribose dose. (B) Activity of NADH dehydrogenase 1 in SCH-R and clinical isolates by D-ribose dose. (C) Percent survival of SCH-R and clinical isolates by rotenone dose and 1 MIC gentamicin plus 24mM D-ribose. (D) QRT-PCR of key electron transport chain genes in the presence 24mM D-ribose. *nuoI*, NADH dehydrogenase I chain I; *ndh*, NADH:quinone reductase; *cyoB*, cytochrome o ubiquinol oxidase subunit I; *cydA*, cytochrome BD2 subunit I; *atpA*, *atpD*, *atpG*, *atpH* and *atpC*, membrane-bound ATP synthase, F1 sector, alpha-subunit, beta-subunit, gamma-subunit, delta-subunit, and epsilon-subunit. Results are displayed as the mean±SEM and three biological repeats are carried out. Significant differences are identified (* $p < 0.05$ and ** $p < 0.01$).

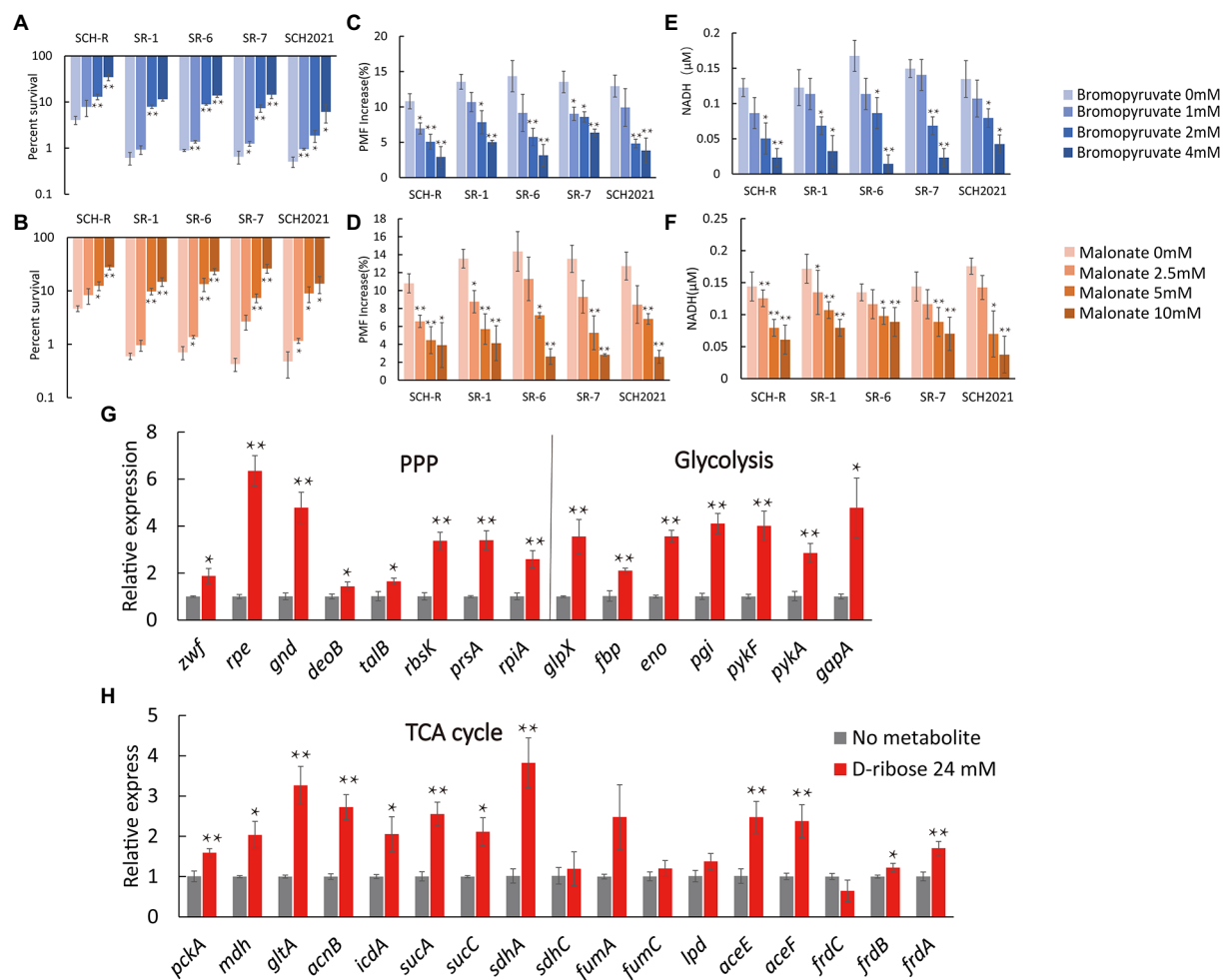


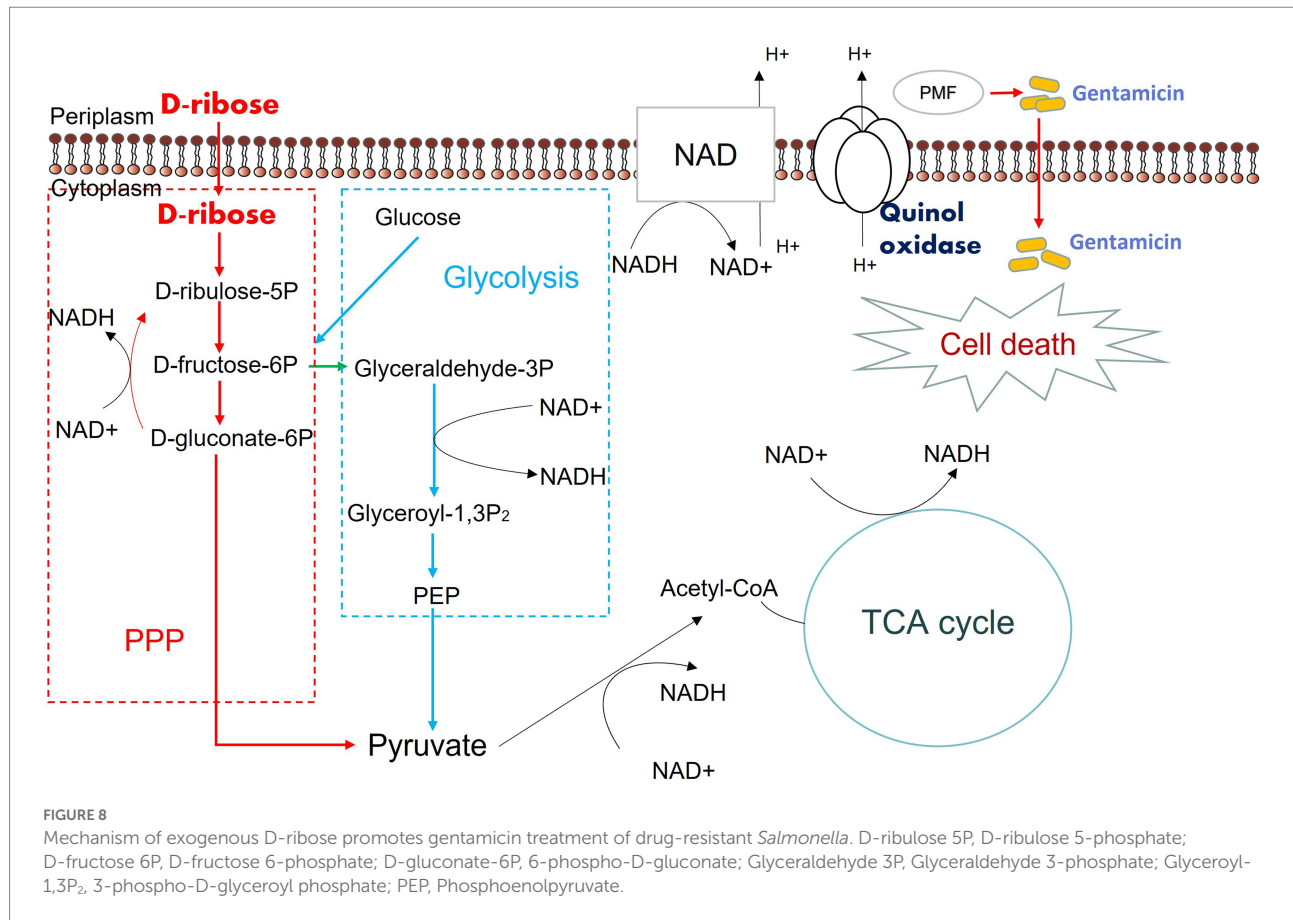
FIGURE 7

Effect of exogenous D-ribose on central carbon metabolism. (A,B) Percent survival of SCH-R and clinical isolates by (A) bromopyruvate and (B) malonate dose and 1 MIC gentamicin plus 24mM D-ribose. (C,D) PMF of SCH-R and clinical isolates by (C) bromopyruvate and (D) malonate dose with 24mM D-ribose. (E,F) Intracellular NADH concentration of SCH-R and clinical isolates by (E) bromopyruvate and (F) malonate dose with 24mM D-ribose. (G,H) QRT-PCR for expression of key central carbon metabolism genes in the presence of 24mM D-ribose. Results are displayed as the mean \pm SEM and three biological repeats are carried out. Significant differences are identified (* $p < 0.05$ and ** $p < 0.01$).

metabolism, involving glycolysis, the pentose phosphate pathway, and the TCA cycle, is the core component of cell metabolism, responsible for converting nutrients into biomass to maintain life (Baughn and Rhee, 2014; Barbier et al., 2018; Dolan et al., 2020). Disrupted central carbon metabolism and energy metabolism result in drug inactivation in bacterial cells (Chen et al., 2022). While the TCA cycle was not affected in SCH-R, the fluctuation of amino acid metabolism and other metabolic pathways, as well as the qPCR results, suggested that the TCA cycle was disrupted. These results suggest that bacteria may require central carbon metabolism and energy metabolism to acquire resistance.

A recent study confirmed that activated purine metabolism could restore the sensitivity of multidrug-resistant bacteria to antibiotics. This may be due to increased purine metabolism, which activates the CpxA/CpxR two-component system, promotes *OmpF* expression, and induces drug uptake (Zhao et al., 2021).

Coincidentally, both purine and pyrimidine metabolism were seriously impacted in SCH-R and the pentose phosphate pathway and alanine, aspartate, and glutamate metabolism were shown to directly affect purine metabolism through 5-phosphoribosyl diphosphate and 5-phosphoribosylamine, respectively. Furthermore, it is worth noting that nutrients can also contribute to riboflavin metabolism through the pentose phosphate pathway, leading to ROS production, a cause of bacterial death induced by bactericidal antibiotics (Kohanski et al., 2007; Chen et al., 2022). Whether purine and pyrimidine metabolism are involved in the inactivation of gentamicin, and whether there is a certain co-action between them and central carbon metabolism mediating the resistance of SCH-R to gentamicin remains to be further studied. Meanwhile, disrupted central carbon metabolism and increased fatty acid synthesis mediate ceftazidime and ciprofloxacin resistance jointly (Liu et al., 2019; Su et al., 2021). While fatty acid synthesis was not enriched in



SCH-R, glycerolipid and glycerophospholipid metabolism indirectly reflect the impact on fatty acid synthesis. These results suggested that SCH-R acquires gentamicin resistance through a universal metabolic shift, including upstream amino acid metabolism, central carbon metabolism at the core, and downstream metabolism including nucleotide metabolism and fatty acid synthesis. Thus, it is evident that fluctuations in central carbon metabolism, accompanied by changes in other metabolic pathways, are critical for drug inactivation.

Antibiotic efficacy is enhanced by altering the metabolic state of bacteria (Allison et al., 2011). Importantly, repressing metabolites through exogenous supplementation can alter the sensitivity of resistant strains (Peng et al., 2015a). Such a strategy was first implemented in resistant *Escherichia coli* and *Staphylococcus aureus* (Allison et al., 2011). This study found that glucose, fructose, and mannitol can promote glycolysis, stimulate the ETC, induce PMF, promote gentamicin uptake, and eliminate *E. coli* persister cells and *Staphylococcus aureus* biofilm. Metabolite-dependent aminoglycoside potentiation has also been applied to aminoglycoside-resistant bacteria, such as *Edwardsiella tarda* (Su et al., 2015), *Vibrio alginolyticus* (Li et al., 2020), and *Pseudomonas aeruginosa* (Meylan et al., 2017). Thus, it was probable that metabolome-reprogramming could also enhance the effect of antibiotics against SCH-R and other drug-resistant *Salmonella*. Indeed, D-ribose was shown to significantly enhance

the gentamicin-mediated killing of both SCH-R and multidrug-resistant *S. Choleraesuis*, *S. Derby*, and *S. Typhimurium*. Allison et al. (2011) found that metabolites enter metabolism through glycolysis rather than the pentose phosphate pathway, inducing rapid gentamicin killing of persisters. However, D-ribose, which enters metabolism via the pentose phosphate pathway, also promotes the gentamicin-mediated killing of drug-resistance *Salmonella*. Notably, glucose, fructose, and mannitol failed to increase the effect of aminoglycosides against SCH-R and multidrug-resistant *Salmonella* (data not shown), but are shown to enhance the impact of aminoglycosides on *Escherichia coli*, *Staphylococcus aureus*, *Pseudomonas aeruginosa*, and *Edwardsiella tarda* (Peng et al., 2015b). This finding suggests that the strengthening effect of D-ribose may target drug-resistant bacteria rather than persisters.

The current study demonstrated that D-ribose significantly increased the gentamicin-, tobramycin-, and apramycin-mediated killing of *S. Choleraesuis*, *S. Derby*, and *S. Typhimurium* (Figures 4A–G). D-ribose does not have the same impact on kanamycin and spectinomycin (Supplementary Figures S2A,B), however, which may be explained by the higher MIC of these drugs in the wild strains (Table 1). Alternatively, this mechanism of metabolite-mediated killing may be used by bactericidal antibiotics but not bacteriostatic drugs (Allison et al., 2011; Peng et al., 2015b; Meylan et al., 2017). Whether there are

additional factors that prevent D-ribose from impacting kanamycin and spectinomycin requires further investigation. Interestingly, in the presence of 1 MIC gentamicin and 24 mM D-ribose, the percent survival of SCH-R was significantly higher than the clinical isolates (Supplementary Figure S3A). As illustrated by Su et al. (2015), this may be attributable to the weaker growth capacity of SCH-R than the clinical isolates and SCH-S after 6 h (Supplementary Figures S3B,C). Additional studies are needed to determine whether this is common among lab and clinical strains or whether it occurs sporadically.

Increased central carbon metabolism, especially the TCA cycle, is the core of metabolome reprogramming. Our previous work confirmed that citrulline and glutamine enhanced the apramycin-mediated killing of *Salmonella* via the TCA cycle (Yong et al., 2021). In the current study, D-ribose significantly increased central carbon metabolism. D-ribose promoted the uptake of drugs by drug-resistant bacteria, which is attributed to the elevated PMF maintained by the ETC. Importantly, CCCP and rotenone significantly increased cell survival. Exogenous D-ribose also stimulated NADH and NADH dehydrogenase and promoted central carbon metabolism, an important source of NADH. These findings suggested that D-ribose-induced central carbon metabolism is critical for gentamicin potentiation. While D-ribose indirectly affects other metabolic pathways, such as purine metabolism and riboflavin metabolism, the effect of D-ribose on these pathways requires further exploration.

In summary, we utilized a metabolomics approach to explore the metabolic mechanism of gentamicin resistance in *S. Choleraesuis*. Disturbed central carbon metabolism, accompanied by fluctuations in metabolic pathways such as amino acid, nucleotide, vitamin, and cofactor metabolism, were identified as characteristics of gentamicin-resistant *S. Choleraesuis*. In addition, D-ribose, which can promote the effect of gentamicin on multidrug-resistant *Salmonella*, was identified as a potential new antibiotic adjuvant. We confirmed that D-ribose promoted the central carbon metabolism of drug-resistant bacteria, increasing glycolysis, the pentose phosphate pathway and TCA cycle, NADH production, ETC activation, PMF, and subsequent drug uptake and cell death. This study characterizes the metabolic mechanism of gentamicin-resistant *Salmonella* and provides evidence that D-ribose can serve as a potential adjuvant to enhance the efficacy of aminoglycosides.

Data availability statement

The original contributions presented in the study are included in the article/Supplementary material, further inquiries can be directed to the corresponding author.

References

Allison, K. R., Brynildsen, M. P., and Collins, J. J. (2011). Metabolite-enabled eradication of bacterial persisters by aminoglycosides. *Nature* 473, 216–220. doi: 10.1038/nature10069

Author contributions

YZ carried out the main experiments and data analysis and wrote the manuscript. YY and CZ participated in the *in vitro* validation tests. HY participated in the isolation and identification of clinical drug-resistant bacteria. BF conceived and designed the experiments. All authors contributed to the article and approved the submitted version.

Funding

This work was funded by the Local Innovative and Research Teams Project of Guangdong Pearl River Talents Program (No. 2019BT02N054).

Acknowledgments

We thank the native English-speaking scientists of Charlesworth Data Services (Beijing) Co., Ltd. (Beijing, China) for editing the manuscript.

Conflict of interest

YY is employed by Guangdong Wens Dahuanong Biotechnology Limited Company.

The remaining authors declare that the research was conducted in the absence of any commercial or financial relationships that could be construed as a potential conflict of interest.

Publisher's note

All claims expressed in this article are solely those of the authors and do not necessarily represent those of their affiliated organizations, or those of the publisher, the editors and the reviewers. Any product that may be evaluated in this article, or claim that may be made by its manufacturer, is not guaranteed or endorsed by the publisher.

Supplementary material

The Supplementary material for this article can be found online at: <https://www.frontiersin.org/articles/10.3389/fmicb.2022.1053330/full#supplementary-material>

Bald, D., Villellas, C., Lu, P., and Koul, A. (2017). Targeting energy metabolism in mycobacterium tuberculosis, a new paradigm in antimycobacterial drug discovery. *MBio* 8, e00272–e00217. doi: 10.1128/mBio.00272-17

- Barbier, T., Zuniga-Ripa, A., Moussa, S., Plovier, H., Sternon, J. F., Lazaro-Anton, L., et al. (2018). Brucella central carbon metabolism: an update. *Crit. Rev. Microbiol.* 44, 182–211. doi: 10.1080/1040841X.2017.1332002
- Baughn, A. D., and Rhee, K. Y. (2014). Metabolomics of central carbon metabolism in mycobacterium tuberculosis. *Microbiol. Spectr.* 2:2.3.02. doi: 10.1128/microbiolspec.MGM2-0026-2013
- Bottger, E. C., and Crich, D. (2020). Aminoglycosides: time for the resurrection of a neglected class of Antibacterials? *ACS Infect. Dis.* 6, 168–172. doi: 10.1021/acinfed.9b00441
- Breijyeh, Z., Jubeh, B., and Karaman, R. (2020). Resistance of gram-negative bacteria to current antibacterial agents and approaches to resolve it. *Molecules* 25:1340. doi: 10.3390/molecules25061340
- Bush, K., Courvalin, P., Dantas, G., Davies, J., Eisenstein, B., Huovinen, P., et al. (2011). Tackling antibiotic resistance. *Nat. Rev. Microbiol.* 9, 894–896. doi: 10.1038/nrmicro2693
- Castanheira, M., Simner, P. J., and Bradford, P. A. (2021). Extended-spectrum beta-lactamases: an update on their characteristics, epidemiology and detection. *JAC Antimicrob. Resist.* 3:dlab092. doi: 10.1093/jacamr/dlab092
- Castro-Santos, P., Laborde, C. M., and Diaz-Pena, R. (2015). Genomics, proteomics, and metabolomics: their emerging roles in the discovery and validation of rheumatoid arthritis biomarkers. *Clin. Exp. Rheumatol.* 33, 279–286.
- Castro-Vargas, R. E., Herrera-Sanchez, M. P., Rodriguez-Hernandez, R., and Rondon-Barragan, I. S. (2020). Antibiotic resistance in salmonella spp. isolated from poultry: a global overview. *Vet. World* 13, 2070–2084. doi: 10.14202/vetworld.2020.2070-2084
- CDC (2019). Antibiotic resistance threats in the United States [online]. Available at: <https://www.cdc.gov/drugresistance/pdf/threats-report/2019-ar-threats-report-508.pdf> (Accessed July 8, 2022).
- Chang, C. C., Lin, Y. H., Chang, C. F., Yeh, K. S., Chiu, C. H., Chu, C., et al. (2005). Epidemiologic relationship between fluoroquinolone-resistant salmonella enterica Serovar Choleraesuis strains isolated from humans and pigs in Taiwan (1997 to 2002). *J. Clin. Microbiol.* 43, 2798–2804. doi: 10.1128/JCM.43.6.2798-2804.2005
- Chen, Y. T., Yang, K. X., Dai, Z. Y., Yi, H., Peng, X. X., Li, H., et al. (2022). Repressed central carbon metabolism and its effect on related metabolic pathways in Cefoperazone/Sulbactam-resistant *Pseudomonas aeruginosa*. *Front. Microbiol.* 13:847634. doi: 10.3389/fmicb.2022.847634
- Cheng, Z. X., Gong, Q. Y., Wang, Z., Chen, Z. G., Ye, J. Z., Li, J., et al. (2017). Edwardsiella tarda tunes Tricarboxylic acid cycle to evade complement-mediated killing. *Front. Immunol.* 8:1706. doi: 10.3389/fimmu.2017.01706
- Chiu, C. H., Su, L. H., and Chu, C. (2004). Salmonella enterica serotype Choleraesuis: epidemiology, pathogenesis, clinical disease, and treatment. *Clin. Microbiol. Rev.* 17, 311–322. doi: 10.1128/CMR.17.2.311-322.2004
- Ciorba, V., Odone, A., Veronesi, L., Pasquarella, C., and Signorelli, C. (2015). Antibiotic resistance as a major public health concern: epidemiology and economic impact. *Ann. Ig.* 27, 562–579. doi: 10.7416/ai.2015.2048
- Cohen, J. I., Bartlett, J. A., and Corey, G. R. (1987). Extra-intestinal manifestations of salmonella infections. *Medicine (Baltimore)* 66, 349–388. doi: 10.1097/00005792-198709000-00003
- Dolan, S. K., Kohlstedt, M., Trigg, S., Vallejo Ramirez, P., Kaminski, C. F., Wittmann, C., et al. (2020). Contextual flexibility in *Pseudomonas aeruginosa* central carbon metabolism during growth in single carbon sources. *MBio* 11, e02684–e02619. doi: 10.1128/mBio.02684-19
- Ernholm, L., Sternberg-Lewerin, S., Agren, E., Stahl, K., and Hulten, C. (2022). First detection of salmonella enterica Serovar Choleraesuis in free ranging European wild boar in Sweden. *Pathogens* 11:723. doi: 10.3390/pathogens11070723
- Fisher, R. A., Gollan, B., and Helaine, S. (2017). Persistent bacterial infections and persister cells. *Nat. Rev. Microbiol.* 15, 453–464. doi: 10.1038/nrmicro.2017.42
- Gao, M., Yi, J., Zhu, J., Minikes, A. M., Monian, P., Thompson, C. B., et al. (2019). Role of mitochondria in Ferroptosis. *Mol. Cell* 73, 354–363.e3. doi: 10.1016/j.molcel.2018.10.042
- Gil Molino, M., Risco Perez, D., Goncalves Blanco, P., Fernandez Llarrio, P., Quesada Molina, A., Garcia Sanchez, A., et al. (2019). Outbreaks of antimicrobial resistant salmonella Choleraesuis in wild boars piglets from Central-Western Spain. *Transbound. Emerg. Dis.* 66, 225–233. doi: 10.1111/tbed.13003
- Hendriksen, R. S., Vieira, A. R., Karlsmose, S., Wong, L. F., Danilo, M., Jensen, A. B., et al. (2011). Global monitoring of salmonella serovar distribution from the World Health Organization global foodborne infections network country data Bank: results of quality assured laboratories from 2001 to 2007. *Foodborne Pathog. Dis.* 8, 887–900. doi: 10.1089/fpd.2010.0787
- Hogberg, L. D., Heddini, A., and Cars, O. (2010). The global need for effective antibiotics: challenges and recent advances. *Trends Pharmacol. Sci.* 31, 509–515. doi: 10.1016/j.tips.2010.08.002
- Johnson, C. H., Ivanisevic, J., and Siuzdak, G. (2016). Metabolomics: beyond biomarkers and towards mechanisms. *Nat. Rev. Mol. Cell Biol.* 17, 451–459. doi: 10.1038/nrm.2016.25
- Kohanski, M. A., Dwyer, D. J., Hayete, B., Lawrence, C. A., and Collins, J. J. (2007). A common mechanism of cellular death induced by bactericidal antibiotics. *Cells* 130, 797–810. doi: 10.1016/j.cell.2007.06.049
- Kok, M., Maton, L., van der Peet, M., Hankemeier, T., and van Hasselt, J. G. C. (2022). Unraveling antimicrobial resistance using metabolomics. *Drug Discov. Today* 27, 1774–1783. doi: 10.1016/j.drudis.2022.03.015
- Kovac, J. R., Pastuszak, A. W., and Lamb, D. J. (2013). The use of genomics, proteomics, and metabolomics in identifying biomarkers of male infertility. *Fertil. Steril.* 99, 998–1007. doi: 10.1016/j.fertnstert.2013.01.111
- Li, L., Su, Y. B., Peng, B., Peng, X. X., and Li, H. (2020). Metabolic mechanism of colistin resistance and its reverting in vibrio alginolyticus. *Environ. Microbiol.* 22, 4295–4313. doi: 10.1111/1462-2920.15021
- Li, H., Wang, Y., Meng, Q., Wang, Y., Xia, G., Xia, X., et al. (2019). Comprehensive proteomic and metabolomic profiling of mcr-1-mediated colistin resistance in Escherichia coli. *Int. J. Antimicrob. Agents* 53, 795–804. doi: 10.1016/j.ijantimicag.2019.02.014
- Liu, S. R., Peng, X. X., and Li, H. (2019). Metabolic mechanism of ceftazidime resistance in vibrio alginolyticus. *Infect Drug Resist.* 12, 417–429. doi: 10.2147/IDR.S179639
- Longo, A., Losasso, C., Vitulano, F., Mastrorilli, E., Turchetto, S., Petrin, S., et al. (2019). Insight into an outbreak of salmonella Choleraesuis var. Kunzendorf in wild boars. *Vet. Microbiol.* 238:108423. doi: 10.1016/j.vetmic.2019.108423
- Luk-In, S., Chatsuwan, T., Pulsrikarn, C., Bangtrakulnonth, A., Rirerm, U., and Kulwichit, W. (2018). High prevalence of ceftriaxone resistance among invasive salmonella enterica serotype Choleraesuis isolates in Thailand: the emergence and increase of CTX-M-55 in ciprofloxacin-resistant S. Choleraesuis isolates. *Int. J. Med. Microbiol.* 308, 447–453. doi: 10.1016/j.ijmm.2018.03.008
- Mahon, B. E., and Fields, P. I. (2016). Invasive infections with Nontyphoidal salmonella in sub-Saharan Africa. *Microbiol. Spectr.* 4:4.3.18. doi: 10.1128/microbiolspec.EI10-0015-2016
- Meylan, S., Porter, C. B. M., Yang, J. H., Belenky, P., Gutierrez, A., Lobritz, M. A., et al. (2017). Carbon sources tune antibiotic susceptibility in *Pseudomonas aeruginosa* via Tricarboxylic acid cycle control. *Cell Chem Biol.* 24, 195–206. doi: 10.1016/j.chembiol.2016.12.015
- Molino, G. M., Garcia, A., Zurita, S. G., Martin-Cano, F. E., Garcia-Jimenez, W., Risco, D., et al. (2020). Spread of antimicrobial resistance by salmonella enterica Serovar Choleraesuis between close domestic and wild environments. *Antibiotics (Basel)* 9:750. doi: 10.3390/antibiotics9110750
- Oransathid, W., Sukhchat, P., Margulieux, K., Wongpatcharamongkol, N., Kormanee, R., Pimsawat, T., et al. (2022). First report: Colistin resistance gene mcr-3.1 in salmonella enterica serotype Choleraesuis isolated from human blood sample from Thailand. *Microb. Drug Resist.* 28, 102–105. doi: 10.1089/mdr.2020.0553
- Otto, M. (2013). Community-associated MRSA: what makes them special? *Int. J. Med. Microbiol.* 303, 324–330. doi: 10.1016/j.ijmm.2013.02.007
- Papic, B., Kusar, D., Micunovic, J., Vidrih, S., Pirs, M., Ocepik, M., et al. (2021). Genomic insights into salmonella Choleraesuis var. Kunzendorf outbreak reveal possible interspecies transmission. *Vet. Microbiol.* 263:109282. doi: 10.1016/j.vetmic.2021.109282
- Peng, B., Li, H., and Peng, X. X. (2015a). Functional metabolomics: from biomarker discovery to metabolome reprogramming. *Protein Cell* 6, 628–637. doi: 10.1007/s13238-015-0185-x
- Peng, B., Su, Y. B., Li, H., Han, Y., Guo, C., Tian, Y. M., et al. (2015b). Exogenous alanine and/or glucose plus kanamycin kills antibiotic-resistant bacteria. *Cell Metab.* 21, 249–262. doi: 10.1016/j.cmet.2015.01.008
- Poulidakos, P., and Falagas, M. E. (2013). Aminoglycoside therapy in infectious diseases. *Expert. Opin. Pharmacother.* 14, 1585–1597. doi: 10.1517/14656566.2013.806486
- Provenzani, A., Hospodar, A. R., Meyer, A. L., Leonardi Vinci, D., Hwang, E. Y., Butrus, C. M., et al. (2020). Multidrug-resistant gram-negative organisms: a review of recently approved antibiotics and novel pipeline agents. *Int. J. Clin. Pharm.* 42, 1016–1025. doi: 10.1007/s11096-020-01089-y
- Reyes, K., Bardossy, A. C., and Zervos, M. (2016). Vancomycin-resistant enterococci: epidemiology, infection prevention, and control. *Infect. Dis. Clin. N. Am.* 30, 953–965. doi: 10.1016/j.idc.2016.07.009
- Ryan, D. G., Yang, M., Prag, H. A., Blanco, G. R., Nikitopoulou, E., Segarra-Mondejar, M., et al. (2021). Disruption of the TCA cycle reveals an ATF4-dependent integration of redox and amino acid metabolism. *elife* 10:e72593. doi: 10.7554/eLife.72593
- Stokes, J. M., Lopatkin, A. J., Lobritz, M. A., and Collins, J. J. (2019). Bacterial metabolism and antibiotic efficacy. *Cell Metab.* 30, 251–259. doi: 10.1016/j.cmet.2019.06.009

- Su, Y. B., Kuang, S. F., Ye, J. Z., Tao, J. J., Li, H., Peng, X. X., et al. (2021). Enhanced biosynthesis of fatty acids is associated with the Acquisition of Ciprofloxacin Resistance in *Edwardsiella tarda*. *mSystems* 6:e0069421. doi: 10.1128/mSystems.00694-21
- Su, Y. B., Peng, B., Han, Y., Li, H., and Peng, X. X. (2015). Fructose restores susceptibility of multidrug-resistant *Edwardsiella tarda* to kanamycin. *J. Proteome Res.* 14, 1612–1620. doi: 10.1021/pr501285f
- Taber, H. W., Mueller, J. P., Miller, P. F., and Arrow, A. S. (1987). Bacterial uptake of aminoglycoside antibiotics. *Microbiol. Rev.* 51, 439–457. doi: 10.1128/mr.51.4.439-457.1987
- Touati, A. (2019). Aminoglycoside resistance mechanism inference algorithm: implication for underlying resistance mechanisms to aminoglycosides. *EBioMedicine* 46:8. doi: 10.1016/j.ebiom.2019.07.045
- Tyson, G. H., Li, C., Harrison, L. B., Martin, G., Hsu, C. H., Tate, H., et al. (2021). A multidrug-resistant salmonella *Infantis* clone is spreading and recombining in the United States. *Microb. Drug Resist.* 27, 792–799. doi: 10.1089/mdr.2020.0389
- WHO (2017). List of critically important antimicrobials for human medicine [online]. Available at: <https://apps.who.int/iris/bitstream/handle/10665/255027/9789241512220-eng.pdf?sequence=1> (Accessed 21 August, 2022).
- Yang, C. C., Chuang, F. R., Wu, C. H., Chen, J. B., Lee, C. H., and Lee, C. T. (2012). Refractory salmonella enterica serotype Choleraesuis-related renal cyst infection in a patient with autosomal dominant polycystic kidney disease undergoing hemodialysis treated successfully with intracystic ciprofloxacin infusion. *Med. Princ. Pract.* 21, 576–578. doi: 10.1159/000339199
- Yin, W., Wang, Y., Liu, L., and He, J. (2019). Biofilms: the microbial "protective clothing" in extreme environments. *Int. J. Mol. Sci.* 20:3423. doi: 10.3390/ijms20143423
- Yong, Y., Zhou, Y., Liu, K., Liu, G., Wu, L., and Fang, B. (2021). Exogenous Citrulline and glutamine contribute to reverse the resistance of salmonella to Apramycin. *Front. Microbiol.* 12:759170. doi: 10.3389/fmicb.2021.759170
- Zhao, X. L., Chen, Z. G., Yang, T. C., Jiang, M., Wang, J., Cheng, Z. X., et al. (2021). Glutamine promotes antibiotic uptake to kill multidrug-resistant uropathogenic bacteria. *Sci. Transl. Med.* 13:eabj0716. doi: 10.1126/scitranslmed.abj0716



OPEN ACCESS

EDITED BY

Vijay Soni,
Weill Cornell Medical Center, United States

REVIEWED BY

Arka Banerjee,
Weill Cornell Medical Center, United States
Brendon Lee,
Cornell University, United States
Bhupendra Singh Rawat,
Rutgers University,
Newark, United States
Saurabh Mishra,
Cornell University, United States

*CORRESPONDENCE

Yashwant Kumar

✉ y.kumar@thsti.res.in

Niraj Kumar

✉ nkumar@thsti.res.in

[†]These authors have contributed equally to this work

RECEIVED 27 January 2023

ACCEPTED 10 April 2023

PUBLISHED 27 April 2023

CITATION

Singh R, Thakur L, Kumar A, Singh S, Kumar S,
Kumar M, Kumar Y and Kumar N (2023)
Comparison of freeze-thaw and sonication
cycle-based methods for extracting
AMR-associated metabolites from
Staphylococcus aureus.
Front. Microbiol. 14:1152162.
doi: 10.3389/fmicb.2023.1152162

COPYRIGHT

© 2023 Singh, Thakur, Kumar, Singh, Kumar,
Kumar, Kumar and Kumar. This is an open-
access article distributed under the terms of
the [Creative Commons Attribution License](https://creativecommons.org/licenses/by/4.0/)
(CC BY). The use, distribution or reproduction
in other forums is permitted, provided the
original author(s) and the copyright owner(s)
are credited and that the original publication in
this journal is cited, in accordance with
accepted academic practice. No use,
distribution or reproduction is permitted which
does not comply with these terms.

Comparison of freeze-thaw and sonication cycle-based methods for extracting AMR-associated metabolites from *Staphylococcus aureus*

Rita Singh^{1,2†}, Lovnish Thakur^{1,2†}, Ashok Kumar¹, Sevaram Singh^{1,2},
Shailesh Kumar¹, Manoj Kumar¹, Yashwant Kumar^{1*} and
Niraj Kumar^{1*}

¹Translational Health Science and Technology Institute, NCR Biotech Science Cluster, Faridabad, India,

²Jawaharlal Nehru University, Delhi, India

Emerging antimicrobial resistance (AMR) among Gram-positive pathogens, specifically in *Staphylococcus aureus* (*S. aureus*), is becoming a leading public health concern demanding effective therapeutics. Metabolite modulation can improve the efficacy of existing antibiotics and facilitate the development of effective therapeutics. However, it remained unexplored for drug-resistant *S. aureus* (gentamicin and methicillin-resistant), primarily due to the dearth of optimal metabolite extraction protocols including a protocol for AMR-associated metabolites. Therefore, in this investigation, we have compared the performance of the two most widely used methods, i.e., freeze-thaw cycle (FTC) and sonication cycle (SC), alone and in combination (FTC+SC), and identified the optimal method for this purpose. A total of 116, 119, and 99 metabolites were identified using the FTC, SC, and FTC+SC methods, respectively, leading to the identification of 163 metabolites cumulatively. Out of 163, 69 metabolites were found to be associated with AMR in published literature consisting of the highest number of metabolites identified by FTC (57) followed by SC (54) and FTC+SC (40). Thus, the performances of FTC and SC methods were comparable with no additional benefits of combining both. Moreover, each method showed biasness toward specific metabolite(s) or class of metabolites, suggesting that the choice of metabolite extraction method shall be decided based on the metabolites of interest in the investigation.

KEYWORDS

antimicrobial resistance, *Staphylococcus aureus*, Gram-positive, metabolites extraction method, freeze-thaw cycle, sonication cycle

1. Introduction

Antimicrobial resistance (AMR) among bacterial pathogens has become a leading cause of morbidity and mortality and hence a global public health concern demanding immediate action to develop strategies to combat such antimicrobial resistant difficult-to-treat bacterial infections (Dhingra et al., 2020). This recent trend indicates the emerging prevalence of Multidrug-resistant (MDR) is not only among Gram-negative (i.e., *Klebsiella pneumoniae*, *Acinetobacter*

baumannii, and *Pseudomonas aeruginosa*, etc.) but also Gram-positive bacterial pathogens [primarily methicillin and gentamicin-resistant *Staphylococcus aureus* (MRSA)] making them also difficult to treat (Bassetti et al., 2019; Mulani et al., 2019). Tremendous efforts are being made to understand the pathogen and disease biology and develop relevant diagnostics and therapeutics for the effective treatment of Gram-negative pathogens; however, the same has been comparatively limited for Gram-positive pathogens (Vazquez-Guillamet and Kollef, 2014; Breijyeh et al., 2020).

World Health Organization (WHO) and the centers for disease control and prevention (CDC) have placed MRSA under a list of serious threat causing drug-resistant pathogens (WHO, 2021). MRSA alone has been responsible for more than 100,000 deaths worldwide in 2019 globally (Oxford, U.o, 2019). In India, the prevalence of MRSA has been recorded to be around 30–70% with high mortality rates among patients developing MRSA bacteremia (Antimicrobial Resistance, C, 2022). Originally, MRSA was common in the healthcare setting contributing to nosocomial/hospital-acquired (HA-MRSA) infections like those associated with surgical procedures, indwelling catheters, or prosthetic devices (Mehta et al., 2020). However, over the last decade, there has been an upsurge of community-associated MRSA (CA-MRSA) infections also like bone, joint and skin infections (Masimen et al., 2022). These HA- and CA-*S. aureus* infections are spread through direct contact with an infected wound or contaminated hands and can be fatal if remains untreated (Masimen et al., 2022). Further, limited therapeutic options and an increasing rate of emergence of AMR even against the available last-resort antibiotics have worsened the problem. Altogether, *S. aureus* infection is associated with a greater occurrence of complications, longer hospital stays, duration of therapy, as well as higher costs of treatment (Lee et al., 2018).

Therefore, understanding the molecular changes driving antibiotic resistance among Gram-positive bacteria, specifically *S. aureus*, has become critically important. This can be achieved using various new-generation biological tools, such as genomic, transcriptomic, proteomic, and metabolomics. However, metabolomics allows the identification and quantification of metabolites that are the end product of any genomic- and proteomic-based biological activity of an organism at a given point of time and hence provide a characteristic chemical fingerprint of a specific cellular process (Xiao et al., 2012). Recently, studies have shown that modulation of the pathogen's metabolome can be used to deal with the emerging problem of AMR. One recent example is the conjugating antibiotics with small metabolites like aminoglycosides with fructose and fumarate, resulting in increased potency of aminoglycosides against *S. aureus* and *Escherichia coli* (Rosenberg et al., 2020). A central metabolite of the energy-generation pathway, pyruvate, has been reported to be associated with the virulence and pathogenicity of *S. aureus*, indicating it as a potential target for controlling infection (Harper et al., 2018). Further exogenous administration of L-valine, L-leucine, L-isoleucine, and L-proline in *S. aureus* bloodstream infection animal models has also been shown to have anti-infective effects (Pang et al., 2020). A decrease in intracellular ATP levels has been linked to the development of the *S. aureus* persister phenotype making them resistant to antibiotics (Conlon et al., 2016). However, existing knowledge of target(s) for regulating metabolomic modulation to treat resistant infections is still limited, owing to limited attempts to investigate the comprehensive metabolome of *S. aureus* (Kumar et al., 2022). This may potentially be due to the

unavailability of the appropriate protocols and pipeline for investigating the metabolome of the Gram-positive bacteria, *S. aureus* (specifically drug-resistant strains), including the very first step of extracting AMR-associated metabolites.

Therefore, the goal of this study was to determine the optimal method for extraction of AMR-associated metabolites from *S. aureus* because the method of metabolite extraction dictates the possible range of metabolites that can be detected in the sample and thus has a large impact on the potential outcome(s) of the metabolomic studies. Most of the metabolomic investigations employ FTC or SC-based methods for extracting bacterial metabolites; however, their efficacy for extraction of AMR-associated metabolite from Gram-positive bacteria has not been investigated yet (Conlon et al., 2016). In this study, we have employed both methods, i.e., FTC and SC individually as well as their combination FTC followed by SC (FTC + SC) to extract the metabolites from the *S. aureus* pathogen. Further, Electrospray Ionization-Liquid Chromatography-Mass Spectrometry/Mass Spectrometry (ESI-LC-MS/MS; Orbitrap Fusion Tribrid, Thermo-Scientific), a highly sensitive and advanced mass-spectrometer was used to potentially increase the metabolomic coverage. Finally, the list of identified metabolites was subjected to an intensive literature search for finding the potential association of identified metabolites with AMR. Altogether, this information was utilized to identify the optimal metabolite extraction method for investigating AMR-associated metabolites.

2. Materials and methods

2.1. Harvesting of *Staphylococcus aureus* cell pellets

The primary culture of *S. aureus* (ATCC®33592) was inoculated in 5 ml Mueller Hinton Broth (MHB), followed by incubation for approximately 16 h at 37°C at 220 rpm. The secondary culture was inoculated (1% from primary culture) in fresh MHB and incubated till the exponential growth phase (Optical density, OD_{600nm}: ~0.6–0.7, i.e., 4 h post-inoculation) was achieved. Approximately 10⁷ cells (OD-based measurement) were harvested using centrifugation and washing with LC-MS grade cold water and kept at –80°C. The cell pellets were generated for 6 independent biological replicates. Since the cellular architecture and composition of member pathogens among a species are highly expected to be similar, a single strain of *S. aureus* was used for the study.

2.2. Bacterial metabolism quenching and extraction

For metabolite extraction, the stored cell pellet was thawed for 10 min on ice, followed by resuspension in 500 µl of mass spectrometry (MS) grade chilled methanol (Sigma). To evaluate the metabolites extraction efficiency of three extraction methods, i.e., FTC, SC, FTC + SC, 13C-labeled L-valine (40 ng/ml), an internal standard, was added to each sample before metabolite extraction (Kumar et al., 2022). For the freeze-thaw cycle-based metabolite extraction method, the resuspended cells were subjected to repeated freeze-thaw cycles (10 min at –80°C followed by 10 min on ice) three times. For the

sonication-based metabolite extraction method, the mixture was sonicated for 2 min at 35 A° (10-s on-and-off cycles). Similarly, for FTC + SC, the resuspended cell pellet was subjected to a freeze-thaw cycle three times and followed by a sonication cycle as described above. The sample mixture following FTC, SC, or FTC + SC methods was collected as supernatant after centrifugation at 12,500 RPM for 10 min (4°C), aliquoted and stored at −80°C till further analysis. The metabolites were extracted using each method (FTC, SC and FTC + SC) from 6 independent biological replicate samples.

2.3. Separation and quantitation of metabolites using ESI-LC–MS/MS

The standard workflow for metabolite separation and measurement using ESI-LC–MS/MS was as followed. An aliquot (100 µl) of the sample was vacuum dried and the pellet was resuspended in 3:17, methanol: water mixture (25 µl), followed by vortexing for 15 min, and 10 min centrifugation at 11000 rpm at 4°C. Data acquisition was done on C18 Reversed Phase HPLC Columns (C18) and Hydrophilic interaction LC (HILIC) columns with positive and negative mode separately. The collected metabolites were separated using C18 (HSS T3) and HILIC (XBridge BEH Amide) columns on UPLC ultimate 3,000 maintained at 40°C and 35°C temperature, respectively. A gradient of mobile phase A consisting of water +0.1% formic acid and mobile phase B (methanol +0.1% formic acid) was used as a mobile phase for the C18 column. For the HILIC column, 20 mM ammonium acetate in the water of pH 9.0 (mobile phase A) and 100% acetonitrile (mobile phase B) were used for separation. For separation in the reverse phase, a gradient of 1% mobile phase B to 99% mobile phase B over 14 min (flow rate of 0.3 ml/min) was set and for the HILIC column, 85% mobile phase B to 10% B over 16 min (flow rate of 0.35 ml/min) was used. 5 µl sample was injected into the column and for data acquisition. The Orbitrap Fusion Tribrid Mass Spectrometer (Thermo-Scientific) equipped with heated electrospray ionization (HESI) source was used for processing the sample using the following settings: 4000 positive mode spray voltage, 35,000 V for negative mode, 60–900 m/z mass range, AGC (Automatic gain control) was targeted at 100,000 ions. For data acquisition, 120,000 resolutions in MS1 mode and 30,000 resolutions in data-dependent MS2 scan mode were used. For MS, 50 ms was used as the maximum injection time while for MS/MS, an AGC target of 20,000 ions and a maximum injection time of 60 ms was used.

2.4. Metabolites identification and data analysis

The untargeted workflow of Progenesis QI software for metabolomics from Water Corporation was used at default settings for acquiring the data and its analysis. The MetaScope plugin of Progenesis QI metabolites was used for matching the mass, fragmented ions pattern and retention time of identified compounds with a list of 950 metabolites from our in-house library followed by an online spectral library search to confirm the identified metabolites. Peak detected in ≥4 replicates (out of 6 independent biological replicates) with intensity ≥100 (confidence interval >95%) receives an identification by spectral match. Further, ±1 min and 5 ppm retention time error for MS and

MS/MS with fragmentation pattern match were also considered as a criterion for identifying metabolites (Supplementary Table 1).

For data analysis, the list of identified metabolites in HILIC and C18 (both positive and negative mode) was combined, and duplicates were removed (Supplementary Table 2). MetaboAnalyst 5.0 was used for statistical and functional analysis like principal component analysis (PCA) and heat map analysis. Outlier intensities of metabolite(s) were excluded and the data were loaded in a matrix and statistical analysis was performed using peak intensities thereby using a statistical filter of interquartile range. Sample normalization was performed using “normalization by sum” methods followed by data transformation using log transformation (base 10) thereby scaling the data using Pareto scaling (mean-centered and divided by the square root of the standard deviation of each variable) (shown in MetaboAnalyst report, i.e., Supplementary Data sheet 3). Univariate analysis was performed using one-way analysis of variance (ANOVA) and post-hoc tests using a value of *p* (FDR) cutoff of ≤0.05. 2-D PCA was performed displaying 95% confidence regions to observe the inner clusters and find the apparent outliers. Hierarchical clustering heat maps were prepared using *t*-test/one-way ANOVA and Euclidean distance measure and Ward clustering method.

For quantitation, the peak intensity average of replicates for each metabolite extraction method (SC, FTC, and FTC + SC) was considered and used to identify differences among the extraction method. Chemical class-based analysis and functional categorization of metabolites were done using Metabolomics Workbench.¹

2.5. Identification of AMR-associated metabolites

A majority of antibiotics work by targeting cellular processes like (1) cell wall synthesis, (2) cell metabolism, (3) nucleotide biosynthesis and/or (4) protein synthesis. So, it is evident that establishing and identifying metabolites associated with these processes can help us in understanding the metabolic fingerprint and mechanism of antibiotic resistance. Therefore, a literature search to identify the role of each metabolite in nucleotide synthesis, protein synthesis, cell wall biosynthesis, cell proliferation (potential representative of resistant phenotypes as they can grow even in presence of selective pressure, i.e., antibiotics) and cell death (representative drug sensitive bacterial population) was performed using Google Scholar and PubMed and the resulting information was utilized to fetch the AMR-associated metabolites and followed by data interpretation.

3. Results

3.1. Identification of metabolites

Metabolites extracted from *S. aureus* using three methods, FTC, SC, and their combination FTC + SC, were separated using UPLC ultimate 3,000 (C18 and HILIC column), detected and quantified using an Orbitrap Fusion Mass Spectrometer and identified using the

¹ <https://www.metabolomicsworkbench.org/>

untargeted workflow of Progenesis QI software for metabolomics (Water Corporation). The list of identified non-polar and polar metabolites from the C18 and HILIC columns, respectively, was merged to get a collated list of metabolites extracted from each method-FTC, SC, and FTC+SC (Table 1).

The data of identified metabolites were subjected to PCA analysis to identify the distribution of the metabolomic profiles generated using FTC, SC and FTC+SC methods (Table 1). Noticeable differences between the three extraction protocols (3 distinct clusters) were observed indicating the characteristic fingerprint of each method (Figure 1A). The separation and clustering in PCA analysis also indicated the biasness of the individual method for different classes of metabolites and the quality of the sample generated for metabolomics experiments, respectively. Overall, a total of 116, 119, and 99 metabolites were identified using the FTC, SC, and FTC+SC methods of metabolite extraction, respectively, leading to the identification of 163 metabolites cumulatively (Tables 1, 2).

Overall, 62 metabolites were common among all three methods. FTC and SC yielded 25 common metabolites, 14 were common between FTC+SC and SC methods, and eight metabolites were identified by both FTC and FTC+SC methods (Figure 1B). Whereas 21 metabolites were uniquely identified in the FTC method followed by 18 unique metabolites by the sonication method, and only 15 unique metabolites by FTC+SC (Table 2).

3.2. Chemical classification of identified metabolites

All the metabolite extraction methods (FTC, SC, and FTC+SC) predominantly enabled the identification of different chemical classes of amino acids followed by saturated fatty acids and dicarboxylic acid [Figures 1–4 (Supplementary File-4)]. Similar pattern was observed in uniquely identified metabolites.

The dominant class of metabolites identified as amino acids (29% by FTC and 27% by SC and FTC+SC) followed by saturated fatty acids. Interestingly, the class “Naphthalene carboxylic acid” was uniquely identified in the FTC+SC method only (Figure 2). However, uniquely identified metabolites from individual methods showed biases toward specific chemical classes/subclass of metabolites (Figure 2).

3.3. Differential abundance of identified metabolites from FTC, SC, and FTC+SC method

The difference in intensity of metabolites was observed with different methods of extraction (Figure 3 and Supplementary Figure 5).

A few metabolites were observed to be more intense in a specific method compared to others (Figure 4). For example, Alloisoleucine, nonanoate, palmitoleate, leucine, sucrose, tyrosine, glutamate, and prolylleucine were more abundant in the FTC method. Fucose, risperidone, hexazinone, and isoleucine were found to be more abundant in the SC method. Decanoate, succinate, leucylproline, and melibiose were found to be higher in intensity in FTC+SC. A few metabolites were identified by two methods. For example, maltose, suberate, pentadecanoic acid, palmitoleic acid, arachidate, fipronil, adenosine, and urocanate were more abundant in FTC and SC. Phenylalanine, pyruvic acid, sebacic acid, arabinose, palatinose, fumaric acid, laurate, palmitic acid, and serine were found to be more abundant in FTC+SC and SC methods. Guanine, azelaic acid, linoleate, adenine, and uracil were highly abundant in FTC and FTC+SC methods. Whereas a few metabolites like carnitine and glucose were identified by all three methods. This altogether indicates the biasness of metabolite extraction methods toward particular metabolite(s).

3.4. AMR-associated metabolites

Out of 163, a total of 69 metabolites were found to be related with AMR-associated phenotypes (cell proliferation and cell death) (Table 3). Of these, 57, 54, and 40 AMR-associated metabolites were found in metabolite samples extracted from FTC, SC or FTC+SC method, whereas 12, 7, and 2 were unique to each method (Table 3).

4. Discussion

Infections caused by Gram-positive bacteria have become a serious public health threat causing high morbidity and mortality (Jubeh et al., 2020). Limited treatment options and rapid development of resistance to even the last-line antibiotics is the main reason for deaths, especially in the case of *S. aureus* (MRSA infections) (Chambers and Deleo, 2009; Alos, 2015). Besides enormous efforts, very few has been discovered over the last few decades, and this necessitates identifying new strategies to combat the emerging problem of AMR (WHO, 2020). Thus, understanding the molecular changes driving AMR among *S. aureus* becomes very important. Metabolomics can decode the real biochemical state of any organism and help in analyzing the emergence and/or spread of AMR phenomena (Pinu et al., 2019). To date metabolomics has been employed to identify new metabolic pathways (Deng et al., 2020), identification of bacterial species/strains (Zhang and Zhu, 2022), study the influence of external factors on bacteria (Tang, 2011), and

TABLE 1 Number of identified metabolites with respect to different metabolite extraction methods and chromatographic surfaces (polar/non-polar).

Metabolite extraction method	Total metabolites identified from C18	Total metabolites identified from HILIC	Common among C18 and HILIC	Total metabolites
FTC	71	55	10	116
SC	68	61	10	119
FTC+SC	49	54	4	99
Total	188	171	24	335

The table contains all metabolites data, overlapping/similar metabolites were not removed while preparing this table.

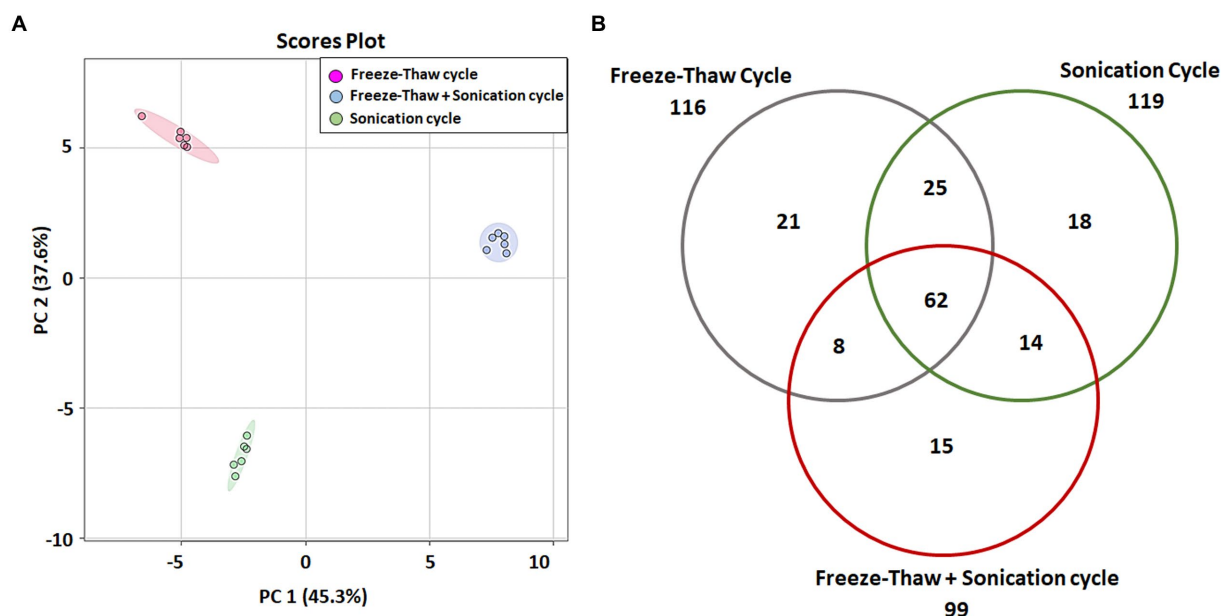


FIGURE 1

Multi-variate analysis of identified metabolites. (A) Principal component analysis (PCA) showing score plots of the metabolic differences between 3 methods (consisting a total 6 independent biological replicates for each method), red: freeze-thaw Cycle (FTC), green: Sonication Cycle (SC), blue: freeze-thaw Cycle followed by Sonication Cycle (FTC+SC). All three methods clustered distinctly having replicates of each method together indicating the consistency of sample preparation and downstream analysis. (B) Venn diagram representing unique and common metabolites among the three different methods of metabolite extraction [freeze-thaw cycle (FTC), Sonication Cycle (SC) and freeze-thaw cycle followed by Sonication Cycle (FTC+SC)]. A total of 62 metabolites were common among all 3 methods, whereas 21, 18, and 15 were uniquely identified in FTC, SC, and FTC+SC, respectively, indicating the potential biasness of the individual methods. Data from $n \geq 4$ (out of six independent biological replicates were used in this analysis). One-way ANOVA was used to select the significant metabolites, i.e., 163 total metabolites (cutoff value of $p \leq 0.05$) for the analysis.

in some cases reported to be of diagnostic use to detect bacterial infections (Fernández-García et al., 2018). However, so far, very few studies and efforts have been made to understand the spread and/or emergence of AMR and this may be primarily due to the unavailability of appropriate protocols and pipelines for investigating global and AMR-associated metabolites. As of now, even the performance of existing protocols for extracting AMR-associated intracellular metabolites from Gram-positive pathogen, *S. aureus*, are not established and hence the optimal method for the purpose remains unknown.

4.1. Analysis of metabolite extraction method and identified metabolites

The metabolites were extracted from *S. aureus* (gentamicin and methicillin resistant) using the two most commonly used protocols, i.e., FTC, and SC, alone and in the combination [FTC followed by SC (FTC+SC)] and identified using ESI-LC-MS/MS (Orbitrap Fusion Tribrid Mass Analyzer), a highly sensitive and advanced mass-spectrometer to potentially achieve increased metabolomic coverage. Further, we have used 2 different Liquid Chromatography (LC) columns, i.e., HILIC and C18 which are specific for separating compounds with different physico-chemical properties were also used. Generally, HILIC columns are very well known for separating polar amino acids, organic acids, sugars, phosphorylated sugars, nucleobases, nucleotides, phosphorylated metabolites, hydrophilic vitamins, and coenzymes (Galeano Garcia et al., 2019). C18 columns

are usually employed to separate semi-polar and non-polar compounds like alkaloids, flavonoids, phenolic acids, and other glycosylated species (Liu et al., 2019). Data analysis from individual LC columns (HILIC and C18) revealed that C18 enabled a higher number of metabolite identification compared to HILIC among all the metabolite extraction methods used (Table 1). This may potentially be because of poor retention of very polar metabolites during chromatographic separation and hence is in line with published literature (Harrieder et al., 2022). Only a few metabolites were common among the metabolites identified using C18 and HILIC columns. A total of 163 metabolites were cumulatively identified using all chromatographic surfaces and extraction methods. The SC method showed the highest number of metabolites though comparable with FTC among the total identified metabolites (116 by FTC and 119 by SC out of a total of 163 metabolites). The most likely reason for low yield in FTC+SC methods might be the degradation of already extracted metabolites during sonication. Among 163 metabolites, 21, 18, and 15 were uniquely identified in FTC, SC, and FTC+SC methods indicating the potential bias of the method toward specific metabolite(s) (Table 2). Chemical class-based functional categorization and analysis revealed that amino acids were the major chemical class of metabolites identified by all methods. The FTC method was observed to be more biased toward saturated fatty acids (17%), and disaccharides (17%) (Supplementary Figure 2). The SC method showed biasness toward hexoses (2%), C24 bile acids (2%), and pyrimidines (3%) (Supplementary Figure 3). Disruption of the peptidoglycan layer (mesh-like network of amino acids and sugar) during metabolite extraction might be the possible reason for yielding

TABLE 2 List of identified metabolites specific to metabolite extraction protocols (FTC, SC, and FTC+SC) as well as commonly identified metabolites among all methods.

Common metabolites						Freeze thaw		Sonication		Freeze thaw+sonication	
S. no	Metabolite name	S. no	Metabolite name	S. no	Metabolite name	S. no	Metabolite name	S. no	Metabolite name	S. no	Metabolite name
1	1-(Carboxymethyl) cyclohexanecarboxylic Acid	22	Dipentyl phthalate	43	N-acetylmethionine	1	3-methyladenine	1	2-Hydroxy-4-methylpentanoic acid	1	16-Hydroxyhexadecanoic acid
2	1-Phenyl-2-butanone	23	Diphenylamine	44	N-acetylserine	2	3-Phosphoglyceric acid	2	Tetrahydroxy-5- α -pregnan-20-one 3,21-diacetate	2	1-Hydroxy-2-naphthoate
3	2'-Deoxyuridine 5'-mono-phosphate	24	Elaidate	45	Nad	3	Abietic acid	3	3-Oxochohic acid	3	3-Hydroxy-3-methylglutaric acid
4	2-Methyl-S-benzothiazole	25	Ethyl paraben	46	N- α -acetyl-L-lysine	4	Alanine	4	4-[[3-(Diethylamino)propyl]amino]-4-oxobut-2-enoic acid	4	3-Hydroxypropanoic acid
5	2-Naphthalenesulfonic acid	26	Glucose	47	N-Epsilon-acetyllysine	5	Alloisoleucine	5	Acetylenedicarboxylic acid	5	Decanoate
6	3-Hydroxyphenylacetic acid	27	Glutamic acid	48	Norvaline	6	Azelate	6	Adipic acid	6	Erythronolactone
7	3-Tert-Butyladipic acid	28	Glutamine	49	Oleamide	7	Erucate	7	Dihydrouracil	7	Leucylproline
8	6-Carboxyhexanoate	29	Glyceraldehyde	50	O-phosphoserine	8	Glutamate	8	Ethylmethylacetic acid	8	Lithocholyltaurine
9	Ab-chminaca metabolite M6	30	Glyceric acid	51	Penbutolol	9	Leucine	9	Isoleucine	9	Melibiose
10	Adenine	31	Guanine	52	Phosphonoacetate	10	Mag	10	Linoleic acid	10	N-acetylaspartate
11	Adenosine monophosphate	32	Heptadecanoate	53	Phthalic acid	11	Methyl jasmonate	11	Melatonin	11	Peg N12
12	Alpha-lactose	33	Homoserine	54	Pyroglutamate	12	Nonanoate	12	N-acetyl-Dl-methionine	12	Suberic acid
13	Aspartate	34	Hydrochlorothiazide	55	Ribose	13	Palmitoleate	13	N- α -acetyl-L-asparagine	13	Succinate
14	Aspartic acid	35	Lactic acid	56	Salicylic acid	14	Peg N10	14	Peg N8	14	Triphenylphosphine oxide
15	Benzophenone	36	Malic acid	57	Serine	15	Pge2	15	P-toluenesulfonic acid		
16	Betaine	37	Myristate	58	Stearate	16	Prolylleucine	16	Risperidone		
17	Bmpea	38	N-(4-methoxy-5-morpholino-2-nitrophenyl)-N-(2-pyridyl)amine	59	Suberate	17	Stearic acid	17	Tartrate		
18	Carnitine	39	N-acetylaspartic acid	60	Uracil	18	Sucrose	18	Taurodeoxycholic acid		
19	Citroflex A-4	40	N-acetylhistidine	61	Uridine-5-monophosphate	19	Trehalose				
20	Dibutyl maleate	41	N-acetyl-L-aspartic acid	62	Urocanic acid	20	Tyrosine				
21	Dihydrosphingosine	42	N-acetyl-L-glutamine			21	Uridine 5'-diphospho-N-acetylglucosamine				

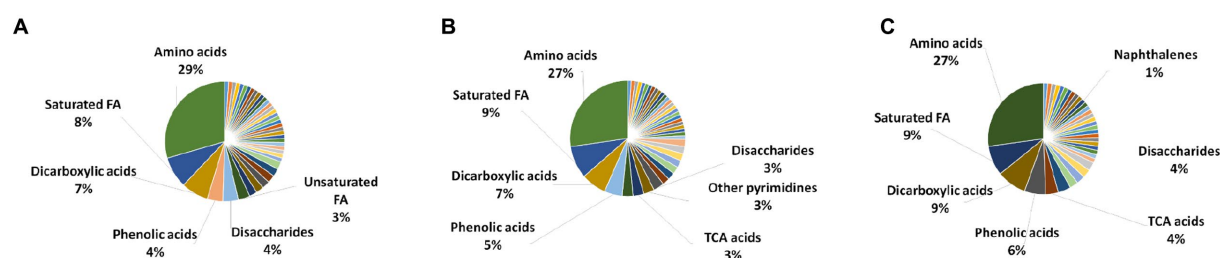


FIGURE 2

Chemical class analysis of identified metabolites. Pie-Chart of metabolite chemical class composition, identified using three different metabolite extraction methods $n \geq 4$ (out of 6 independent experiments, selected using one-way ANOVA test with cutoff value of $p \leq 0.05$) biological replicates were utilized to analyze the chemical class distribution. (A) freeze-thaw Cycle; (B) sonication Cycle; and (C) freeze-thaw Cycle followed by Sonication Cycle. The major metabolite class identified using each method was amino acids, followed by saturated fatty acids, dicarboxylic acids and phenolic acids (only major classes are shown in the figure). FA, fatty acids; TCA acids, trichloroacetic acids.

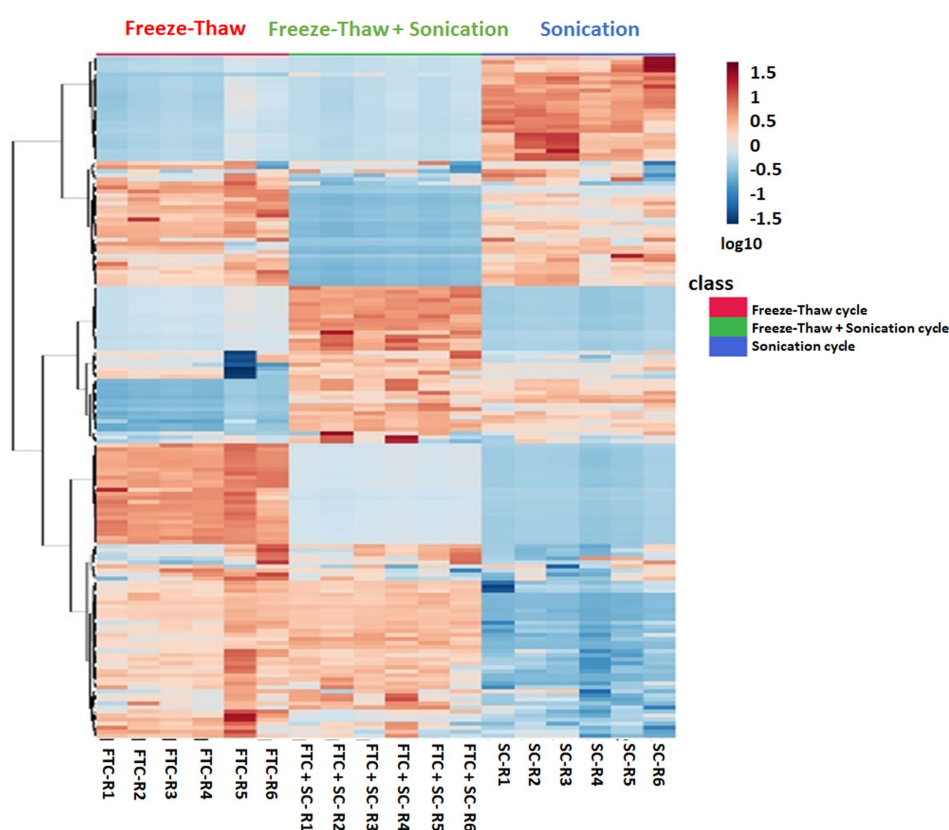


FIGURE 3

Heatmap profile depicting the relative expression levels of 163 metabolites (selected using one-way ANOVA test with cutoff value of $p \leq 0.05$) from all three different extraction methods, i.e., freeze-thaw Cycle (FTC), Sonication Cycle (SC) and freeze-thaw Cycle followed by Sonication Cycle (FTC+SC) as indicated. Each column represents a specific biological replicates sample and row represent the metabolite. The raw intensities of metabolites from $n \geq 4$ (from six independent biological replicates) were parsed by Pareto scaling (mean-centered and divided by the square root of the standard deviation of each variable) and rendered using the MetaboAnalyst 5.0 software. The clustering of the rows is based on Euclidean distance measure and Ward clustering method. A few metabolite clusters were observed to be more intensely expressed (indicated by Red) in a specific method compared to others showing biasness of the method(s). The information of the members in these clusters was utilized to explore their AMR-related biological function. The color is representing \log_{10} transformed metabolite intensities (red: highest; blue: lowest).

a high number of amino acids, dipeptides, sugar derivatives like hexoses, disaccharides, and sugar acids (Vollmer et al., 2008). However, a combination of FTC + SC methods showed an enrichment of hydroxy fatty acids (28%) (Supplementary Figure 4). This altogether indicates the potential bias of each method for investigating specific

metabolites or classes of metabolites. Therefore, the method of metabolite extraction shall primarily be chosen based on the specific metabolite(s) of interest or classes of metabolites. A few attempts have been made by researchers to establish the metabolome of this clinically relevant Gram-positive pathogen, *S. aureus*. Recently, 109 metabolites

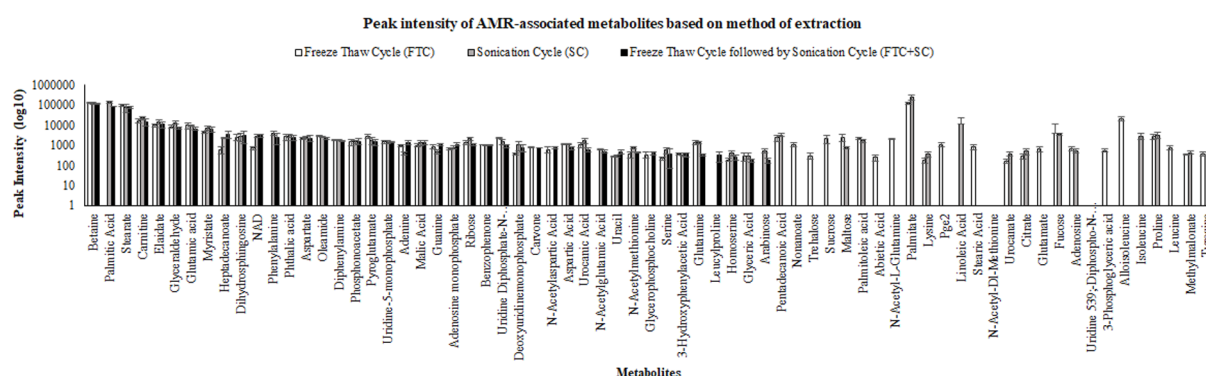


FIGURE 4

Pictorial representation of peak intensities of identified metabolites (selected using one-way ANOVA, means \pm SD, with cutoff value of $p \leq 0.05$) using three different metabolite extraction methods (FTC, SC and FTC+SC). The data represents the metabolites (intensity) from the $n \geq 4$ (out of six independent biological replicate-Supplementary Table 1) samples. FTC, freeze-thaw cycle; SC, sonication cycle; FTC+SC, freeze-thaw cycle followed by sonication cycle.

(RN450) and 107 (450M) metabolites were identified using cold methanol and vortexing (vigorously for ~ 1 min) based metabolite extraction method with HPLC coupled with a TSQ Quantiva Triple Quadrupole mass spectrometer in (methicillin-resistant *S. aureus*) MRSA and (methicillin sensitive *S. aureus*) MSSA strains, respectively, after exposure to a sublethal dose of antibiotic (ampicillin, kanamycin, norfloxacin) (Schelli et al., 2017). However, the number of identified metabolites was low compared to our study potentially due to the use of only the HILIC column, one extraction method, i.e., vortexing (instead of freeze-thaw and vortexing or sonication) and the low-sensitive equipment (Schelli et al., 2017). Another attempt to differentiate MSSA and MRSA biofilm and planktonic phenotypes using an (Nuclear magnetic resonance spectroscopy) NMR-based metabolomics study has been reported. They have identified a total of 120 metabolites (Ammons et al., 2014). Although the reason for identifying a lower number of metabolites in this study might be because of the technology used, NMR is already known to be less sensitive than ESI-LC-MS/MS (Ammons et al., 2014). Among them, 19 and 26 common metabolites were identified when compared to our study, respectively, (Table 4 and Figure 5) (Ammons et al., 2014; Schelli et al., 2017). Similarly, a total of 173 metabolites were identified in MRSA and MSSA using a combination of hydrophilic interaction liquid chromatography and PFP columns (pentafluorophenyl-propyl) coupled with high-resolution mass spectrometry (Aros-Calt et al., 2019). The possible reason for yielding a higher number of metabolites in comparison to our study may be due to a bigger library size compared to our in-house library (~ 950 metabolites). Notably, none of the above-discussed studies have mentioned the identified AMR-associated metabolites.

4.2. Analysis of AMR-associated metabolites

Of the identified 163 metabolites, 69 (42.0%) were observed to be associated with AMR in published literature (Table 3). Among these, the majority of identified AMR-associated metabolites were primarily linked with cell wall biosynthesis (52.1%), followed by cellular metabolism (14.4%), nucleotide biosynthesis (11.5%), and

protein synthesis (21.7%) indicating the potential bias of the method of metabolite extraction or the technique. A comparison of identified AMR-associated metabolites list with previously reported study has shown only 16 and 19 common metabolites (Table 4) (Ammons et al., 2014; Schelli et al., 2017). Interestingly, the FTC method yielded a slightly higher number of AMR-associated metabolites (57 metabolites) compared to SC (54 metabolites) with 42 commonly identified metabolites. Whereas only 40 AMR-associated metabolites were identified using the FTC+SC method potentially due to the degradation of extracted metabolites (after FTC) during sonication. This altogether indicates the suitability of both the methods, FTC or SC, for investigating AMR-associated metabolites in *S. aureus* and Gram-positive pathogens; however, the metabolite of interest shall be key in choosing the method for metabolite extraction.

4.3. Analysis of metabolite extraction methods between Gram-positive pathogen, *Staphylococcus aureus* and Gram-negative pathogen, *Klebsiella pneumoniae*

In this investigation, the maximum number of metabolites from *S. aureus* were identified using SC (119 metabolites) and subsequently by FTC (116 metabolites) and FTC+SC (99 metabolites). Whereas for *K. pneumoniae*, the maximum number of metabolites were identified by the FTC (151) method followed by FTC+SC (132 metabolites) and SC (103 metabolites; Supplementary Table 2) (Kumar et al., 2022). Notably, the number of metabolites identified in *K. pneumoniae* was more when compared to *S. aureus* and the potential reason remains unknown. Among these, only a few metabolites were commonly identified between *S. aureus* and *K. pneumoniae* (26 by FTC, 45 by SC and 31 by FTC+SC). A similar pattern was observed in AMR-associated metabolites. This supports that the metabolomic architecture and AMR-associated metabolites among *S. aureus* (a Gram-positive pathogen) may be different than the *K. pneumoniae* (a Gram-negative pathogen). This also suggests that the optimal method for extracting metabolites from Gram-positive pathogens may be different than the method for Gram-negative pathogens.

TABLE 3 Comparative overview of identified antimicrobial resistance (AMR)-associated metabolites among three different methods of metabolite extraction used in the study.

Peak intensity of AMR-associated metabolites and method of detection						
S. no.	Cell wall biosynthesis	Bacterial strain and species	FTC (Intensity±standard deviation)	SC (Intensity±standard deviation)	FTC+SC (Intensity±standard deviation)	References
1	Pentadecanoic Acid	<i>Actinomycetes</i>	2,347 ± 849	3195.2 ± 602.5	-	Kumari et al. (2022)
2	Carnitine	<i>Escherichia coli</i>	16756.2 ± 3614.4	21936.2 ± 3016.3	14811.4 ± 5519.2	Eichler et al. (1996)
3	Phthalic acid	<i>Staphylococcus arlettae</i>	2709.1 ± 907.8	2901.3 ± 519	2382.4 ± 586	Acharyya et al. (2021)
4	Nonanoate	<i>Escherichia coli</i>	1076.4 ± 210.8	-	-	Lee et al. (2022)
5	Stearate	<i>Actinobacteria</i>	94998.9 ± 10206.5	77041.9 ± 35251.8	74,741 ± 10727.8	Tan et al. (2022)
6	Benzophenone	<i>Rhizobium</i>	1062.1 ± 51.5	1040.6 ± 48.1	1050.8 ± 69.4	Zhang et al. (2022)
7	Betaine	<i>Listeria monocytogenes</i>	125,016 ± 6628.1	124601.5 ± 11719.1	113966.6 ± 6,515	Whiteley et al. (2017)
8	Oleamide	<i>Pseudomonas aeruginosa</i>	2824.6 ± 98.3	2666.7 ± 212.2	2219.3 ± 210.5	Pyke (2022)
9	Trehalose	<i>Selaginella lepidophylla</i>	291.2 ± 97.4	-	-	Vanaporn and Titball (2020)
10	Sucrose	<i>Klebsiella pneumoniae</i>	2119.8 ± 923.8	-	-	Kumar et al. (2011)
11	Maltose	<i>Vibrio alginolyticus</i>	2505.4 ± 944.7	764.6 ± 113.8	-	Jiang et al. (2020)
12	Palmitoleic acid	<i>Mycobacterium tuberculosis</i>	2222.2 ± 239.6	1694.5 ± 307.5	-	Morris et al. (2005)
13	Uridine-5-monophosphate	<i>Pseudomonas aeruginosa</i>	1425.2 ± 212	1388.5 ± 239.1	1433.6 ± 81.9	Niu and Tan (2015)
14	Heptadecanoate	<i>Klebsiella pneumoniae</i>	618.1 ± 232.2	2260.7 ± 189.2	3408.2 ± 1251.1	Kumar et al. (2022)
15	Abietic Acid	<i>Streptococcus mutans</i>	248 ± 84.3	-	-	Ito et al. (2020)
16	Aspartic Acid	<i>Streptococcus faecalis</i> ATCC 9790	1116.5 ± 118.1	1126.7 ± 107	706.3 ± 125.8	Rahmanian et al. (1971)
17	Malic Acid	<i>Aeromonas hydrophila</i>	995.2 ± 147.4	1274.5 ± 363.4	1369.5 ± 276.3	Yao et al. (2016)
18	Dihydrospingosine	<i>Porphyromonas gingivalis</i>	2520.4 ± 744.8	2611.6 ± 1170.9	3130.8 ± 1997	Ranjit et al. (2022)
19	Diphenylamine	<i>Bacillus licheniformis</i> , <i>Bacillus subtilis</i>	1731.9 ± 123.6	1826.2 ± 166.7	1594.6 ± 94	Salton and Schmitt (1967)
20	Elaidate	<i>Escherichia coli</i> and <i>Klebsiella pneumoniae</i>	9651.2 ± 1323.1	14,726 ± 3837.2	10965.1 ± 4004.4	Stahl et al. (2020)
21	Carvone	<i>Hafnia alvei</i>	779.6 ± 23.8	-	754.7 ± 30.6	Li et al. (2018)
22	Myristate	<i>Escherichia coli</i>	4434.1 ± 436.6	7039.8 ± 1414.1	6271.2 ± 1988.9	Somerville et al. (1996)
23	N-Acetylaspartic Acid	<i>Clostridium acetobutylicum</i>	618.1 ± 185.5	728.1 ± 80.1	719.4 ± 84.7	Reith et al. (2011)
24	N-Acetyl-L-Glutamine	<i>Escherichia coli</i>	2064.4 ± 122.4	-	-	Konopka (2012)

(Continued)

TABLE 3 (Continued)

Peak intensity of AMR-associated metabolites and method of detection						
S. no.	Cell wall biosynthesis	Bacterial strain and species	FTC (Intensity±standard deviation)	SC (Intensity±standard deviation)	FTC+SC (Intensity±standard deviation)	References
25	N-Acetylmethionine	<i>Escherichia coli</i>	345.2±119.9	739.2±55.4	451.4±34.1	Viola et al. (2015)
26	Phosphonoacetate	<i>Pseudomonas fluorescens</i>	1423.2±449	1464.8±231	1560.7±488.6	Kulakova et al. (2001)
27	Palmitic Acid	<i>Xanthomonas oryzae</i>	-	131,350±12548.4	84982.3±3847.9	Wang et al. (2021)
28	Palmitate	<i>Vibrio alginolyticus</i>	117837.2±10,837	229951.2±64518.4	-	Liu et al. (2019)
29	Aspartate	<i>Aeromonas hydrophila</i>	2142.3±154.8	2472.7±253.8	2237.4±660.6	Zhao et al. (2018)
30	Lysine	<i>Thermotoga maritima</i> , <i>Escherichia coli</i>	172.9±42.8	376.8±110.7	-	Serganov et al. (2008)
31	Pge2	<i>Staphylococcus aureus</i>	1,066±257.1	-	-	Wang et al. (2017)
32	Linoleic Acid	<i>Staphylococcus aureus</i>	-	11023.3±11921.9	-	Antti et al. (2013)
33	Stearic Acid	<i>Vibrio</i> spp.	824.6±213.6	-	-	Liu et al. (2019)
34	N-Acetyl-DL-Methionine	<i>Escherichia coli</i>	-	530.2±139.05	-	Usuda and Kurahashi (2005)
35	N-Acetylglutamic Acid	<i>Pseudomonas chlororaphis</i> O6	-	619.1±53.9	483±87.4	Park et al. (2018)
36	Uridine Diphosphate-N-Acetylglucosamine	<i>Corynebacterium glutamicum</i>	2239.6±203.3	1523.1±440.3	902.1±143	Gauttam et al. (2021)
	Total		31	29	23	
Cellular metabolism						
37	Urocanate	<i>Pseudomonas aeruginosa</i>	168.8±38.8	374.3±95.7	-	Zhang et al. (2014)
38	Urocanic Acid	<i>Pseudomonas aeruginosa</i>	1092.1±306.8	1677.2±419.6	584.9±119.5	Zhang et al. (2014)
39	Arabinose	<i>Mycobacterium tuberculosis</i>	-	520.8±112.2	174±51.3	Wolucka (2008)
40	Citrate	<i>Streptococcus diacetilactis</i>	280±77.3	514.4±179.7	-	Harvey and Collins (1963)
41	Glutamate	<i>Listeria monocytogenes</i>	646.1±203.6	-	-	Feehily and Karatzas (2013)
42	Glutamine	<i>Salmonella</i>	1331.2±303.9	1306.5±162.6	336.7±38.6	Yong et al. (2021)
43	Glyceric Acid	<i>Staphylococcus aureus</i> and <i>Pseudomonas aeruginosa</i>	277.9±117.8	303.3±92.7	175.8±38.4	Thomas et al. (2016)
44	Leucylproline	<i>Bifidobacterium bifidum</i>	-	-	314±175.9	Berg et al. (2015)
45	Fucose	<i>Klebsiella pneumoniae</i>	3968.6±7013.9	3495.5±511.1	-	Hudson (2022)

(Continued)

TABLE 3 (Continued)

Peak intensity of AMR-associated metabolites and method of detection						
S. no.	Cell wall biosynthesis	Bacterial strain and species	FTC (Intensity±standard deviation)	SC (Intensity±standard deviation)	FTC+SC (Intensity±standard deviation)	References
46	Glyceraldehyde	<i>Stenotrophomonas maltophilia</i>	8322.3 ± 1120.3	13281.7 ± 2500.2	6,880 ± 984.1	Gil-Gil et al. (2022)
	Total		6	8	6	
Nucleotide metabolism						
47	Adenosine	<i>Vibrio splendidus</i>	693 ± 154.7	530 ± 120.6	-	Li et al. (2023)
48	Ribose	<i>Staphylococcus aureus</i>	1413.4 ± 299.8	2034.2 ± 296.8	1068.7 ± 152.4	Baysarowich et al. (2008)
49	Adenine	<i>Escherichia coli</i>	933.4 ± 90.3	407 ± 70	1420.3 ± 346.2	Holt et al. (2017)
50	Adenosine monophosphate	<i>Salmonella enterica</i>	692 ± 81.8	786.2 ± 110.7	1086.6 ± 196	Pontes and Groisman (2019)
51	Guanine	<i>Staphylococcus aureus</i>	880.3 ± 227.9	487.4 ± 100.3	1099.8 ± 110.8	Dersch et al. (2017)
52	Uracil	Methicillin-resistant <i>Staphylococcus aureus</i> (MRSA)	281.8 ± 23.9	285.3 ± 36.5	476 ± 88.9	Fan et al. (2023)
53	Uridine 539;-Diphospho-N-Acetylglucosamine	<i>Bacillus subtilis</i>	2239.6 ± 203.3	-	-	Patel et al. (2023)
54	Deoxyuridine monophosphate	<i>Escherichia coli</i>	371.1 ± 54.3	1016.1 ± 482.1	772.9 ± 317.2	Zampieri et al. (2017)
	Total		7	7	5	
Protein synthesis						
55	3-Phosphoglyceric acid	<i>Aeromonas caviae</i>	549.7 ± 96.2	-	-	Wang et al. (2023)
56	Glutamic acid	<i>Pseudomonas chlororaphis</i> O6	9577.1 ± 3,662	9769.6 ± 613.1	6497.5 ± 986.6	Park et al. (2018)
57	Alloisoleucine	<i>Clostridioides difficile</i>	20562.5 ± 4961.2	-	-	Robinson et al. (2019)
58	Isoleucine	<i>Edwardsiella piscicida</i>	-	2854.6 ± 951.3	-	Ye et al. (2018)
59	NAD	<i>Chromobacterium</i>	725 ± 147.2	2858.6 ± 494.9	2939.5 ± 412.2	Banerjee et al. (2017)
60	Proline	<i>Escherichia coli</i>	2674.8 ± 664.2	3196.7 ± 1046.7	-	Lin et al. (2019)
61	Leucine	<i>Edwardsiella piscicida</i>	737.4 ± 173.2	-	-	Ye et al. (2018)
62	3-Hydroxyphenylacetic Acid	<i>Pseudomonas aeruginosa</i>	360.5 ± 32.6	336.8 ± 54.9	346.3 ± 83.1	Pahalagedara et al. (2020)
63	Glycerophosphocholine	<i>Klebsiella pneumoniae</i> and <i>Mycoplasma</i>	339.6 ± 116.6	-	397 ± 77	Low et al. (2018)
64	Homoserine	<i>Variovorax paradoxus</i>	189.9 ± 39.3	402.8 ± 99.8	250.3 ± 78.4	Leadbetter and Greenberg (2000)
65	Methylmalonate	<i>Pseudomonas aeruginosa</i>	337.1 ± 29.1	436.1 ± 64.8	-	Su et al. (2010)

(Continued)

TABLE 3 (Continued)

S. no.	Peak intensity of AMR-associated metabolites and method of detection					References
	Cell wall biosynthesis	Bacterial strain and species	FTC (Intensity±standard deviation)	SC (Intensity±standard deviation)	FTC+SC (Intensity±standard deviation)	
66	Pyroglutamate	<i>Saccharolobus solfataricus</i>	2748.9 ± 612.7	1738.5 ± 646.1	1,441 ± 537.4	Vetter et al. (2019)
67	Serine	<i>Edwardsiella piscicida</i>	215.4 ± 43.3	558.1 ± 178	352.5 ± 283.6	Ye et al. (2018)
68	Tyrosine	<i>Porphyromonas gingivalis</i>	367.2 ± 85	-	-	Whitmore and Lamont (2012)
69	Phenylalanine	<i>Escherichia coli</i> and <i>Pseudomonas putida</i>	-	3985.3 ± 1032.4	2567.6 ± 1449.6	Teufel et al. (2010)
	Total		13	10	8	

Shaded cells show the maximum intensity yielding method for each metabolite, —symbol shows metabolite not identified, (metabolite intensity data from $n \geq 4$ out of six independent biological replicates) was considered while preparing this table. Supporting (raw data) data is available in (Supplementary Table 1).

5. Conclusion

The increasing emergence of AMR among Gram-positive pathogens such as *S. aureus* is becoming a global health concern and urgently demands strategies to control it. Understanding the metabolomic footprint of antibiotic-resistant/sensitive pathogens has been shown to improve our understanding of the emergence/spread of AMR superbugs. However, very few efforts have been made in this direction possible due to the lack of appropriate methods of metabolite extraction.

Therefore, in this investigation, we have compared the performance of the two most common methods, i.e., FTC and SC alone and in combination (FTC+SC), for extracting metabolites from *S. aureus* (gentamicin and methicillin-resistant) using a highly sensitive and advanced HPLC-coupled mass-spectrometer (ESI-LC-MS/MS). The SC and FTC methods were observed to identify a comparable number of total metabolites as well as AMR-associated metabolites and hence may be utilized for investigating the metabolome of *S. aureus* or other Gram-positive bacteria after further validation. FTC+SC gave a lower yield of metabolites possible due to the degradation of already extracted metabolites by FTC during sonication. The methods of metabolite extraction were also observed to have biasness toward specific metabolite(s) or class of metabolites (“Tryptamines” was unique to the SC method, “C20 isoprenoids and Jasmonic acids” were unique to FTC, and “Naphthalenes” were unique to FTC+SC method) and hence can potentially impact the overall finding of the metabolomics-based studies. Therefore, the method of metabolite extraction shall be primarily chosen based on the metabolites of interest in the investigation. Altogether, our data can help in designing/planning pathway specific/directed metabolomics studies which could improve understanding of the emergence/spread of AMR superbugs and ultimately contribute to improving the efficacy of existing antimicrobial therapies.

Data availability statement

The datasets presented in this study can be found in online repositories (MetaboLights study identifier-MTBLS7338). The names of the repository/repositories and accession number(s) can be found in the article/Supplementary material.

Author contributions

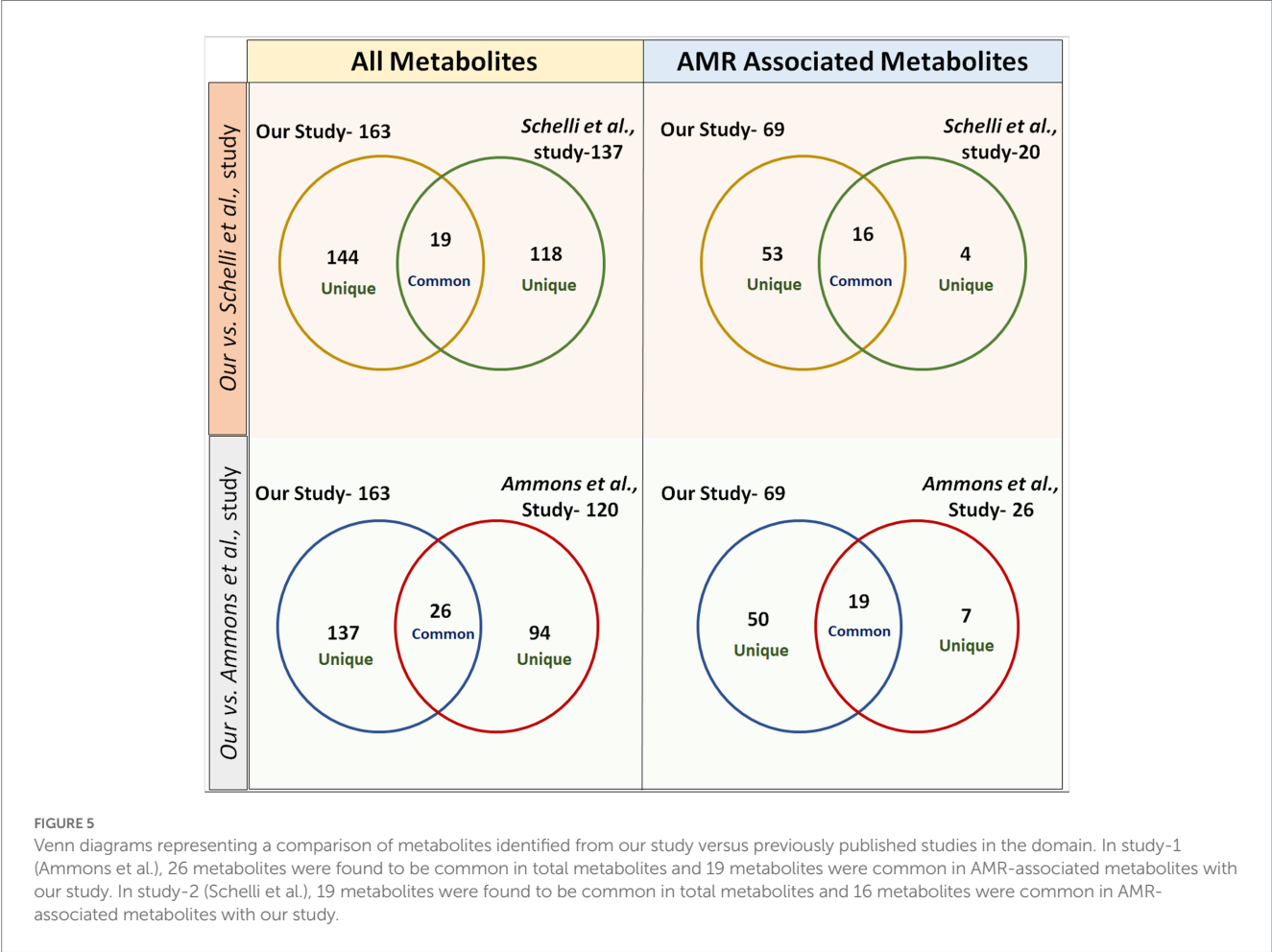
NK conceived, designed, and coordinated the study. SK and MK generated the study material. AK and YK performed most of the experiments. RS, LT, AK SK, YK, and NK performed the data analysis. LT, RS, and SR wrote the manuscript. NK and YK supervised the manuscript writing and revisions. All authors contributed to the article and approved the submitted version.

Funding

This work was supported by grants awarded to NK from the Indian Council of Medical Research Govt. of India (Grant No. AMR/Adhoc/233/2020-ECD-II) and Translational Health Science and Technology Institute Faridabad, India. RS received Senior Research Fellowship from the Council of Scientific and Industrial Research,

TABLE 4 Comparison of metabolites [total and antimicrobial resistance (AMR) associated] identified from our study versus other reported studies.

All metabolites				
Total metabolites identified in Schelli et al. study Schelli et al. (2017)	Common metabolites identified in Schelli et al. versus our study	Total metabolites identified in our study	Common metabolites identified in Ammons et al. versus our study	Total metabolites identified in Ammons et al. study Ammons et al. (2014)
137	19	163	26	120
AMR associated metabolites				
20	16	69	19	26



Govt. of India, and SS and LT received Junior Research Fellowship from the Department of Biotechnology, Govt. of India.

Acknowledgments

We are grateful to Pramod Kumar Garg (Executive Director) and M. V. Santo (Head Administration) of Translational Health Science and Technology Institute Faridabad, India, for providing administrative support.

Conflict of interest

The authors declare that the research was conducted in the absence of any commercial or financial relationships that could be construed as a potential conflict of interest.

Publisher’s note

All claims expressed in this article are solely those of the authors and do not necessarily represent those of their affiliated organizations, or those of the publisher, the editors and the reviewers. Any product that may be evaluated in this article, or claim that may be made by its manufacturer, is not guaranteed or endorsed by the publisher.

Supplementary material

The Supplementary material for this article can be found online at: <https://www.frontiersin.org/articles/10.3389/fmicb.2023.1152162/full#supplementary-material>

References

- Acharyya, S., Saha, S., Majumder, S., and Bhattacharya, M. (2021). Characterization of a mercury tolerant strain of staphylococcus arletiae from Darjeeling hills with an account of its antibiotic resistance pattern and metabolome. *Arch. Microbiol.* 203, 5745–5754. doi: 10.1007/s00203-021-02563-5
- Alos, J. I. (2015). Antibiotic resistance: A global crisis. *Enferm. Infecc. Microbiol. Clin.* 33, 692–699. doi: 10.1016/j.eimc.2014.10.004
- Ammons, M. C., Tripet, B. P., Carlson, R. P., Kirker, K. R., Gross, M. A., Stanisch, J. J., et al. (2014). Quantitative NMR metabolite profiling of methicillin-resistant and methicillin-susceptible *Staphylococcus aureus* discriminates between biofilm and planktonic phenotypes. *J. Proteome Res.* 13, 2973–2985. doi: 10.1021/pr500120c
- Antimicrobial Resistance, C (2022). Global burden of bacterial antimicrobial resistance in 2019: a systematic analysis. *Lancet* 399, 629–655. doi: 10.1016/S0140-6736(21)02724-0
- Antti, H., Fahlgren, A., Näsström, E., Kouremenos, K., Sundén-Cullberg, J., Guo, Y., et al. (2013). Metabolic profiling for detection of *Staphylococcus aureus* infection and antibiotic resistance. *PLoS One* 8:e56971. doi: 10.1371/journal.pone.0056971
- Aros-Calt, S., Castelli, F. A., Lamourette, P., Gervasi, G., Junot, C., Muller, B. H., et al. (2019). Metabolomic investigation of *Staphylococcus aureus* antibiotic susceptibility by liquid chromatography coupled to high-resolution mass spectrometry. *Methods Mol. Biol.* 1871, 279–293. doi: 10.1007/978-1-4939-8814-3_18
- Banerjee, D., Parmar, D., Bhattacharya, N., Ghanate, A. D., Panchagnula, V., and Raghunathan, A. (2017). A scalable metabolite supplementation strategy against antibiotic resistant pathogen *Chromobacterium violaceum* induced by NAD(+)/NADH(+) imbalance. *BMC Syst. Biol.* 11:51. doi: 10.1186/s12918-017-0427-z
- Bassetti, M., Peghin, M., Vena, A., and Giacobb, D. R. (2019). Treatment of infections due to MDR gram-negative bacteria. *Front. Med. (Lausanne)* 6:74. doi: 10.3389/fmed.2019.00074
- Baysarowich, J., Koteva, K., Hughes, D. W., Ejim, L., Griffiths, E., Zhang, K., et al. (2008). Rifamycin antibiotic resistance by ADP-ribosylation: structure and diversity of *Arr. Proc. Natl. Acad. Sci. U. S. A.* 105, 4886–4891. doi: 10.1073/pnas.0711939105
- Berg, M., García-Hernández, R., Cuypers, B., Vanaerschot, M., Manzano, J. I., Poveda, J. A., et al. (2015). Experimental resistance to drug combinations in *Leishmania donovani*: metabolic and phenotypic adaptations. *Antimicrob. Agents Chemother.* 59, 2242–2255. doi: 10.1128/AAC.04231-14
- Breijyeh, Z., Jubeh, B., and Karaman, R. (2020). Resistance of gram-negative bacteria to current antibacterial agents and approaches to resolve it. *Molecules* 25:1340. doi: 10.3390/molecules25061340
- Chambers, H. F., and Deleo, F. R. (2009). Waves of resistance: *Staphylococcus aureus* in the antibiotic era. *Nat. Rev. Microbiol.* 7, 629–641. doi: 10.1038/nrmicro2200
- Conlon, B. P., Rowe, S. E., Gandt, A. B., Nuxoll, A. S., Donegan, N. P., Zalis, E. A., et al. (2016). Persister formation in *Staphylococcus aureus* is associated with ATP depletion. *Nat. Microbiol.* 1, 1–7. doi: 10.1038/nrmicrobiol.2016.51
- Deng, L., Guo, F., Cheng, K. K., Zhu, J., Gu, H., Raftery, D., et al. (2020). Identifying significant metabolic pathways using multi-block partial least-squares analysis. *J. Proteome Res.* 19, 1965–1974. doi: 10.1021/acs.jproteome.9b00793
- Dersch, P., Khan, M. A., Mühlén, S., and Görke, B. (2017). Roles of regulatory RNAs for antibiotic resistance in bacteria and their potential value as novel drug targets. *Front. Microbiol.* 8:803. doi: 10.3389/fmicb.2017.00803
- Dhingra, S., Rahman, N. A. A., Peile, E., Rahman, M., Sartelli, M., Hassali, M. A., et al. (2020). *Microbial resistance movements: an overview of global public health threats posed by antimicrobial resistance, and how best to counter.* *Front. Public Health* 8:535668. doi: 10.3389/fpubh.2020.535668
- Eichler, K., Buchet, A., Lemke, R., Kleber, H. P., and Mandrand-Berthelot, M. A. (1996). Identification and characterization of the *caif* gene encoding a potential transcriptional activator of carnitine metabolism in *Escherichia coli*. *J. Bacteriol.* 178, 1248–1257. doi: 10.1128/jb.178.5.1248-1257.1996
- Fan, L., Pan, Z., Liao, X., Zhong, Y., Guo, J., Pang, R., et al. (2023). Uracil restores susceptibility of methicillin-resistant *Staphylococcus aureus* to aminoglycosides through metabolic reprogramming. *Front. Pharmacol.* 14. doi: 10.3389/fphar.2023.1133685
- Feehily, C., and Karatzas, K. A. (2013). Role of glutamate metabolism in bacterial responses towards acid and other stresses. *J. Appl. Microbiol.* 114, 11–24. doi: 10.1111/j.1365-2672.2012.05434.x
- Fernández-García, M., Rojo, D., Rey-Stolle, F., García, A., and Barbas, C. (2018). Metabolomic-based methods in diagnosis and monitoring infection progression. *Exp. Suppl.* 109, 283–315. doi: 10.1007/978-3-319-74932-7_7
- Galeano García, P., Zimmermann, B. H., and Carazzzone, C. (2019). Hydrophilic interaction liquid chromatography coupled to mass spectrometry and multivariate analysis of the De novo pyrimidine pathway metabolites. *Biomolecules* 9:328. doi: 10.3390/biom9080328
- Gauttam, R., Desiderato, C. K., Radoš, D., Link, H., Seibold, G. M., and Eikmanns, B. J. (2021). Metabolic engineering of *Corynebacterium glutamicum* for production of UDP-N-Acetylglucosamine. *Front. Bioeng. Biotechnol.* 9:748510. doi: 10.3389/fbioe.2021.748510
- Gil-Gil, T., Ochoa-Sánchez, L. E., and Martínez, J. L. (2022). The antibiotic fosfomycin mimics the effects of the intermediate metabolites phosphoenolpyruvate and glyceraldehyde-3-phosphate on the *Stenotrophomonas maltophilia* transcriptome. *Int. J. Mol. Sci.* 23:159. doi: 10.3390/ijms23010159
- Harper, L., Balasubramanian, D., Ohneck, E. A., Sause, W. E., Chapman, J., Mejia-Sosa, B., et al. (2018). *Staphylococcus aureus* responds to the central metabolite pyruvate to regulate virulence. *MBio* 9, e02272–e02217. doi: 10.1128/mBio.02272-17
- Harrieder, E. M., Kretschmer, F., Böcker, S., and Witting, M. (2022). Current state-of-the-art of separation methods used in LC-MS based metabolomics and lipidomics. *J. Chromatogr. B Anal. Technol. Biomed. Life Sci.* 1188:123069. doi: 10.1016/j.jchromb.2021.123069
- Harvey, R. J., and Collins, E. B. (1963). Roles of citrate and Acetoin in the metabolism of *Streptococcus Diacetylactis*. *J. Bacteriol.* 86, 1301–1307. doi: 10.1128/jb.86.6.1301-1307.1963
- Holt, G. S., Lodge, J. K., McCarthy, A. J., Graham, A. K., Young, G., Bridge, S. H., et al. (2017). Shigatoxin encoding bacteriophage varphi24(B) modulates bacterial metabolism to raise antimicrobial tolerance. *Sci. Rep.* 7:40424. doi: 10.1038/srep40424
- Hudson, A. W. (2022). Role of FUCOSE utilization on *Klebsiella Pneumoniae* gut colonization and pathogenesis. [Doctoral dissertation]. Wake Forest University.
- Ito, Y., Ito, T., Yamashiro, K., Mineshima, F., Hirai, K., Omori, K., et al. (2020). Antimicrobial and antibiofilm effects of abietic acid on cariogenic *Streptococcus mutans*. *Odontology* 108, 57–65. doi: 10.1007/s10266-019-00456-0
- Jiang, M., Yang, L., Chen, Z. G., Lai, S. S., Zheng, J., and Peng, B. (2020). Exogenous maltose enhances Zebrafish immunity to levofloxacin-resistant *Vibrio alginolyticus*. *Microb. Biotechnol.* 13, 1213–1227. doi: 10.1111/1751-7915.13582
- Jubeh, B., Breijyeh, Z., and Karaman, R. (2020). Resistance of gram-positive bacteria to current antibacterial agents and overcoming approaches. *Molecules* 25:2888. doi: 10.3390/molecules25122888
- Konopka, J. B. (2012). N-acetylglucosamine (GlcNAc) functions in cell signaling. *Scientifica (Cairo)* 2012, 1–15. doi: 10.6064/2012/489208
- Kulakova, A. N., Kulakov, L. A., Akulenko, N. V., Ksenzenko, V. N., Hamilton, J. T. G., and Quinn, J. P. (2001). Structural and functional analysis of the phosphonate hydrolase (*phnA*) gene region in *Pseudomonas fluorescens* 23F. *J. Bacteriol.* 183, 3268–3275. doi: 10.1128/JB.183.11.3268-3275.2001
- Kumar, A., Singh, S., Gupta, S. K., Kumar, S., Kumar, S., Singh, R., et al. (2022). Identification of metabolite extraction method for targeted exploration of antimicrobial resistance associated metabolites of *Klebsiella pneumoniae*. *Sci. Rep.* 12:8939. doi: 10.1038/s41598-022-12153-0
- Kumar, V., Sun, P., Vamathevan, J., Li, Y., Ingraham, K., Palmer, L., et al. (2011). Comparative genomics of *Klebsiella pneumoniae* strains with different antibiotic resistance profiles. *Antimicrob. Agents Chemother.* 55, 4267–4276. doi: 10.1128/AAC.00052-11
- Kumari, N., Pandey, S., and Menghani, E. J. I. O. G.-M. S. (2022). Evaluation of actinomycetes isolated antimicrobial metabolites as potent inhibitor of multidrug resistant organisms. *Indian J. Mar. Sci.* 50, 29–36. doi: 10.56042/ijms.v50i01.66080
- Leadbetter, J. R., and Greenberg, E. P. (2000). Metabolism of acyl-homoserine lactone quorum-sensing signals by *Variovorax paradoxus*. *J. Bacteriol.* 182, 6921–6926. doi: 10.1128/JB.182.24.6921-6926.2000
- Lee, A. S., de Lencastre, H., Garau, J., Kluytmans, J., Malhotra-Kumar, S., Peschel, A., et al. (2018). Methicillin-resistant *Staphylococcus aureus*. *Nat. Rev. Dis. Primers.* 4:18033. doi: 10.1038/nrdp.2018.33
- Lee, Y., Sathesh-Prabu, C., Kwak, G. H., Bang, I., Jung, H. W., Kim, D., et al. (2022). Enhanced production of nonanedioic acid from nonanoic acid by engineered *Escherichia coli*. *Biotechnol. J.* 17:e2000416. doi: 10.1002/biot.202000416
- Li, Y., Liang, W., and Li, C. J. M. R. (2023). Exogenous adenosine and/or guanosine enhances tetracycline sensitivity of *Vibrio splendidus* persister cells. *Microbiol. Res.* 270:127321. doi: 10.1016/j.micres.2023.127321
- Li, T., Mei, Y., He, B., Sun, X., and Li, J. (2018). Reducing quorum sensing-mediated virulence factor expression and biofilm formation in *Hafnia alvei* by using the potential quorum sensing inhibitor L-Carvone. *Front. Microbiol.* 9:3324. doi: 10.3389/fmicb.2018.03324
- Lin, Y., Li, W., Sun, L., Lin, Z., Jiang, Y., Ling, Y., et al. (2019). Comparative metabolomics shows the metabolic profiles fluctuate in multi-drug resistant *Escherichia coli* strains. *J. Proteome* 207:103468. doi: 10.1016/j.jpro.2019.103468
- Liu, Q., Cai, J., Nichols, R. G., Tian, Y., Zhang, J., Smith, P. B., et al. (2019). A quantitative HILIC-MS/MS assay of the metabolic response of Huh-7 cells exposed to 2,3,7,8-Tetrachlorodibenzo-p-dioxin. *Meta* 9:118. doi: 10.3390/metabo9060118
- Liu, S. R., Peng, X. X., and Li, H. (2019). Metabolic mechanism of ceftazidime resistance in *Vibrio alginolyticus*. *Infect. Drug Resist.* 12, 417–429. doi: 10.2147/IDR.S179639

- Low, Y. M., et al. (2018). Elucidating the survival and response of carbapenem resistant *Klebsiella pneumoniae* after exposure to imipenem at sub-lethal concentrations. *Pathog Glob Health*. 112, 378–386. doi: 10.1080/20477724.2018.1538281
- Masimen, M. A. A., Harun, N. A., Maulidiani, M., and Ismail, W. I. W. (2022). Overcoming methicillin-resistance *Staphylococcus aureus* (MRSA) using antimicrobial peptides-silver nanoparticles. *Antibiotics (Basel)* 11:951. doi: 10.3390/antibiotics11070951
- Mehta, Y., Hegde, A., Pande, R., Zirpe, K. G., Gupta, V., Ahdal, J., et al. (2020). Methicillin-resistant *Staphylococcus aureus* in intensive care unit setting of India: a review of clinical burden, patterns of prevalence, preventive measures, and future strategies. *Indian J. Crit. Care Med.* 24, 55–62. doi: 10.5005/jp-journals-10071-23337
- Morris, R. P., Nguyen, L., Gatfield, J., Visconti, K., Nguyen, K., Schnappinger, D., et al. (2005). Ancestral antibiotic resistance in *Mycobacterium tuberculosis*. *Proc. Natl. Acad. Sci. U. S. A.* 102, 12200–12205. doi: 10.1073/pnas.0505446102
- Mulani, M. S., Kamble, E. E., Kulkarni, S. N., Tawre, M. S., and Pardesi, K. R. (2019). Emerging strategies to combat ESKAPE pathogens in the era of antimicrobial resistance: a review. *Front. Microbiol.* 10:539. doi: 10.3389/fmicb.2019.00539
- Niu, G., and Tan, H. (2015). Nucleoside antibiotics: biosynthesis, regulation, and biotechnology. *Trends Microbiol.* 23, 110–119. doi: 10.1016/j.tim.2014.10.007
- Oxford, U. O. (2019). An estimated 1.2 million people died in 2019 from antibiotic-resistant bacterial infections. 7 10 22. Available from: <https://www.ox.ac.uk/news/2022-01-20-estimated-12-million-people-died-2019-antibiotic-resistant-bacterial-infections#:~:text=One%20pathogen%2Ddrug%20combination%20%E2%80%9320methicillin,between%2050%2C00020and20100%2C000%20deaths.>
- Pahalagedara, A., Flint, S., Palmer, J., Subbaraj, A., Brightwell, G., and Gupta, T. B. (2020). Antimicrobial activity of soil *Clostridium* enriched conditioned media against *Bacillus mycoides*, *Bacillus cereus*, and *Pseudomonas aeruginosa*. *Front. Microbiol.* 11:608998. doi: 10.3389/fmicb.2020.608998
- Pang, R., Su, Y. B., Zhou, H., and Chen, X. (2020). Metabolites alleviate staphylococcal bloodstream infection in a NO-dependent manner via arginase inhibition. *bioRxiv*.
- Park, J. Y., Kang, B. R., Ryu, C. M., Anderson, A. J., and Kim, Y. C. (2018). Polyamine is a critical determinant of *Pseudomonas chlororaphis* O6 for GacS-dependent bacterial cell growth and biocontrol capacity 19, 1257–1266. doi: 10.1111/mpp.12610
- Patel, Y., Soni, V., Rhee, K. Y., and Helmann, J. D. (2023). Mutations in *rpoB* that confer rifampicin resistance can alter levels of peptidoglycan precursors and affect β -lactam susceptibility. *MBio*, e03168–e03122. doi: 10.1128/mbio.03168-22
- Pinu, F. R., Goldansaz, S. A., and Jaïne, J. (2019). Translational metabolomics: current challenges and future opportunities. *Meta* 9:108. doi: 10.3390/metabo906108
- Pontes, M. H., and Groisman, E. A. (2019). Slow growth determines nonheritable antibiotic resistance in *Salmonella enterica*. *Sci. Signal.* 12:eaax3938. doi: 10.1126/scisignal.aax3938
- Pye, S. (2022). Effects of small molecules produced by commensal bacteria on antibiotic resistant *Pseudomonas aeruginosa*. [Master's thesis, Cumming School of Medicine]. University of Calgary.
- Rahmanian, M., Waller, G. R., and Smith, W. G. (1971). Biosynthesis of D-aspartic acid by *Streptococcus faecalis*. *J. Biol. Chem.* 246, 823–830. doi: 10.1016/S0021-9258(18)62483-4
- Ranjit, D. K., Moye, Z. D., Rocha, F. G., Ottenberg, G., Nichols, F. C., Kim, H. M., et al. (2022). Characterization of a bacterial kinase that phosphorylates Dihydrospingosine to form dhS1P. *Microbiol. Spectr.* 10, e00002–e00022. doi: 10.1128/spectrum.00002-22
- Reith, J., Berking, A., and Mayer, C. (2011). Characterization of an N-acetylmuramic acid/N-acetylglucosamine kinase of *Clostridium acetobutylicum*. *J. Bacteriol.* 193, 5386–5392. doi: 10.1128/JB.05514-11
- Robinson, J. I., Weir, W. H., Crowley, J. R., Hink, T., Reske, K. A., Kwon, J. H., et al. (2019). Metabolomic networks connect host-microbiome processes to human *Clostridioides difficile* infections. *J. Clin. Invest.* 129, 3792–3806. doi: 10.1172/JCI126905
- Rosenberg, C. R., Fang, X., and Allison, K. R. (2020). Potentiating aminoglycoside antibiotics to reduce their toxic side effects. *PLoS One* 15:e0237948. doi: 10.1371/journal.pone.0237948
- Salton, M. R., and Schmitt, M. D. (1967). Effects of diphenylamine on carotenoids and menaquinones in bacterial membranes. *Biochim. Biophys. Acta* 135, 196–207. doi: 10.1016/0005-2736(67)90114-9
- Schelli, K., Zhong, F., and Zhu, J. (2017). Comparative metabolomics revealing *Staphylococcus aureus* metabolic response to different antibiotics. *Microb. Biotechnol.* 10, 1764–1774. doi: 10.1111/1751-7915.12839
- Serganov, A., Huang, L., and Patel, D. J. N. (2008). Structural insights into amino acid binding and gene control by a lysine riboswitch. *Nature*. 455, 1263–1267. doi: 10.1038/nature07326
- Somerville, J. E., Cassiano, L., Bainbridge, B., Cunningham, M. D., and Darveau, R. P. (1996). A novel *Escherichia coli* lipid mutant that produces an antiinflammatory lipopolysaccharide. *J. Clin. Invest.* 97, 359–365. doi: 10.1172/JCI118423
- Stahl, R. S., Bisha, B., Mahapatra, S., and Chandler, J. C. (2020). A model for the prediction of antimicrobial resistance in *Escherichia coli* based on a comparative evaluation of fatty acid profiles. *Diagn. Microbiol. Infect. Dis.* 96:114966. doi: 10.1016/j.diagmicrobio.2019.114966
- Su, H. C., Ramkissoon, K., Doolittle, J., Clark, M., Khatun, J., Secrest, A., et al. (2010). The development of ciprofloxacin resistance in *Pseudomonas aeruginosa* involves multiple response stages and multiple proteins. *Antimicrob. Agents Chemother.* 54, 4626–4635. doi: 10.1128/AAC.00762-10
- Tan, R., Jin, M., Shao, Y., Yin, J., Li, H., Chen, T., et al. (2022). High-sugar, high-fat, and high-protein diets promote antibiotic resistance gene spreading in the mouse intestinal microbiota. *Gut Microbes* 14:2022442. doi: 10.1080/19490976.2021.2022442
- Tang, J. (2011). Microbial metabolomics. *Curr. Genomics* 12, 391–403. doi: 10.2174/138920211797248619
- Teufel, R., Mascaraque, V., Ismail, W., Voss, M., Perera, J., Eisenreich, W., et al. (2010). Bacterial phenylalanine and phenylacetate catabolic pathway revealed. *Proc. Natl. Acad. Sci. U. S. A.* 107, 14390–14395. doi: 10.1073/pnas.1005399107
- Thomas, N., Thorn, C., Richter, K., Thierry, B., and Prestidge, C. (2016). Efficacy of poly-lactic-co-glycolic acid micro- and nanoparticles of ciprofloxacin against bacterial biofilms. *J. Pharm. Sci.* 105, 3115–3122. doi: 10.1016/j.xphs.2016.06.022
- Usuda, Y., and Kurahashi, O. (2005). Effects of deregulation of methionine biosynthesis on methionine excretion in *Escherichia coli*. *Appl. Environ. Microbiol.* 71, 3228–3234. doi: 10.1128/AEM.71.6.3228-3234.2005
- Vanaporn, M., and Titball, R. W. (2020). Trehalose and bacterial virulence. *Virulence* 11, 1192–1202. doi: 10.1080/21505594.2020.1809326
- Vazquez-Guillamet, C., and Kollef, M. H. (2014). Treatment of gram-positive infections in critically ill patients. *BMC Infect. Dis.* 14:92. doi: 10.1186/1471-2334-14-92
- Vetter, A. M., Helmecke, J., Schomburg, D., and Neumann-Schaal, M. (2019). The impact of pyroglutamate: *Sulfolobus acidocaldarius* has a growth advantage over *Saccharolobus solfataricus* in glutamate-containing media. *Archaea*. 3208051. doi: 10.1155/2019/3208051
- Viola, R. E., Zhao, M., Blumenthal, R. M., Wijayasinghe, Y. S., and Bhansali, P. (2015). A surprising range of modified-methionyl S-adenosylmethionine analogues support bacterial growth. *Microbiology (Reading)* 161, 674–682. doi: 10.1099/mic.0.000034
- Vollmer, W., Blanot, D., and de Pedro, M. A. (2008). Peptidoglycan structure and architecture. *FEMS Microbiol. Rev.* 32, 149–167. doi: 10.1111/j.1574-6976.2007.00094.x
- Wang, Q., Lin, M., Shen, P., and Guan, Y. (2021). Elevation of fatty acid biosynthesis metabolism contributes to *Zhongshengmycin* resistance in *Xanthomonas oryzae*. *Antibiotics (Basel)* 10:1166. doi: 10.3390/antibiotics10101166
- Wang, Q., Wang, H., Lv, M., Wang, X., and Chen, L. (2023). *Sulfamethoxazole degradation by Aeromonas caviae and co-metabolism by the mixed bacteria*. *Chemosphere* 317:137882. doi: 10.1016/j.chemosphere.2023.137882
- Wang, Y., Ren, B., Zhou, X., Liu, S., Zhou, Y., Li, B., et al. (2017). Growth and adherence of *Staphylococcus aureus* were enhanced through the PGE2 produced by the activated COX-2/PGE2 pathway of infected oral epithelial cells 12:e0177166. doi: 10.1371/journal.pone.0177166
- Whiteley, A. T., Garelis, N. E., Peterson, B. N., Choi, P. H., Tong, L., Woodward, J. J., et al. (2017). C-di-AMP modulates *Listeria monocytogenes* central metabolism to regulate growth, antibiotic resistance and osmoregulation 104, 212–233. doi: 10.1111/mmi.13622
- Whitmore, S. E., and Lamont, R. J. (2012). Tyrosine phosphorylation and bacterial virulence. *Int. J. Oral Sci.* 4, 1–6. doi: 10.1038/ijos.2012.6
- WHO (2020). Lack of new antibiotics threatens global efforts to contain drug-resistant infections. [cited 2020 10 9 22]. Available from: <https://www.who.int/news/item/17-01-2020-lack-of-new-antibiotics-threatens-global-efforts-to-contain-drug-resistant-infections>.
- WHO (2021). Antimicrobial resistance. [cited 2022 13 9 22]. Available from: <https://www.who.int/news-room/fact-sheets/detail/antimicrobial-resistance>.
- Wolucka, B. A. J. T. F. J. (2008). Biosynthesis of D-arabinose in mycobacteria—a novel bacterial pathway with implications for antimycobacterial therapy 275, 2691–2711. doi: 10.1111/j.1742-4658.2008.06395.x
- Xiao, J. F., Zhou, B., and Ransom, H. W. (2012). Metabolite identification and quantitation in LC-MS/MS-based metabolomics. *Trends Anal. Chem.* 32, 1–14. doi: 10.1016/j.trac.2011.08.009
- Yao, Z., Li, W., Lin, Y., Wu, Q., Yu, F., and Lin, W. (2016). Proteomic analysis reveals that metabolic flows affect the susceptibility of *Aeromonas hydrophila* to antibiotics. *Sci. Rep.* 6:39413. doi: 10.1038/srep39413
- Ye, J. Z., Lin, X. M., Cheng, Z. X., Su, Y. B., Li, W. X., Ali, F. M., et al. (2018). Identification and efficacy of glycine, serine and threonine metabolism in potentiating kanamycin-mediated killing of *Edwardsiella piscicida*. *J. Proteome* 183, 34–44. doi: 10.1016/j.jpro.2018.05.006
- Yong, Y., Zhou, Y., Liu, K., Liu, G., Wu, L., and Fang, B. (2021). Exogenous Citrulline and glutamine contribute to reverse the resistance of salmonella to Apramycin. *Front. Microbiol.* 12:759170. doi: 10.3389/fmicb.2021.759170
- Zampieri, M., Enke, T., Chubukov, V., Ricci, V., Piddock, L., and Sauer, U. (2017). Metabolic constraints on the evolution of antibiotic resistance. *Mol. Syst. Biol.* 13:917. doi: 10.15252/msb.20167028

Zhang, P., Lu, G., Sun, Y., Yan, Z., Dang, T., and Liu, J. (2022). Metagenomic analysis explores the interaction of aged microplastics and roxithromycin on gut microbiota and antibiotic resistance genes of *Carassius auratus*. *J. Hazard. Mater.* 425:127773. doi: 10.1016/j.jhazmat.2021.127773

Zhang, S., and Zhu, J. (2022). Untargeted metabolomics sensitively differentiates gut bacterial species in single culture and co-culture systems. *ACS Omega* 7, 14643–14652. doi: 10.1021/acsomega.1c07114

Zhang, X. X., Ritchie, S. R., and Rainey, P. B. (2014). Urocanate as a potential signaling molecule for bacterial recognition of eukaryotic hosts. *Cell. Mol. Life Sci.* 71, 541–547. doi: 10.1007/s00018-013-1527-6

Zhao, X., Chen, H., Jin, Z., Li, L., Zhang, J., and Kong, X. (2018). GC-MS-based metabolomics analysis reveals L-aspartate enhances the antibiotic sensitivity of neomycin sulfate-resistant *Aeromonas hydrophila*. *J. Fish Dis.* 41, 1831–1841. doi: 10.1111/jfd.12894



OPEN ACCESS

EDITED BY

Maria Rosalia Pasca,
University of Pavia, Italy

REVIEWED BY

Garima Khare,
University of Delhi, India
Lenny Jose,
Indiana University–Purdue University
Indianapolis, United States
Hiroyuki Yamada,
Japan Anti-Tuberculosis Association, Japan

*CORRESPONDENCE

Zhe Wang
✉ wangz@sjtu.edu.cn

†These authors have contributed equally to this work

RECEIVED 20 January 2023

ACCEPTED 05 May 2023

PUBLISHED 18 May 2023

CITATION

Xu Y, Ma S, Huang Z, Wang L, Raza SHA and Wang Z (2023) Nitrogen metabolism in mycobacteria: the key genes and targeted antimicrobials.
Front. Microbiol. 14:1149041.
doi: 10.3389/fmicb.2023.1149041

COPYRIGHT

© 2023 Xu, Ma, Huang, Wang, Raza and Wang. This is an open-access article distributed under the terms of the [Creative Commons Attribution License \(CC BY\)](https://creativecommons.org/licenses/by/4.0/). The use, distribution or reproduction in other forums is permitted, provided the original author(s) and the copyright owner(s) are credited and that the original publication in this journal is cited, in accordance with accepted academic practice. No use, distribution or reproduction is permitted which does not comply with these terms.

Nitrogen metabolism in mycobacteria: the key genes and targeted antimicrobials

Yufan Xu^{1,2†}, Shiwei Ma^{1,2†}, Zixin Huang^{1,2}, Longlong Wang^{1,2}, Sayed Haidar Abbas Raza³ and Zhe Wang^{1,2*}

¹Shanghai Collaborative Innovation Center of Agri-Seeds, School of Agriculture and Biology, Shanghai Jiao Tong University, Shanghai, China, ²Shanghai Key Laboratory of Veterinary Biotechnology, School of Agriculture and Biology, Shanghai Jiao Tong University, Shanghai, China, ³Guangdong Provincial Key Laboratory of Food Quality and Safety/Nation-Local Joint Engineering Research Center for Machining and Safety of Livestock and Poultry Products, South China Agricultural University, Guangzhou, China

Nitrogen metabolism is an important physiological process that affects the survival and virulence of *Mycobacterium tuberculosis*. *M. tuberculosis*'s utilization of nitrogen in the environment and its adaptation to the harsh environment of acid and low oxygen in macrophages are closely related to nitrogen metabolism. In addition, the dormancy state and drug resistance of *M. tuberculosis* are closely related to nitrogen metabolism. Although nitrogen metabolism is so important, limited research was performed on nitrogen metabolism as compared with carbon metabolism. *M. tuberculosis* can use a variety of inorganic or organic nitrogen sources, including ammonium salts, nitrate, glutamine, asparagine, etc. In these metabolic pathways, some enzymes encoded by key genes, such as GlnA1, AnsP2, etc, play important regulatory roles in the pathogenesis of TB. Although various small molecule inhibitors and drugs have been developed for different nitrogen metabolism processes, however, long-term validation is needed before their practical application. Most importantly, with the emergence of multidrug-resistant strains, eradication, and control of *M. tuberculosis* will still be very challenging.

KEYWORDS

nitrogen metabolism, antimicrobials, drug targets, tuberculosis, TB

1. Introduction

The first recorded case of tuberculosis (TB) can be traced back to 9000 years ago in the Eastern Mediterranean (Holzheimer et al., 2021). Human and zoonotic TB is normally caused by the infection of *Mycobacterium tuberculosis complex* which includes several species. They share highly conserved genomic sequences and possibly evolved from a single ancestor. During the past 200 years, TB kills more than 1 billion people (Gagneux, 2018). Furthermore, TB can also co-infected with other disease, leading to more serious symptoms (Huang and Zhao, 2022). As a matter of fact, co-infection with *Mycobacterium tuberculosis* (*M. tuberculosis*), becomes the primary reason of death to HIV-1 infectors. Despite some progress in diagnosis in recent years (Liao et al., 2022), the situation is still not promising. The mortality increased to 423,000 in 2020 (from 209,000 in 2019) (Bell and Noursadeghi, 2018; Harding, 2020), suggests that high rates of HIV infection have more TB cases and

higher mortality rates (Dean et al., 2022). This increase shows that TB poses a significant threat to people's lives whether they are co-infected with HIV or not.

In 2020, *M. tuberculosis*, the etiological agent of TB, caused 5.8 million new cases around the world and there may be 4.1 million people who haven't been diagnosed or reported as WHO estimated (Harding, 2020). Despite the enormous financial and human resources invested in combating this deadly disease, they remain inadequate. Targets set in 2015 to reduce the number of infections and deaths have both not been met, with only half (11–20%) and a quarter (9.2–35%) of the plans achieved, respectively (Kirby, 2021). Especially with the COVID-19 pandemic, massive medical resources have been taken up, suggesting that we are facing a great hardship even more difficult to overcome than preceded. More worrying is that some studies suggest that the immune suppression and storm of inflammatory cytokines caused by COVID-19 may contribute to the development of TB (Hildebrand et al., 2022). The recent emergence of a case of latent TB reactivation due to COVID-19 infection (Leonso et al., 2022) has heightened this concern, as the proposed causes were the immunosuppressive sequelae of COVID-19, the effects of the chemotherapy (steroids and remdesivir), or a combination of both. Given the large numbers of people infected by both diseases, we must be alert to the potentially serious consequences of co-infection.

As a kind of facultative intercellular pathogen, *M. tuberculosis* can multiply in macrophages despite the acidic environment rich in radicals, and lacking in oxygen and nutrition, which usually kills most other bacteria (Höner zu Bentrup and Russell, 2001). In the dilemma, *M. tuberculosis* reduces metabolic activity and enters a dormant state which increases its resistance. However, most antibiotics target the processes of DNA replication, translation, or cell wall formation which are active in rapidly dividing cells. This makes it really hard to treat the infection. Patients are advised to use 4 drugs combination including isoniazid, rifampin, ethambutol, and pyrazinamide for 2–6 months and the therapy for multidrug-resistant cases even costs more time, 9–20 months (Caño-Muñoz et al., 2018). Even after a long period of treatment, if a small percentage of the pathogen is not killed, the probability of recurrence is very high. Therefore, exploring how *M. tuberculosis* survives in macrophages is really important and it's attractive to develop novel drugs based on these studies.

There have been lots of studies on carbon metabolism reported in the literature, which have shown various carbon sources that *M. tuberculosis* used, the ways the bacterium obtained them from hosts, and specific metabolic pathways that it exploited during infection (Ehrt et al., 2018). By contrast, studies on the metabolism of nitrogen, another equally important element involved in the synthesis of many biomolecules including amino acids, proteins, nucleotides, some cofactors, and peptidoglycan, in this pathogen have just begun. A great deal of mystery remains about the processes of acquiring and assimilating nitrogen. In this review, we describe some of the key genes identified so far in the regulation of nitrogen metabolism, as well as some small molecule inhibitors.

2. Key genes in nitrogen metabolism

Central nitrogen metabolism, the best-studied part of nitrogen metabolism so far, concerned with the intake and utilization of

ammonium, is indispensable to all living organisms around the world to balance internal and adapt to the external environment. *In vivo*, ammonium assimilation metabolism can be divided into two kinds according to the different conditions of glutamic acid synthesis. One is the formation of glutamate from ammonium and α -ketoglutaric acid in response to glutamate dehydrogenase and the other is a molecule of glutamine and a molecule of α -ketoglutarate catalyzed by glutamine synthetase to form two glutamates. The former has a lower K_m value and is therefore referred to as a low-affinity pathway, while the latter is referred to as a high-affinity pathway. The major assimilation pathway in *M. tuberculosis* is the high-affinity pathway related to glutamine synthetase and glutamine oxoglutarate aminotransferase (GOGAT), which catalyze the production of glutamine or glutamate, respectively. Although a low-affinity pathway for ammonium assimilation using glutamate dehydrogenase exists in other bacteria, in *M. tuberculosis* the enzyme acts primarily on glutamine catabolism which breaks down glutamine into α -ketoglutaric acid and ammonium. Besides ammonium, the source of nitrogen can be various either inorganic substances such as nitrate or organics including alanine, aspartate, asparagine, glutamate, and glutamine (Agapova et al., 2019). Furthermore, nitrogen from different amino acids goes to different places. For example, according to the results of the isotope tracer, more than 50% of ^{15}N from $^{15}\text{N1-Asp}$ was transferred to Glu/n, $^{15}\text{N1-Glu}$ to six amino acids, $^{15}\text{N2-Gln}$ to eight amino acids, and $^{15}\text{N1-Leu}$ to Ile. Nitrogen from glutamine is the major source and can turn into many other amino acids. While alanine is used directly as a component of thallus rather than transformed (Borah et al., 2019). Interestingly, *M. tuberculosis* grows faster when utilizes organic nitrogen sources. Some of the metabolic pathways involved in this review are shown in Figure 1 and the structures of proteins encoded by key genes are shown in Figure 2.

2.1. glnA1

Glutamine and glutamate are two molecules that play irreplaceable roles in central nitrogen metabolism. When ammonium in the medium is used as primary nitrogen donors by the bacterium, it must combine with glutamine and glutamate first (Leigh and Dodsworth, 2007). And because of lacking of a low-affinity pathway for ammonium assimilation, *M. tuberculosis* cannot assimilate ammonia directly into glutamate. Thus glutamine synthetase and glutamate synthetase are the sole means of ammonia assimilation (Tullius et al., 2003). There are 4 kinds of isoforms of glutamine synthetase, GlnA1, GlnA2, GlnA3, and GlnA4. Among these, GlnA1, GlnA3, and GlnA4 synthesize L-glutamine, whereas GlnA2 synthesizes the D-glutamine and D-isoglutamine required for cell wall biosynthesis. However, only *glnA1* expresses abundantly, the three other genes being 9–15-fold less expressed (Harth et al., 2005). Though *glnA3* will overexpress when GlnA1 is inhibited, the quantity is less than fold which is too little to compensate for the lack of *glnA1* (Lee et al., 2006; Carroll et al., 2011), thus GlnA1 provides the main activity in *M. tuberculosis*. The gene *glnA1* consists of 1437 base pairs and encodes 478 amino acids (57.3 kDa) (Couturier et al., 2015). In addition to its internal role in bacteria, GlnA1 can also be secreted

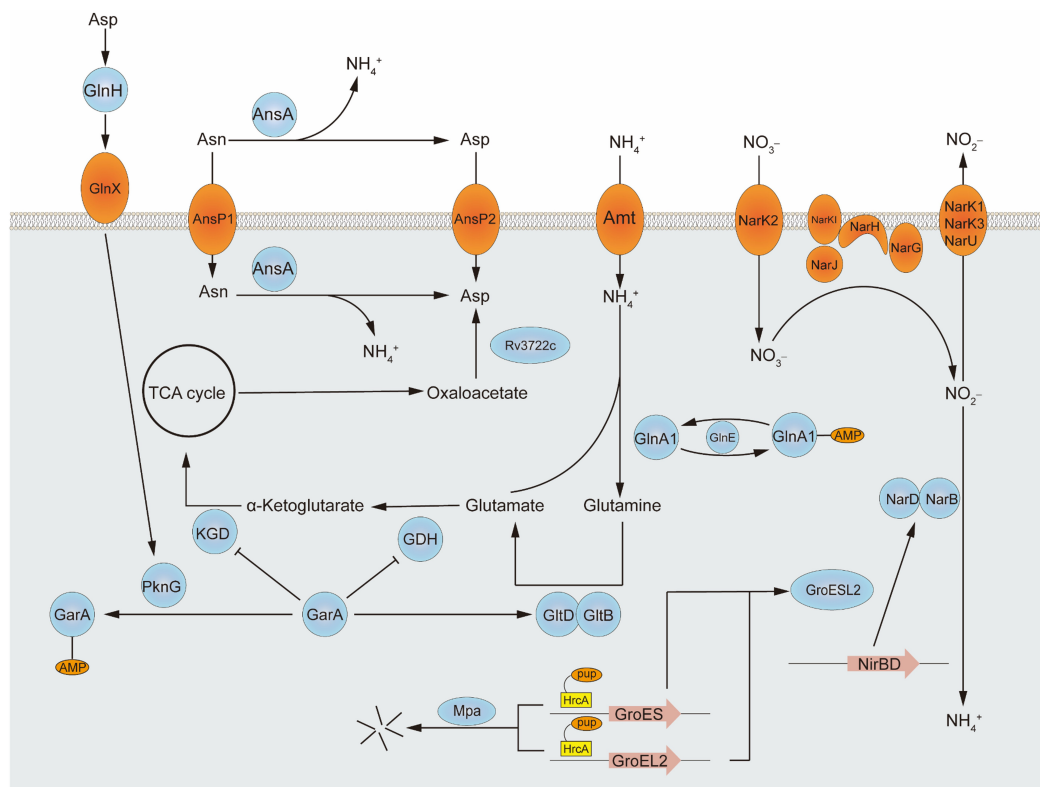


FIGURE 1
The sketch of nitrogen metabolism pathway in mycobacteria.

into the external environment as a secreted protein, which may affect phagosomal pH and phagosomal lysosomal fusion, thus allowing *M. tuberculosis* to survive phagocytosis by macrophages (Harth et al., 1994). What's more, as reported, GlnA1 is related to the synthesis of poly-L-glutamate/glutamine. This component, which is absent in non-pathogenic mycobacteria, corresponds to 10% of the cell wall of pathogenic mycobacteria (Couturier et al., 2015). These all imply the importance of the gene *glnA1*.

In other bacteria represented by *E. coli*, the regulation of GlnA1 is a cascade reaction, mainly dependent on three proteins, PI protein, PII protein, and Gln D. Among them, PI has adenylyl transferase activity, which can adenylylate or deadenylylate GlnA1, thereby regulating its activity. There are two forms of PII: PII-UMP and dephosphorylated. PII can promote PI-catalyzed adenylation, while PI-UMP can promote deadenylation. Different forms of PII are regulated by the uridylyl transferase GlnD (Read et al., 2007). In *M. tuberculosis*, the homologous proteins of the three proteins are GlnE, GlnK, and GlnD. But there are some differences between its function and that of *E. coli*.

According to many studies, both GlnA1 and GlnE are necessary for the growth of *M. tuberculosis*. This is specific to *M. tuberculosis*, studies have shown that GlnE is not necessary for *E. coli* and *Streptomyces* (Fink et al., 1999). GlnE has both adenylation and deadenylation activities, which regulate the activity of glutamine synthetase by transferring AMP to, or removing AMP from GlnA1. When GlnA1 binds to AMP, it becomes inactive. But studies that deleted adenylation or deadenylation domains separately showed that only the former was necessary for growth, and that the absence

of the latter had no significant effect on growth (Carroll et al., 2008). This may be because if all the highly expressed GlnA1 is in the active state, the intracellular glutamate and ATP will be rapidly depleted. Given that glutamate is required for the sole pathway for *M. tuberculosis* to assimilate external ammonium, this could explain the lethality of the mutation.

In addition, GlnD showed adenylyl transferase but not uridylyl transferase activity in *M. tuberculosis*, controlling GlnK adenylation or deadenylation (Williams et al., 2013). Unlike *E. coli*, GlnK and GlnA1 adenylation appear to be independent of each other in *M. tuberculosis*. Studies have shown that *glnD-null* mutants do not show growth defects, although the expression of *amt*, *glnD*, and *glnK* genes is upregulated under nitrogen deficiency conditions (Read et al., 2007). Therefore, the role of GlnK and GlnD in *M. tuberculosis* nitrogen metabolism needs to be further studied.

Furthermore, it is also reported that GlnA1 has the activity of acyltransferase in active sites different from typical theories (Baghel et al., 2011). It means that *glnA1* may not only regulate nitrogen metabolism by controlling the use of sources but also by modulating the activity of other proteins while being regulated by GlnE.

2.2. *pknG*

The GOGAT of *M. tuberculosis* is composed of two subunits, GltB and GltD (Cole et al., 1998), which play a very important role in nitrogen metabolism and adaptation to adverse environments.

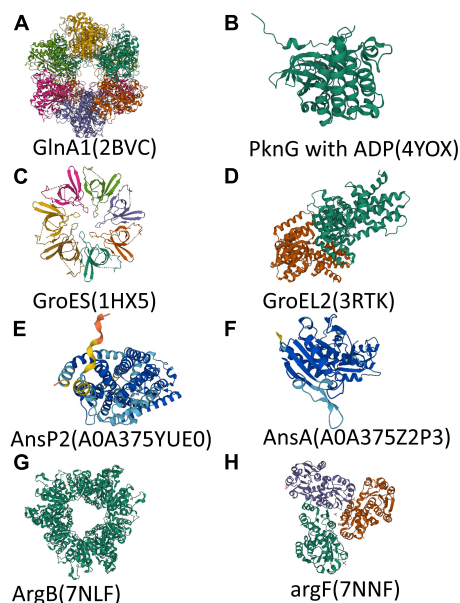


FIGURE 2

Structure of polypeptide chains encoded by key genes. (A–H) Overall structure of protein or polypeptide chain encoded by *glnA1*, *pknG*, *groES*, *groEL2*, *ansP2*, *ansA*, *argB*, and *argF*. The 3D model of AnsP2 and AnsA came from AlphaFold protein structure database (<https://alphafold.com>). Different colors in a 3D model represent per-residue confidence score (pLDDT) between 0 and 100 (Dark blue: pLDDT > 90, Light blue: 90 > pLDDT > 70, Yellow: 70 > pLDDT > 50, Orange: pLDDT < 50). The 3D model of other proteins came from RCSB PDB (<https://www.rcsb.org/>).

Some studies have shown that GltB/D catalyzed reactions can be used to neutralize cytoplasmic pH that is acidified while consuming host propionate carbon through the methylcitrate cycle. In contrast, there are defects in *M. bovis* BCG, which is not pathogenic and is less adaptable (Lee et al., 2018). Prior to this, it has been reported that the loss of *gltB* or *gltD* in *M. bovis* BCG would cause glutamatergic nutrient deficiency, resulting in inadequate growth of the strain in a medium with glutamate as the sole nitrogen source (Viljoen et al., 2013). These all implied that *gltB* and *gltD* may be related to the pathogenicity of *M. tuberculosis*.

Similar to GlnA1 above, GOGAT activity is regulated by a series of reactions. The glycogen accumulation regulator A (GarA) plays a regulating role in GOGAT and GDH. On the one hand, it can activate GOGAT to promote glutamate synthesis, on the other hand, it can inhibit GDH to inhibit glutamate decomposition. When GarA is phosphorylated, it becomes inactive, and metabolism shifts to glutaminolysis. The interconversion between glutamate and α -ketoglutarate can be regulated by phosphorylation and the dephosphorylation of GarA.

Further studies revealed that GarA phosphorylation and dephosphorylation were regulated by Serine-threonine protein kinase PknG (O'Hare et al., 2008). Disruption of *pknG* or *garA* has opposite effects on metabolism: defects in glutamate catabolism or intracellular glutamate depletion, respectively. Interestingly, disruption of GarA phosphorylation sites caused the same defects as *pknG* depletion (Rieck et al., 2017). In conclusion, a slight change in *pknG* expression can sensitively regulate metabolism through cascade amplification.

According to the crystal structure, there is no direct amino acid binding site for glutamine on PknG, so its activity needs the help of auxiliary components (Scherr et al., 2007). PknG consists of three distinct structural domains: rubredoxin domain (RD), kinase domain (KD), and tetratricopeptide repeat-containing domain (TPRD). The KD is sandwiched between RD and TPRD (Lisa et al., 2015). Some studies have shown that the activity of PknG is related to the environment outside the bacteria. The conserved aspartate-specific solute binding protein GlnH links extracellular amino acid concentration to PknG activity via the periplasmic transmembrane protein GlnX. There is a specific binding site for aspartic acid on GlnH. When amino acids are abundant in the environment, the conformation of GlnH bound to aspartic acid will be changed and bind to the transmembrane protein GlnX, and the signal will be transmitted to the cell, causing the activation of PknG. Activated PknG phosphorylates and inactivates GarA, thereby regulating glutamate metabolism (Bhattacharyya et al., 2018). In addition, studies of PknG substrates by affinity purification-mass spectrometry revealed that PknG may regulate many physiological processes, such as nitrogen and energy metabolism, cell wall synthesis, and protein translation (Gil et al., 2019). Metabolomic analysis showed that PknG was necessary to adapt to hypoxia and maintain REDOX balance, and was associated with a dormancy state (Khan et al., 2017).

2.3. groES and groEL2

In addition to ammonia, nitrate is also an important source of nitrogen available to *M. tuberculosis*. It was a few decades ago, researchers have found that nitrate can be the only nitrogen source to support the growth of *M. tuberculosis* (Hedgecock and Costello, 1962). Nitrate is also essential for the survival of *M. tuberculosis* under hypoxic conditions. It can act as a terminal electron acceptor in the respiratory chain under hypoxic conditions, causing *M. tuberculosis* to enter a dormant state instead of dying (Aly et al., 2006; Via et al., 2008). In addition, nitrite produced by reduction during nitrate metabolism can protect bacteria from the damage of reactive oxygen species and reactive nitrogen species *in vivo*. The metabolic pathway of nitrate is quite conservative. It is reduced to nitrite, which is further reduced to ammonia by NirBD, and then enters the central nitrogen metabolism. The nitrite that is not immediately reduced during this process is expelled from the cell (Malm et al., 2009).

Recent studies have found that the reduction of nitrate by *M. tuberculosis* requires chaperones expressed by *groES* and *groEL2*. They're all heat shock proteins (HSP) due to their increased levels of expression at elevated temperatures. As chaperone proteins, HSPs are widely and highly conserved in various organisms. They perform ATP-dependent folding of proteins to ensure cell viability at different temperatures (Ellis, 1999). The most characterized one among them is the GroEL/ES complex, or called Cpn60/Cpn10, from *E. coli*. GroEL forms two heptamer rings, which are then stacked back-to-back to form a complex of tetradecamers. GroES, on the other hand, bind to one or both ends of the GroEL complex after forming a heptamer ring driven by ATP. Both Cpn are required for *E. coli* (Xu et al., 1997; Grallert and Buchner, 2001). But in *M. tuberculosis*, the situation is different. Although there

are also homologous GroEL and GroES co-expressed by *groE* operon, there is another HSP in *M. tuberculosis* that belongs to the HSP60 family, commonly referred to as GroEL2. The gene that encodes the protein is not on *groE* operon (Qamra et al., 2005). And experiments showed that when the genes encoding GroES or GroEL2 were deleted, *M. tuberculosis* growth was completely inhibited. However, the lack of GroEL only prevented granulomatous inflammation in infected mice or guinea pigs (Hu et al., 2008). In addition, unlike *E. coli*, neither GroEL nor GroEL2 forms tetradecamers in *M. tuberculosis* cells, but exists as oligomers (Qamra et al., 2004). Crystal structures show that GroEL2 forms dimers in *M. tuberculosis* (Qamra and Mande, 2004). Furthermore, it has been proposed that GroEL2 has only weak ATPase activity and can function in an ATP-independent mode (Qamra et al., 2004). This may be due to the slower growth of mycobacteria, which helps it survive in harsh environments such as hypoxia and poor nutrition. The HrcA acts as a transcriptional repressor to block the expression of *groES* and *groEL2* though binding to their cognate DNA elements. Together with the pup-proteasome system, they regulate nitrate utilization. When the pup-proteasome system is absent and HrcA cannot be degraded, *M. tuberculosis* is deficient in nitrate utilization (Becker et al., 2019). Furthermore, the GroESL2 complex may also be able to fold other proteins involved in nitrogen metabolism. Researchers can explore the role of this regulatory mechanism in other pathways and there may be more discoveries.

2.4. ansP2, ansA, and Rv3722c

Asparagine is also important or even known as one of the best nitrogen sources for *M. tuberculosis*. There should be systems in place to transport and utilize this amino acid. It has been previously reported that *M. tuberculosis* can capture aspartate through membrane transporters and use the amino as a source of nitrogen during infection. Interestingly, AnsP2 (Rv0346c), the homolog of AnsP1 whose expression is markedly induced in the lungs of patients (Rachman et al., 2006), was recently predicted to be an asparagine transporter. However, although the growth of the knockout strain was affected when asparagine was used as the sole nitrogen source, the pathogenicity to mice was not reduced (Gouzy et al., 2014), suggesting that there may be other unknown transporters waiting to be discovered.

There are also some new achievements in the study of asparaginase. This enzyme was discovered decades ago in various mycobacteria, including *M. tuberculosis* (Kirchheimer and Whittaker, 1954). The AsnA/Rv1358c was previously found to hydrolyze aspartate *in vitro* in *Mycobacterium bovis* (Cai et al., 2012), and its homolog in *M. tuberculosis* was recently found to perform the same function. The activity of AsnA/Rv1358c has been reported and annotated, indicating that Rv1358c, as a secretory protein, can help *M. tuberculosis* resist an acidic environment by hydrolyzing asparagine to aspartic acid and ammonia. In addition, it is also recognized to induce stress to primary immune cells and compromise the host immune response (Gouzy et al., 2014; Kataria et al., 2021). Compared with central nitrogen metabolism, the research in this area is less and still in its infancy. Studying the function of genes involved in this metabolic pathway is an alternative research direction in the future.

In addition, as mentioned above, Glu is the primary portal of nitrogen assimilation and 27% of nitrogen is distributed via Asp for the dedicated biosynthesis of several cofactors, nucleotides, and amino acids (Reitzer, 2004). It highlights the importance of aspartate aminotransferase which connects metabolisms of glutamate and aspartate. Gratifyingly, Rv3722c was found to encode the main aspartate aminotransferase in *M. tuberculosis* (Jansen et al., 2020). What's more, Rv3722c belongs to a recently described and structurally distinct subclass of AspATs, designated type Ic, whose members are absent in humans and almost exclusively present in bacteria (Son and Kim, 2016; El-Gebali et al., 2019). It lays an avenue between carbon and nitrogen metabolisms.

2.5. Gene of arginine synthesis

Mycobacterium tuberculosis preserves most of the essential nutrient synthesis pathways, allowing it to survive in a variety of nutrient-deficient environments, which may be one of the important reasons for its success. In previous studies, *M. tuberculosis* strains deficient in leucine or glutamate showed reduced growth but did not die (Hondalus et al., 2000; Lee et al., 2006). Only the absence of methionine or arginine causes bactericidal effects (Berney et al., 2015). Strains with knockdown of *argB* or *argF*, coding two key enzymes in the *de novo* arginine synthesis pathway, are unable to grow in an arginine-deficient medium. Of particular interest, although *M. tuberculosis* has two carriers for arginine transport and sufficient amino acids in host serum, this cannot compensate for the absence of *de novo* arginine synthesis (Tiwari et al., 2018). This was reflected in the experimental results that when *argB*- or *argF*-deficient *M. tuberculosis* was injected into mice, the mutants failed to replicate. It has previously been reported that *Mycobacterium bovis* cannot utilize *in vitro* arginine as the sole nitrogen source (Peteroy-Kelly et al., 2003). Given the similarity between the two bacteria, this may imply that *M. tuberculosis* is unable to utilize or only inefficiently transport exogenous arginine. In addition, oxidative damage caused by ROS accumulation was observed in *argB* or *argF* null mutants, which is the bactericidal mechanism of the commonly used anti-tuberculosis drug isoniazid (Middlebrook et al., 1954; Dhandayuthapani et al., 1996), suggesting the research direction of new bactericidal or adjuvant drugs. And since there is no metabolic pathway for *de novo* arginine synthesis in the body, it might be a target with fewer side effects.

3. Inhibitors of nitrogen metabolism

After long-term studies, a variety of anti-tuberculosis drugs are being used in clinical practice. For drug-sensitive *M. tuberculosis*, the combination of several common drugs, such as rifampicin, isoniazid, pyrazinamide and ethambutol, can achieve good results. But because of the existence of the dormant state, many patients suffer from a long course of treatment and easy to relapse. In addition, the large number of multi-drug resistant bacteria also put forward an urgent need for the development of new drugs. The inhibitors involved and their dosages are shown in Table 1 and the docking view of ligands and proteins is shown in Figure 3.

3.1. Inhibitor of glutamine synthetase

As one of the most important enzymes in central nitrogen metabolism, glutamine synthetase is a natural candidate drug target. In addition, although GlnA1 is also present in humans, its homology with *M. tuberculosis* is low, less than 20% (Krajewski et al., 2008). Therefore, drugs developed with this target will have limited risks of on-target *in vivo* toxicity. Earlier drugs were mostly glutamine analogs that competitively bind glutamine synthetase. For example, L-methionine-Sr-sulfoximine (MSO) has been reported to reduce the number of *M. tuberculosis* in the lungs and spleen of diseased animals, and can synergize with isoniazid and ascorbic acid to improve the efficacy. As expected, MSO showed high selectivity for *M. tuberculosis* protein. The compound was 100-fold less active against human glutamine synthetase (Harth and Horwitz, 2003). Unfortunately, although the drug markedly reduced the amount of poly real-L-glutamate/glutamine cell wall structure in *M. tuberculosis*, the drug can't cross the cell wall of mycobacteria. Therefore, only extracellular glutamine synthetase can be inhibited, but the effect on cellular glutamine synthetase is very small (Harth and Horwitz, 1999). For other mycobacteria, there is few report about the antibacterial efficacy of MSO. However, *in vitro* biochemical result shown that MSO can largely inhibit the enzymatic activity of glutamine synthetase in *Mycobacterium avium*, the representative strain of non-tuberculosis mycobacteria (NTM) (Alvarez and McCarthy, 1984).

Consider the process catalyzed by glutamine synthetase, ATP phosphorylates glutamate to form an intermediate, and then the amino group replaces the phosphate group to form glutamine, glutamine synthetase functions as an ATP-dependent process. Drugs that interact with ATP binding have been developed in recent years. Bedaquiline (BDQ), the first new drug approved

in decades, is an inhibitor of *M. tuberculosis* ATP synthase. As expected, there has been some evidence supporting the synergy between MSO and BDQ (Wang et al., 2019). Several bisphosphonic acid derivatives have been reported to have potential as new drugs, and given their bone-targeting properties, these compounds are promising for the treatment of bone tuberculosis (Kosikowska et al., 2016). In addition, 4-(2-Tert-Butyl-4-(6-Methoxynaphthalen-2-Yl)-3 h-Imidazol-4-Yl) pyridin-2-Amine was also found to has antibacterial activity by high-throughput screening (Gising et al., 2012) (the drug-target interaction is shown as Figure 3A). However, it is highly toxic to human cells, so its specificity needs to be enhanced to develop its clinical use.

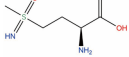
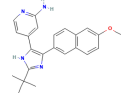
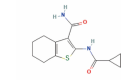
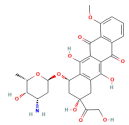
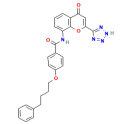
Recently, it has been reported that the anticancer drug linsitinib can act as a competitive inhibitor of ATP binding and affect GlnA activity, thereby inhibiting the growth of *M. tuberculosis*. It can also enhance the resistance to *M. tuberculosis* by activating autophagy in host cells. Similarly, it also showed a certain synergistic effect of bedaquiline (Wang et al., 2022). As a drug developed in the past, its safety is relatively guaranteed. However, its anti-tuberculosis effect needs to be strengthened and further optimized in subsequent studies.

These molecules with different roles and different sources provide a broad prospect for the development of new drugs.

3.2. Inhibitor of PknG

As mentioned in the previous content, PknG is related to many physiological processes in *M. tuberculosis*, participating in the regulation of various metabolism, and its metabolites connect carbon metabolism and nitrogen metabolism. In particular, it is associated with the survival and dormant state of *M. tuberculosis*

TABLE 1 Chemical inhibitors targeted to nitrogen metabolism.

Name	Structural formula	IC50	MIC	Target	References	PubChem ID
L-methionine-SR-sulfoximine		/	10 µM	Glutamine synthetase	Harth and Horwitz, 2003	801860
4-(2-Tert-Butyl-4-(6-Methoxynaphthalene-2-Yl)-3 h-Imidazole-4-Yl) pyridine-2-Amine		0.049 µM	2 µg/ml	Glutamine synthetase	Gising et al., 2012	56928064
AX20017		0.39 µM	/	PknG	Scherr et al., 2007	673481
Doxorubicin		56 µM	/	Asparaginase	Kataria et al., 2019	31703
Pranlukast		2.7 µg/ml	5.2 µg/ml	ArgJ	Mishra et al., 2019	4887

“/” Means the values are not mentioned in the references. The structure of L-methionine-SR-sulfoximine was drawn using Chemdraw and others came from PubChem database (<https://pubchem.ncbi.nlm.nih.gov/>).

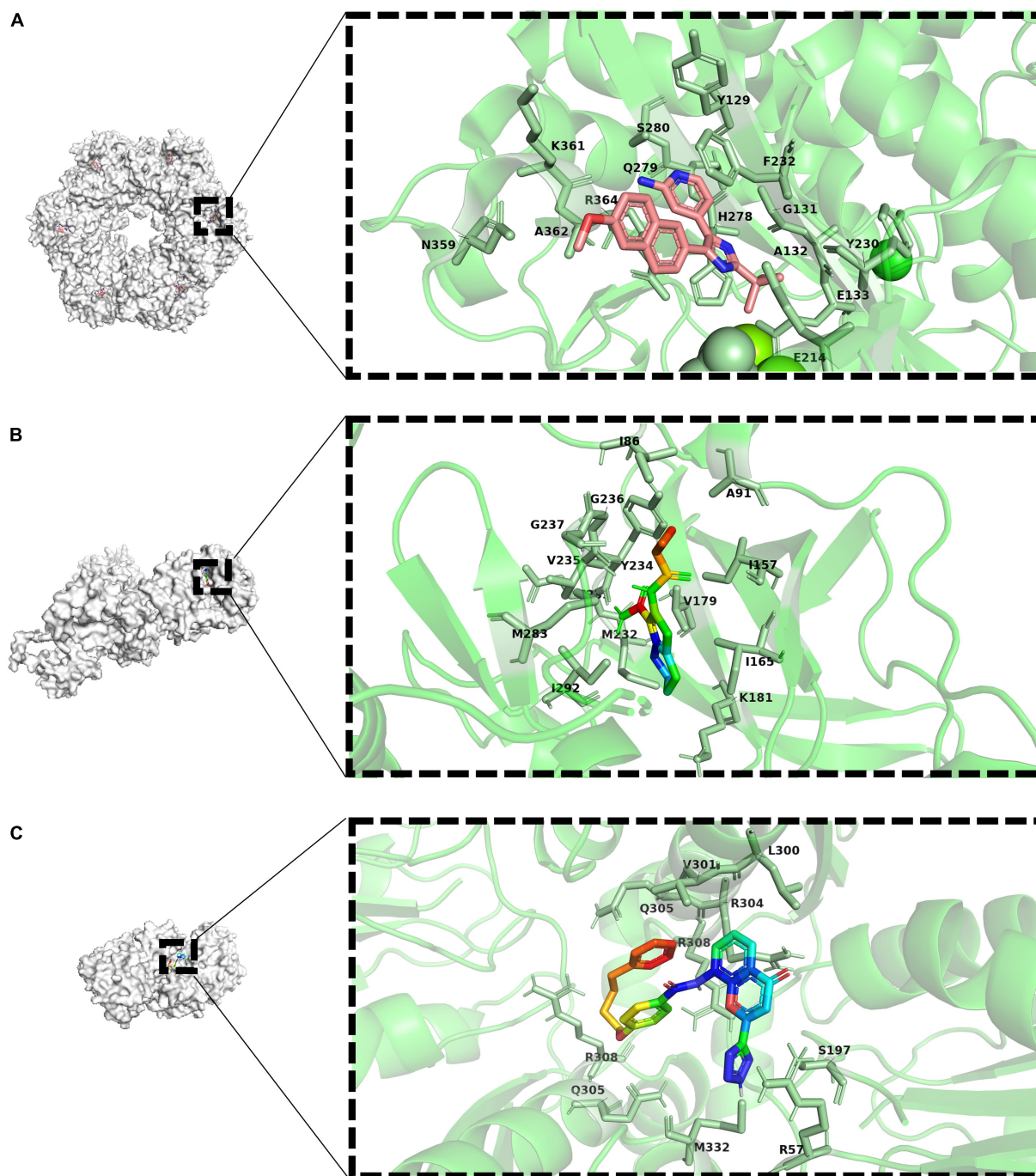


FIGURE 3

Docking view or co-crystal complexes of ligands and proteins. (A) Co-crystal complex of 4-(2-Tert-Butyl-4-(6-Methoxynaphthalene-2-Yl)-3 h-Imidazole-4-Yl) pyridine-2-Amine (PubChem-ID: 673481) as ligand and GlnA1 (Co-crystallization PDB-D: 3ZXV). Sticks representation of residues with 4Å around ligand in a zoomed view. (B) Co-crystal complex of ax20017 (PubChem-ID: 673481) as ligand and PknG (Co-crystallization PDB-D: 2PZI). Sticks representation of residues with 4Å around ligand in a zoomed view. (C) Docking view of Pranlukast (PubChem-ID: 4887) as ligand and ArgJ (PDB-ID: 3IT4). Sticks representation of residues with 4Å around ligand in a zoomed view.

under hypoxia. This is crucial for the survival of *M. tuberculosis* in macrophages and the development of drug resistance. It is well known that many TB drugs, such as isoniazid, mainly target bacteria in the replicating phase but have little effect on bacteria in the non-replicating dormant state. Therefore, PknG as a drug target may play a role in killing bacteria and weakening drug resistance, so as to achieve a better therapeutic effect.

Compound AX20017 was reported to occupy the binding site for ATP whose structure is out of the ordinary, inhibits PknG, and causes mycobacterial transfer into lysosomes, thereby killing mycobacteria (the drug-target interaction is shown as Figure 3B). Moreover, kinase-dependent processes within the macrophage host cell, such as the capacity to proliferate, synthesize proteins, and phagocytosis do not interfere, so as the cellular morphology

demonstrating that AX20017 is a highly specific inhibitor of PknG (Scherr et al., 2007). To improve the affinity, selectivity and potency of AX20017, the cyclopropyl ring which does not exploit binding capacity fully may be an alternative modification site. In recent years, although some studies have found RO9021 and a few flavonoids by computer virtual screening and simulation docking, no subsequent experiments based on cells or animals have been found (Qasaymeh et al., 2019; Arica-Sosa et al., 2022), so its effectiveness still needs to be verified and it is still far from clinical use. It is worth nothing that targeting PknG can also cause the growth inhibition of *M. bovis*, which has been proven through several independent reports (Singh et al., 2015; Kanehiro et al., 2018; Kidwai et al., 2019). The similar sequence of PknG among MTBC therefore let it become a promising broad-spectrum anti-mycobacteria drug target.

3.3. Inhibitor of asparaginase

As mentioned above, asparagine is one of the important nitrogen sources for *M. tuberculosis*. Asparaginase is mainly categorized into type I, II, and III. Type I and II are found in most bacteria, while type III, which has a distinct mode of catalysis is usually found in mammals and plants (Nomme et al., 2012). This difference makes the enzyme a good candidate as a drug target. Specific inhibitors targeting the active site of this enzyme, the potential inhibitors were predicted and screened from ZINC database, TCM database and FDA-approved drug database, according to the structure. Excitingly, M3 (ZINC 4740895), M26 (ZINC 33535) and doxorubicin were screened out and showed satisfactory results in *M. smegmatis* (Kataria et al., 2019). The experiment in *M. tuberculosis* has not been reported, which is worthy of further study. The result can also be extended to *Salmonella typhi*, *H. pylori*, and *L. donovan*, which encode significant overlaps in the conserved catalytic residues. This makes it possible that these compounds could be used as a basis for further development of broad-spectrum antimicrobial drugs to help patients with multiple bacterial co-infections. It was also reported that three kinds of phytochemicals, Physalin D, Withanone, and Withaferin A, can competitively bind asparaginase (Sharma et al., 2022). However, the effect on *M. tuberculosis* remains to be studied.

3.4. Inhibitor of arginine synthesis

Arginine is very important for the growth of *M. tuberculosis*, and the abundant arginine in the outside world cannot compensate for the influence caused by the blockage of its own synthetic pathway. In addition, there is no metabolic pathway for *de novo* arginine synthesis in human body. These make it possible to find drug targets in arginine anabolic metabolism. Most of the substrates for arginine synthesis are common small molecules, so if they are used as the targets of inhibitors, the drugs may have serious off-target effects. However, the allosteric sites of enzymes required for metabolism are less conserved in evolution, which can be used as drug-targeting sites to enhance specificity and reduce side effects (Wenthur et al., 2014). Recently, it has been reported that Pranlukast (PRK) can act as an allosteric inhibitor of ArgJ during

arginine biosynthesis in *M. tuberculosis* and inhibit its ornithine acetyltransferase activity, thereby inhibiting bacterial survival and virulence (Mishra et al., 2019) (the drug-target interaction is predicted as shown in Figure 3C). Further metabolomics studies showed that PRK caused significant differential expression of 50 metabolites (Yelamanchi et al., 2022). This will contribute to a deeper understanding of PRK-mediated metabolic changes and provide a basis for the development of new therapeutic approaches. Because it has already been approved by the FDA, PRK could be ready for use much faster than a new drug. And as an approved drug, there are no excessive concerns about its safety, and patients are more likely to accept it.

4. Way forward

In this review, we describe some of the key genes involved in nitrogen metabolism in *M. tuberculosis* using ammonium and nitrate as inorganic nitrogen sources and some amino acids as organic nitrogen sources. Some inhibitors or drugs targeting nitrogen metabolism were also introduced. The action sites of the inhibitors are mainly some key enzymes in the metabolic process, which also indicates the direction of developing new anti-tuberculosis drugs in the future. Many new inhibitors have been discovered, giving hope for the development of new anti-TB drugs. However, many research results remain at the level of computer prediction or biochemical experiments, and the subsequent results of cell and animal experiments are lacking, which may be related to the greater risk of *Mycobacterium tuberculosis* and the higher requirements of laboratory safety level for research. Considering previous studies have reported some nanomolar inhibitions of GlnA1 inhibitors, none of which were active against whole-cell *M. tuberculosis* (Couturier et al., 2015), cautious optimism is warranted.

In addition, it is worth noting that some drugs not only act on the metabolic process of *M. tuberculosis*, but also kill the pathogen by affecting host cells. Recent studies have reported that mitochondrial metabolism regulated by mTOR limits mycobacteria-induced cytotoxicity (Pagán et al., 2022) suggesting that screening new anti-TB drugs from existing drugs that target mTOR may be a good direction. And compared with developing new drugs, existing drugs have great advantages in terms of safety and time to approval.

Like we have been through in the past, the clinical application of nitrogen-targeted antimicrobials will inevitably lead to drug resistance in the future. However, finding a synergistic drug combination includes 1, 2, or more extra antibiotics could be an effective way to overcome drug resistance. The previous research from our team has shown that inhibiting both ATP synthesis and glutamine synthesis causes a synergistic killing effect (Wang et al., 2019), it is therefore worth to keep exploring the combination between BDQ and other nitrogen metabolism targeted drugs, since ATP is the crucial factor driving hundreds of biochemical reactions to maintain the bacterial nitrogen homeostasis.

There are still many possible drug targets that have not been studied or rarely studied, leaving a wide range of possibilities for new drugs. However, due to the complexity of metabolic processes and the need to consider the effects of drugs on the patient's body,

the real development of effective and safe drugs will still be a long and arduous process.

Author contributions

ZW and YX: conceptualization. YX, SM, and LW: literature search. ZH and YX: protein structure analysis. ZW, YX, and SM: writing—original draft preparation. ZW, YX, SM, LW, and SR: writing—review and editing. All authors read and agreed to the published version of the manuscript.

Funding

This research was kindly supported by a grant from the National Natural Science Foundation of China (No. 32070128), National Key Research and Development Plans of China

References

- Agapova, A., Serafini, A., Petridis, M., Hunt, D., Garza-Garcia, A., Sohaskey, C., et al. (2019). Flexible nitrogen utilisation by the metabolic generalist pathogen *Mycobacterium tuberculosis*. *eLife* 8:e41129. doi: 10.7554/eLife.41129
- Alvarez, M., and McCarthy, C. (1984). Glutamine synthetase from *Mycobacterium avium*. *Can. J. Microbiol.* 30, 353–359. doi: 10.1139/m84-052
- Aly, S., Wagner, K., Keller, C., Malm, S., Malzan, A., Brandau, S., et al. (2006). Oxygen status of lung granulomas in *Mycobacterium tuberculosis*-infected mice. *J. Pathol.* 210, 298–305. doi: 10.1002/path.2055
- Arica-Sosa, A., Alcántara, R., Jiménez-Avalos, G., Zimic, M., Milón, P., and Quiliano, M. (2022). Identifying RO9021 as a Potential Inhibitor of PknG from *Mycobacterium tuberculosis*: combinative computational and *in vitro* studies. *ACS Omega* 7, 20204–20218. doi: 10.1021/acsomega.2c02093
- Baghel, A., Tandon, R., Gupta, G., Kumar, A., Sharma, R., Aggarwal, N., et al. (2011). Characterization of protein acyltransferase function of recombinant purified GlnA1 from *Mycobacterium tuberculosis*: a moon lighting property. *Microbiol. Res.* 166, 662–672. doi: 10.1016/j.micres.2011.02.001
- Becker, S., Jastrab, J., Dhabaria, A., Chaton, C., Rush, J., Korotkov, K., et al. (2019). The *Mycobacterium tuberculosis* Pup-proteasome system regulates nitrate metabolism through an essential protein quality control pathway. *Proc. Natl. Acad. Sci. U.S.A.* 116, 3202–3210. doi: 10.1073/pnas.1819468116
- Bell, L., and Noursadeghi, M. (2018). Pathogenesis of HIV-1 and *Mycobacterium tuberculosis* co-infection. *Nat. Rev. Microbiol.* 16, 80–90. doi: 10.1038/nrmicro.2017.128
- Berney, M., Berney-Meyer, L., Wong, K., Chen, B., Chen, M., Kim, J., et al. (2015). Essential roles of methionine and S-adenosylmethionine in the autarkic lifestyle of *Mycobacterium tuberculosis*. *Proc. Natl. Acad. Sci. U.S.A.* 112, 10008–10013. doi: 10.1073/pnas.1513033112
- Bhattacharyya, N., Nkumama, I., Newland-Smith, Z., Lin, L., Yin, W., Cullen, R., et al. (2018). An aspartate-specific solute-binding protein regulates protein kinase G activity to control glutamate metabolism in mycobacteria. *mBio* 9:e00931-18. doi: 10.1128/mBio.00931-18
- Borah, K., Beyß, M., Theorell, A., Wu, H., Basu, P., Mendum, T., et al. (2019). Intracellular *Mycobacterium tuberculosis* exploits multiple host nitrogen sources during growth in human macrophages. *Cell Rep.* 29, 3580.e4–3591.e4. doi: 10.1016/j.celrep.2019.11.037
- Cai, X., Wu, B., Fang, Y., and Song, H. (2012). [Asparaginase mediated acid adaptation of mycobacteria]. *Acta Microbiol. Sin.* 52, 1467–1476.
- Caño-Muñiz, S., Anthony, R., Niemann, S., and Alffenaar, J. (2018). New approaches and therapeutic options for *Mycobacterium tuberculosis* in a dormant state. *Clin. Microbiol. Rev.* 31:e00060-17. doi: 10.1128/CMR.00060-17
- Carroll, P., Pashley, C., and Parish, T. (2008). Functional analysis of GlnE, an essential adenylyl transferase in *Mycobacterium tuberculosis*. *J. Bacteriol.* 190, 4894–4902. doi: 10.1128/JB.00166-08
- (No. 2021YFD1800401), and Shanghai Biomedical Science and Technology Support Special Project (No. 21S11900200).

Conflict of interest

The authors declare that the research was conducted in the absence of any commercial or financial relationships that could be construed as a potential conflict of interest.

Publisher's note

All claims expressed in this article are solely those of the authors and do not necessarily represent those of their affiliated organizations, or those of the publisher, the editors and the reviewers. Any product that may be evaluated in this article, or claim that may be made by its manufacturer, is not guaranteed or endorsed by the publisher.

- and resist acid stress during infection. *PLoS Pathog.* 10:e1003928. doi: 10.1371/journal.ppat.1003928
- Grallert, H., and Buchner, J. (2001). Review: a structural view of the GroE chaperone cycle. *J. Struct. Biol.* 135, 95–103. doi: 10.1006/jbsi.2001.4387
- Harding, E. (2020). WHO global progress report on tuberculosis elimination. *Lancet Respir Med.* 8:19. doi: 10.1016/S2213-2600(19)30418-7
- Harth, G., Clemens, D., and Horwitz, M. (1994). Glutamine synthetase of *Mycobacterium tuberculosis*: extracellular release and characterization of its enzymatic activity. *Proc. Natl. Acad. Sci. U.S.A.* 91, 9342–9346. doi: 10.1073/pnas.91.20.9342
- Harth, G., and Horwitz, M. (1999). An inhibitor of exported *Mycobacterium tuberculosis* glutamine synthetase selectively blocks the growth of pathogenic mycobacteria in axenic culture and in human monocytes: extracellular proteins as potential novel drug targets. *J. Exp. Med.* 189, 1425–1436. doi: 10.1084/jem.189.9.1425
- Harth, G., and Horwitz, M. (2003). Inhibition of *Mycobacterium tuberculosis* glutamine synthetase as a novel antibiotic strategy against tuberculosis: demonstration of efficacy *in vivo*. *Infect. Immun.* 71, 456–464. doi: 10.1128/IAI.71.1.456-464.2003
- Harth, G., Maslesa-Galia, S., Tullius, M., and Horwitz, M. (2005). All four *Mycobacterium tuberculosis* glnA genes encode glutamine synthetase activities but only GlnA1 is abundantly expressed and essential for bacterial homeostasis. *Mol. Microbiol.* 58, 1157–1172. doi: 10.1111/j.1365-2958.2005.04899.x
- Hedgecock, L., and Costello, R. (1962). Utilization of nitrate by pathogenic and saprophytic mycobacteria. *J. Bacteriol.* 84, 195–205. doi: 10.1128/jb.84.2.195-205.1962
- Hildebrand, R., Chandrasekar, S., Riel, M., Touray, B., Aschenbroich, S., and Talaat, A. (2022). Superinfection with SARS-CoV-2 has deleterious effects on *Mycobacterium bovis* BCG immunity and promotes dissemination of *Mycobacterium tuberculosis*. *Microbiol. Spectr.* 10:e0307522. doi: 10.1128/spectrum.03075-22
- Holzheimer, M., Buter, J., and Minnaard, A. (2021). Chemical synthesis of cell wall constituents of *Mycobacterium tuberculosis*. *Chem. Rev.* 121, 9554–9643. doi: 10.1021/acs.chemrev.1c00043
- Hondalus, M., Bardarov, S., Russell, R., Chan, J., Jacobs, W., and Bloom, B. (2000). Attenuation of and protection induced by a leucine auxotroph of *Mycobacterium tuberculosis*. *Infect. Immun.* 68, 2888–2898. doi: 10.1128/IAI.68.5.2888-2898.2000
- Höner zu Bentrup, K., and Russell, D. (2001). Mycobacterial persistence: adaptation to a changing environment. *Trends Microbiol.* 9, 597–605. doi: 10.1016/S0966-842X(01)02238-7
- Hu, Y., Henderson, B., Lund, P., Tormay, P., Ahmed, M., Gurucha, S., et al. (2008). A *Mycobacterium tuberculosis* mutant lacking the groEL homologue cpn60.1 is viable but fails to induce an inflammatory response in animal models of infection. *Infect. Immun.* 76, 1535–1546. doi: 10.1128/IAI.01078-07
- Huang, F., and Zhao, Y. (2022). Global control of tuberculosis: current status and future prospects. *Zoonoses* 2:9. doi: 10.15212/ZOONOSSES-2021-0021
- Jansen, R., Mandyoli, L., Hughes, R., Wakabayashi, S., Pinkham, J., Selbach, B., et al. (2020). Aspartate aminotransferase Rv3722c governs aspartate-dependent nitrogen metabolism in *Mycobacterium tuberculosis*. *Nat. Commun.* 11:1960. doi: 10.1038/s41467-020-15876-8
- Kanehiro, Y., Tomioka, H., Pieters, J., Tatano, Y., Kim, H., Iizasa, H., et al. (2018). Identification of novel mycobacterial inhibitors against mycobacterial protein kinase G. *Front. Microbiol.* 9:1517. doi: 10.3389/fmicb.2018.01517
- Kataria, A., Patel, A., and Kundu, B. (2021). Distinct functional properties of secretory L-asparaginase Rv1538c involved in phagosomal survival of *Mycobacterium tuberculosis*. *Biochimie* 182, 1–12. doi: 10.1016/j.biochi.2020.12.023
- Kataria, A., Singh, J., and Kundu, B. (2019). Identification and validation of L-asparaginase as a potential metabolic target against *Mycobacterium tuberculosis*. *J. Cell. Biochem.* 120, 143–154. doi: 10.1002/jcb.27169
- Khan, M., Bhaskar, A., Upadhyay, S., Kumari, P., Rajmani, R., Jain, P., et al. (2017). Protein kinase G confers survival advantage to *Mycobacterium tuberculosis* during latency-like conditions. *J. Biol. Chem.* 292, 16093–16108. doi: 10.1074/jbc.M117.797563
- Kidwai, S., Bouzeyen, R., Chakraborti, S., Khare, N., Das, S., Priya Gosain, T., et al. (2019). NU-6027 inhibits growth of *Mycobacterium tuberculosis* by targeting protein kinase D and protein kinase G. *Antimicrob. Agents Chemother.* 63:e00996-19. doi: 10.1128/AAC.00996-19
- Kirby, T. (2021). Global tuberculosis progress reversed by COVID-19 pandemic. *Lancet Respir Med.* 9, e118–e119. doi: 10.1016/S2213-2600(21)00496-3
- Kirchheimer, F., and Whittaker, C. (1954). Asparaginase of mycobacteria. *Am. Rev. Tuberc.* 70, 920–921.
- Kosikowska, P., Bochno, M., Macegoniuk, K., Forlani, G., Kafarski, P., and Berlicki, Ł. (2016). Bisphosphonic acids as effective inhibitors of *Mycobacterium tuberculosis* glutamine synthetase. *J. Enzyme Inhib. Med. Chem.* 31, 931–938. doi: 10.3109/14756366.2015.1070846
- Krajewski, W., Collins, R., Holmberg-Schiavone, L., Jones, T., Karlberg, T., and Mowbray, S. (2008). Crystal structures of mammalian glutamine synthetases illustrate substrate-induced conformational changes and provide opportunities for drug and herbicide design. *J. Mol. Biol.* 375, 217–228. doi: 10.1016/j.jmb.2007.10.029
- Lee, J., Lim, J., Gao, S., Lawson, C., Odell, M., Raheem, S., et al. (2018). Glutamate mediated metabolic neutralization mitigates propionate toxicity in intracellular *Mycobacterium tuberculosis*. *Sci. Rep.* 8:8506. doi: 10.1038/s41598-018-26950-z
- Lee, S., Jeon, B., Bardarov, S., Chen, M., Morris, S., and Jacobs, W. (2006). Protection elicited by two glutamine auxotrophs of *Mycobacterium tuberculosis* and *in vivo* growth phenotypes of the four unique glutamine synthetase mutants in a murine model. *Infect. Immun.* 74, 6491–6495. doi: 10.1128/IAI.00531-06
- Leigh, J., and Dodsworth, J. (2007). Nitrogen regulation in bacteria and archaea. *Annu. Rev. Microbiol.* 61, 349–377. doi: 10.1146/annurev.micro.61.080706.093409
- Leonso, A., Brown, K., Prol, R., Rawat, S., Khunger, A., and Bromberg, R. (2022). A rare case of latent tuberculosis reactivation secondary to a COVID-19 infection. *Infect. Dis. Rep.* 14, 446–452. doi: 10.3390/idr14030048
- Liao, Z., Yang, S., Li, Q., and Lu, H. (2022). The role of metagenomic next-generation sequencing as a promising technology for diagnosing HIV-TB coinfection. *Zoonoses* 2, 1–4. doi: 10.15212/ZOONOSSES-2022-0032
- Lisa, M., Gil, M., André-Leroux, G., Barilone, N., Durán, R., Biondi, R., et al. (2015). molecular basis of the activity and the regulation of the eukaryotic-like S/T protein kinase PknG from *Mycobacterium tuberculosis*. *Structure* 23, 1039–1048. doi: 10.1016/j.str.2015.04.001
- Malm, S., Tiffert, Y., Micklinghoff, J., Schultze, S., Joost, I., Weber, I., et al. (2009). The roles of the nitrate reductase NarGHJI, the nitrite reductase NirBD and the response regulator GlnR in nitrate assimilation of *Mycobacterium tuberculosis*. *Microbiology* 155(Pt 4), 1332–1339. doi: 10.1099/mic.0.023275-0
- Middlebrook, G., Cohn, M., and Schaefer, W. (1954). Studies on isoniazid and tubercle bacilli. III. The isolation, drug-susceptibility, and catalase-testing of tubercle bacilli from isoniazid-treated patients. *Am. Rev. Tuberc.* 70, 852–872.
- Mishra, A., Mamidi, A., Rajmani, R., Ray, A., Roy, R., and Surolia, A. (2019). An allosteric inhibitor of *Mycobacterium tuberculosis* ArgJ: implications to a novel combinatorial therapy. *EMBO Mol. Med.* 11:e11209. doi: 10.15252/emmm.201911209
- Nomme, J., Su, Y., Konrad, M., and Lavie, A. (2012). Structures of apo and product-bound human L-asparaginase: insights into the mechanism of autoprolysis and substrate hydrolysis. *Biochemistry* 51, 6816–6826. doi: 10.1021/bi300870g
- O'Hare, H., Durán, R., Cerveñansky, C., Bellinzoni, M., Wehenkel, A., Pritsch, O., et al. (2008). Regulation of glutamate metabolism by protein kinases in mycobacteria. *Mol. Microbiol.* 70, 1408–1423. doi: 10.1111/j.1365-2958.2008.06489.x
- Pagán, A., Lee, L., Edwards-Hicks, J., Moens, C., Tobin, D., Busch-Nentwich, E., et al. (2022). mTOR-regulated mitochondrial metabolism limits *mycobacterium*-induced cytotoxicity. *Cell* 185, 3720.e13–3738.e13. doi: 10.1016/j.cell.2022.08.018
- Peteroy-Kelly, M., Venketaraman, V., Talaue, M., Seth, A., and Connell, N. (2003). Modulation of J774.1 macrophage L-arginine metabolism by intracellular *Mycobacterium bovis* BCG. *Infect. Immun.* 71, 1011–1015. doi: 10.1128/IAI.71.2.1011-1015.2003
- Qamra, R., and Mande, S. (2004). Crystal structure of the 65-kilodalton heat shock protein, chaperonin 60.2, of *Mycobacterium tuberculosis*. *J. Bacteriol.* 186, 8105–8113. doi: 10.1128/JB.186.23.8105-8113.2004
- Qamra, R., Mande, S., Coates, A., and Henderson, B. (2005). The unusual chaperonins of *Mycobacterium tuberculosis*. *Tuberculosis* 85, 385–394. doi: 10.1016/j.tube.2005.08.014
- Qamra, R., Srinivas, V., and Mande, S. (2004). *Mycobacterium tuberculosis* GroEL homologues unusually exist as lower oligomers and retain the ability to suppress aggregation of substrate proteins. *J. Mol. Biol.* 342, 605–617. doi: 10.1016/j.jmb.2004.07.066
- Qasaymeh, R., Rotondo, D., Oosthuizen, C., Lall, N., and Seidel, V. (2019). Predictive binding affinity of plant-derived natural products towards the protein kinase G enzyme of *Mycobacterium tuberculosis* (Mt PknG). *Plants* 8:477. doi: 10.3390/plants8110477
- Rachman, H., Strong, M., Ulrichs, T., Grode, L., Schuchhardt, J., Mollenkopf, H., et al. (2006). Unique transcriptome signature of *Mycobacterium tuberculosis* in pulmonary tuberculosis. *Infect. Immun.* 74, 1233–1242. doi: 10.1128/IAI.74.2.1233-1242.2006
- Read, R., Pashley, C., Smith, D., and Parish, T. (2007). The role of GlnD in ammonia assimilation in *Mycobacterium tuberculosis*. *Tuberculosis* 87, 384–390. doi: 10.1016/j.tube.2006.12.003
- Reitzer, L. (2004). Biosynthesis of glutamate, aspartate, asparagine, L-alanine, and D-alanine. *EcoSal Plus* 1, 1–18. doi: 10.1128/ecosal.3.6.1.3
- Rieck, B., Degiacomi, G., Zimmermann, M., Cascioferro, A., Boldrin, F., Lazar-Adler, N., et al. (2017). PknG senses amino acid availability to control metabolism and virulence of *Mycobacterium tuberculosis*. *PLoS Pathog.* 13:e1006399. doi: 10.1371/journal.ppat.1006399
- Scherr, N., Honnappa, S., Kunz, G., Mueller, P., Jayachandran, R., Winkler, F., et al. (2007). Structural basis for the specific inhibition of protein kinase G, a virulence factor of *Mycobacterium tuberculosis*. *Proc. Natl. Acad. Sci. U.S.A.* 104, 12151–12156. doi: 10.1073/pnas.0702842104
- Sharma, D., Saini, R., and Mishra, A. (2022). Natural phytochemicals physalin D, withaferin A and withanone target L-asparaginase of *Mycobacterium tuberculosis*

- : a molecular dynamics study. *J. Biomol. Struct. Dyn.* 41, 2645–2659. doi: 10.1080/07391102.2022.2036239
- Singh, N., Tiwari, S., Srivastava, K., and Siddiqi, M. (2015). Identification of novel inhibitors of *Mycobacterium tuberculosis* PknG using pharmacophore based virtual screening, docking, molecular dynamics simulation, and their biological evaluation. *J. Chem. Inform. Model.* 55, 1120–1129. doi: 10.1021/acs.jcim.5b00150
- Son, H., and Kim, K. (2016). Structural insights into a novel class of aspartate aminotransferase from *Corynebacterium glutamicum*. *PLoS One* 11:e0158402. doi: 10.1371/journal.pone.0158402
- Tiwari, S., van Tonder, A., Vilch  ze, C., Mendes, V., Thomas, S., Malek, A., et al. (2018). Arginine-deprivation-induced oxidative damage sterilizes *Mycobacterium tuberculosis*. *Proc. Natl. Acad. Sci. U.S.A.* 115, 9779–9784. doi: 10.1073/pnas.1808874115
- Tullius, M., Harth, G., and Horwitz, M. (2003). Glutamine synthetase GlnA1 is essential for growth of *Mycobacterium tuberculosis* in human THP-1 macrophages and guinea pigs. *Infect. Immun.* 71, 3927–3936. doi: 10.1128/IAI.71.7.3927-3936.2003
- Via, L., Lin, P., Ray, S., Carrillo, J., Allen, S., Eum, S., et al. (2008). Tuberculous granulomas are hypoxic in guinea pigs, rabbits, and nonhuman primates. *Infect. Immun.* 76, 2333–2340. doi: 10.1128/IAI.01515-07
- Viljoen, A., Kirsten, C., Baker, B., van Helden, P., and Wiid, I. (2013). The role of glutamine oxoglutarate aminotransferase and glutamate dehydrogenase in nitrogen metabolism in *Mycobacterium bovis* BCG. *PLoS One* 8:e84452. doi: 10.1371/journal.pone.0084452
- Wang, H., Bi, J., Zhang, Y., Pan, M., Guo, Q., Xiao, G., et al. (2022). Human kinase IGF1R/IR inhibitor linsitinib controls the *in vitro* and intracellular growth of *Mycobacterium tuberculosis*. *ACS Infect. Dis.* 8, 2019–2027. doi: 10.1021/acsinfectdis.2c00278
- Wang, Z., Soni, V., Marriner, G., Kaneko, T., Boshoff, H., Barry, C., et al. (2019). Mode-of-action profiling reveals glutamine synthetase as a collateral metabolic vulnerability of *M. tuberculosis* to bedaquiline. *Proc. Natl. Acad. Sci. U.S.A.* 116, 19646–19651. doi: 10.1073/pnas.1907946116
- Wenthur, C., Gentry, P., Mathews, T., and Lindsley, C. (2014). Drugs for allosteric sites on receptors. *Annu. Rev. Pharmacol. Toxicol.* 54, 165–184. doi: 10.1146/annurev-pharmtox-010611-134525
- Williams, K., Bennett, M., Barton, G., Jenkins, V., and Robertson, B. (2013). Adenylation of mycobacterial Glnk (PII) protein is induced by nitrogen limitation. *Tuberculosis* 93, 198–206. doi: 10.1016/j.tube.2012.12.003
- Xu, Z., Horwich, A., and Sigler, P. (1997). The crystal structure of the asymmetric GroEL-GroES-(ADP)7 chaperonin complex. *Nature* 388, 741–750. doi: 10.1038/41944
- Yelamanchi, S., Arun Kumar, S., Mishra, A., Keshava Prasad, T., and Surolia, A. (2022). Metabolite dysregulation by pranlukast in *Mycobacterium tuberculosis*. *Molecules* 27:1520. doi: 10.3390/molecules27051520

Frontiers in Microbiology

Explores the habitable world and the potential of microbial life

The largest and most cited microbiology journal which advances our understanding of the role microbes play in addressing global challenges such as healthcare, food security, and climate change.

Discover the latest Research Topics

[See more →](#)

Frontiers

Avenue du Tribunal-Fédéral 34
1005 Lausanne, Switzerland
frontiersin.org

Contact us

+41 (0)21 510 17 00
frontiersin.org/about/contact

